Marine predator foraging strategies in response to broad- and fine-scale resource variability

---

Malcolm Daniel O'Toole

Bachelor of Science (Hons), University of Tasmania

Submitted in fulfilment of the requirements for the degree of Doctor of Philosophy

Institute for Marine and Antarctic Studies, University of Tasmania

Antarctic Climate and Ecosystem Cooperative Research Centre, University of Tasmania

June 2015

Declaration of originality

This thesis contains no material which has been accepted for a degree or diploma by the University or any other institution, except by way of background information and duly acknowledged in the thesis, and to the best of my knowledge and belief no material previously published or written by another person except where due acknowledgement is made in the text of the thesis, nor does the thesis contain any material that infringes copyright.

Malcolm Daniel O'Toole 27th February 2015

Statement of authority of access

This thesis may be made available for loan and limited copying in accordance with the copyright act 1968

Malcolm Daniel O'Toole 27th February 2015

Abstract

Foraging ecology is key to understanding the drivers of habitat selection, elucidating the abiotic and biotic factors associated with animal decision-making and the ecological context within which these choices occur. In particular, the resilience and response of upper-trophic-level populations to trans-seasonal resource variability is an ongoing question in marine ecology. New analytical tools are now opening new avenues for understanding such questions in the marine environment. However, while a considerable body of literature exists on the effects of *in situ* physical conditions on marine species; few studies have investigated the effects of *in situ* biological conditions. The overall aim of this thesis was to assess the feasibility of using light, collected by a marine predator, to estimate biological conditions in the water column, and demonstrate its application, in an ecological context.

First, light level and depth data collected by elephant seals were used as a relative index to estimate plankton density in the water column, and subsequently compared with trans-seasonal chlorophyll-a patterns as revealed by satellite-derived ocean colour. Second, different aspects of broad-scale elephant seal foraging behaviour (search intensity, dive effort and mass gain rate) estimated from time-depth recorders was tested in response to the daily plankton density index. Seal foraging strategies were compared between summer and winter foraging trips. Finally, feeding activity of elephant seals (prey encounter events - PEE) estimated from high-resolution accelerometry was examined in relation to concurrent light data used to estimate both plankton density and possible bioluminescent prey encounter events ($Biolum_{PEE}$), within the recurrent "Kerguelen" phytoplankton plume in summer, at both the meso- and dive-scale.

Thesis results demonstrated that light collected by elephant seals, used as an index for plankton density in open waters of the Southern Ocean, correlated well with seasonal chlorophyll-a estimates derived from satellite ocean colour. Despite contrast phytoplankton production between summer (bloom period) and winter (oligotrophic waters), the foraging behaviour of elephant seals responded positively to plankton density at the broad-scale, regardless of time of year. This provided insight into how marine predators may utilise different foraging strategies to exploit prey resources throughout the year. High-resolution data collected within the Kerguelen plume alluded to the possible function of plankton in relation to seal foraging behaviour within the frontal zones of the Antarctic Circumpolar Current; plankton density is likely to facilitate seal vertical access to prey as the predator moves towards the Kerguelen plume 'front' where the system is less mature (*i.e.* less time has passed for energy to transfer from lower-trophic to higher-trophic species).

Fine-scale data collected by bio-logging devices in remote polar regions can provide useful biological information that is concurrent with predator foraging behaviour at relevant scales. Differences in behavioural responses reflect resource variability during the period of prey acquisition at sea. My results suggest likely foraging strategies adopted by elephant seals (that targets meso-pelagic fish) in response to trans-seasonal resource variability, while scale-dependent analysis alludes to their foraging plasticity in a system largely structured by a phytoplankton plume.

Statement of publication and co-authorship

Publications produced as part of this thesis:

O'Toole, M.D., Lea, M.-A., Guinet, C., and Hindell, M.A. (2014). Estimating Trans-Seasonal Variability in Water Column Biomass for a Highly Migratory, Deep Diving Predator. *Plos One* 9, e113171. doi: 10.1371/journal.pone.0113171.

O'Toole, M.D., Lea, M.-A., Guinet, C., Schick, R., and Hindell, M.A. (In Review). Influence of seasonal resource differences on foraging strategies of a top marine predator. *Frontiers in Marine Science.*

O'Toole, M.D., Guinet, C., Lea, M.-A., and Hindell, M.A. (In Preparation). Making the link: light collected by post-breeding elephant seals reveal trophic dynamics within the recurrent Kerguelen plume. *Progress in Oceanography*.

The following people and institutes contributed to the publication of the research undertaken as part of this thesis:

Mark A. Hindell (University of Tasmania), Mary-Anne Lea (University of Tasmania) and Christophe Guinet (Centre détudes biologiques de Chizé) assisted with guidance and supervision in all aspects of the PhD research and producing publishable manuscripts.

Robert Schick (University of St Andrews) provided daily mass gain estimates used in chapter 3.

We the undersigned agree with the above stated “proportion of work undertaken” for each of the above published (or submitted) peer-reviewed manuscripts contributing to this thesis:

Mark Hindell
(Candidate’s supervisor)

Richard Coleman
(Deputy Director of IMAS)

Acknowledgements

This thesis would not have been possible without the support of my primary supervisors Mark Hindell and Mary-Anne Lea (IMAS), as well as Christophe Guinet (CNRS). Their guidance and encouragement helped me push through some of the more challenging stages of my PhD to become a much more competent and confident researcher for which I am very grateful.

I am also indebt to Mark and Christophe for providing me with the opportunity to work in both the Antarctic and sub-Antarctic as part of the French-Australian marine predator tagging programs. I would like to thank Ian Field and Andy Doube for imparting their knowledge to me while working in the field at Davis Station. Both Ian and Andy provided me with skills and experience that will be invalulable for any future fieldwork, and I will always admire their approach to working with animals in the wild.

Thanks also to Sophie Bestley for making herself available to discuss statistical methods used in this thesis, and to Pete Strutton for his advice on using light to measure bio-optic properties in the water column.

I would like to thank Christophe for inviting me to work at CNRS in Chize (France) and sharing with me some amazing datasets and his extensive knowledge on marine predator ecology, as well as his hospitality. I am also indebt to Baptiste Picard for helping me to access datasets stored at the lab in Chize, as well as Jade Vacquie-Garcia for her advice on the detection of bioluminescent events using animal-borne light sensors. Thanks also to Jean-Benoit Charrassin for inviting me to work at the LOCEAN in Paris and always making himself available if ever I needed advice. A huge thanks to Karine and Anne-Marie for welcoming me into their home while in Paris and making me feel part of the family. Special thanks also to Karine for her comments and general support.

Finally, I want to thank my family for helping to get me this far.

Table of Contents

Chapter 1: Introduction

1.1 Marine predators in a heterogeneous environment

The dispersal of organisms is considered an important aspect of many ecological processes including biological invasions, habitat colonisation, avoidance of predators and competitors, as well as allowing individuals to access resources (Cantrell et al., 2010). The principal ecological factors that influence the evolution of dispersal involve environmental heterogeneity in time and/or space (Sahrhage, 1988;McPeek and Holt, 1992). Because resources are often patchily distributed, individuals must sense local environmental conditions and adjust behaviour accordingly (Cantrell et al., 2010). The occurrence of species is not primarily determined by habitat area (or its connectivity), but rather habitat quality and spatial variation in habitat quality from one area to another (reviewed by Fahrig, 2003;Pellet et al., 2007). A major goal in ecology is therefore to measure the role of biotic and abiotic factors that influence the habitat selection at both the individual- and population level.

1.2 Trophic dynamics

Species can be categorised according to their dietary position in the food web (trophic level), ranging from primary producers (lower-trophic-level) to tertiary consumers (top predators). Top predator species are downstream of the energy transfer chain within an ecosystem and resource availability can therefore affect their feeding and reproductive success (and ultimately population dynamics) (Erikstad et al., 1998;Hindell et al., 2003b;Forcada et al., 2005;Le Boeuf and Crocker, 2005;McMahon and Burton, 2005). However, trophic links (interactions between two levels in a food web) are either direct (*e.g.* predators feed on grazers (Estes and Palmisano, 1974)) or indirect (*e.g.* predators control the grazing pressure of grazers on primary producers (Estes and Palmisano, 1974)) . At the base of the marine food web, phytoplankton responds to increased nutrients and light by increasing production (growth and reproduction) (Kiørboe, 1993;Boyd et al., 2000;Boyd, 2002), while primary and mid-trophic (*e.g.* mesopelagic fish) production are coupled and controlled by secondary producers (*i.e.* zooplankton) (Cury et al., 2000;Ware and Thomson, 2005). Changes in zooplankton biomass often lag primary productivity by weeks to months, depending on numerous biotic and abiotic factors such as species composition and water temperature (Hayward and Venrick, 1998). Grémillet et al. (2008) has shown how spatio-temporal mismatch between lower-trophic-level groups can have a marked influences on seabird populations along the Atlantic coast of South Africa. This demonstrates the importance for understanding biotic factors across all major trophic levels and how they interact with marine predators in their environment. The resilience and response of upper-trophic-level populations to trans-seasonal resource variability is an ongoing question in

marine ecology, and novel analytical tools are opening new avenues for answering these questions (Bolker, 2010). This comes at a time when signs of important changes are being observed in the Southern Ocean (Walther et al., 2002;Meredith and King, 2005;Parmesan, 2006;Trathan et al., 2007), and when concerns about the conservation of the region are increasing (e.g. managing future fisheries; Constable et al., 2000;Constable et al., 2014).

1.3 Biophysical processes in the Southern Ocean and its importance to marine biota

The Southern Ocean is of major importance in the global system (Convey et al., 2009), encompassing three deep ocean basins (exceeding 3000 m in depth) including the Atlantic, the Pacific, and the Indian Oceans (figure 1.1). Although relatively unproductive, the large pelagic province of the Southern Ocean is thought to account for approximately 90% of the overall primary production of circumpolar waters, with the contribution of ice-edge bloom production to overall production considered to be low relative to open water productivity (Arrigo et al., 2008). The Ross Sea is considered to be the most productive sector within the Southern Ocean (Arrigo et al., 2008). The biophysical environment of these regions, however, is highly dynamic on both spatial and temporal scales and is heavily influenced by the circulation of the Antarctic Circumpolar Current (ACC), as it flows from west to east around the Southern Ocean (Post et al., 2014). The ACC itself, consists of numerous narrow, deep reaching fronts with distinct water mass properties (Sokolov and Rintoul, 2007). The two most distinct and continuous fronts are the sub-Antarctic front (SAF) and the Polar Front (PF) (Sokolov and Rintoul, 2009) (figure 1.1), both of which are important for fish (Bestley et al., 2010), as well as seabird and marine mammal populations in the Southern Ocean (Bost et al., 2009b). The location of these fronts is strongly influenced by bathymetric obstacles, such as the Kerguelen and Campbell Plateaus, and to a lesser extent the mid-ocean ridges in the Pacific and Indian Oceans (Moore et al., 1999;Moore and Abbott, 2002). These features divert the flow of major fronts and create meandering small scale eddies downstream (Park et al., 1991) that bring nutrient-rich Circumpolar Deep Water (CDW) to the surface (Park et al., 2014). Iron enhancement in the euphotic zone, a critical limiting factor to phytoplankton growth (Martin and Fitzwater, 1988;Martin et al., 1990), can be partly facilitated by vertical mixing when currents flow across shallow plateaus (Park et al., 2008a;Park et al., 2008b). Indeed, the Kerguelen Plateau sustains the most productive waters in the ACC (Moore and Abbott, 2000;Chever et al., 2010), which also enrich surface waters thousands of kilometres downstream of the iron source via lateral advection (Blain et al., 2001;Sokolov and Rintoul, 2007;Mongin et al., 2009). These conditions are thought to facilitate recurrent chlorophyll

blooms in these areas (Boyd, 2002;Sokolov and Rintoul, 2007), driven by nutrient dispersal via upwelling and advection by mesoscale eddies across the ACC (Palter et al., 2010), as well as the eastward flow of the ACC itself (Olbers et al., 2004).

The seasonal cycle of productivity is quite marked in polar regions, largely driven by the variability of light levels (in response to seasonal solar angle or vertical mixing of particulates in the water column or both), iron availability, temperature, and ice cover (Thomalla et al., 2011). Ocean mixed layer depth (MLD) is also an important structure in the upper water column because it defines the quasi-homogeneous surface region significant in determining ocean biology (Polovina et al., 1995); seasonal winds and water temperatures being the main drivers of the MLD (Kara et al., 2003). The MLD deepens following a period of sustained strong winds or surface cooling in winter months. Deeper mixed layers bring more nutrients to the surface, but phytoplankton spends less time near the surface where light for photosynthesis is highest, limiting phytoplankton growth rates (Mitchell et al., 1991;Boyd et al., 2001). High phytoplankton biomass chlorophyll is found in iron-rich waters where the light-mixing regime is favourable (Blain et al., 2001). Indeed, phytoplankton biomass is generally high in the frontal zones during early summer, especially the PF (Moore and Abbott, 2002). These physical controls are critical for initiating the recurrent spring blooms, but are also responsible for the relatively oligotrophic conditions that follow in winter (Behrenfeld and Falkowski, 1997;Garibotti et al., 2005;Thomalla et al., 2011). Consequently, phytoplankton biomass and food web processes vary more seasonally than on daily or annual cycles.

Biological resources in the Southern Ocean also vary in the vertical dimension in both space and time. Deep chlorophyll maxima (DCM) are often found in regions where the concentration of chlorophyll (green pigments found in cells of algae and plants, including phytoplankton) are very low in the upper mixed layer (Holm-Hansen et al., 2005), and decrease to a depth of 200 m, below which the chlorophyll concentration is generally negligible (El-Sayed et al., 1983;Teo et al., 2009). Although chlorophyll can be found below the euphotic zone, it is sometimes assumed that the chlorophyll measured near the surface is indicative phytoplankton distribution in the entire water column (see examples given by Knox, 2007, p. 32). However, stratification of the water column is the major factor determining the distribution of phytoplankton throughout the water column (Mellard et al., 2011). Adaptive features such as diel vertical migration also dictate the distribution of higher-trophic-level groups including zooplankton (Hays, 2003) and mid-trophic fish (Sutton, 2013), as well as their predators (e.g. McIntyre et al., 2010).

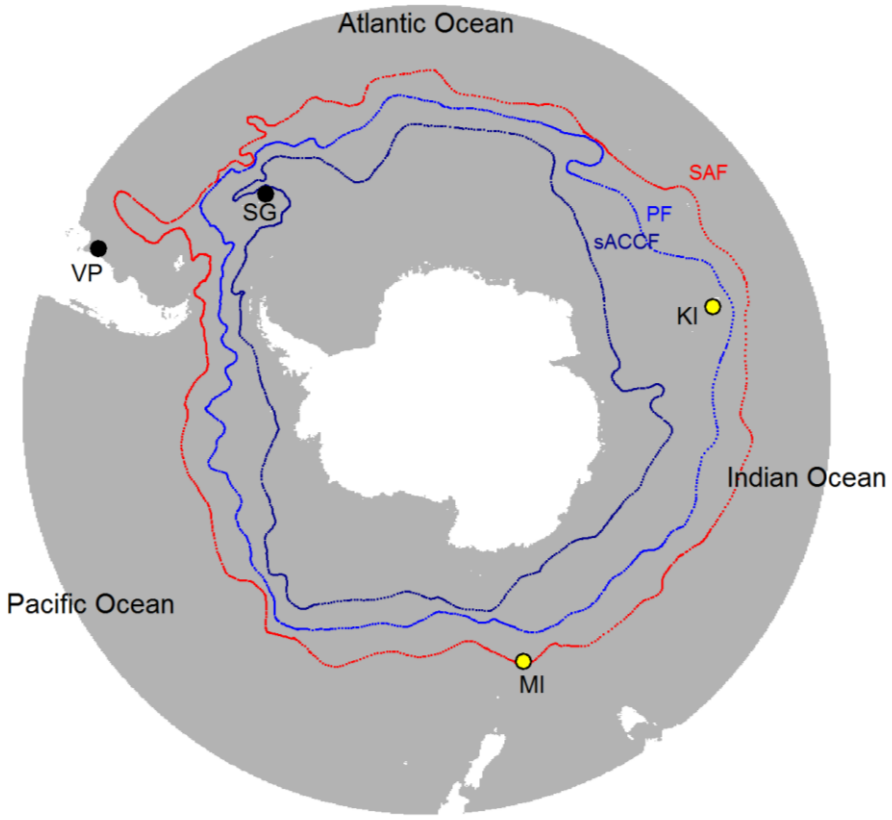

Figure 1.1. The Southern Ocean showing the major ocean basins (Atlantic, Pacific and Indian Ocean sectors) and polar fronts (Sub-Antarctic Front [SAF] – red; Polar Front [PF] – blue; and southern Antarctic Circumpolar Current Front [sACCF] – dark blue), as well as the main breeding islands of southern elephant seals (South Georgia [SG]; Ilse Kerguelen [KI]; Macquarie Island [MI]; and Valdes Peninsula [VP]). Datasets included in this thesis were collected from southern elephant seal breeding populations coloured yellow (*i.e.* Ilse Kerguelen and Macquarie Island).

While the trophic structure of food webs is thought to be an important concept in ecology (Martinez and Lawton, 1995), our ability to model food web dynamics is still rudimentary in many aspects due to limited sampling of biological data and poor food web information (Purves et al., 2013). This is particularly true for open ocean pelagic systems, and even more so at high latitudes, that are remote and difficult to sample and/or observe. Guisan and Thuiller (2005) highlight three main factors that determine biological patterns: (i) the dispersal capacities of species; (ii) the spatial distribution of environmental conditions that favour species' habitat (*e.g.* temperature and solar radiation); and (iii) the biotic environment, including the availability and dynamics of resources. Datasets for (ii) are on broad scales and are becoming increasingly available globally (Turner et al., 2003), whereas datasets

for (iii) tend to have much more fine-scale spatial structures and are limited to detailed field studies due to measurement difficulties over extensive areas (Araújo and Guisan, 2006).

1.4 Analysing animal foraging behaviour and biological conditions simultaneously

For more than 20 years, the development and deployment of electronic tags on marine animals (*e.g.* fish, turtles, seabirds, seals, whales) has provided detailed information on their migration and behaviour in the three-dimensional environment over extensive areas and for long periods of time (Evans et al., 2013). As this technology has evolved, ocean data sensors have been added to these tags, used to measure light (e.g. Teo et al., 2004;Teo et al., 2009;Vacquié-Garcia et al., 2012), temperature and salinity (e.g. Charrassin et al., 2002;Charrassin et al., 2008), and more recently, chlorophyll estimated by fluorometers (Charrassin et al., 2010). While a considerable body of literature exists on the effects of *in situ* physical conditions on marine predators (see review, Costa et al., 2010a), few studies have investigated predator response to *in situ* biological conditions in the water column. The advent of fluorometer from instruments carried by marine animals is now enabling researchers to investigate animal responses to three-dimensional distribution of chlorophyll, though only a few datasets have been collected so far (e.g. Charrassin et al., 2010;Laidre et al., 2010;Guinet et al., 2013).

Prior to the advent of fluorometer sensors on tags, studies commonly used remotely-sensed data, such as ocean colour (*e.g.* Sea-viewing Wide Field-of-view sensor, SeaWiFS; Moderate-resolution Imaging Spectroradiometer, MODIS), to examine potential biological influences on focal animal behaviour and/or distribution (e.g. Jaquet et al., 1996;Guinet et al., 2001;Grémillet et al., 2008;Bestley et al., 2010). The use of satellite-derived ocean colour data as a proxy for phytoplankton concentration has become standard in marine ecology (Chavez et al., 2011). However, there are several fundamental problems with using satellite-derived data, particularly in ecological studies. First, global calibrations of chlorophyll algorithms tend to be poorly correlated with actual values at high latitudes (Johnson et al., 2013). Second, the quantity and quality of ocean colour information obtained by satellites is affected by cloud cover, so that data during the winter months and at high latitudes are often sparse (Sumner et al., 2003), and consequently correspond poorly with marine animal behaviour (Bradshaw et al., 2004). To improve data availability, these patchy satellite data are often aggregated at spatio-temporal scales not necessarily relevant to marine animal behaviour. Third, satellite sensors are unable to provide information at depth, and cannot consider deep chlorophyll maxima (Guinet et al., 2013). Finally, satellite-derived data do not provide

any information on the distribution or abundance of upper-trophic-level groups such as zooplankton or mid-trophic fish. Water column parameters are particularly difficult to quantify, as direct water sampling and/or catch data recorded from ship-based surveys are both costly and logistically difficult to collect (Schofield et al., 2013), and are rarely measured simultaneously with animal behaviour (Day, 2008).

Alternatively, light data recorded by time-depth-light recorders (TDLRs) deployed on marine animals can be used to measure the bio-optical properties of the water column (McCafferty et al., 2004). Although originally developed for geo-location purposes (Hill and Braun, 2001;e.g. Bradshaw et al., 2002;Bost et al., 2009a;Cleeland et al., 2013), this additional, contextual application has led to researchers attempting to quantify different biological aspects of the environment using recorded light data, to either (1) estimate plankton density on the basis of its attenuating effects within the water column (Teo et al., 2009;Jaud et al., 2012), or (2) detect possible encounters with mid-trophic fish that emit bioluminescent light (Campagna et al., 2001;Vacquié-Garcia et al., 2012). Thus, light data collected by marine animals can provide useful indices for biological conditions concurrent with animal movement and behaviour.

1.5 A diving predator: southern elephant seals

Southern elephant seals (*Mirounga leonina*) are long-lived, upper-trophic-level predators with a circumpolar distribution (Laws, 1994) (figure 1.1). Although southern elephant seals have the capacity to travel long distances (e.g. Hindell and McMahon, 2000), there are four genetically-distinct populations comprising the South Georgia, Kerguelen, Macquarie and Valdes Peninsula populations (Slade et al., 1998;Hoelzel et al., 2001) (figure 1.1). As a consequence, each of these populations is thought as a discrete ecological entity (McMahon and Burton, 2005). Over the past 30 years there has been a shift in the focus of research on elephant seals from fundamental biology to primary ecological research such as their foraging ecology, with marine macroecology becoming an important topic for understanding how environmental changes will modify species biogeography (Koubbi et al., 2014). For elephant seals, a considerable body of literature already exists regarding their physical habitat characteristics (Field et al., 2001;Costa et al., 2002;Bailleul et al., 2007;Bailleul et al., 2010b;Dragon et al., 2010;Hindell et al., 2011), but information on preferred biological conditions remains elusive.

The species are deep diving and spends most of its life cycle at sea. While at sea they continuously dive to an average depth of 500 m (sometimes up to 2000 m) (McIntyre et al., 2010;McIntyre et al., 2012) around 60 times per day (Hindell et al., 1991a) to feed predominately on small mesopelagic fish (Cherel et al., 2008) or squid (Newland et al., 2009). As diving predators, elephant seals must return repeatedly to the surface to breathe and can therefore be studied under the framework of central-place foraging (Orians and Pearson, 1979) with the surface acting as the central place (Houston and McNamara, 1985). A major assumption is that central-placed foragers will make a decision so as to maximise the net rate of energy intake during a foraging bout (Charnov, 1976). As central-place foragers, diving predators should increase their energy gain to compensate for travel costs as distances to food increases (Mori, 1998).

Adult female elephant seals perform two foraging trips annually. Following the 3-4 week breeding season on land, most will spend 2 – 3 months (October – December/early January) foraging at sea, before returning to land to moult for one month between December and March (age-dependent) (Hindell et al., 1991a;Hindell et al., 1991b;Stewart and DeLong, 1995). Following the moult, females forage at sea for an extended period (5 – 8 months) to build body reserves for the next breeding season, and migrate to two broad foraging habitats: the inter-frontal zone (between the subtropical front and polar front) or Antarctic zone (between polar and the southern boundary of the Antarctic Circumpolar Current) (Bailleul et al., 2007;Bailleul et al., 2010a;Dragon et al., 2010). Post-breeding migrations coincide with peak primary productivity in late spring through to mid-summer, while post-moulting migrations extend across the entire austral winter when primary productivity is relatively low. Although elephant seals largely target mid-trophic prey (*i.e.* fish and squid), past work has attempted to relate their foraging behaviour to primary productivity estimated from satellite data; though with limited success (Bradshaw et al 2004). More recent work, using data from seal-borne light sensors to estimate phytoplankton concentration, has suggested that phytoplankton may influence seal prey availability in the horizontal and vertical dimension (Jaud et al., 2012;Guinet et al., 2014).

The overall objective of this thesis was to use *in situ* light to estimate biological conditions and relate this to southern elephant seals foraging in an ecological context, using two datasets collected by female southern elephant seals from Macquarie Island and Iles Kerguelen (figure 1.1). Specific aims were to (1) assess the concept of using light to estimate plankton concurrent with animal behaviour; (2) examine broad-scale foraging strategies in response to trans-seasonal plankton distribution; and

(3) use high-resolution data to examine feeding activity in response to scale-dependent plankton densities within a major phytoplankton plume.

1.6 Thesis outline

Each data chapter of the thesis (chapter 2 – 4) was written as an independent manuscript that has either been published, is currently in review, or is in preparation for submission to a scientific journal. Malcolm O'Toole was the primary author for each chapter and was involved in some of the data collection on Iles Kerguelen. He was also responsible for the data analysis, its interpretation and manuscript preparation. However, co-authors helped facilitate the project, collection of data, data analysis and preparation of the manuscripts. These co-authors are listed at the start of each chapter and in the statement of publication and co-authorship.

1.6.1 Chapter 2: estimating water column biomass concurrent with deep diving predator behaviour

In chapter two, light level and depth data collected by elephant seals over a six-year period were used to generate a phytoplankton index that was concurrent with seal movements and behaviour. This work aimed to demonstrate that a light-based index was consistent with typical trans-seasonal satellite-derived chlorophyll-a patterns, and examine the efficacy of using a light-based index to estimate phytoplankton distribution. This was an essential first step, as analysis in the following chapters relied on its outcome.

1.6.2 Chapter 3: predator response to seasonal variability in plankton

Little is known about the links between marine predators and ocean productivity, specifically, how plankton density influences their foraging behaviour. In chapter three, elephant seal post-breeding (summer) and post-moult (winter) foraging trips provided year-round data that allowed an investigation into the relationship between plankton density and seal foraging behaviour at sea. Due to distinct biological change between the summer bloom period and the winter post-bloom period, I expected fundamental differences in seal foraging strategy in relation to seasonal plankton density (indicative of a change in the seal prey field distribution).

1.6.3 Chapter 4: making the link between a predator and plankton in a recurrent phytoplankton plume

In chapter four, light-depth data collected by elephant seals was not only used to estimate plankton density, but also bioluminescent prey encountered by the seal. In addition, seals were equipped with accelerometers to measure lunge activity, which was used to detect prey encounter events. These data provided a unique opportunity to conduct multi-scale analyses (meso- and dive-scale) of seal feeding response to different biological conditions within a major recurrent phytoplankton plume downstream of the Kerguelen Plateau. The primary aims were to propose (1) the dynamic structure of the plume ecosystem and (2) an underlying function of the plankton influence on seal foraging behaviour.

1.6.4 Chapter 5: general discussion

In the final chapter, the thesis concludes with a general discussion that synthesises trans-seasonal and season-specific differences in the foraging behaviour of southern elephant seals in response to biological conditions encountered in the water column. A summary of how seals likely use biophysical features of the Southern Ocean to locate and detect prey at different times of the year is provided. Results are discussed in relation to foraging plasticity in highly variable and changing environments. The advantages and shortcomings of light as an index for quantifying biological conditions in the water column are also discussed.

Chapter 2: Estimating trans-seasonal variability in water column biomass for a highly migratory, deep diving predator

Published as: O'Toole, M.D., Lea, M.-A., Guinet, C., and Hindell, M.A. (2014). Estimating Trans-Seasonal Variability in Water Column Biomass for a Highly Migratory, Deep Diving Predator. *Plos One* 9, e113171. doi: 10.1371/journal.pone.0113171.

2.1 Abstract

The deployment of animal-borne electronic tags is revolutionizing our understanding of how pelagic species respond to their environment, by providing *in situ* oceanographic information such as temperature, salinity, and light measurements. These tags, deployed on pelagic animals, provide data that can be used to study the ecological context of their foraging behaviour and surrounding environment. Satellite-derived measures of ocean colour reveal temporal and spatial variability of surface chlorophyll-a (a useful proxy for phytoplankton distribution). However this information can be patchy in space and time resulting in poor correspondence with marine animal behaviour. Alternatively, light data collected by animal-borne tag sensors can be used to estimate chlorophyll-a distribution. Here, we use light level and depth data to generate a phytoplankton index that matches daily seal movements. Time-depth-light recorders (TDLRs) were deployed on 89 southern elephant seals (*Mirounga leonina*) over a period of 6 years (1999 – 2005). TDLR data were used to calculate integrated light attenuation of the top 250 m of the water column (LA_{250}), which provided an index of phytoplankton density at the daily scale that was concurrent with the movement and behaviour of seals throughout their entire foraging trip. These index values were consistent with typical seasonal *chl-a* patterns as measured from 8-day Sea-viewing Wide Field-of-view Sensor (SeaWiFS) images. The availability of data recorded by the TDLRs was far greater than concurrent remotely sensed *chl-a* at higher latitudes and during winter months. Improving the spatial and temporal availability of phytoplankton information concurrent with animal behaviour has ecological implications for understanding the movement of deep diving predators in relation to lower trophic levels in the Southern Ocean. Light attenuation profiles recorded by animal-borne electronic tags can be used more broadly and routinely to estimate lower trophic distribution at sea in relation to deep diving predator foraging behaviour.

2.2 Introduction

Chlorophyll-a is an important biological parameter in the Southern Ocean and is considered a useful indicator of spatial and temporal variability of primary productivity (Smith and Baker, 1978;Behrenfeld and Falkowski, 1997;Arrigo et al., 2008). To understand the foraging behaviour and habitat utilisation of higher trophic organisms requires knowledge of lower trophic dynamics, coupled with information on how organisms respond to these changes. Indeed, satellite measurements of ocean colour have revealed the complex temporal and spatial variability of weighted average near-surface chlorophyll-a concentration (Moore and Abbott, 2002), but the

quantity and quality of information obtained in this way is affected by cloud cover. Consequently, information from high latitudes and during the winter months is often sparse (Sumner et al., 2003;Bradshaw et al., 2004) and correspond poorly with marine animal behaviour. Moreover, to improve data availability, these patchy satellite data are often merged at spatio-temporal scales not necessarily relevant to marine animal behaviour. While fluorometers and water samples from ship-based surveys are the only *in-vivo* and *in-vitro* measurements to determine chlorophyll-a concentration, it is both costly and logistically difficult if collecting simultaneously with animal behaviour. In recent years, additional ocean data recorded by animal-borne electronic tags have been used to supplement other data from buoys and satellites (e.g. Charrassin et al., 2008;Fedak, 2013) and have improved our understanding of the relationship between marine predator distribution and environmental parameters, including chlorophyll-a (Biuw et al., 2007;Teo et al., 2009). Indeed, miniaturised fluorometers have now been deployed, in some instances simultaneously with light sensors, on elephant seals to estimate chlorophyll-a in the water column (Jaud et al., 2012;Guinet et al., 2013) but are costly and available data are scarce. Therefore, understanding lower trophic variability (*i.e.* phytoplankton) and its influence on marine predators in the Southern Ocean is still hampered by a lack of concurrent data.

Time-depth-light recorders (TDLRs) provide detailed information on dive behaviour of a wide range of animals over extensive areas (Boyd and Croxall, 1996;Hindell et al., 2010), and are often coupled with sensors that record environmental data (*e.g.* temperature and salinity). Southern elephant seals (*Mirounga leonina*) are ideal platforms for these oceanographic sensors due to their circumpolar distribution extensive foraging across the Southern Ocean (Biuw et al., 2007). They are also a deep diving animals, diving up to 2000 m (McIntyre et al., 2012) while performing on average 60 dives per day (Hindell et al., 1991a). Elephant seals can be used to measure *in situ* environmental conditions and provide important habitat information for the seals (Biuw et al., 2007). Seals equipped with sensors that collect information such as temperature, salinity can cover areas not sampled by conventional techniques (*e.g.* ship-based survey, satellite images), including within the sea-ice zone (*i.e.* south of 60°S) where it is particularly difficult to sample physical parameters of the ocean (Charrassin et al., 2008). Furthermore, post-moult elephant seals are also at sea throughout winter when data collected by conventional techniques is scarce.

Light levels recorded by animal-borne sensors are commonly used to infer day length as a means of estimating geographical position (Delong, 1992;Sumner et al., 2009), and can also be used as means of recording light levels at depth during animal diving (Campagna et al., 2001;McCafferty et al.,

2004;Vacquié-Garcia et al., 2012). Experiments have demonstrated the concept of estimating chlorophyll-a distribution from light-depth data compared to fluorescence (e.g. Teo et al., 2009;Jaud et al., 2012). Fluorometers estimate chlorophyll-a by measuring its fluorescence intensity. Light sensors instead measures ambient light, which is attenuated throughout the water column for two reasons: (1) physical properties of the seawater and (2) quantity of inorganic and organic particles suspended (or dissolved) in the water column (Morel and Maritorena, 2001). The Southern Ocean is typically characterised by Case I waters, whereby phytoplankton comprises the main source of particles suspended within the euphotic zone (Morel and Prieur, 1977;Morel and Maritorena, 2001), and is consequently the main cause of light attenuation if we assume related coloured dissolved organic matter (CDOM) and detritus degradation products covary with phytoplankton (Bricaud et al., 1981) and physical properties are constant(Bricaud et al., 1998). Indeed, it was Smith and Baker (1978) that introduced the concept of measuring the bio-optical properties of the water column to estimate the concentration of chlorophyll-a in the ocean. A study by Teo et al. (2009), one of the first to use light levels collected by Pacific blue fin tuna (*Thunnus orientalis*) to estimate chlorophyll-a distribution, found a positive relationship between light attenuation at depth and *in situ* chlorophyll-a collected by both water samples and fluorometers. Light levels collected by elephant seals equipped with light sensors were also strongly correlated with concurrent *in situ* fluorometer data (Jaud et al., 2012). Despite their findings, these studies were not performed over multiple seasons; instead tested over a much shorter time scale. Nor was light attenuation compared with satellite-derived chlorophyll-a estimates (hereafter *chl-a*). More recently, Guinet et al. (2013) used a multi-seasonal dataset over several years and found *chl-a* to be related to surface chlorophyll-a estimates from seal-borne fluorometers. The bio-optical relationship between chlorophyll-a and phytoplankton and does vary according to phytoplankton taxonomic composition (Stramski et al., 2001) but are still considered to correlate well with each other. To our knowledge, no study has used light level and depth data to generate a phytoplankton index that matches daily seal movements while at sea.

This study examined the feasibility of using light collected from TDLRs to calculate an index of phytoplankton distribution that is concurrent with marine animal behaviour in the Southern Ocean. We also highlight the advantages of a phytoplankton index recorded simultaneously with the foraging behaviour of a top marine predator, particularly at times of the year where *chl-a* data is lacking. Analyses were performed in Case 1 waters over multiple seasons between 1999 and 2005. Our primary objectives included:

(i) providing an index of phytoplankton density at the daily scale that is concurrent with the movement and behaviour of seals throughout their entire foraging trip;

(ii) demonstrating that our index is consistent with typical seasonal chl-a patterns;

(iii) examining the efficacy of using a light-based index to estimate phytoplankton distribution.

2.3 Materials and methods

2.3.1 Ethics statement

All necessary permits were obtained for the described field studies. Elephant seal research was sanctioned by the University of Tasmania Animal Ethics Committee (permit A6738) and the Australian Antarctic Science Advisory Council Ethics Committee (project 2794). Permits and permission to carry out research on Macquarie Island was obtained from Parks and Wildlife Service Tasmania.

TDLRs (Mk6, Mk7, Mk8 and Mk9; Wildlife Computers, Redmond, WA, USA) were attached to both post-breeding and post-moult adult female southern elephant seals (n=89) at Macquarie Island (54°35´S, 158°58´E, Table 2.1) from 1999 to 2005. The seals were approached by foot and temporarily restrained with a head bag and anaesthetised intravenously with a 1:1 mixture of tiletamine and zolazepam (0.5 mg kg^{-1}) (McMahon et al., 2000;Field et al., 2002). TDLRs were attached to the pelage above the shoulders using a two component industrial epoxy (Araldite AW 2101) (Hindell and Slip, 1997). Seals were observed during recovery from anaesthesia and allowed to enter the water when no longer sedated. TDLRs were retrieved at the end of the foraging trip once the seal had hauled out on land by repeating the above restraint procedures. These tracking devices or attachment method did not adversely affect individual performance and fitness over the short (seal growth) or long (seal survival) term (McMahon et al., 2008).

2.3.2 Tag data

TDLRs measured time, depth and light at 30 s intervals for the duration of each foraging trip. Mk6 – Mk8 tags used uncorrected watch crystals to measure time. They were offset to spread the time error (TE) over the likely range of seawater temperatures (T) ($TE = (1x10^{-5} – 3.5x10^{-8} x (T – 25)^2) x 10^6$ µs). Mk9 tags used a temperature correction algorithm to keep the time error within 1 ppm. Depth measurements were made by a pressure transducer calibrated by the manufacturer (± 6 m). Light

values are converted on-board the logger via a log treatment (see appendix S2.7.1) to compress the light measurements to a three digit value, thereby giving a linear relationship and increase the resolution at lower light levels. The light sensor data can be used to identify dawn/dusk events down to 300 m in clear waters and is temperature-compensated for the entire light level range (Wildlife Computers). The wavelength at the centre of the light sensor parabolic-shaped pass-band filter is ~430 nm and consequently the sensor only reads the violet/blue light band (370 nm – 470 nm). All other bands of light are rejected and not measured. The light sensor measures on a scale of 20 readings per decade, so the light level error is considered to be $1/20^{th}$ of a decade. Tags also recorded temperature (± 0.1°C). The lag in temperature measurement (inherent in the design of the TDLRs) was accounted for (see Boyd et al., 1999;Bradshaw et al., 2002).

2.3.3 Data extraction

Twice daily at-sea location estimates were derived from the recorded light levels for sunrise and sunset using the geo-location procedure outlined inThums et al. (2008b). Geo-location by light enables animal movement estimation, based on measurements of light intensity over time recorded by the in-built light sensor of each TDLR (Sumner et al., 2009). However, an inherent problem with this approach is that an array of factors may change the natural light intensity pattern, thereby affecting the accuracy and precision of location estimates calculated from these light patterns (Hill, 1994;Hill and Braun, 2001;Ekstrom, 2004). With the incorporation of the 'tripEstimation' method (see Sumner et al., 2009) geo-location mean longitudinal and latitudinal error is shown to be estimated at ~57 ± 9 km (*i.e.* 0.83°) and ~54 ± 8 km (*i.e.* 0.49°) respectively (Chew unpublished). All dive recorders were corrected for drift in the pressure sensor using a customised zero-offset correction routine. We then identified individual dive cycles, defined as the first sub-surface record until the last surface interval of the subsequent post-dive surface interval below 10 m. The surface interval encompassed depth values between 0 and 10 m. This tolerance accounted for subsurface movements of seals between dives.

Table 2.1.Summary of tag deployments for 89 female elephant seals: year, trip, tag type used, number of individuals tagged, and period of data records (start to finish dates). *PB* - post-breeding, *PM* - post-moult.

				Period of data records	
Year	**Trip**	**Tag type**	**No. individuals**	**Start**	**Finish**
1999	PB	mk6	4	23-Oct-1999	12-Jan-2000
1999	PB	mk7	15	15-Oct-1999	17-Jun-2000
2000	PM	mk7	9	26-Jan-2000	15-Oct-2000
2000	PB	mk7	11	21-Oct-2000	14-Jun-2001
2001	PM	mk7	3	9-Feb-2001	3-Oct-2001
2001	PM	mk8	3	15-Jan-2001	13-Oct-2001
2002	PM	mk7	3	30-Jan-2002	22-Sep-2002
2002	PM	mk8	12	26-Jul-2001	7-Nov-2002
2004	PM	mk8	12	30-Jan-2004	19-Oct-2004
2004	PB	mk8	7	18-Oct-2004	31-Jan-2005
2004	PM	mk9	3	24-Jan-2004	15-Dec-2004
2004	PB	mk9	2	22-Oct-2004	5-May-2005
2005	PM	mk8	3	11-Jan-2005	13-Oct-2005
2005	PM	mk9	2	19-Jan-2005	15-Oct-2005

2.3.4 Environmental data

2.3.4.1 Satellite-derived chlorophyll-a estimates

The *chl-a* data (mg m^{-3}) was estimated from Sea-viewing Wide Field-of-view Sensor (SeaWiFS) images (McClain et al., 1998). Because of the patchy nature of these data at high latitudes, particularly during winter, we used 8-day *chl-a* composites at 0.1° resolution (http://oceancolor.gsfc.nasa.gov/).

2.3.4.2 Sea ice

We extracted sea ice data from daily satellite images (grid cell size of 25 km x 25 km) (Cavalieri et al., 2012, updated yearly). Satellite *chl-a* data in regions with >20% sea ice coverage were excluded from analyses as reflective irradiance from the ice may affect the accuracy of satellite imagery (P. Strutton, Personal Communication). Sea ice data were also used to calculate the seasonal mean sea ice extent between 1999 and 2005. The sea ice extent was defined by the open ocean (*i.e.* ice-free pelagic region) – sea ice (> 50% concentration) interface.

2.3.4.3 Bathymetry

We aggregated bathymetry data, derived from the ETOPO2 bathymetry data set at 2' resolution (http://www.ngdc.noaa.gov/mgg/global/global-.html), to calculate mean bathymetric depth of each 1° x 1° grid cell associated with each seal location.

2.3.5 Mixed layer

In order to assess changes to phytoplankton density using integrated light attenuation we consider total phytoplankton in the water column, the bulk of which is found within the mixed layer (de Baar et al., 2005). Temperature and profiles recorded by the TDLRs were used to identify the mixed layer depth (hereafter MLD) for each dive to establish the vertical extent of phytoplankton in the water column. A custom broken stick method was used to find the greatest inflection point along each temperature-depth profile to a depth of 350 m (limit of light sensor sensitivity is ~300 m). The inflection point was considered the MLD if the difference between temperature at the surface (~10 m) and temperature inflection point was greater than 0.2°C (Thomalla et al., 2011).

The same procedure was applied to light profiles, also recorded by the TDLRs, to identify the depth of the most significant light inflection point for each dive. It is important to note consistent light-depth profile differences between the descent and ascent phase of each dive (figure 2.1), owing to a time-response lag inherent in the light sensor that is greatest at low light levels (Wildlife Computers), as well as possible changes in water properties, surface irradiance and animal behaviour. We calculated the average depth of the most significant light inflection point for each dive to account for this bias. From the surface to the depth of the most significant light inflection point was considered the section of the water column that incorporated the bulk of phytoplankton.

These analyses showed the proportion of dives with a given temperature and light inflection depth closely corresponds with each other (figure 2.2). According to these results we conclude that the mixed layer depth and bulk of phytoplankton were frequently above 250 m (82.6% and 74.3% of dives respectively), and fewer dives encountered mixed layer depths or the bulk of phytoplankton exceeding 300 m (17.4% and 25.7%) (figure 2.2).

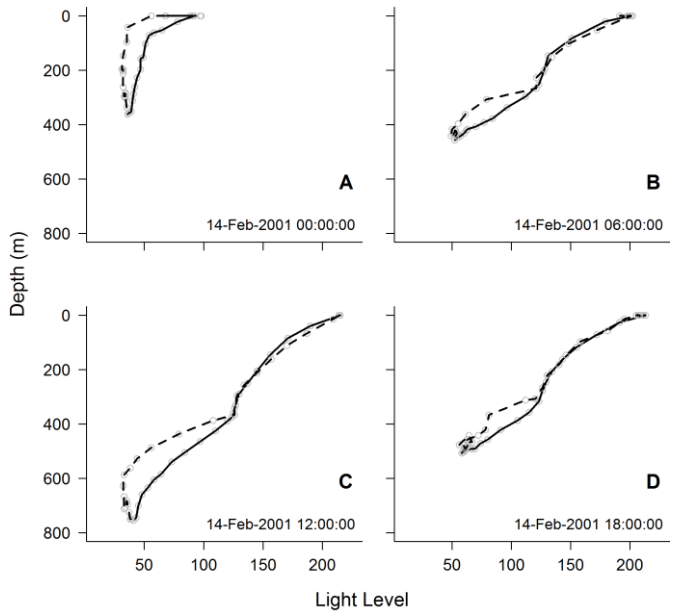

Figure 2.1. Examples of light-depth profiles collected from the descent (solid) and ascent (dashed) phases of dives. Profiles recorded at local (A) midnight, (B) 6am, (C) noon and (D) 6pm on 14 February 2001. Light level values are related to blue light intensity (W cm^{-2}). Calibrations are checked at levels 10^{-5}, 10^{-7} and 10^{-9} W cm^{-2}, which correlated to light level values around 150, 110 and 70 respectively (see appendix S2.7.1).

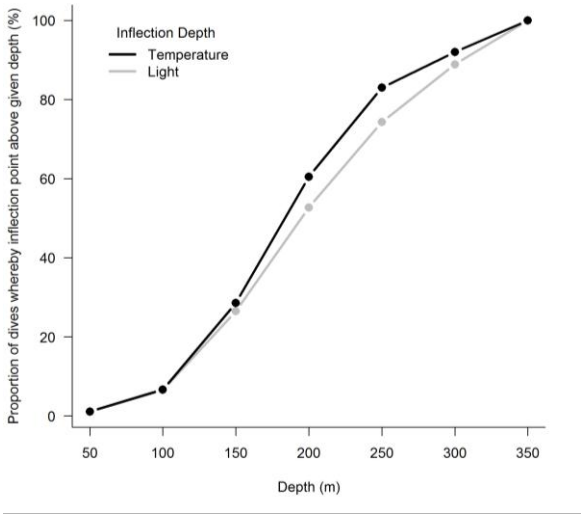

Figure 2.2. Proportion of dives whereby greatest temperature and light inflection points are above a given depth.

2.3.6 Frontal zones

Frontal structures in the Southern Ocean are sharp, horizontal gradients in water properties that mark the boundaries between different frontal zones (FZ) (figure 2.3– represented by historical mean front positions). The general position for each front can be marked using representative values of temperature and salinity at approximately 200 m depth. The FZ occupied by the seal was identified by water temperatures at 200 m depth (T_{200}), as indicated by Park et al. (1998) and Orsi et al. (1995). The sub-Antarctic Front (SAF) limit was defined by sub-surface values of 7°C, the Polar Front (PF) was defined by the northern limit of 2.8°C, and the Southern Antarctic Circumpolar Current Front (SACCF) was defined by a temperature of 1.6°C (Guinet et al., 2014). In this study we use these subsurface boundaries to distinguish between three major FZ: the Polar Frontal Zone (PFZ) was where seals encountered temperatures greater than 2.8°C; north of the southern Antarctic Circumpolar Current Front (SACCF-N) was where seals encountered temperatures between 2.8°C and 1.6°C; and south of the SACCF (SACCF-S) was where seals encountered temperatures below 1.6°C.

Temperature recorded for both the descent and ascent phase of individual dives were used and a temperature value at 200 m (T_{200}) was derived for both the descent and ascent phase of each dive using a linear interpolation between the non-regular series of depths and temperature. Temperature values from the two phases were averaged. Because we only retained local noon light

attenuation values for our analyses only local noon temperature estimates were used to calculate the mean daily noon T_{200}. Each daily noon light level profile was assigned to a given FZ based on these mean daily noon T_{200} values (appendix S2.7.2 – figure S2.7.2).

2.3.7 Light attenuation

By examining the mixed-layer depths and light-depth profiles encountered by the seals we determined that the bulk of phytoplankton was likely found in the top 250 m of the water column (see mixed layer section). Moreover, light levels recorded at depths of 300 m or more become unreliable as the light sensors reach their sensitivity limit. Consequently, integrated light attenuation between the surface and a depth of 250 m (LA_{250}) was used as an index of phytoplankton in the water column (based on the assumptions outlined in our introduction).

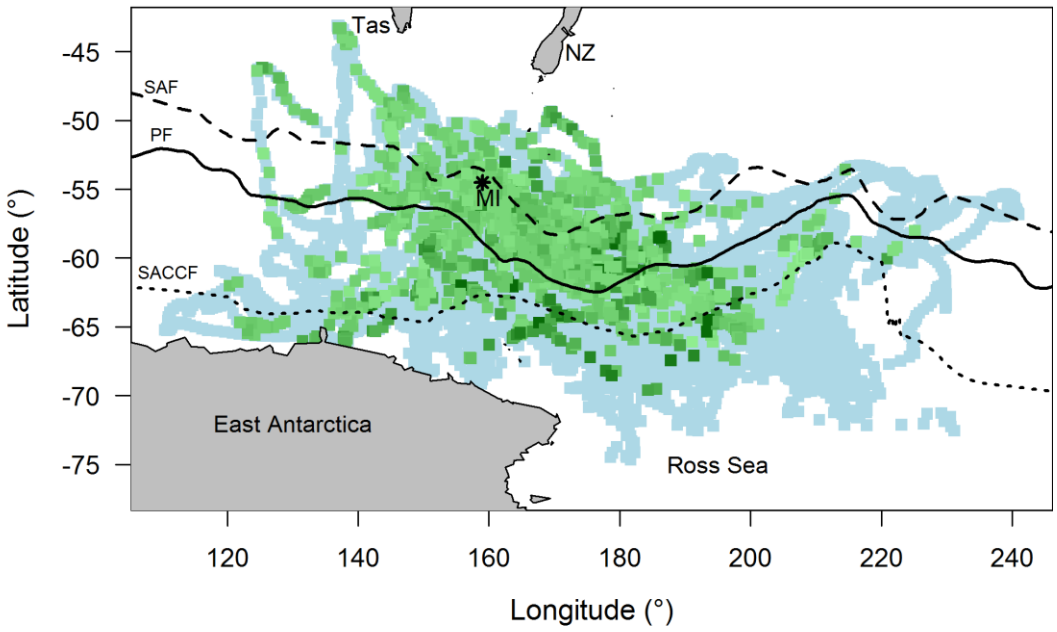

Figure 2.3. Noon locations for all seals with and without concurrent *chl-a*. Includes locations during post-moult and post-breeding foraging trips collectively (light blue), and of these, all that correspond with *chl-a* (green). Scale of *chl-a* values denoted by grading from light green (0.03 mg m^{-3}) to dark green (2.48 mg m^{-3}). Map shows the bottom of Tasmania (Tas) and New Zealand (NZ) and the coast of East Antarctica and Ross Sea (bottom). The black asterisk shows Macquarie Island (MI). Lines represent the historical mean positions of the Sub-Antarctic Front (SAF - dashed), Polar Front (PF - solid) and Southern Antarctic Circumpolar Current Front (SACCF - dotted).

To calculate LA_{250}, light data were first interpolated linearly between the non-regular series of depths to estimate light levels at 250 m for each dive (LL_{250}). We used light levels recorded for both the descent and ascent phase due to sensor and measurement error (see mixed layer section). The surface light level for each dive was estimated from the mean sub-surface light levels in the top 10 m of the water column at the end of the ascent phase (LL_0) (Jaud et al., 2012). Light levels above the surface (indicated by the wet/dry sensor on the tag) were excluded from LL_0 estimates. For each dive, LL_{250} was subtracted from LL_0 and divided by the depth (z) of LL_{250} (*i.e.* 250 m) to calculate the LA_{250} (m^{-1}):

$$LA_{250} = \frac{LL_0 - LL_{250}}{z}$$

Only LA_{250} values 1h either side of local noon (1100-1300) were used in order to minimise variability in the ambient light field (see discussion in Teo et al., 2009). The interpolation of geo-locations was done to attempt best correspondence with noon dives and *chl-a* (see maps – appendix S2.7.2). This was based on the assumption that the seals' trajectory between consecutive locations was straight. Data recorded 1h either side of local noon encompassed, on average, 4.3±1.3 light profiles per seal per day. Since we assume Southern Ocean waters are Case-1, attenuation will be dominated by phytoplankton (see introduction for details).

2.3.8 Statistical analysis

As part of this study we aimed to demonstrate that LA_{250} values (our phytoplankton index) are consistent with typical seasonal *chl-a* patterns. However, spatial error associated with positions derived by geo-location (Sumner et al., 2009) impart uncertainty in the true position of the recorded light attenuation. If then compared to *chl-a* values, for which the spatial errors were considerably less, any resulting correlation may be subsequently weakened. We attempt to account for spatial bias in geo-location position errors by spatial averaging of the data into 1° x 1° grid cells. Grid cells with less than 3 dive profiles were excluded from the analysis as these were likely to give unreliable estimates of the resulting mean LA_{250} and mean *chl-a* per grid cell. Moreover, *chl-a* data were sparse at high latitudes (> 64°S) and during winter months due to elevated cloud cover (Table 2.2).

Conversely, the seal light data were sparse at low latitudes (< 52°S) as few seals travelled north of this region (Table 2.2). Focal analysis was therefore based on data collected between 52°S and 64°S,

and excluded winter months; for two reasons: (i) it is not possible to establish interaction effects when there are missing data in the dataset; and (ii) low data frequency may result in interaction effect bias.

We investigated the relationship between *chl-a* and LA_{250} aggregated at 1° resolution. We used the mixed effect model (*nlme*) package in R (Pinheiro et al., 2012a) to assess this relationship with and without the random intercept term and slope effect to determine whether individual seals were contributing to the model fit. Season and latitude (and their interaction terms) were included in our analysis because of their likely effect on phytoplankton abundance in the water column (for details see discussion). Season was divided according to the austral seasonal cycle: summer (Dec – Feb); autumn (Mar – May); winter (Jun – Aug); and spring (Sep – Nov). Because FZ is largely influenced by latitude in the Southern Ocean (e.g. Field et al., 2001;Bost et al., 2009a) we expect the inclusion of FZ and latitude in our mixed model to have a confounding effect on *chl-a* distribution. For that reason we assessed the inclusion of each of these effects in our mixed model relative to each other and found that latitude was more useful for the purpose of this study (see appendix S2.7.2 – Table S2.7.2). We therefore tested the individual fixed effects (including LA_{250}, season, latitude and their interactions) by sequentially removing non-significant terms from the model according to Zuur et al. (2009). In all cases, models were ranked via Akaike Information Criterion (Burnham and Anderson, 2002), the most parsimonious model having the lowest AIC value. Model selection was carried out using Maximum Likelihood (ML) estimation. In addition, we used *F* and *t* statistics to examine the significance of individual fixed effects. The final model is presented using restricted maximum likelihood (REML) methods. Both *chl-a* and LA_{250} values were log-transformed to ensure a normal distribution.

2.4 Results

We used data from entire foraging trips for 67 (75%) of the 89 deployments (31 post-breeding/ 36 post-moult trips). Twenty one trips were excluded due to light sensor failure at some point during the time at sea. Data for one seal were also omitted due to unrealistic track estimates (*i.e.* the track passed over land). Data were obtained over 1561 days from 22 Oct 1999 through to 8 Oct 2005. A total of 31614 light profiles at 9552 noon locations were recorded during this period (Table 2.3). There were 7212 noon locations available that included 3 or more light profiles (*i.e.* LA_{250} values) and did not coincide with heavy sea-ice, of which only 1461 noon locations coincided with *chl-a* values (20.3%) (table 2.3, figure 2.3). This showed approximately one-fifth of seal locations (with daily LA_{250}

values) coincided with *chl-a* values. Filtered data (*i.e.* included 3 or more light profiles, did not coincide with heavy sea-ice) were then gridded into 3940 1° x 1° cells for model analysis, of which only 1066 cells (25.1%) corresponded with gridded *chl-a* data (Table 2.3). Each cell incorporated 1.26±0.02 locations (4.77±0.09 light profiles). Seals travelled either to the sea ice zone in the north of the Ross Sea and off the coast of East Antarctica, or to the shelf break of East Antarctica (figure 2.3). Most seals travelled to areas south of the SACCF.

2.4.1 Relationship between light attenuation and chl-a

The best model relating LA_{250} to *chl-a* included individual variability (random intercept term *seal*), the random slope term (LA_{250}); most parsimonious model included fixed effects LA_{250}, season, latitude, and the 2-way interaction terms LA_{250} : latitude and latitude : season (table 2.4). The LA_{250} was positively related to *chl-a* (estimated coefficient = 0.76 ± 0.13, $p < 0.0001$, table 2.5, figure 2.4). Predicted *chl-a* values from our model show no obvious latitudinal or longitudinal error pattern over the study region (figure 2.5A, B). However, results indicated that predicted *chl-a* values largely overestimated *chl-a* by 10-30%, particularly over water depths greater than 4000 m, those most frequented by seals (figure 2.5C).

Table 2.2. Frequency of daily locations for each season by 1° latitudinal bins.

	Season			
Latitude (°S)	**Autumn**	**Spring**	**Summer**	**Winter**
44	-	-	-	6
45	-	-	-	4
47	4	-	-	1
48	1	-	-	2
49	1	4	-	1
50	2	7	3	1
51	1	8	5	6
52	3	6	8	2
53	5	10	5	-
54	2	18	11	-
55	4	63	38	-
56	6	72	44	1
57	3	51	50	-
58	12	41	43	-
59	14	21	53	-
60	21	27	46	-
61	22	26	47	-
62	27	17	40	-
63	24	12	27	-
64	33	2	15	-
65	40	-	13	-
66	28	-	14	-
67	10	-	4	-
68	5	-	-	-
69	3	-	-	-
70	2	-	-	-

Table 2.3. Data summary for each deployment (*i.e.* trip) by year: number of seals (*n*); total light profiles and locations at noon and concurrent *chl-a*; filtered[†] light profiles and locations at noon and concurrent *chl-a*; number of 1° grid cell locations and concurrent *chl-a*.

			Total			**Filtered[†]**			**Grid Cells**	
Year	**Trip**	**Seals (n)**	**Light profiles**	**Locations**	**Concurrent *chl-a***	**Light profiles**	**Locations**	**Concurrent *chl-a***	**Locations**	**Concurrent *chl-a***
1999	PB	14	4319	984	307	4096	939	306	514	207
2000	PB	10	2954	713	167	2805	681	165	365	115
2001	PB	-	-	-	-	-	-	-	-	-
2002	PB	-	-	-	-	-	-	-	-	-
2004	PB	7	1733	433	180	1644	415	177	255	129
2005	PB	-	-	-	-	-	-	-	-	-
		31	*9006*	*2130*	*654*	*8545*	*2035*	*648*	*1134*	*451*
1999	PM	-	-	-	-	-	-	-	-	-
2000	PM	6	4120	1328	113	3385	1051	111	544	89
2001	PM	5	3091	951	93	2659	808	85	433	69
2002	PM	10	6199	2001	269	4241	1262	254	689	188
2004	PM	11	6832	2292	297	5034	1632	283	892	205
2005	PM	4	2366	850	81	1312	424	80	248	64
		36	*22608*	*7422*	*853*	*16631*	*5177*	*813*	*2806*	*615*
	Total	**67**	**31614**	**9552**	**1507**	**25176**	**7212**	**1461**	**3940**	**1066**
	%	**-**	**-**	**-**	**15.8**		**-**	**20.3**	**-**	**27.1**

[†]locations with > 3 light profiles that do not coincide with heavy sea-ice

Table 2.4. Ranked mixed models. The *chl-a* explained by light attenuation at 250 m (LA_{250}), season (S) and latitude (lat) (*n*=67 seals). Mixed models are ranked by decreasing Akaike's Information Criterion (AIC) and change in AIC (ΔAIC). The most parsimonious model is in bold.

Candidate models	***df***	**AIC**	**ΔAIC**	**logLik**
LA_{250} + lat + S + LA_{250} : lat + S : lat	**12**	**547.8**	**0**	**-261.9**
LA_{250} + lat + S + S : lat	11	550.7	2.9	-264.3
LA_{250} + lat + S + LA_{250} : S + LA_{250} : lat + S : lat	14	551.7	4	-261.9
LA_{250} + lat + S + LA_{250} : S + S : lat	13	553.9	6.2	-264
LA_{250} + lat + S + LA_{250} : S + LA_{250} : lat + S : lat + LA_{250} : S : lat	16	554.2	6.5	-261.1
LA_{250} + lat + S + LA_{250} : lat	10	554.5	6.7	-267.2
LA_{250} + lat + S	9	557.1	9.3	-269.5
LA_{250} + lat + S + LA_{250} : S + LA_{250} : lat	12	558.5	10.7	-267.2
LA_{250} + lat + S + LA_{250} : S	11	560.3	12.5	-269.1
LA_{250} + S	8	568.1	20.4	-276.1
LA_{250}	6	662	114.2	-325
LA_{250} + lat	7	662.7	115	-324.4
S + lat	6	664.8	117.1	-326.4
S	5	685.2	137.5	-337.6
Lat	4	787.1	239.3	-389.5
~ 1	3	794.5	246.7	-394.2

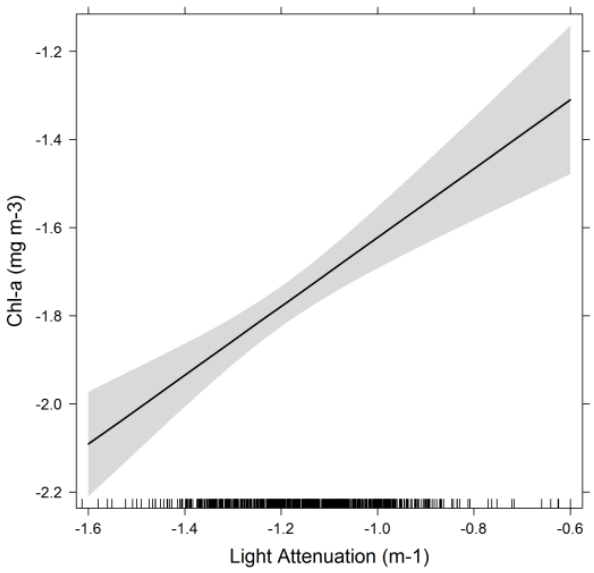

Figure 2.4. Relationship between *chl-a* and light attenuation (LA_{250}) from our mixed model. Shaded area indicates the confidence level. Both axes are log transformed.

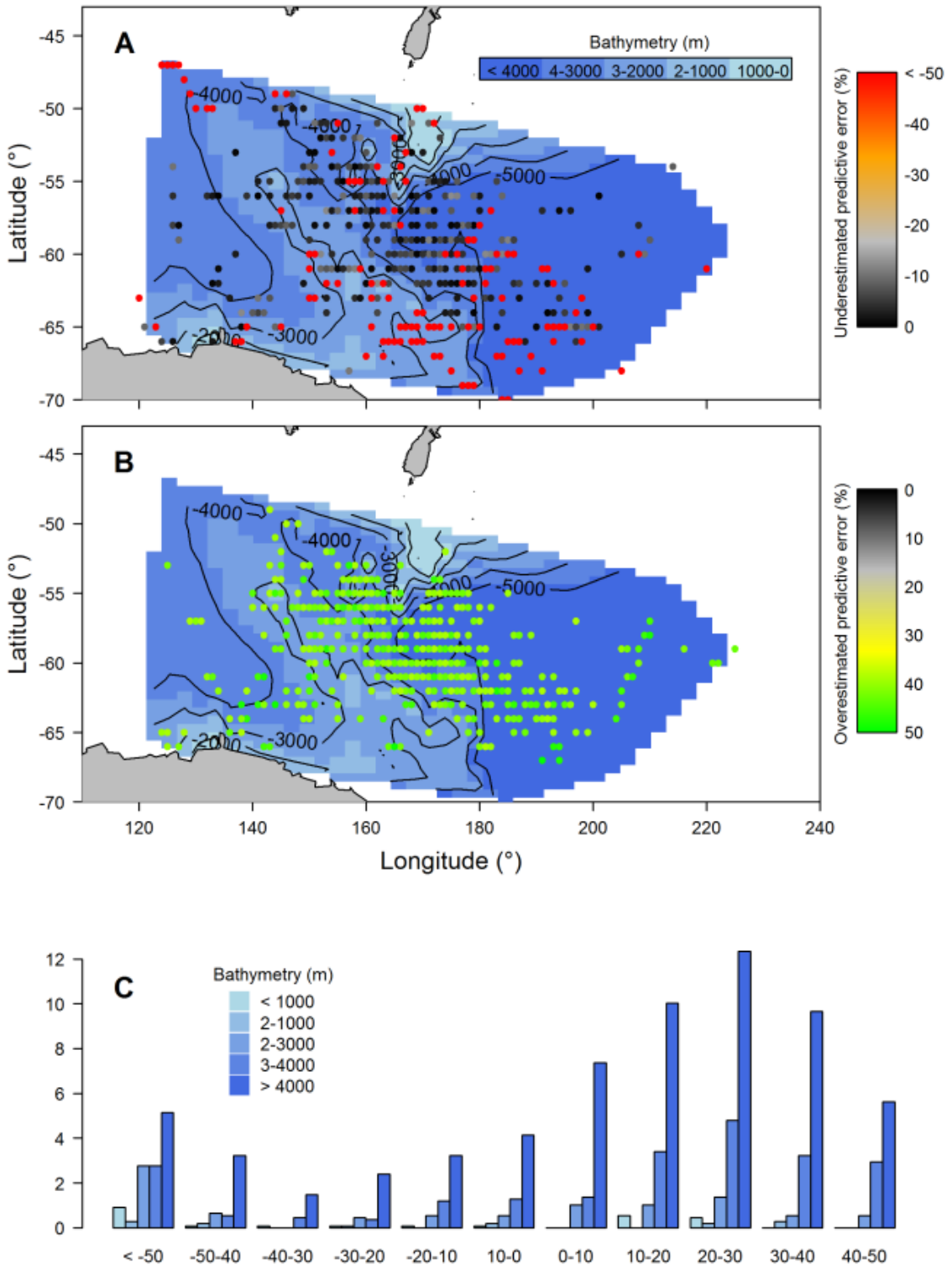

Figure 2.5. Spatial distribution of predictive chlorophyll-a error from our mixed model. Plots show locations associated with (A) underestimated predictive error (%), (B) overestimated predictive error (%), and (C) proportion (%) of locations with associated predictive error (%) in relation to bathymetric bands.

2.4.2 Distribution of light-based chl-a estimates

Fitted values from the mixed model results (*i.e.* phytoplankton index) were used to calculate the spatial distribution of light-based *chl-a* collected by TDLRs (hereafter $TDLR_{chl}$) encountered by the focal seals (figure 2.6A), revealing different seasonal patterns in relation to latitude (figure 2.6B). During summer months, seals encountered generally higher $TDLR_{chl}$ compared to other times of the year, particularly at latitudes between 60°S and 65°S, south-east of Macquarie Island (north of the Ross Sea). Conversely, seals encountered uniformly low $TDLR_{chl}$ across latitudes during autumn. In spring, $TDLR_{chl}$ encountered by seals were marginally greater (figure 2.6B), and levels gradually elevated toward the mean spring-time sea ice extent.

These same fitted values were also used to calculate inter-annual $TDLR_{chl}$ variability and were compared with *chl-a* within the 55-65°S latitudinal band (figure 2.7). Mean monthly $TDLR_{chl}$ agreed well with *chl-a* inter-annual variability, despite large differences for January 2002 and 2004, and to a lesser extent, December 2005. These large differences correspond well with the few available data (figure 2.7).

2.4.3 Light verses chl-a data coverage

The $TDLR_{chl}$ data sets provided more information than the *chl-a* data that corresponded with seal locations (hereafter corresponding *chl-a*), but both followed similar spatial and temporal trends (figure 2.8A and figure 2.8B respectively). However, coverage of $TDLR_{chl}$ and the overall *chl-a* available within the focal study region (hereafter overall *chl-a*) each followed different spatial and temporal trends (figure 2.8C and figure 2.8D respectively).

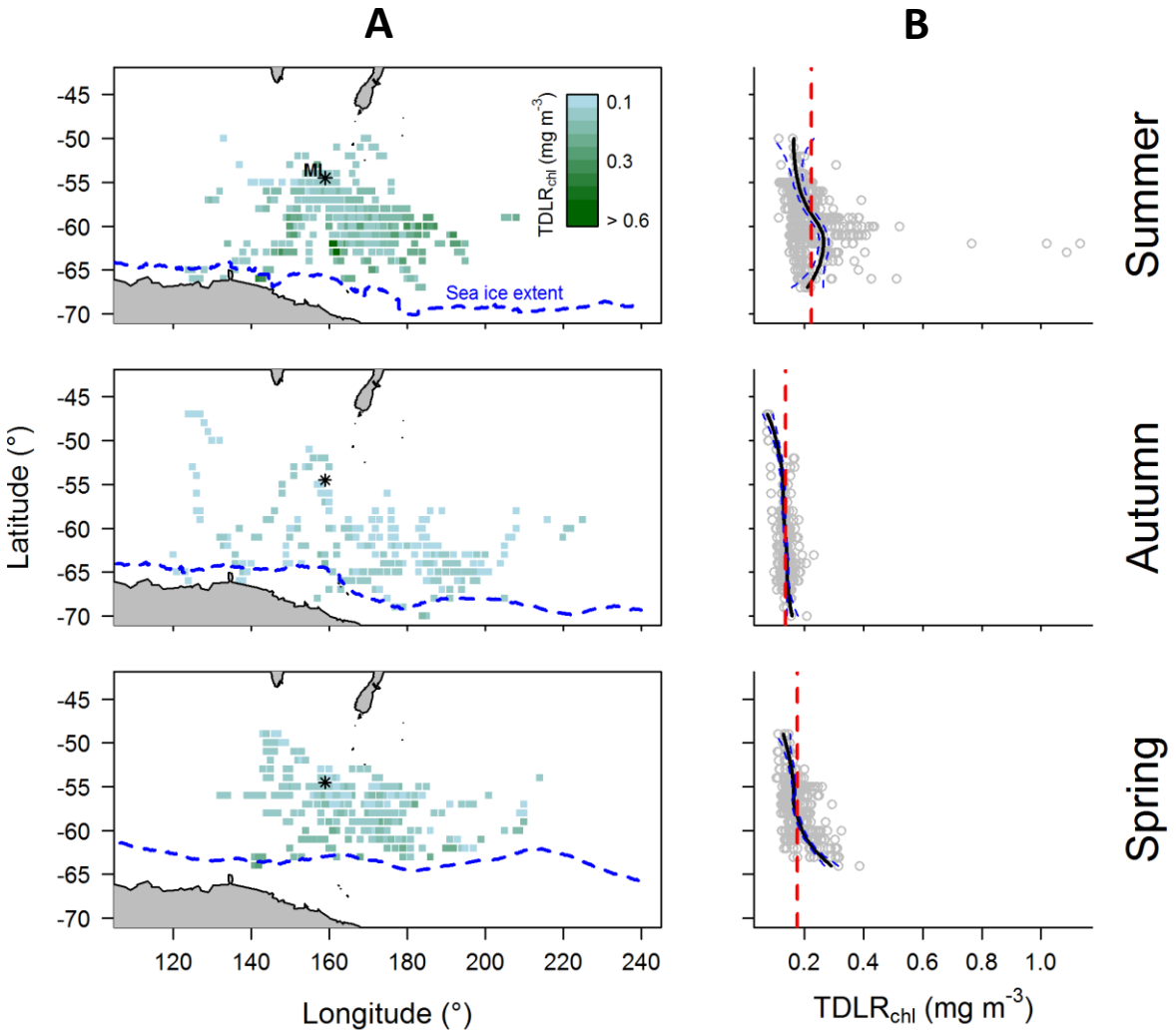

Figure 2.6. (A) Seasonal spatial distribution and (B) latitudinal patterns of $TDLR_{chl}$† from the final mixed model. Each map shows the bottom of Tasmania and New Zealand (top), the coast of East Antarctica and Ross Sea (bottom), and the sea ice extent (blue dashed line). The black asterisk shows Macquarie Island. For each corresponding plot (B) the black line represents a loess fit and blue dashed lines represent the 95% confidence level, and the vertical red dashed line represents the mean $TDLR_{chl}$. †Light-based *chl-a* estimates from our final mixed model collected by TDLRs.

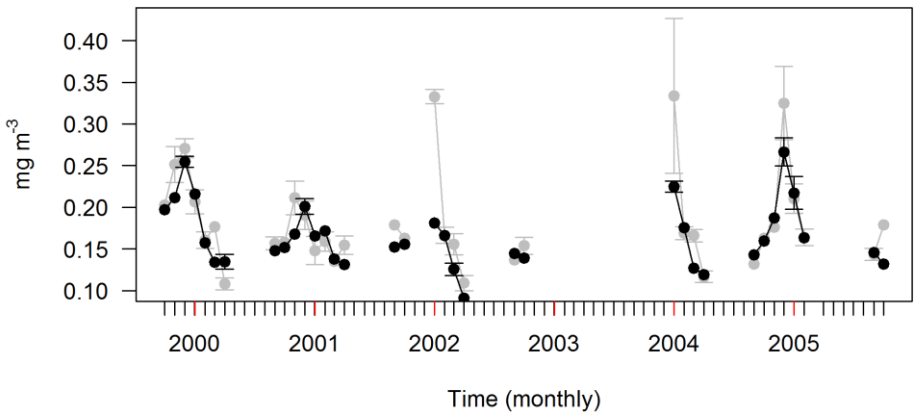

Figure 2.7. Mean inter-annual cycles. The *chl-a* (grey) and light-based *chl-a* estimates from our final mixed model collected by TDLRs ($TDLR_{chl}$) (black) mean inter-annual cycles within a 55°S to 60°S latitudinal band of the study site (*i.e.* where seal density is highest – see table 2.2). Values include standard error bars. Red ticks on the x-axis represent January of each year. Mean inter-annual trends are incomplete because study lacked PB deployments for 2001, 2002 and 2003, and PM deployments for 2003 (see table 2.1). Furthermore, mixed model analysis excluded winter months (see 2.4 Results).

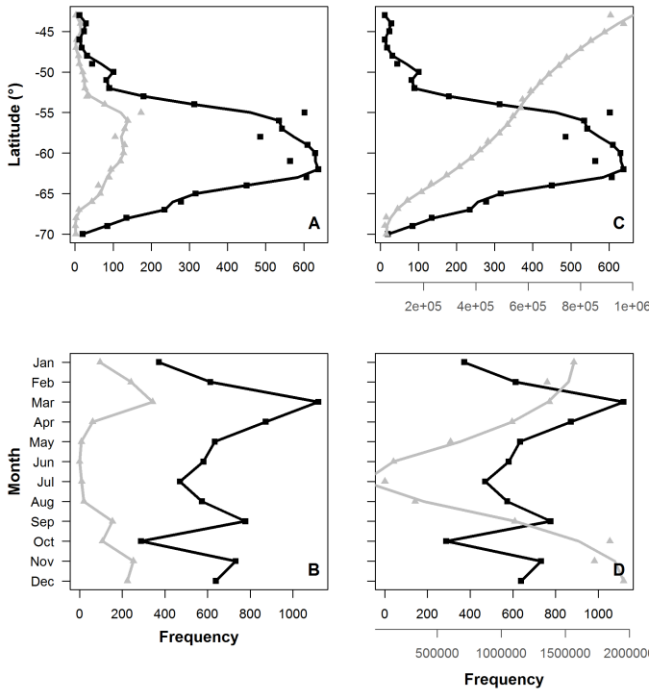

Figure 2.8. Data frequency coverage of *chl-a* and LA_{250}: data coverage of the study region is shown by (A) latitude (at 1° increments) and (B) months (between 1999 and 2005). Black represents LA_{250} coverage and grey represents *chl-a* coverage. Lines represent a loess fit.

Spatial coverage of $TDLR_{chl}$ and corresponding *chl-a* peaked at latitudes between 55°S and 64°S; however peak corresponding *chl-a* coverage was considerably less than $TDLR_{chl}$ coverage (figure 2.8A). In general, peak $TDLR_{chl}$ coverage increased with latitude up to 64°S only to drop with increasing proximity to the Antarctic Continent. However, the extent of $TDLR_{chl}$ coverage was still considerable at latitudes as high as 67°S. Conversely, peak corresponding *chl-a* data coverage steadily decreased from 56°S, becoming virtually negligible at 66°S. Overall, *chl-a* data coverage was greatest at 44°S, but was inversely related to latitude; virtually negligible at latitudes greater than ~ 67°S (figure 2.8C).

Temporal coverage of $TDLR_{chl}$ and corresponding *chl-a* data peaked twice over a 12-month period; the largest peak during March, the other during spring with the exception of a sharp drop of coverage in October (figure 2.8B). However, the two peaks in $TDLR_{chl}$ coverage were considerably greater than that of corresponding *chl-a* data (figure 2.8B). Less coverage of $TDLR_{chl}$ and corresponding *chl-a* data was evident at the beginning of summer, during winter and in October. Specifically, minimal coverage of $TDLR_{chl}$ occurred in October during the breeding season, although still maintained moderate-to-low coverage at this time compared to virtually nil coverage of corresponding *chl-a* data throughout winter. Overall *chl-a* data coverage was poor during the winter months, particularly in July when overall *chl-a* data coverage was completely unavailable (figure 2.8D).

2.5 Discussion

This is the first multi-year dataset (67 elephant seals) used to provide a light-based index of phytoplankton density that is concurrent with a marine animal's entire foraging trip over multiple seasons. Of the 3940 LA_{250} gridded cells recorded over 5 years, only 25.1% cells coincided with *chl-a* measurements demonstrating the deficiency of remotely sensed data sources concurrent with animal behaviour. Model output also revealed that seasonal trends detected by our phytoplankton index were in agreement with data collected by remote sensing. It demonstrates how our phytoplankton index is consistent with near-surface *chl-a* values in the Southern Ocean, and that phytoplankton changes at depth generally reflect near-surface primary producer conditions. This opens the way for the use of simple light data as a bio-optical index for phytoplankton in the Southern Ocean that is concurrent with animal at-sea behaviour.

2.5.1 Relationship between water column light and chl-a

The Southern Ocean is characterised by Case I waters, where phytoplankton organisms are the most optically significant components of the water column (Morel and Prieur, 1977). It is therefore likely that bio-optical differences detected by TDLR light sensors at depth are representative of plankton densities. Our results show that *chl-a* (derived from satellite images) is significantly related to our phytoplankton index estimated from the integrated light attenuation recorded by TDLRs in the top 250 m of the water column. Light at 250 m generally coincides with the limit of the euphotic zone, so all photosynthetic organisms in the water column influence light attenuation to this depth. In general, there is a good relationship between *chl-a* concentration within the top 30 m (as detected by satellite images) and chlorophyll-a integrated over the entire euphotic zone (Guinet et al., 2013). Nevertheless, because the density of phytoplankton particulates is particularly low in the Southern Ocean (Smith and Baker, 1978;Fenton et al., 1994) perhaps the compounding effect of phytoplankton cells on LA_{250} enables TDLR sensors to detect variability that correlate well with *chl-a*. Furthermore, because phytoplankton is virtually negligible below the euphotic zone (Kirk, 1994) no further information is likely to be gained by considering depths greater than 250 m.

We only used data from a 2 h period around the local noon to reduce the influence of ambient light field variability, thereby improving the accuracy and reducing the variability of light attenuation between dives (for details see Teo et al., 2009). However, solar elevation angle at local noon is affected by latitude and time of year (*i.e.* season), invariably altering light penetration at depth, and ultimately, integrated light attenuation to 250 m. This would consistently affect the relationship between *chl-a* and LA_{250} as seals travel extensively across the Southern Ocean. We suggest that the interactions between LA_{250} and latitude, as well as latitude and season, were retained in our final model to account for changes to the solar elevation angle at local noon. Variability of light attenuation in the water column is also due partly to differences in optical properties between phytoplankton species (Stramski et al., 2001;Loisel et al., 2002). Different phytoplankton groups (based on their bio-optical characteristics) can be highly influenced by latitude (e.g. haptophytes and diatoms are found mostly in high latitudes, Alvain et al., 2005) and season (e.g. diatoms blooms dominate during spring and summer, Alvain et al., 2005). Moreover, different FZ can influence distribution of phytoplankton groups (D'Ovidio et al., 2010;Garcia-Munoz et al., 2013;Zhao et al., 2013), and therefore, light attenuation variability, although we suggest that latitude can account for this effect in the Southern Ocean. It is possible, however, that distinct phytoplankton assemblages are not closely associated with our defined FZs. Perhaps a better understanding of FZ and their associated phytoplankton assemblages may show, in fact, that FZ is a useful contributing predictor

to our light-based index of phytoplankton distribution. Another consideration is that the light sensors are not tested for angular sensitivity and are photodiodes without angular compensation; originally intended only for geolocation (Wildlife Computers). Finally, one of the reasons for using LA_{250} (*i.e.* relative decrease in irradiance), rather than integrated light attenuation values closer to the surface, is that it normalises out small variations in sensor sensitivity or calibration. Nonetheless, seal was included as a random term in mixed model analyses despite Wildlife Computers checking light sensor calibrations (see appendix S2.7.1). We expect light values still vary between individual seals and potentially influence the relationship between light and *chl-a* if not accounted for.

These findings show the value of using existing datasets collected from animal-borne light sensors to calculate an index for phytoplankton density in the water column. Indeed, our results revealed that seasonal trends detected by our phytoplankton index were in agreement with data collected by remote sensing. This is despite temporal and spatial accuracy issues associated with both *chl-a* and LA_{250} data that were a potential source of persistent error in our analysis. First, typically dense cloud cover in the Southern Ocean (particularly during winter and at high latitudes) required use of 8-day composite SeaWiFS data (rather than 1-day) to improve data coverage, thereby compromising temporal resolution. Second, we expect spatial error inherent in our geo-location estimates (see methods) to result in spatial mismatch between LA_{250} and *chl-a*. Analyses were performed at 1° degree resolution to minimise location error bias. Third, it is possible that body position of the diving seals affects detection of irradiance by the light sensor. Indeed Sala et al. (2011) have shown how body roll is incorporated into typical diving bouts throughout a seal's entire foraging trip, although we see little evidence of body position affecting light profiles (for examples refer to figure 2.1) and expect error due to roll to be minimal. Although these issues may exist in our analysis we were still able to show how our phytoplankton index revealed seasonal trends consistent with data from *chl-a*.

It is likely that much of the discrepancy in our model between *chl-a* and LA_{250} largely originates from our data sources. Satellites do not provide a direct measure of *chl-a* and instead measure radiance and use empirically derived algorithms to estimate values. The SeaWiFS algorithm used for estimating *chl-a* tends to underestimate values in the Southern Ocean (Hirawake et al., 2000;Johnson et al., 2013). Surface prey aggregation may also contribute to the overestimation of *chl-a* detected during spring when zooplankton in particular become more abundant (Robins et al., 1995). However, it is also possible that these prey aggregations could consistently coincide with elevated *chl-a* and therefore still correlate well with surface (or shallow subsurface) *chl-a* in any case.

Nonetheless, we would expect that subsurface biology accounts for some of the discrepancy between our phytoplankton index and *chl-a*. Prey aggregations (*e.g.* zooplankton, fish), for instance, may affect light attenuation (Teo et al., 2009;Jaud et al., 2012), which become increasingly likely with depth. Moreover, deep chlorophyll-a maxima (DCM) can be more than 30% that of surface values in some regions (Guinet et al., 2013) and may cause further decoupling of *chl-a* and LA_{250}. Holm-Hansen et al. (2005) showed that DCMs are located predominately over the deep ocean basins, regions regularly frequented by the focal elephant seals. Indeed, model predictions were more likely to overestimate *chl-a* by 10-30% when light was recorded over bathymetry greater than 4000 m (figure 2.5). Our light-based phytoplankton index may therefore be useful for estimating total phytoplankton densities in the water column, rather than only providing near-surface *chl-a* information where seals dive.

2.5.2 Ecological significance

The light-based phytoplankton index from our model (hereafter phytoplankton index) produced seasonal patterns typical of *chl-a* distribution in the Southern Ocean south of Australia and New Zealand (Sokolov and Rintoul, 2007). Summer values were consistent with Sokolov and Rintoul (2007) that showed relatively high phytoplankton south of the Antarctic Circumpolar Current, and where the Polar Front interacted with the Mid-Ocean Ridge (*i.e.* regions between 60°S and 65°S). Phytoplankton index values also show typical seasonal patterns that are in agreement with *chl-a* values for the same region (Sokolov and Rintoul (2007): low *chl-a* across the entire Southern Ocean leading into austral winter and a rise in early spring in the vicinity of the sea ice extent. It is important to consider, however, that locations visited by the seals may result in biased phytoplankton distributional trends. For example, in spring, seals may target slightly elevated phytoplankton patches at high latitudes and therefore not sample the relatively low phytoplankton densities of surrounding areas. We did, however, show that an inter-annual trend in mean monthly phytoplankton estimates corresponded well with *chl-a* within a latitudinal band most frequented by the focal seals; further validating that light-based estimates are detecting biological activity.

This study also shows that TDLRs record data in areas where satellite coverage is limited or completely absent. Specifically, satellite coverage is poor at high latitudes and during winter where cloud and ice coverage is more prevalent. This lack of data potentially limits our understanding of resource distribution in the Southern Ocean in relation to seal movement and their foraging behaviour (Bradshaw et al., 2004). Electronic tags deployed on animals have already been used to

collect *in situ* temperature and salinity data along its track to improve our understanding of habitat utilisation (Costa et al., 2010a). Using light to estimate relative phytoplankton distribution may prove a useful covariate recorded simultaneously with elephant seal behaviour in future studies, particularly at the large scale and where *chl-a* data is sparse as described here. Indeed, our phytoplankton index recorded at depth could be more relevant to a deep diving apex predator rather than *chl-a* data taken at the near-surface, although this is beyond the scope of this study. Regardless, these light data are already widely available, for a range of marine species, as light is traditionally recorded for estimating geo-location. This provides an opportunity to augment the application of light data in this study with data collected by multiple species.

Phytoplankton blooms typically support high zooplankton densities (Robins et al., 1995;Burghart et al., 1999;Lizorre, 2001), and this in turn provides an important food resource for pelagic fish and higher predators. Traditionally, *chl-a* data has been the primary source of resource information in the marine environment, but are often limited by cloud cover at high latitudes and lack information at depth. Studies have often not found any significant relationship between *chl-a* and top predators foraging movements (e.g. Bost et al., 2009a), unless at large scales, where general associations are apparent (e.g. Lea et al., 2006). In some instances foraging behaviour has even been shown to be inversely related to *chl-a* (e.g. Bradshaw et al., 2004). However such studies cite either a lack of *chl-a* data (Sumner et al., 2003;Bradshaw et al., 2004), limited satellite resolution (Guinet et al., 2001;Sumner et al., 2003) or "downstream" effects decoupling phytoplankton from its physical conditions of origin (Guinet et al., 2001) as possible explanations. It is therefore crucial that concurrent data is used where possible in efforts to model and understand trophic linkages in Southern Ocean ecosystems. Recording animal behaviour and light data simultaneously may enable researchers to help improve the predictive capacity of ecological models. Light data may provide important biological context in regions of the Southern Ocean and during specific months of the year that are historically poorly understood. Tag configuration that incorporates both fluorometer and light sensors could improve our ability to discriminate between phytoplankton and zooplankton distribution in the 3D marine environment. These data could give new insight into the biology of foraging habitat and/or oceanographic structures (*e.g.* upwelling eddies, ocean fronts) visited by tagged animals by providing information on resource distribution.

2.6 Acknowledgements

We thank Michele Thums, Steve Wall and Corey Bradshaw for field assistance. We thank the Australian Antarctic Division for providing logistical support. We wish to thank Pete Strutton for his advice. Finally, we would like to thank the three anonymous reviewers for their constructive comments.

2.7 Appendix

Appendix 2.7.1

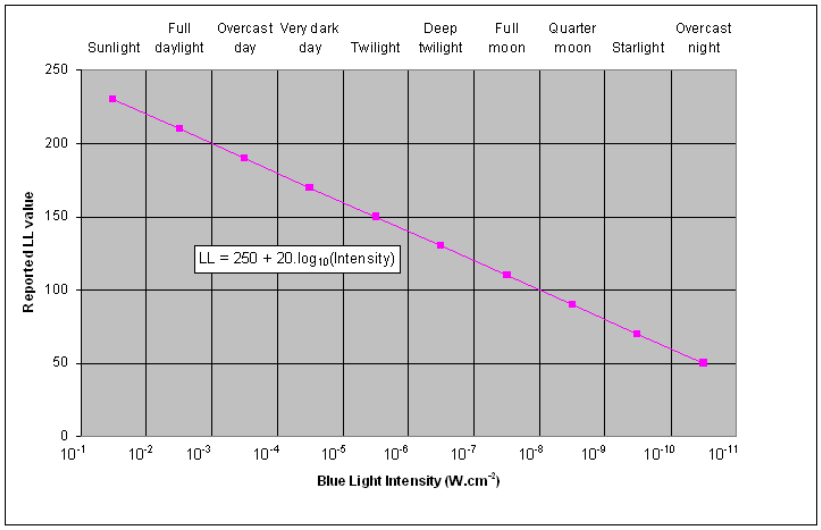

Figure S2.7.1. The relationship between relative light level and blue light intensity (W cm^{-2}) for a typical tag. Calibrations are checked by Wildlife Computers at levels 10^{-5}, 10^{-7} and 10^{-9} W cm^{-2}, which correlates to light level values around 150, 110 and 70 respectively. Furthermore, these light level values roughly equate to specific daylight conditions ranging from full sunlight to overcast night. Source: Wildlife Computers, USA.

Appendix S2.7.2

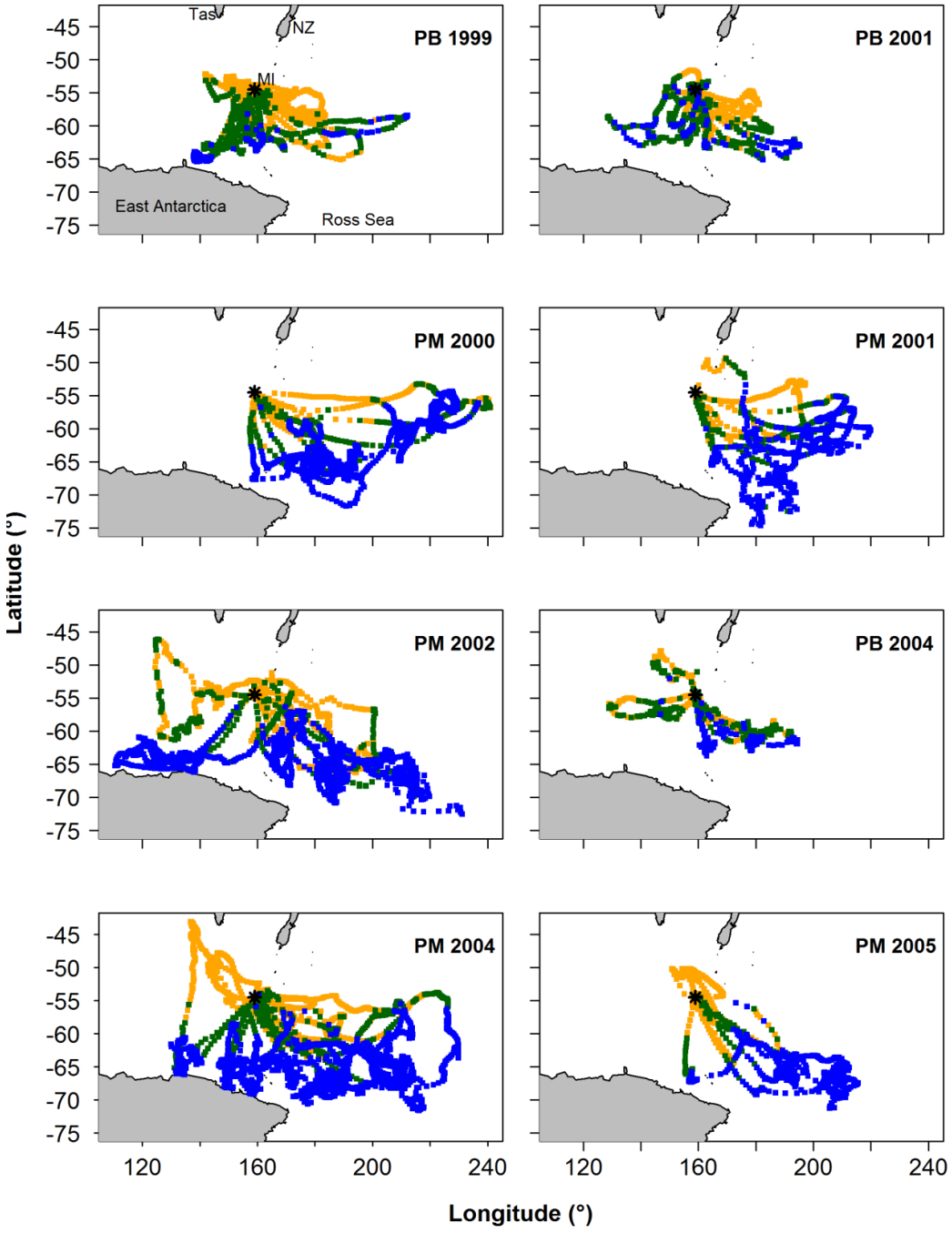

Figure S2.7.2. Locations of each annual deployment cohort. Each location is assigned to one of three frontal zones: Polar Frontal Zone (PFZ – orange); north of the southern Antarctic Circumpolar Current (SACCF-N - green); south of the Southern Antarctic Circumpolar Current Front (SACCF-S - blue). Maps show the bottom of Tasmania (Tas) and New Zealand (NZ, top) and the coast of East Antarctica and Ross Sea (bottom). The black asterisks show Macquarie Island (MI).

Table S2.7.2. Ranked mixed models at 1° resolution. Satellite-derived chlorophyll (*chl-a*) explained by integrated light attenuation above 250 m (LA_{250}), season, latitude and frontal zone (FZ) (*n*=67 seals)[†]. Mixed models are ranked by decreasing Akaike's Information Criterion (AIC) and change in AIC (ΔAIC) [41]; the most parsimonious model having the lowest AIC.

Model*	**df**	**AIC**	**ΔAIC**	**BIC**	**logLik**
LA_{250} * season * latitude	16	697.0	0	777.8	-332.5
LA_{250} * season * FZ	22	740.8	43.7	851.8	-348.4

[†]season (levels: summer, autumn and spring); latitude (between 52°S and 64°S at 1° intervals); FZ (levels: SAFZ, PFZ and sSAACF).

Chapter 3: Foraging strategy switch of a top marine predator according to seasonal resource differences

Submitted as: O'Toole, M.D., Lea, M.-A., Guinet, C., Schick, R., and Hindell, M.A. (2015). Foraging strategy switch of a top marine predator according to seasonal resource differences. *Frontiers in Marine Science* 2. doi: 10.3389/fmars.2015.00021.

3.1 Abstract

The spatio-temporal variability in marine resources influences the foraging behaviour and success of top marine predators. However, little is known about the links between these animals and ocean productivity, specifically, how plankton density influences their foraging behaviour. Southern elephant seals (*Mirounga leonina*) have two annual at-sea foraging trips: a two month post-breeding foraging trip (Nov – Jan) that coincides with elevated summer productivity; and an eight month post-moulting foraging trip (Feb – Oct) over winter, when productivity is low. Physical parameters are often used to describe seal habitat, whereas information about important biological parameters is lacking. We used electronic tags deployed on elephant seals during both trips to determine their movement and foraging behaviour. The tags also recorded light, which measured the bio-optical properties of the water column, the bulk of which is presumably influenced by phytoplankton. We investigated the relationship between plankton density and seal foraging behaviour; comparing trends between summer and winter trips. We found a positive relationship between plankton density and foraging behaviour, which did not vary seasonally. We propose that profitable concentrations of seal prey are more likely to coincide with planktonic aggregations, but we also acknowledge that trophic dynamics may shift in response to seasonal trends in productivity. Seal prey (mid-trophic level) and plankton (lower-trophic level) are expected to overlap in space and time during summer trips when peak phytoplankton blooms occur. In contrast, aggregated patches of lower trophic levels are likely to be more dispersed during winter trips when plankton density is considerably lower and heterogeneous. These results show that southern elephant seals are able to exploit prey resources in different ways throughout the year as demonstrated by the variation observed between seal foraging behaviour and trophic dynamics.

3.2 Introduction

The Southern Ocean (SO) is one of the world's most productive oceans, supporting a highly dynamic and heterogeneous marine ecosystem where food resources are patchy in both time and space (Arrigo et al., 2008). Seasonal climatic conditions in the SO are quite distinct as abiotic factors such as light levels, iron availability, temperature and ice cover vary markedly between summer and winter which affects the abundance and timing of primary and secondary production (Thomalla et al., 2011 and references within). Most marine productivity takes place in late spring and summer, with levels declining in autumn and conditions becoming oligotrophic in winter. Many marine predators have evolved migratory patterns that allow them to adjust their foraging behaviour in

relation to seasonal variability (Costa et al., 2012). However, it is often unclear how marine predators resident in the SO year round respond to heterogeneous resources that fluctuate seasonally.

The development of electronic tags for marine animals has provided detailed information on their movement and behaviour in the horizontal, vertical and temporal dimensions over extensive areas and for extended periods of time (Boyd et al., 2004;Kooyman, 2004;Naito, 2007;Costa et al., 2012;Evans et al., 2013), and in relation to oceanographic structures and processes (Costa et al., 2010a). Tagging programs have revealed the diverse assemblage of marine vertebrates in the North Pacific (Tagging of Pacific Predators [TOPP]; Block et al., 2011), as well as significant migratory corridors for endemic species (e.g. flatback marine turtle Natator depressus; Pendoley et al., 2014). More specifically, sensory devices deployed on marine animals can reveal their behaviour and the dynamic nature of the surrounding environment. For example, physical parameters used to identify meso-scale eddies (potential sites of elevated productivity) have been related to southern elephant seal (*Mirounga leonina*) foraging activity (Bailleul et al., 2010b). However, these studies often do not directly assess the links existing between these physical structures, the biological activity associated with them (*e.g.* plankton aggregations) and the foraging strategies of top predators, due to the paucity of data on lower and mid-trophic levels in the SO. Efforts to model predator movements and behaviour using only physical parameters typically result in relatively weak relationships and poor model fits (e.g. O'Toole et al., 2014a), likely due to the poor connectivity between seals and the physical environment. Biological information would prove invaluable for fitting such habitat models, but these data are difficult to obtain.

Satellite measurements of ocean colour have revealed the complex temporal and spatial variability of surface chlorophyll-a (e.g. Arrigo et al., 2008), a useful proxy for phytoplankton distribution. While marine predators do not feed on phytoplankton, but rather on mid trophic level resources (*e.g.* myctophid), it is possible to use primary producer distribution to assess indirect relationships between predators and their prey (Guinet et al., 2001). However, satellite-derived chlorophyll-a information can be patchy in space and time due to cloud cover, particularly in winter (Sumner et al., 2003), and provide no information on plankton concentration at depth. This can be important as deep maximum chlorophyll-a concentration are reported in the Southern Ocean and cannot be detected from ocean colour satellite images (Guinet et al., 2013). Animal-borne fluorometers are the only *in-vivo* measurements taken simultaneously with animal movement that can determine

chlorophyll-a concentration (e.g. Guinet et al., 2013). These sensors, however, are limited by memory capacity and short battery life both of which hinder application in large-scale studies.

An alternative is to use light data recorded by time-depth-light recorders (TDLRs) deployed on marine predators to measure the bio-optical properties of the water column (McCafferty et al., 2004). Ambient light is attenuated throughout the water column due to physical properties of the seawater, but also because of the quantity of inorganic and organic particulates suspended in the water column (Morel and Maritorena, 2001). The Southern Ocean is typically characterised by Case I waters, whereby phytoplankton are the main source of particles suspended within the euphotic zone (Morel and Prieur, 1977;Morel and Maritorena, 2001). Phytoplankton is consequently the main cause of light attenuation if it is assumed coloured dissolved organic matter (CDOM) and detritus degradation products covary with phytoplankton (Bricaud et al., 1981) and physical properties are constant (Bricaud et al., 1998). Light data collected during daylight hours by marine animals can therefore provide a useful index for plankton density concurrent with animal movement (Teo et al., 2009;Guinet et al., 2013;O'Toole et al., 2014b) and have revealed seasonal trends typical of Southern Ocean productivity south of Iles Kerguelen and Macquarie Island (Jaud et al., 2012;O'Toole et al., 2014b).

Southern elephant seals (SESs) have a circumpolar distribution and spend most of their life at sea feeding, mainly on squid and fish, across extensive areas of the Southern Ocean (Biuw et al., 2007). Adult elephant seals annually perform two foraging trips: following their breeding season on land in October, seals go to sea for two to three months returning to land to moult for one month in December-March (depending on age and sex) (Stewart and DeLong, 1995). Following the moult, they forage at sea for an extended period (5 – 8 months) to build body reserves for the next breeding season. Post-breeding migrations coincide with peak productivity in late spring through to mid-summer (summer trips); however, post-moulting migrations extend over the entire austral winter (Mar – Oct) when productivity is relatively low (winter trips).

Here we investigate the relationship between the foraging behaviour of a wide-ranging apex marine predator with a continuously recorded *in-situ* index for plankton density. We aim to advance our understanding of seasonal trophic interactions between low trophic levels and a top marine predator in the Southern Ocean. Our primary objectives were to examine seasonal plankton distribution in the pelagic environment north of the Ross Sea and how it influences adult female SES foraging behaviour. Due to distinct biological change between the summer bloom period and the

winter post-bloom period, we expect fundamental differences in SES foraging strategy in relation to seasonal plankton densities. The diet of female SES is thought to consist largely of mesopelagic fish, primarily myctophid, during the two foraging periods (Cherel et al., 2008;Guinet et al., 2014). Therefore, seasonal changes in seal behaviour may be indicative of a change in the prey field distribution relative to lower trophic (*i.e.* plankton) distribution.

3.3 Methods

3.3.1 Tag deployment and data extraction

Eighty-nine adult female SES were instrumented at Macquarie Island (54°35´S, 158°58´E) between 1999 and 2005. Deployments were made either before their summer or winter foraging trips (October or January/February respectively). All necessary permits were obtained for the described field studies. Elephant seal research was sanctioned by the University of Tasmania Animal Ethics Committee (permit A6738) and the Australian Antarctic Science Advisory Council Ethics Committee (project 2794). Permits and permission to carry out research on Macquarie Island was obtained from Parks and Wildlife Service Tasmania.

The seals were approached by foot and temporarily restrained with a head bag and anaesthetised intravenously with a 1:1 mixture of tiletamine and zolazepam (0.5 mg kg^{-1}) (McMahon et al., 2000;Field et al., 2002). Time-depth-light recorders (TDLRs) (Wildlife Computers, Redmond, WA, USA: MK7s, MK8s or MK9s) were attached to the pelage above the shoulders using a two component industrial epoxy (Araldite AW 2101) (Hindell and Slip, 1997). Seals were observed during recovery from anaesthesia and allowed to enter the water when no longer sedated. Time-depth-light recorders were retrieved at the end of the foraging trip once the seal had hauled out on land by repeating the above restraint procedures. The tracking devices or attachment method did not adversely affect individual performance and fitness over the short (seal growth) or long (seal survival) term (McMahon et al., 2008).

TDLRs (Mk6, Mk7 and Mk8s) measured time, depth (pressure), light and temperature at 30 s intervals for the duration of each foraging trip. The details of all tag specifications for the time, depth, light and temperature sensors are available in appendix S3.7.1. Raw data from TDLRs were extracted using DAP Instrument Helper software (Wildlife Computers, Redmond, WA, USA). Individual dive cycles were identified using the procedure outlined in appendix S3.7.2.

3.3.2 Plankton density index

Light data recorded by the TDLRs were used as an index of plankton density by measuring the integrated light attenuation within the mixed layer depth. Because the sensitivity of the on-board light sensors become diminished below 300 m (*see* appendix S2.7.1) we only consider the influence of plankton on light attenuation in the top 250 m of the water column to give an index of plankton density (PDI). For each dive, the light level at 250 m (LL_{250}) was subtracted from the mean surface light level (LL_0) and divided by depth (z) to provide a PDI (for details see appendix S3.7.3). We only considered PDI values 1h either side of local midday (1100-1300) to minimise variability in the ambient light field (see discussion in Teo et al., 2009), and excluded dives in heavy sea ice cover to avoid light attenuation bias due to sea ice shading (see appendix S3.7.4).

3.3.3 Path analysis and behavioural metric estimates

Twice daily at-sea locations (at dawn and dusk) were derived from the logged light levels with the R package tripEstimation (R Development Core Team, 2014) (for details see Thums et al., 2011) and were processed using state-space model analysis (SSM, Jonsen et al., 2005) to produce an estimated track for each seal trip at 6 hourly interpolated intervals local time (*i.e.* 0h, 6h, 12h, 18h). To match daily PDI values only the interpolated locations at 12h were considered in any further analyses. Output from SSMs was also used to quantify the first of three behavioural metric, known as behavioural state, by giving a probability of the seal exhibiting search behaviour at each location, ranging from 0 (low probability) to 1 (high probability) on a continuous scale (details of this behavioural state metric are available in appendix S3.7.5). A method adapted from Bailleul et al. (2008) was used to quantify the second behavioural metric, dive effort, which was based on vertical dive behaviour only that measures the relative time spent at the bottom of a dive (details of this dive effort metric, known as bottom time residuals, are available in appendix S3.7.6). Dive effort is thought to be linked to foraging activity (Bailleul et al., 2008;Gallon et al., 2013). Finally, estimates of *in situ* body composition can be used as a measure of foraging success (Biuw et al., 2003), and can be related to movement patterns and prey distribution. We used a hierarchical Bayesian state-space approach developed by Schick et al. (2013) to estimate daily mass gain rates for each individual while at sea (details of this foraging success metric are available in appendix S3.7.7).

3.3.4 Statistical analysis

We fitted generalised linear mixed-effect models (GLMMs) using the R software package *nlme* (R Development Core Team, function lme; Pinheiro et al., 2012b) following the steps described in Zuur et al. (2009) to examined the relationship between PDI and each behavioural metric calculated at the mean daily scale:

(i) Behavioural state (horizontal state space analysis)
(ii) Dive effort (residual bottom time)
(iii) Foraging success (fat content)

Variables were transformed, where necessary, prior to analyses to correct for non-Gaussian distributions. Behavioural state is the proportional likelihood of exhibiting search behaviour and ranged between 0 (transit) and 1 (search), therefore suffering from unit constraints, so values were logit transformed.

Model selection was achieved using the following the steps described in (Zuur et al., 2009). First, we determined the optimal structure of each model by assessing the full model with fixed effects (PDI, season) and their interaction term with and without individual seals (*seal*) and latitude fitted as random intercept terms (latitude was nested within *seal*) to ensure that these terms were contributing to the model fit. Random intercept models were then compared with random slope models (a random slope for PDI was added to the random slope models). Both *seal* and latitude were included as random terms in our analysis to allow for potential tag measurement variability and likely effect on phytoplankton abundance in the water column respectively (for details see chapter 2). Second, we assessed the effect of inclusion of an autocorrelation term in the resulting optimal model by using the AR-1 autocorrelation (corAR1) argument. Finally, we tested the individual fixed and interaction terms by sequentially removing non-significant terms from the model. Model selection was made using the likelihood ratio test, based on maximum likelihood (ML). Terms were only retained if they improved the fit ($p < 0.05$; Zuur et al., 2009;Bestley et al., 2010). In all cases, models were ranked via Akaike Information Criterion (AIC) (Burnham and Anderson, 2002), to ensure the most parsimonious (*i.e.* lowest AIC value) model was selected. In addition, we used *F* and *t* statistics to examine the significance of individual fixed and interaction terms. The final model was presented using restricted maximum likelihood (REML) methods. The normality of the residuals was checked graphically and the fitted values of the model were plotted against the observed.

Latitude at 2° intervals was normalised by subtracting the overall mean from each value and was included as a random term. Time of year was expressed as a 4-level factor: late spring – summer (Nov – Jan); autumn (Feb – Apr); winter (May – Jul); early spring (Aug – Oct). Post-breeding (or summer) trips coincided with the late spring – summer period (Nov – Jan) and post-moulting (or winter) trips encompassed autumn through to early spring. Time of year was included as a fixed term as we were particularly interested in the seasonal interaction effect on the relationship between plankton densities and each behavioural metric.

3.4 Results

We used data from entire foraging trips for 50 (23 summer; 27 winter) of the 89 deployments (table S3.1). Thirty-one trips were excluded due to either light or depth sensor failure. Data from one seal were also omitted due to unrealistic track estimates (*i.e.* track passed over land). Another seven trips could not be included because they lacked the necessary morphometric data to estimate daily lipid gain. Summer trips were considerably shorter than winter trips (79 ± 31 (SD) days and 234 ± 26 (SD) days respectively). All GLMMs included both random intercept terms (*seal* and nested latitude) as well as the random slope term (LA_{250}) and an autocorrelation term. According to model parsimony, both fixed effects (LA_{250} and season) were retained in each model (table 3.1). A seasonal interaction term was also retained in the dive effort model (table 3.1), suggesting that dive effort response to plankton density was influenced by the time of year (*i.e.* season). No seasonal interaction term was retained in either the behavioural state or foraging success models.

3.4.1 Behavioural metrics in response to seasonal plankton densities

In the most parsimonious models (*see* table 3.1) each behavioural metric exhibited by seals (*i.e.* behavioural state, dive effort and foraging success) was significantly correlated with plankton distribution, although dive effort was also influenced by season (table 3.2). Linear mixed effect models indicated that both the search activity (*i.e.* behavioural state) and foraging success (*i.e.* mass gain rate), increased with plankton densities throughout the year (figure 3.1and figure 3.2 respectively). Dive effort also increased with plankton densities, albeit a slightly stronger trend in winter and spring (table 3.2, figure 3.3). Dive effort was generally higher in summer compared with other times of the year (table 3.2).

Table 3.1. Ranked model parsimony according to the significance of fixed effects (plankton density index – PDI; season – S) and their interaction term (PDI: S) in relation to each behavioural metric. The model parsimony is ranked via Akaike Information Criterion (Burnham and Anderson, 2002) and includes degrees of freedom (*df*); Akaike Information Criterion (AIC); divergence of a candidate model from the most parsimonious model according to AIC (∆AIC); and maximum log-likelihood (LL).

model	***df***	**AIC**	**∆AIC**	**LL**
behavioural state				
PDI + S	13	27170.4	0	-13572.2
PDI + S + PDI : S (full model)	16	27190.3	19.9	-13579.2
S	8	27205.3	34.9	-13594.7
PDI	10	27369.6	199.2	-13674.8
null model	2	38370	11199.6	-19183
foraging success				
PDI + S	13	3703.3	0	-1838.6
PDI + S + PDI : S (full model)	16	3704.1	0.8	-1836
S	8	3722.4	19.1	-1853.2
PDI	10	3745.3	42	-1862.7
null model	2	8194.8	4491.5	-4095.4
dive effort				
PDI + S + PDI : S (full model)	16	-9237.5	0	4634.7
PDI + S	13	-9149.6	87.9	4587.8
S	8	-9091.8	145.7	4553.9
PDI	10	-8170.4	1067.1	4095.2
null model	2	2104	11341.5	-1050

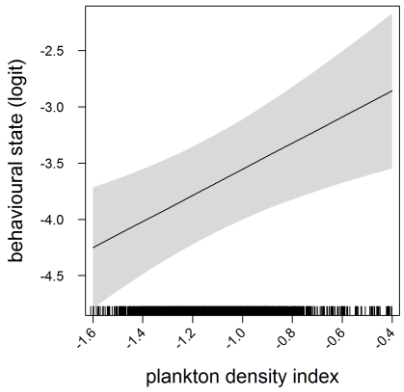

Figure 3.1. Effects plot of the relationship between plankton densities encountered by seals (*i.e.* PDI) and their behavioural state from our mixed model analysis. Shaded area indicates the confidence interval. Behavioural state has been logit transformed (higher values indicated an increasing likelihood of seals exhibiting horizontal search activity).

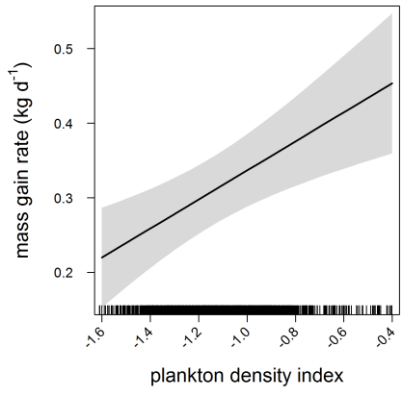

Figure 3.2. Effects plot of the relationship between plankton densities encountered by seals (*i.e.* PDI) and their foraging success (*i.e.* mass gain rate) from our mixed model analysis. Shaded area indicates the confidence interval.

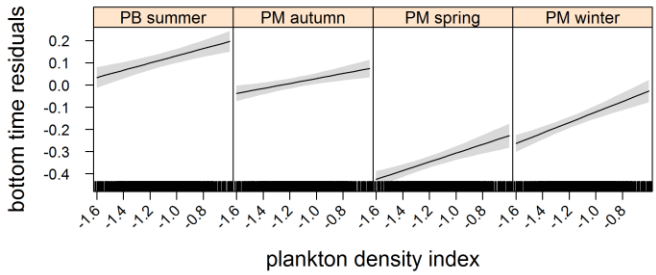

Figure 3.3. Effects plot of the relationship between plankton densities encountered by seals (*i.e.* PDI) and their dive effort (*i.e.* bottom time residuals) according to season from our mixed model analysis. Shaded area indicates the confidence interval.

Table 3.2. Coefficients from our most parsimonious generalised mixed-effects models relating the plankton density index (PDI) to each behavioural metric (i.e. behavioural state, foraging success, dive effort). Term coefficients are presented ± SE and *p*-values for each coefficient are also shown. Significant terms ($p < 0.05$) are denoted by italic characters. Season variable was coded as a factor in the model, thus coefficients for the 3 post-moulting periods (PM-Autumn, PM-Winter, PM-Spring) are given in reference to the post-breeding summer period (PB-Summer).

	coefficient ± SE	**coefficient *p***
behavioural state		
(Intercept)	-2.79 ± 0.55	<0.0001
PDI	1.16 ± 0.36	0.0014
Season (PM-Autumn)	-0.70 ± 0.46	0.1266
Season (PM-Winter)	1.82 ± 0.47	0.0001
Season (PM-Spring)	0.27 ± 0.47	0.5663
foraging success		
(Intercept)	0.62 ± 0.07	<0.0001
PDI	0.19 ± 0.06	0.0005
Season (PM-Autumn)	-0.16 ± 0.05	0.0015
Season (PM-Winter)	-0.12 ± 0.05	0.0237
Season (PM-Spring)	-0.06 ± 0.05	0.2409
dive effort		
(Intercept)	-0.30 ± 0.05	<0.0001
PDI	0.15 ± 0.04	0.0002
Season (PM-Autumn)	-0.17 ± 0.06	0.0086
Season (PM-Winter)	-0.19 ± 0.07	0.0069
Season (PM-Spring)	-0.38 ± -0.07	<0.0001
LA : Season (PM-Autumn)	-0.05 ± 0.06	0.3415
LA : Season (PM-Winter)	0.08 ± 0.06	0.1735
LA : Season (PM-Spring)	0.07 ± 0.06	0.2372

3.4.2 Seasonal spatio-temporal distribution

Predicted mass gain values from our foraging success model also showed that summer seal body condition improved with PDI at the distal end of the trip, within the Polar Front Zone (PFZ), delineated by the sub-Antarctic front (SAF) and the southern Antarctic Circumpolar Current Front (SACCF), and generally north of East Antarctica (figure 3.4). Both PDI and behavioural metric values generally peaked around December (summer) (figure 3.5) at the greatest longitudinal (either 140°E to the west or 200-220°E to the east) and latitudinal (63°S) extents attained by seals (figure 3.6). In contrast, seals migrating during winter were largely south of the SACCF (> 63°S) and shifted progressively eastward by the end of autumn through to spring (up to 240°E) along the maximum sea ice extent (figure 3.4 and figure 3.5). Predicted mass gain values show that body condition improved with PDI in pelagic waters between the SACCF and Ross Sea (63°S – 68°S) from late autumn to the end of winter (figure 3.4B and figure 3.4C), which coincided with intensifying search activity during mid-winter (figure 3.5B) as seals ended their eastward trajectory (figure 3.6A) and slowly moved northward from between 63°S and 68°S to between 55°S and 68°S (figure 3.6B). However, dive effort and PDI values had already declined in early March (figure 3.5B and figure 3.5A respectively) as they began to pass south of the SACCF (figure 3.6B; *also see* figure 3.4B). By spring predicted mass gain rate in response to PDI dropped as their distribution shifted from these waters back towards MI as they returned to the island for the breeding season (figure 3.4).

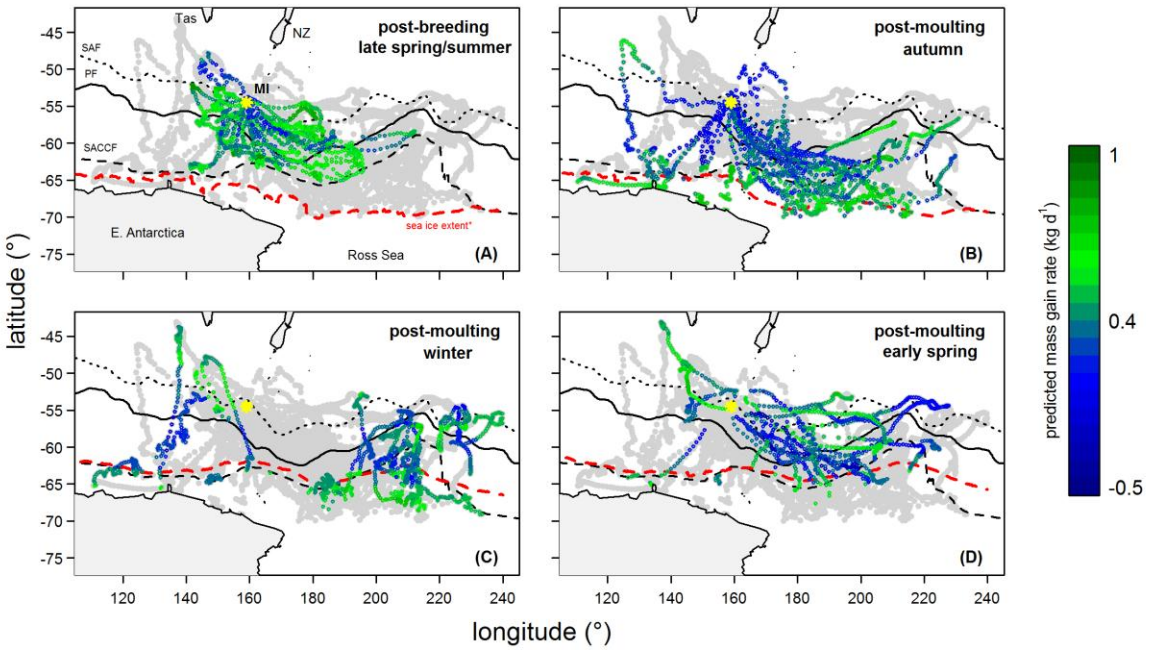

Figure 3.4. Tracks of southern elephant seals (from Macquarie Island) during their (A) summer and (B-D) winter foraging trips after the correction of geo-locations using state-space models (excluding locations in heavy sea ice). Year-round location points are light-grey and are overlaid with predicted mass gain values from our foraging success model (see legend for colour code) according to season. Maps show the bottom of Tasmania (Tas) and New Zealand (NZ, top) and the coast of East Antarctica and Ross Sea (bottom). The yellow asterisk indicates Macquarie Island (MI). Three major fronts are also shown: sub-Antarctic Front (SAF – dotted); Polar Front (PF - solid); and Southern Antarctic Circumpolar Current Front (SACCF - dashed). The seasonal sea ice extent (blue dashed line) is defined as the northern boundary where average sea ice concentration between 1999 and 2005 is >50%.

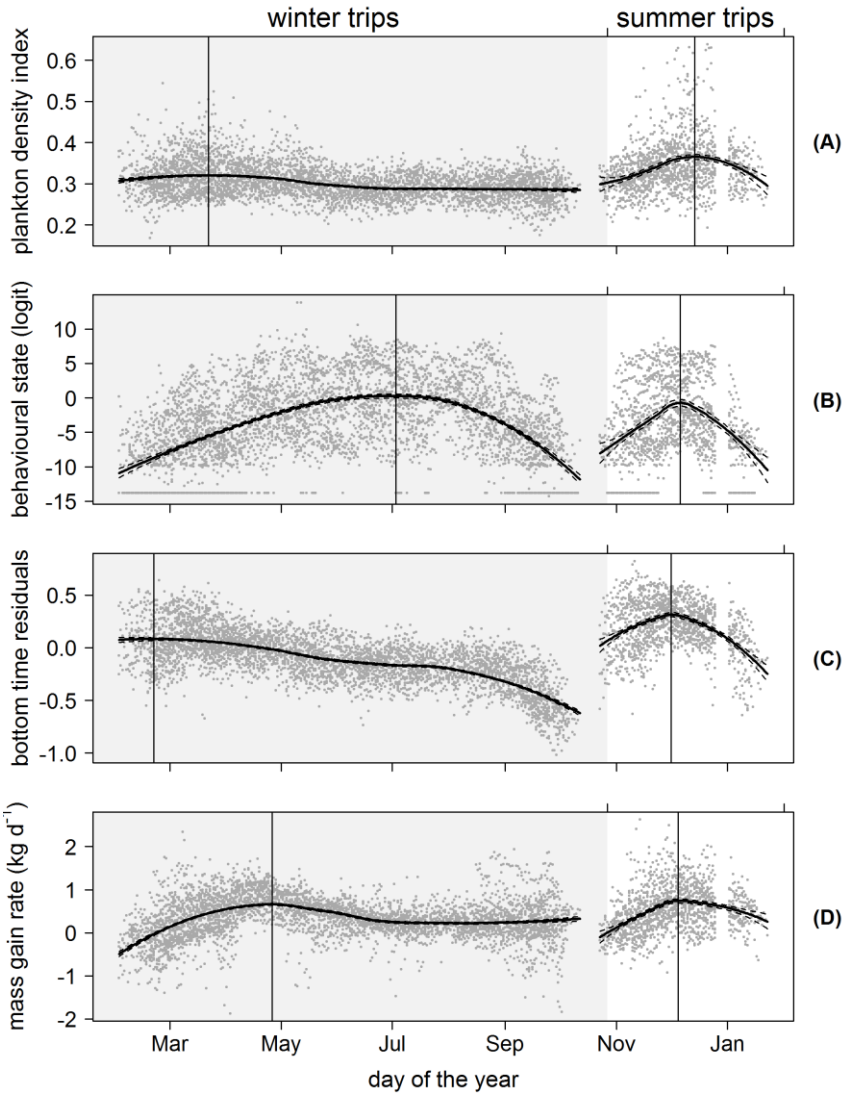

Figure 3.5. Seasonal trends over multiple years of (A) plankton densities encountered, (B) behavioural state, (C) dive effort, and (D) foraging success during the summer (non-shaded area) and winter (shaded area) foraging trips. Data values are represented by dark grey points. A locally-weighted polynomial regression smoother function applied to PDI and behavioural values using the R software package *stats* (function lowess; R Development Core Team, 2014). The loess fit and grey dashed lines represent the 95% confidence level. Vertical lines indicate the temporal peak for each measured metric.

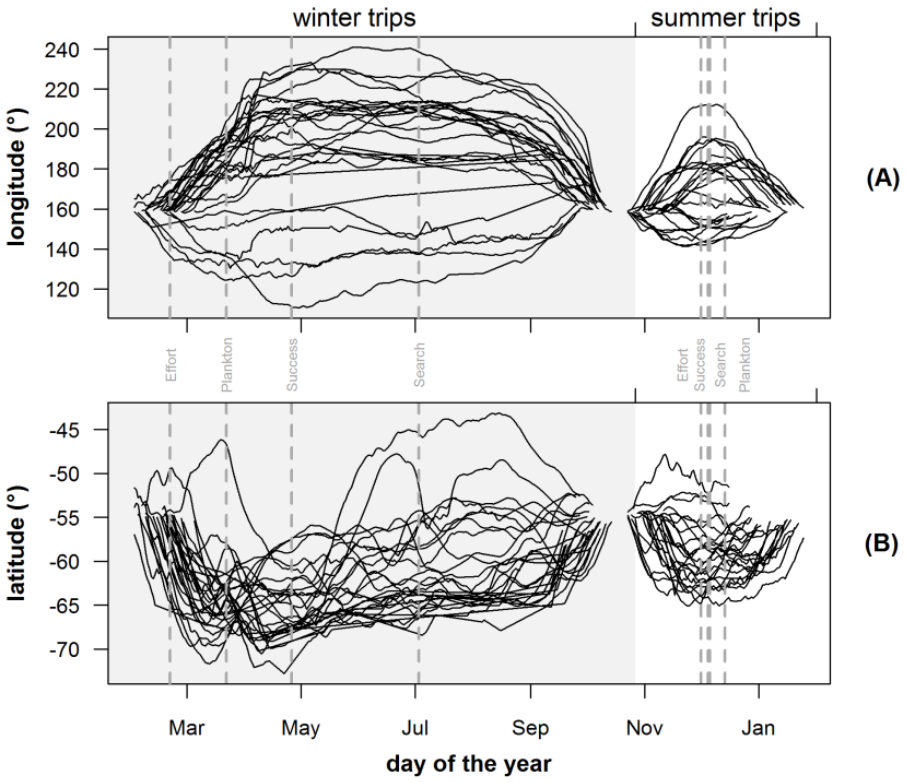

Figure 3.6. Geographical extent of individuals: seasonal trends of (A) longitude and (B) latitude position of individual seals during the summer (non-shaded area) and winter (shaded area) foraging trips. Grey vertical dashed lines in plots indicate peak values for plankton densities (Plankton), foraging behaviour (Search), dive effort (Effort) and foraging success (Success).

3.5 Discussion

In the past it has been difficult to investigate the linkages between lower trophic levels and the foraging behaviour of deep diving predators because concurrent data were often lacking, particularly in the polar regions. Resource distribution in relation to animal behaviour is often estimated from satellite-derived chlorophyll-a (e.g. Guinet et al., 2001;Bradshaw et al., 2004;Suryan et al., 2012), but depth data are lacking. These data also become increasingly scarce and unreliable in polar regions due to cloud cover (Sumner et al., 2003), and are often spatially mismatched with animal behaviour due to error inherent in animal location estimates (Ekstrom, 2004;Costa et al., 2010b). We provide an approach for investigating the trophic link between a deep diving predator and concurrent plankton densities in the 3D marine environment by using light data collected by sensors deployed

on southern elephant seals (SESs). Integrated light attenuation in the top 250 m of the water column were used to infer year-round changes to plankton distribution in the Southern Ocean that followed known seasonal patterns in productivity. This is the first dataset (up to 50 SESs) used to examine how seal movement and feeding behaviour respond to plankton and its seasonal variability in the Southern Ocean, providing rare evidence of regions of elevated plankton influencing seal foraging behaviour. In addition, we demonstrate how the response of seals to resource structuring can give some insight into seasonal foraging strategies at high latitudes.

3.5.1 Seasonally-contrasted foraging strategies in relation to resource distribution

We hypothesized that the contrasting primary production between the spring-summer bloom and post-bloom period in winter required a fundamental change in elephant seal foraging strategy, but found no significant (or very little) seasonal differences. There were no pronounced seasonal differences in the influence of plankton densities on seal behavioural state or foraging success, albeit a small seasonal influence on dive effort. Seal search intensified and foraging success increased in response to elevated plankton densities not only in summer, but also during other times of the year including winter. This is despite the well-documented seasonal decline in phytoplankton biomass from the bloom period during early spring and summer to oligotrophic conditions during winter (Behrenfeld and Falkowski, 1997;Garibotti et al., 2005;Thomalla et al., 2011). These biological changes do not appear to affect the ability of seals to locate elevated plankton densities where prey availability increases. It is therefore likely that lower trophic aggregates are associated with seal prey either directly (feed on plankton) or indirectly (plankton reduce light penetration at depth, thereby improving seals' vertical access to prey (Guinet et al., 2014)).

Marine resources are often heterogeneously distributed because of physical (*e.g.* eddy fields; d'Ovidio et al., 2013) and biological (*e.g.* grazing pressure; Hernández-León et al., 2008) processes (Begon et al., 2006). Optimal foraging theory predicts that animals will make decisions so as to maximise the net rate of energy intake while foraging in these patchy environments (Charnov, 1976). The different spatial distribution between summer and winter foraging trips may be a strategy for maximising encounters with patches of prey. The summer seals intensified their search and dive effort at the distal end of their foraging trip where prey acquisition appeared to increase (according to foraging success). This coincided with known spring bloom events in deep pelagic waters between the major fronts of the Antarctic Circumpolar Current (ACC) (Sokolov and Rintoul, 2007;Sokolov, 2008), but not the blooms that often accompany the receding sea ice extent (*e.g.* Robins et al., 1995)

(*see* figure 3.4). This is perhaps because during their two month summer foraging trip less time is allocated for transit to favourable habitat compared with their much longer winter foraging trip; preferring instead to target blooms that are relatively close within the major fronts. We suspect a high degree of overlap between seal prey (mid-trophic level) and plankton (lower-trophic level) within these productive frontal regions during late spring and summer because the extent of phytoplankton biomass is so vast. Cotté et al. (2014) argue that the prey field may be relatively homogeneous and dense within a bloom in late spring/summer, and exhibit little spatial structure. We suggest that during the summer seals adopt a hierarchical foraging strategy by responding to large-scale biological cues during late spring/summer phytoplankton bloom periods in order to locate profitable prey fields at the smaller scale. These findings are consistent with Guinet et al. (2014) which showed summer seals (females) feeding during the day are more successful (indicated by prey capture attempts derived from accelerometer data) in areas where higher concentration of particles (indicted by the influence of plankton density on light attenuation) are encountered, but did not however consider females feeding in winter.

Despite oligotrophic winter waters the post-moulting foraging trip remains vital for gestating females that must also build fat reserves for the up-coming breeding season. We revealed that winter seals, like summer seals, generally intensified their search, were likely to spend relatively more time foraging at depth, and exhibited increasing foraging success when encountering higher PDI. It is likely prey field distribution becomes increasingly patchy in space as productive waters from summer blooms become increasingly mixed with low-productive waters throughout the winter period (d'Ovidio et al., 2013;Cotté et al., 2014). We expect seals are encountering these increasingly isolated patches of productive waters as winter progresses. Cotté et al. (2014) have demonstrated how winter seals in transit along cold water filaments track water parcels originating from spring bloom patches as they are advected by the flow of the ACC. We suspect turning frequencies, and therefore periods of ARS, of the seals increased in winter in order to locate and follow these filaments. These filaments, which correspond to frontal transportation, are reported to carry high zooplankton densities (Labat et al., 2009;Perruche et al., 2011), which may explain why seals are more likely to increase search intensity in response to sites of elevated plankton densities, even throughout winter. Cotté et al. (2014) also suggest that seals may temporally exploit these rich filaments while also using them to track the most profitable meso-scale features where higher prey densities occur (e.g. eddies - Godo et al., 2012). This is consistent with our results which showed seals foraging in winter were more likely to spend greater time foraging at depth and increase

foraging success in response to elevated plankton densities. Strong meandering meso-scale eddies created by the energetic ACC (Chelton et al., 2007) are thought to facilitate plankton accumulation (Godo et al., 2012) and retention times long enough to transfer energy to different trophic levels (Biggs, 1992;Riandey et al., 2005;Benitez-Nelson and McGillicuddy Jr, 2008), including fish (e.g. Nishimoto and Washburn, 2002;Zainuddin et al., 2006) and apex predators such as SESs (d'Ovidio et al., 2013). These advected water parcels are thought to sustain the pelagic ecosystem east of its origin and could explain the progressively eastward displacement of winter foraging seals. Elephant seals are known to feed opportunistically even while in transit to winter forging grounds (Thums et al., 2011). Continuous foraging during transit has previously been reported in several other pelagic predators that feed over extensive regions, including wandering albatross *Diomedea exulans* (Weimerskirch et al., 2005), leatherback turtles *Dermochelys coriacea* (Hays et al., 2006), southern bluefin tuna *Thunnus maccoyii* (Bestley et al., 2010). This foraging strategy allows animals to efficiently locate highly dispersed prey items or isolated patches of prey (Sims et al., 2006) while still making progress to know areas of higher prey abundance.

By combining information from predator behaviour and a concurrent plankton index (inferred from light measurements) we have developed a tool for describing the relationship between predators and biological activity in space and time, something which is crucial for understanding trophic links in the 3D marine environment. Because deep diving predators feed at depth future work will include separating sub-surface plankton (Guinet et al., 2013) distribution from surface values and comparing this information with predator foraging behaviour. It will also be important to test our findings at a finer resolution to see if these trends persist at the dive scale or whether seals are only responding to large scale features that coincide with elevated plankton densities (*e.g.* summer phytoplankton plumes, mesoscale eddies). Nonetheless, our results provide some insight into the possible foraging strategies used by a marine predator in response to different resource distributions between summer and winter.

3.6 Acknowledgements

We thank Michele Thums, Steve Wall and Corey Bradshaw for field assistance. We thank the Australian Antarctic Division for providing logistical support.

3.7 Appendix

Appendix S3.7.1

Mk6 – Mk8 tags used uncorrected watch crystals to measure time. They were offset to spread the time error (TE) over the likely range of seawater temperatures (T) (TE = $(1x10^{-5} – 3.5x10^{-8} x (T – 25)^2)$ x 10^6 ppm). Mk9 tags used a temperature correction algorithm to keep the time error within 1 ppm. Depth measurements were made by a pressure transducer calibrated by the manufacturer (± 6 m). Light values are converted on-board the logger via a log treatment (*see* figure S2.7.1) to compress the light measurements to a three digit value, thereby giving a linear relationship and increase the resolution at lower light levels. The light sensor is able to identify dawn/dusk events (for details see Sumner et al., 2009) down to 300 m in clear waters and is temperature-compensated for the entire light level range (Wildlife Computers). The wavelength at the centre of the light sensor parabolic-shaped pass-band filter is ~430 nm and consequently the sensor only reads the violet/blue light band (370 nm – 470 nm). All other bands of light are rejected and not measured. The light sensor measures on a scale of 20 readings per decade, so the light level error is considered to be $1/20^{th}$ of a decade. Tags also recorded temperature (± 0.1°C). The lag in temperature measurement (inherent in the design of the TDLRs) was accounted for (see Boyd et al., 1999;Bradshaw et al., 2002).

Appendix S3.7.2

All dive records were corrected for drift in the pressure sensor using a customised zero-offset correction routine (see Heerah et al., 2014). We then identified individual dive cycles; defined here as commencing from the first sub-surface record until the last surface interval of the subsequent post-dive surface interval. Only dives greater than 10 m were used in the subsequent analyses. A diagnostic check of these dive profiles was performed by visualising light-depth data to identify tag and/or sensor failure.

Appendix S3.7.3

To calculate the plankton density index (PDI), light data were first interpolated linearly between the non-regular series of depths to estimate light levels at 250 m for each dive (LL250). We used light levels recorded for both the descent and ascent phase due to sensor temporal resolution (i.e. 30 s intervals). The surface light level for each dive was estimated from the mean sub-surface light levels

in the top 10 m of the water column at the end of the ascent phase (LL0) (Jaud et al., 2012). Light levels above the surface (indicated by the wet/dry sensor on the tag) were excluded from LL_0 estimates. For each dive, LL_{250} was subtracted from LL_0 and divided by the depth (z) of LL_{250} (*i.e.* 250 m) to calculate the PDI:

$$PDI = \frac{LL_0 - LL_{250}}{z}$$

Appendix S3.7.4

We extracted sea ice data from daily satellite images (grid cell size of 25 km x 25 km) (Cavalieri et al., 2012, updated yearly). Light-depth dive profiles in regions with >20% sea ice coverage were excluded from analyses as ice cover may result in light attenuation biases. Sea ice data were also used to calculate the seasonal mean sea ice extent between 1999 and 2005. The sea ice extent was defined by the open ocean (i.e. ice-free pelagic region) – sea ice (> 50% concentration) interface.

Appendix S3.7.5

Importantly, the SSMs also fit multiple random walks to animal movement paths consisting of ordered sets of step lengths and turning angles to allocate two behavioural modes, (i) rapid and directional movement indicative of transit between foraging patches and (ii) comparatively slow and contorted movement indicative of area-restricted search (ARS) (Morales et al., 2004;Jonsen et al., 2005). The modelled behavioural mode is considered a useful proxy for identifying horizontal search intensity along an animal's track (Biuw et al., 2003). Importantly, intensive search behaviour does not necessarily indicate foraging success as some migrating pelagic predators – including wandering albatross *Diomedea exulans* (Weimerskirch et al., 2005), leatherback turtles *Dermochelys coriacea* (Hays et al., 2006), southern bluefin tuna *Thunnus maccoyii* (Bestley et al., 2010), as well as SES (Thums et al., 2011) – are thought to also target prey opportunistically while in transit.

Appendix S3.7.6

Dives with a long bottom time are presumed to represent foraging activity because the seals were expected to maximise the proportion of time spent at a particular depth where prey might be encountered (Schreer et al., 2001). However, travel between the surface and bottom of a dive is greater for deeper dives, meaning less time available to spend at the bottom. We therefore

calculated bottom time residuals (*BTr*) using multivariate linear regression between *bottom time*, maximum depth and total dive duration for each dive within a trip (Bailleul et al., 2008). Dives that included drift behaviour (classified visually, or when velocity is 0 m s^{-1} according to velocity sensors where available) were not included for calculating *BTr* because 'drift' dives have relatively long bottom times but do not involve active foraging behaviour (Dragon et al., 2012). Moreover, dives less than 50 m and/or 2 min were not considered foraging dives and were also excluded from *BTr* calculations. We then calculated the mean values of these residuals for each day. Positive residuals indicated dives with a longer *bottom time* than average for a given maximum dive depth and total dive duration, suggesting increased foraging effort. Conversely, negative residuals indicated a shorter *bottom time* than average and represented reduced foraging effort.

The bottom time residual method does not take into account variations in dive types displayed by SESs (Hindell et al., 1991a;Jonker and Bester, 1998). However seals exhibited dive behaviour predominately in the pelagic zone (see figure 1 in manuscript) and we therefore assume most dives to fall into one dominant dive type (i.e. deep diving square-shaped dives - Thums et al., 2008a).

Appendix S3.7.7

For some marine mammal species, including SESs, changes in relative proportions of lipid and lean body tissue (*i.e.* body condition) at sea can be detected as fluctuations in buoyancy via the rate of vertical passive drift when stationary in the water column (Webb et al., 1998). Drift rates have therefore been used as proxies for relative lipid content and thus foraging success in SESs while foraging at sea (Biuw et al., 2003;Bailleul et al., 2007;Biuw et al., 2007).

We used a hierarchical Bayesian state-space approach developed by Schick et al. (2013) to estimate daily lipid store for each individual while at sea. The model linked drift dive rates to lipid stores by quantifying daily changes in lipid stores as a function of the physiological condition of the seal. Where possible, swim speed readings ≤ stall speed of the velocity turbine were used to identify putative drift dives. Otherwise drift dives were identified from pre-determined drift dive characteristics (see Thums et al., 2008a). We acknowledge that identification in the absence of velocity data can result in some drift dives being missed or incorrectly identified. However, a validation of this classification technique found that misclassification of drift dives was only 2-4% (Thums et al., 2008a). We used the speed through the water column from drift dives (*i.e.* drift rate), as well as lipid estimates at deployment (*i.e.* start of trip) and upon recapture (*i.e.* end of trip) to

estimate daily changes in lipid mass (for further details see Schick et al., 2013). Lipid mass estimates at the start and end of a trip were calculated from mass, morphometric and back fat density measurements taken at deployment and recapture respectively (refer to *Procedures, Protocols and Notes for Elephant Seal Research on Macquarie Island*, https://data.aad.gov.au/aadc/tags for details of specific measurements recorded (Field et al., 2007)). However, not all necessary measurements were recorded for some of the individuals. In these instances we used linear models to examine the relationship between lipid estimates and available mass, morphometric and back fat density measurements to predict lipid mass estimates.

There is likely to be a temporal lag between prey capture and assimilation into the adipose tissue that effects and animal buoyancy. Rosen and Trites (2000) suggested the period between Steller sea lion (*Eumetopias jubatus*) prey ingestion and assimilation was approximately 4 days. Also see Thums et al. (2011); and Dragon et al. (2010) Linking foraging for SES examples. Foraging success is therefore considered as the daily changes of lipid storage that occur 4 days following prey capture events.

Table S3.7.1. Data Summary: year of tag deployment, deployment (post-breeding – PB; post-moult – PM); seal identification; data availability for each behavioural metric in this study.

			behavioural metrics		
year	**deployment**	**seal**	**behavioural state**	**dive effort**	**foraging success**
1999	PB	b362pb_99	√	√	√
1999	PB	b367pb_99	√	√	√
1999	PB	b568pb_99	√	√	√
1999	PB	b889pb_99	√	√	√
1999	PB	b900pb_99	√	√	√
1999	PB	b927pb_99	√	√	√
1999	PB	c023pb_99	√	√	√
1999	PB	c041pb_99	√	√	√
1999	PB	c060pb_99	√	√	NA
1999	PB	c790pb_99	√	√	√
1999	PB	c899pb_99	√	√	√
1999	PB	c933pb_99	√	√	√
2000	PB	b362pb_00	√	√	√
2000	PB	b533pb_00	√	√	-
2000	PB	b771pb_00	√	√	NA
2000	PB	b889pb_00	√	√	√
2000	PB	b900pb_00	√	√	√
2000	PB	c728pb_00	√	√	√
2000	PB	c790pb_00	√	√	√
2000	PB	c899pb_00	√	√	√
2000	PM	b569pm_00	√	√	√
2000	PM	b889pm_00	√	√	√
2000	PM	b900pm_00	√	√	√
2000	PM	c064pm_00	√	√	√
2000	PM	c217pm_00	√	√	√
2001	PM	b131pm_01	√	√	√
2001	PM	b362pm_01	√	√	√
2001	PM	b900pm_01	√	√	√
2001	PM	c064pm_01	√	√	√
2001	PM	c163pm_01	√	√	√
2002	PM	b279pm_02	√	√	NA
2002	PM	b650pm_02	√	√	√
2002	PM	c162pm_02	√	√	√
2002	PM	c200pm_02	√	√	√

2002	PM	c209pm_02	√	√	√
2002	PM	c217pm_02	√	√	NA
2002	PM	c312pm_02	√	√	√
2002	PM	c923pm_02	√	√	√
2004	PB	b889pb_04	√	√	√
2004	PB	c064pb_04	√	√	√
2004	PB	c090pb_04	√	√	√
2004	PB	c162pb_04	√	√	√
2004	PB	c312pb_04	√	√	NA
2004	PB	c790pb_04	√	√	NA
2004	PB	h285pb_04	√	√	√
2004	PM	b143pm_04	√	√	√
2004	PM	b347pm_04	√	√	√
2004	PM	b546pm_04	√	√	NA
2004	PM	b900pm_04	√	√	√
2004	PM	c064pm_04	√	√	√
2004	PM	c161pm_04	√	√	√
2004	PM	c162pm_04	√	√	√
2004	PM	c200pm_04	√	√	√
2004	PM	h233pm_04	√	√	√
2004	PM	h285pm_04	√	√	√
2004	PM	h833pm_04	√	√	√
2005	PM	f993pm_05	√	√	√
		n =	57	57	50

Chapter 4: Making the link using light collected by post-breeding elephant seals reveal trophic dynamics within the recurrent Kerguelen plume

---

Submitted as: O'Toole, M.D., Guinet, C., Lea, M.-A., and Hindell, M.A. (In Preparation). Making the link: light collected by post-breeding elephant seals reveal trophic dynamics within the recurrent Kerguelen plume. *Progress in Oceanography*.

4.1 Abstract

In open ocean ecosystems, meso-scale features such as frontal systems and eddies provide highly productive sites for species at all trophic levels. We used light sensors deployed on marine animals to estimate sub-surface plankton density and encounters with bioluminescent organisms, as well as accelerometry sensors to detect prey capture attempts along an animal's track. Information was collected by southern elephant seals from Isles Kerguelen to examine how the feeding behaviour of a deep-diving marine predator responds to biological activity within the 'Kerguelen plume' during summer. Bioluminescent prey encounter event ($Biolum_{PEE}$) rate drops as the seals move eastward towards the front of the Kerguelen plume, but increasing plankton density (as the seals approach the plume front) improve the seals' vertical access to their prey (via shading effect), buffering prey acquisition rate against the decreasing density of prey field. This may be the primary reason why post-breeding female seals are able to feed at a relatively constant rate throughout a major bloom event. A lack of data has previously hampered our understanding of pelagic ecosystem functions. Our approach reveals biological interactions between elephant seals and lower-trophic-level organisms, and gives insight into how this important marine predator utilises a major recurrent plume in the Southern Ocean.

4.2 Introduction

Resources in the marine environment tend to be patchily distributed, and are clumped rather than distributed randomly or systematically; a feature of many, if not all, natural environments (Hoelzel, 2009). A predator, which forages over a range of scales, must locate continuously changing prey field patterns, and respond to a complex heterogeneous environment at different scales (Russell et al., 1992). As data on prey resources are often limited, lower trophic levels (phytoplankton) which can be inferred from remote sensing sources (surface chlorophyll) have been widely used to characterise habitat quality (e.g. Guinet et al., 2001;Ware and Thomson, 2005;Vilchis et al., 2006). However, it is unclear how the complex meso-scale distribution of phytoplankton influences the multiple trophic links within the ecosystem, particularly the link between higher predators and their meso-pelagic prey (*i.e.* where and how much prey is eaten). Jaquet et al. (1996) attempted to correlate chlorophyll concentration with sperm whale distribution at different scales, but found no relationship. Guinet et al. (2001) showed that diving activity of fur seals was negatively related to near-surface chlorophyll concentration at a small spatial scale, but was positively related at a larger scale. Satellite-derived

chlorophyll is commonly used in studies of this nature, but are often patchy and the relatively coarse spatial resolution (8 km x 8 km) may likely limit small scale analysis.

This has prompted alternative approaches for measuring *in situ* plankton concentrations within an animal's range. Animal-borne fluorometers used to record chlorophyll simultaneously with animal movement (Guinet et al., 2013), but often have limited memory capacity and short battery life, which hinder application in large-scale studies (although this is changing due to recent developments in technology, see Guinet et al. (2013)). Light measurements recorded by time-depth recorders (TDRs) have provided an acceptable alternative method for measuring the bio-optical properties of the water column to infer plankton density in the water column (Teo et al., 2009;O'Toole et al., 2014b). Foraging behaviour of elephant seals (trends in movement and mass gain across their entire trip at sea) from Macquarie Island was positively correlated with an index of plankton density at the daily scale, regardless of the time of year (*see* chapter 3). However, without multi-scale data (*e.g.* dive-scale and meso-scale), including information regarding prey encounter events (PEE), the function of this effect remains elusive.

Past telemetry studies have already revealed important relationships between the foraging behaviour of deep-diving marine animals and the physical environment (e.g. Bradshaw et al., 2004;Dragon et al., 2010;Heerah et al., 2013). For example, physical parameters (such as temperature and salinity) used to identify meso-scale eddies (features characterised by elevated productivity) are known to coincide with elephant seal foraging activity (Bailleul et al., 2010b;Dragon et al., 2010). However, these studies did not quantify biological activity associated with these patches, and furthermore, often used animal movement behaviour to infer foraging success (*e.g.* bottom time residuals, (Bailleul et al., 2010b)). Advances in bio-logging technology now provide much finer-scale intra-dive information using 3-axis accelerometry to measure body lunges indicative of likely PEE (Naito, 2007;Naito et al., 2010;Viviant et al., 2010;Gallon et al., 2013). These data, coupled with an *in situ* light-based plankton index may provide valuable information about the spatio-temporal interaction between top predators and lower-trophic levels. Satellite-mounted colour sensors infer chlorophyll in the upper 30 m of the water column, though deep chlorophyll maxima (DCM) can be more than 30% of that of surface values in some regions (Guinet et al., 2013). These sub-surface conditions may be more relevant to deep-diving predators and can be inferred from light levels recorded along the dive profile of the seal (Teo et al., 2009;O'Toole et al., 2014b). Moreover, estimates of prey density have also been derived from on-board light records by detecting the number of bioluminescent prey encounter events ($Biolum_{PEE}$) by elephant seals

(Vacquié-Garcia et al., 2012). Utilising these data could allow us to disentangle important biological interactions in the vertical dimension of the water column.

The predominately low-phytoplankton conditions of the Southern Ocean are interspersed by regions of elevated phytoplankton biomass, including a large plume that extends for 1500 km downstream of the Isles Kerguelen in the Indian sector of the Southern Ocean (Blain et al., 2013). The dynamics of these plankton blooms are largely controlled by the mixed-layer macronutrient inventory (Blain et al., 2007;Boyd et al., 2007), light availability and the mixed-layer depth (Mitchell et al., 1991;de Baar et al., 2005), as well as grazing pressure from zooplankton (Smetacek et al., 2004). The Polar Front plays a critical role in the annually recurrent Kerguelen plume by facilitating the advection of iron-rich waters from the Kerguelen plateau (Blain et al., 2007;Bown et al., 2012) and dispersion via strong regional meso-scale eddy activity in the open ocean (Kostianoy et al., 2003;Langlais et al., 2011;Park et al., 2014). Work from the recent KEPOPS2 cruise east of the Kerguelen plateau showed that zooplankton grazing may dominate marine processes later in the season (Jouandet et al., 2011) when primary production is more likely to reach higher trophic levels. Moreover, phytoplankton blooms often influence zooplankton and fish larvae (Henson et al., 2009), rather than adult fish species, and we expect a spatial and temporal lag between lower and upper trophic levels.

Southern elephant seals (*Mirounga leonina*), an important Southern Ocean predator (McConnell et al., 1992), spend most of their life cycle at sea, continuously diving to an average of 500 m (Campagna et al., 1999;McIntyre et al., 2010) to feed predominately on small mesopelagic fish (Cherel et al., 2008). These deep-diving predators must return repeatedly to the surface to breathe, and can therefore be studied under the framework of central-place foraging (Orians and Pearson, 1979) with the surface acting as the central place (Houston and McNamara, 1985). A major assumption is that central-placed foragers will make a decision so as to maximise the net rate of energy intake during a foraging bout (Charnov, 1976). As central-place foragers, diving predators should increase their energy gain to compensate for travel costs as distances to food increases (Mori, 1998). Following the breeding season, most female elephant seals from Kerguelen spend 2-3 months (October – December/early January) feeding in the vicinity of the Kerguelen plume (e.g. Dragon et al., 2012). How marine predators utilise the seemingly homogeneous plume environment to maximise prey intake rate is still not well understood (Cotté et al., 2014). We use multi-year records of light-depth data collected by female elephant seals from Iles Kerguelen to identify planktonic conditions, as well as $Biolum_{PEE}$, during their post-breeding foraging trip at sea. Coupled with accelerometry data used to detect PEE, we examined the feeding behaviour of elephant seals within a major

recurrent plume downstream of the Kerguelen Plateau. Our primary objectives included: 1) identifying distinct meso-scale patches of plankton within different layers of the euphotic zone; 2) examining how patterns of plankton density vary with seal behaviour and prey encounter rates (PEE and $Biolum_{PEE}$) at different scales; and 3) proposing an underlying function of planktonic variability in relation to seal foraging strategy in a dynamic plume system.

4.3 Method

4.3.1 Deployment and tag specifications

Fieldwork and data collection were undertaken with approval from IPEV (Institut ploaire francais Paul Emile Victor) and TAAF (Terres Australes et Antarctiques Francaises) animal ethics committee. Thirty-eight female SES were captured at Iles Kerguelen (49°20´S, 70°20´E) during October/November prior to their post-breeding trip from 2010 and 2013 (table 4.1). The seals were approached by foot and temporarily restrained with a head bag and anaesthetised intravenously with a 1:1 mixture of Tiletamine and Zolazepam (0.5 mg kg^{-1}) (McMahon et al., 2000;Field et al., 2002). All seals were equipped with either a GPS logger (n=23) or an Argos transmitter (n=14) (SPLASH10-Fast-Loc GPS/Argos, Wildlife Computers), in addition to a time-depth and accelerometer data logger (MK10-X or TDR10-Daily Diary, Wildlife Computers). Devices were attached to the head (except for TDR10-Daily Diary tags that were attached to the dorsal midline between the scapulae) using a two-component industrial epoxy (Araldite AW 2101) (Hindell and Slip, 1997). Seals were observed during recovery from anaesthesia and allowed to enter the water when no longer sedated. Data loggers were retrieved by repeating the above restraint procedures at the end of the 2 – 3 month foraging trip once the seal had hauled out on land. The tracking devices/data loggers or attachment method did not adversely affect individual performance and fitness over the short (seal growth) or long (seal survival) term (McMahon et al., 2008).

GPS locations were sampled every 20 minutes to maximise the chance of locations coinciding with each surface interval (see Guinet et al., 2014) and the frequency of Argos location depended on the number of available uplinks (generally between 4 to 14 locations per day) . Time-depth recorders (MK10, SPLASH10 TDR and TDR10-Daily Diary) recorded time at a resolution of 16 Hz, and depth (0 – 1500 m, ± 1 m) and light levels (5 x 10^{-2} W cm^{-2} to 5 x 10^{-12} W cm^{-2} in blue wavelength) every 1 s. Acceleration was recorded in 3 axes at 16Hz. Tags do suffer from temporal drift, though its affect is considered negligible because accelerometers only record over a relatively short period of time (*e.g.*

tags drift less than 2 s and 6 Hz over a 2 month period, per. comm. Baptiste Picard). Depth measurements were made by a pressure transducer calibrated by the manufacturer (± 1 m). Light level values (W cm^{-2}) were converted using on-board logarithmic conversion algorithms (per. comm. Wildlife Computers) to compress the light measurements to a 3 digit value, and increase the resolution at lower light levels. The light sensors were able to identify dawn/dusk events (for details see Sumner et al., 2009) down to 300 m in clear waters and were temperature-compensated for the entire light level range (per. comm. Wildlife Computers). The wavelength at the centre of the light sensor parabolic-shaped pass-band filter is ~430 nm and consequently the sensor only read the violet/blue light band (370 nm – 470 nm). All other bands of light were rejected and not measured. The light sensor measured on a scale of 20 readings per decade, so the light level error is considered to be 1/20^{th} of a decade.

4.3.2 Data processing

4.3.2.1 Dive profile

All dive records were corrected for drift in the pressure sensor using a customised zero-offset correction routine (see Heerah et al., 2014). We then identified individual dive cycles; defined here as commencing from the first sub-surface record until the last surface record of the subsequent post-dive surface interval. Only dives deeper than 15 m were used in the subsequent analyses. Each dive was divided into a descent, ascent and bottom phase; the bottom phase corresponding to the period between the seal first reaching 80% of the maximum dive depth threshold and when the seal last swims above this threshold (figure 4.1). In this study the diving depth was defined as the mean depth during the bottom phase of the dive.

Table 1. Data summary: seal identification, trip start and end dates in the pelagic zone; total trip duration in the pelagic zone; number of dives performed during the day in the pelagic zone; and data availability recorded for the trip[†].

Seal ID	Start	End	Trip duration (days)	No. of dives	Full trip[†]
2010-18	30-Oct-10	21-Dec-10	52.3	1554	√√
20110-19	8-Nov-10	8-Jan-11	60.6	2078	√√
2010-21	23-Nov-10	1-Feb-11	70.5	2550	√√
2011-14	27-Oct-11	5-Nov-11	9.1	335	--
2011-16	28-Oct-11	5-Nov-11	8.5	295	√-
2011-18	30-Oct-11	9-Nov-11	10.5	436	√-
2011-21	31-Oct-11	21-Dec-11	51	2090	√-
2011-26	2-Nov-11	26-Dec-11	54.4	1894	√-
2011-27	2-Nov-11	13-Nov-11	11.5	428	√-
2011-28	2-Nov-11	24-Dec-11	52.2	1897	√-
2012-11	4-Nov-12	26-Nov-12	22.2	822	--
2012-14	3-Nov-12	29-Nov-12	25.9	842	--
2012-15	4-Nov-12	25-Nov-12	21.3	747	--
2012-16	4-Nov-12	26-Nov-12	22.4	736	--
2012-17	4-Nov-12	27-Nov-12	23.2	841	--
2012-1	29-Oct-12	20-Nov-12	22.5	839	√-
2012-2	4-Nov-12	23-Nov-12	19.1	622	√-
2012-4	30-Oct-12	20-Nov-12	21.2	720	√-
2012-6	1-Nov-12	21-Nov-12	20.4	688	√-
2012-9	9-Nov-12	10-Dec-12	31.1	1139	√-
2013-1	30-Oct-13	23-Nov-13	24.2	868	√-
2013-10	3-Nov-13	8-Dec-13	35.3	7813	--
2013-11	1-Nov-13	10-Dec-13	39.5	1029	--
2013-12	2-Nov-13	23-Nov-13	21.6	675	--
2013-13	1-Nov-13	23-Nov-13	22.6	887	--
2013-18	3-Nov-13	26-Nov-13	23.6	787	--
2013-2	3-Nov-13	22-Nov-13	18.9	663	√-
2013-3	1-Nov-13	21-Nov-13	20.5	733	√-
2013-4	1-Nov-13	16-Nov-13	15.5	542	√-
2013-5	30-Oct-13	15-Nov-13	16.3	682	√-
2013-6	31-Oct-13	15-Nov-13	15	616	√-
2013-7	31-Oct-13	25-Nov-13	25.6	949	√-

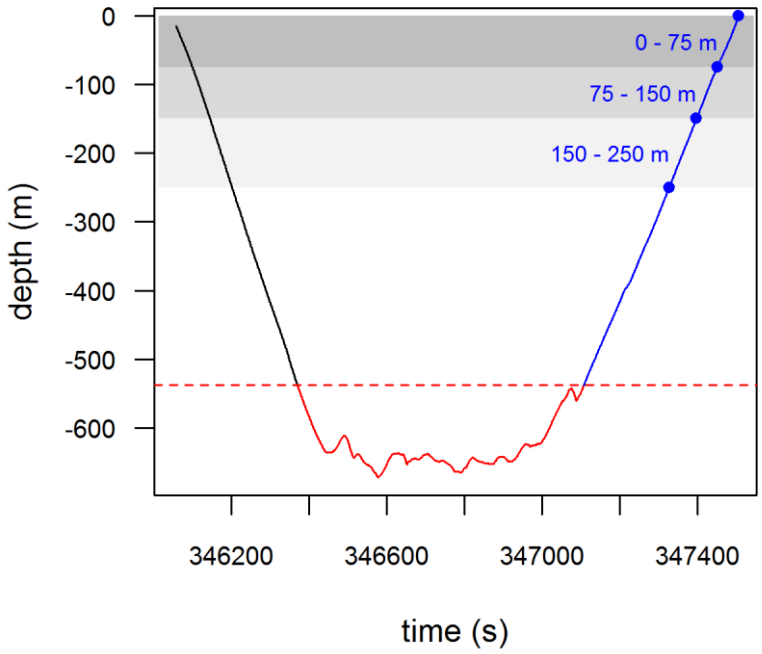

Figure 4. 1. An example of a time-depth (dive) profile extracted from the 2010-18 TDR dataset. The dive profile is divided into 3 phases: descent (black); bottom (red); and ascent (blue). Light level estimates were calculated at 0 m, 75 m, 150 m and 250 m (blue points) during the ascent phase and used to calculate the integrated light attenuation of each depth band [0 – 75 m, upper euphotic (dark grey); 75 – 150 m, lower euphotic (grey); 150 – 250 m, below euphotic (light grey)]. The red dashed line represents the 80% maximum dive depth threshold. Time is given in seconds since the beginning of the trip.

4.3.2.2 Post-location processing

GPS location estimates were up to 5 times greater more frequent than Argos, and location error seldom exceeded a few tens of kilometres (worst-case scenario) (Lopez et al., 2014). Argos measurements were associated with varying classes of error and were processed using a multiple-model Kalman filter (Lopez et al., 2014). Kalman-smoothed Argos locations were provided at the time of each original Argos location. Tracks were interpolated from either GPS or Argos locations and each dive was given a geographical coordinate based on its position in time along the track.

4.3.2.3 Extracting pelagic dives

Female southern elephant seals mainly feed in oceanic waters (but also over the Kerguelen Plateau and Antarctic shelves). We focused on the pelagic phase of the tracks by excluding data associated with shelf waters of the Kerguelen and Crozet plateaux (*i.e.* < 1000 m) where seals are known to perform benthic dives, and therefore utilise a different food-web. Water depth at each seal location was extracted by merging location data with bathymetric data derived from National Geophysical Data Centre ETOPO2 Global 2 Elevations (www.ngdc.noaa.gov/mgg/global/etopo2.html).

4.3.3 Biological indices

Light data from electronic tags deployed on marine animals can be used to measure the bio-optical properties of the water column (McCafferty et al., 2004). This information can help infer aspects of biological activity encountered by the tagged individual at depth, including plankton density and distribution as well as the presence of bioluminescent prey. A visual check of light-dive profiles was performed to identify tag and/or sensor failure.

4.3.3.1 Plankton index at depth

Ambient light is attenuated throughout the water column due to physical properties of the seawater, but also because of the quantity of inorganic and organic particulates suspended in the water column (Morel and Maritorena, 2001). The Southern Ocean is typically characterised by Case I waters, whereby phytoplankton are the main source of particles suspended within the euphotic zone (Morel and Prieur, 1977;Morel and Maritorena, 2001), and is consequently the main cause of light attenuation if we assume that coloured dissolved organic matter (CDOM) and detritus degradation products covary with phytoplankton (Bricaud et al., 1981) and physical properties are constant (Bricaud et al., 1998). We would expect the presence of higher trophic organisms such as zooplankton to also influence light attenuation to some extent (Teo et al., 2009;O'Toole et al., 2014b). Consequently, light data collected during daylight hours by marine animals can provide a useful index for plankton density (including phytoplankton and zooplankton) (Teo et al., 2009;Guinet et al., 2013;O'Toole et al., 2014b) and have revealed seasonal trends typical of Southern Ocean productivity south of Iles Kerguelen and Macquarie Island (Jaud et al., 2012;O'Toole et al., 2014b). However, because the sensitivity of the on-board light sensors is reduced at 300 m (per. comm

Wildlife Computers) we only considered light levels within the top 250 m of the water column. Furthermore, only light levels recorded during the ascent phase were used to minimise bias towards low light levels due to body roll observed during the descent and bottom phase (Sala et al., 2011). Within each dive, light levels were interpolated linearly between the non-regular series of depths to estimate light levels at 75 m, 150 m and 250 m. In addition, light levels recorded during the post-dive surface interval (in the upper 10 m) were averaged to estimate the light level at 0 m. Light level estimates were used to calculate the light attenuation within three different depth bands (LA_d) of each dive: 0 – 75 m (upper euphotic zone); 75 – 150 m (lower euphotic zone); and 150 – 250 m (below euphotic zone) (figure 1) using a simple equation where LL_{z1} and LL_{z2} represent the upper and lower light level estimates of a given depth band respectively; and $\triangle z$ represents the depth difference between the upper and lower depth boundary:

$$LA_d = \frac{(LL_{z1} - LL_{z2})}{(\Delta\, z)}$$

Integrated light attenuation values were used as an index of plankton density within each depth band: upper euphotic zone (P_{upper}), lower euphotic zone (P_{lower}), below the euphotic zone (P_{below}). However, we needed to consider two important factors that affect our estimates of plankton density. First, negative light attenuation values were removed from further analysis as these were likely an artefact of low light level conditions or encounters with bioluminescent events during the ascent phase (for details see appendix S4.7.1). Second, the rate of sun angle change throughout the day is thought to influence light attenuation values calculated from animal-borne data (Teo et al., 2009). Daytime dives were identified by calculating its corresponding solar angle (above the horizon, 0°), based on time and Argos/GPS location, using the R package *tripEstimation* (function astro, Sumner and Wotherspoon, 2014). If the ambient light field is rapidly changing, any change in the light profile might reflect ambient light field changes rather than light attenuation. This is particularly true for light profiles recorded around dawn and dusk (solar angle between 0° and 7° above the horizon). Light attenuation estimates within each depth band were tested for any significant relationship with sun angle (relative to midday sun angle) by grouping values into 10 sun angle bins using analysis of variance. We found that the time of day (as indicated by sun angle) significantly influenced light attenuation estimates within the upper euphotic zone ($F_{1,22496}$=273.8, $p < 0.0001$), but not within the

lower euphotic zone or the depth band below the euphotic zone (see output from analysis of variance models in appendix S4.7.2).

4.3.3.2 Bioluminescent prey encounter events ($Biolum_{PEE}$)

Sudden peaks in ambient light levels at depths below 550 m during the day can be used to detect $Biolum_{PEE}$ along the dive path of the seals (for details see Vacquié-Garcia, In Preparation). We used the *IDPmisc* R package (function peaks, Locher et al., 2012) to identify all peaks in the light data. This function detects all anomalies in the light data, even those that are very low. Moreover, because of light sensor precision (per. comm. Wildlife Computers) any light level anomaly values less than 2 could not be accurately considered a bioluminescent event. Consequently, only light anomalies with a minimum of 3 light level values were used in this study (add term "miniPH=3" to "peaks" function).

4.3.4 Prey encounter events (PEE)

Data from the accelerometers were processed according to Viviant et al. (2010) and Gallon et al. (2013) using custom-written MATLAB code (available on request). Individual feeding events were detected within accelerometry data using procedures outlined in Guinet et al. (2014). The steps in this procedure include (1) a high-pass filter of the 3-axis accelerometer time series to remove noise due to swimming movement and (2) identifying significant accelerations along each axis time series (summed to 1 s resolution). Only movement events that could be detected simultaneously on the 3 axes were considered as true PEE; others were considered to correspond with transit activity within the dive. It is possible that a head lurch could be detected by variability along only one axis; however, we thought it best to take a conservative approach and only consider significant lunge events that involve head/back movements along all three axes. Movement events (or PEE) were detected either from head- (MK10-X) or back-mounted (Daily Diary tags) devices; detection of PEE using data from either device is consistent with one another (C. Guinet unpublished data). PEEs separated by periods longer than 1 s were considered independent PEE. The number of PEEs was determined for each dive and its bottom phase. Detecting PEEs using accelerometry data does not necessarily reflect a true feeding event (Watanabe and Takahashi, 2013), and for this study, is instead considered as a relative index of prey encounter during the dive.

The number of PEEs recorded within a dive was used to calculate the PEE per unit of time (PEE rate) during the bottom phase of the dive where elephant seals are thought to perform most of their foraging activity (Heerah et al., 2014). We do not consider the PEE rate for the total dive because vertical transit time between the surface and bottom phase of the dive will vary depending on dive depth. Deeper dives will mean less time spent at the bottom of the dive where most PEE are expected to occur and could artificially reduce PEE rate.

4.3.5 Defining meso-scale patches of plankton (high- verses low-density)

To identify meso-scale patches a cubic smoothing spline (a simple linear monotonic model) was fitted to the time series of plankton data at each depth band for each trip using the R software package *stats* (R Developmemt Core Team, function smooth.spline; R Development Core Team, 2014). The number of knots applied to this function was based on the total number of days spent in the oceanic zone divided by 4 days. The 4 day interval was used as this is the approximate time taken for an elephant seal to pass across a meso-scale feature (~ 300 km) if we assume the average daily horizontal displacement of a seal is 75 km day^{-1} (average daily displacement of focal seals was 62 ± 42 km day^{-1}). We then identified dives associated with each trough and peak value encountered along each trip. Each peak event, which we considered to be a high-density patch, included all dives bound by the adjacent troughs with predicted plankton values greater than 75 percent of the peak predicted plankton value; all remaining dives were grouped into low-density patches (*e.g.* figure 4.2A and figure 4.2B). Incomplete trip datasets were excluded from analysis.

4.3.6 Statistical analysis

We fitted linear mixed-effect models (LMMs) using the R software package *nlme* (R Development Core Team, function `lme`, Pinheiro 2012) following the steps described in Zuur et al. (2010) to examine interactions between seal feeding behaviour, $Biolum_{PEE}$ and plankton density at multiple scales (meso- and dive-scale). Variables were transformed, where necessary, prior to analyses to correct for non-Gaussian distributions. All models were tested for the inclusion of the random intercept term (*seal*), the random slope term (to account for individual light sensor differences), an autocorrelation term, as well as the removal of fixed and interaction terms in accordance with model selection procedures outlined in Zuur et al. (2009).

4.3.6.1 Meso-scale

We tested the relationship between the seals' distance from the colony (*i.e.* Iles Kerguelen) and the plankton density of meso-scale patches within each layer of the euphotic zone (*i.e.* P_{upper}, P_{lower}, P_{below}). We then tested how PEE rate was influenced by the plankton density of meso-scale patches within each layer of the euphotic zone, as well as $Biolum_{PEE}$ rates, at the meso-scale. $Biolum_{PEE}$ rates were also tested against meso-scale patches within each layer of the euphotic zone. All models at the meso-scale considered patch type as a 2-level fixed term (high- or low-density), maximum dive depth as a 5-level fixed term (100 m depth intervals between 400 m and 800m) and their interaction effects.

4.3.6.2 Dive-scale

We tested how PEE rate was influenced by the plankton density within each layer of the euphotic zone and $Biolum_{PEE}$ rates at the dive-scale. PEE rate was compared with these dive conditions within the focal dive (d_0), but also with the dive conditions encountered in up to 5 dives prior to- and following the focal dive (d_{-5}, d_{-4}, d_{-3}, d_{-2}, d_{-1}, d_{+1}, d_{+2}, d_{+3}, d_{+4}, d_{+5}) to test if trends could be detected beyond the focal dive (*i.e.* when does plankton density influence begin and end at the dive-scale?). Preliminary analysis showed that some dives did not coincide with any PEE or $Biolum_{PEE}$. Indeed, elephant seals will continue to exhibit high foraging activity in the absence of $Biolum_{PEE}$ as their diet also consists of non-bioluminescent species (Vacquié-Garcia et al., 2012 and references within). However, we could not use zero-inflated Poisson or negative binomial models because the response variable was not count data, but rather a rate. Consequently, model analysis at the dive-scale was performed using two different data sets: (1) dives associated with PEE activity; and (2) dives associated with PEE and $Biolum_{PEE}$. The influence of $Biolum_{PEE}$ rate was not tested using data set 1. Dive-scale models that considered P_{upper} also included sun angle (relative to midday sun angle) as a random slope term to account for the influence of sun angle on light attenuation estimates.

Finally, we wanted to test the relationship between maximum dive depth and plankton density within each layer of the euphotic zone. However preliminary results showed that maximum dive depth increased significantly with distance from the colony (appendix S4.7.3), thereby potentially confounding the relationship between maximum dive depth and plankton density. Consequently, we

tested the relationship between maximum dive depth and plankton density at the dive-scale within meso-scale patches encountered by seals (1) at the beginning of their migration (*i.e.* patches closest to the colony) and (2) when furthest from the colony.

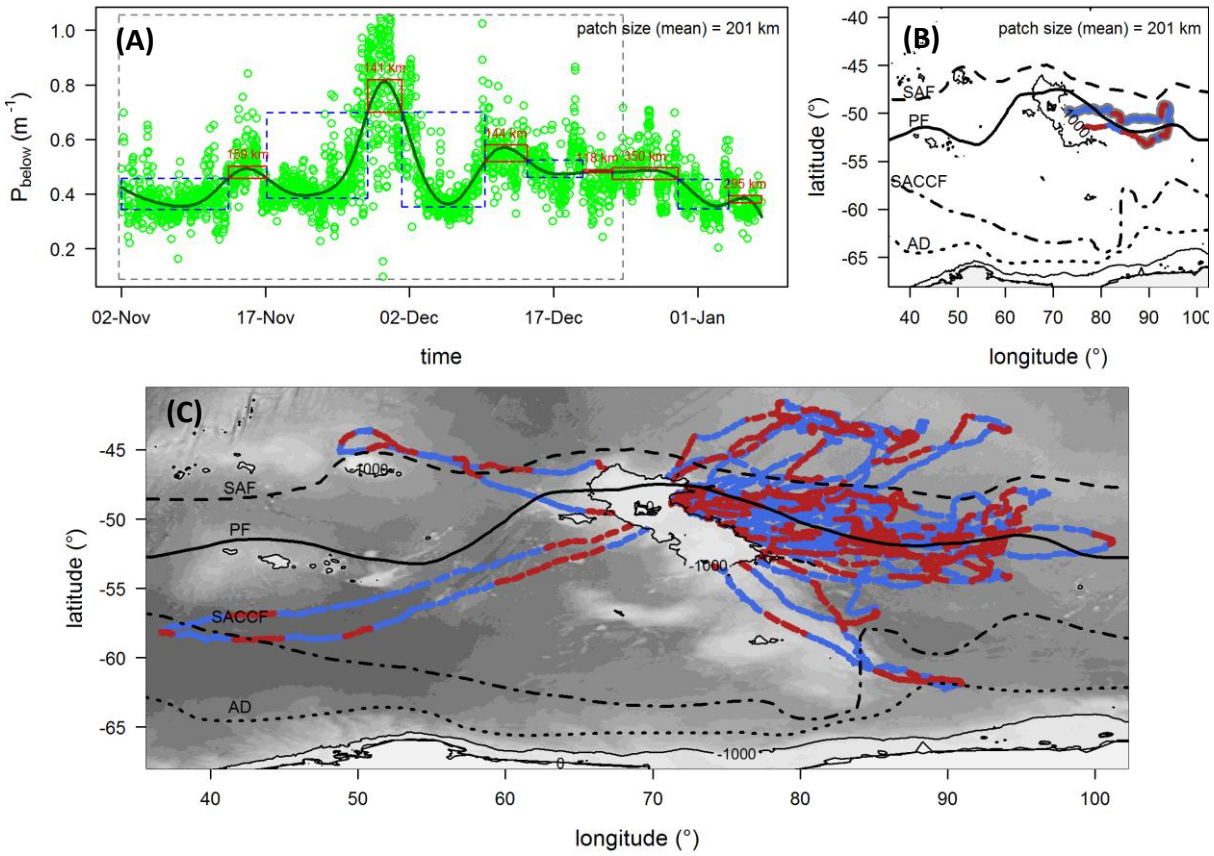

Figure 4.2. Meso-scale patches of high-density (red) and low-density (blue) plankton in the upper euphotic zone: (A) an example of a smoothing function applied to plankton values from seal 2011-28 reveals temporal plankton patterns (red and dashed blue boxes encompass high-density and low-density plankton patches respectively) encountered during the trip; (B) high-density (red) and low-density (blue) plankton patches, and dives that coincided with prey capture records (grey) were mapped spatially, along the seal's track; and (C) all 14 complete seal tracks coinciding high-density and low-density plankton patches. The spatial scale of each high-density patch (at the top of each red box) and the average is shown in the top left plot. Records of prey capture rates are delineated by the dashed grey box in the top left plot. Frontal structures are shown from north to south: Subantarctic Front (SAF, dashed); Polar Front (PF, solid); Southern Antarctic Circumpolar Current Front (SACCF, dot-dashed); and Antarctic divergence (AD, dotted). The Kerguelen and Antarctic shelf

areas are considered from the coast to the 1000 m depth isobath. Meso-scale patches of plankton in the lower euphotic zone and below the euphotic zone are shown in appendix S4.7.5-S4.7.7.

4.4 Results

We used data from 33 of the 38 southern elephant seal female deployments between 2010 and 2013. Five deployments were excluded due to either light or depth sensor failure. Of the deployments retained in this study, three recorded time, depth, light and accelerometer data for the entire trip; nineteen recorded time, depth and light data for the entire trip and accelerometry data for part of the trip; and eleven recorded time, depth, light and accelerometry for part of the trip (table 4.1; see maps of recorded data in appendix S4.7.4). In total, tag deployments recorded 53918 dive profiles during daylight hours (*i.e.* sun above horizon); of which less than 2% were removed (1.02% shelf dives, 0.02% drift dives, and < 1% dives corresponding with negative light attenuation values). Of the remaining dive profiles, 23156 dive profiles contained concurrent accelerometry data. The number of dives associated with PEE (*i.e.* PEE rate > 0) was approximately 80% of dives with accelerometry records. However, less than 9% of these dives were associated with $Biolum_{PEE}$.

Most seals (n=25) travelled eastward within the Polar Frontal Zone (PFZ) and along the southern edge of the Polar Front, and another five seals travelled north-east from Kerguelen to the Subantarctic Zone (SAZ) (figure 4.2C). Three seals travelled well beyond the Kerguelen plume site: one north-west toward Crozet Island; one south-west toward the southern Antarctic Circumpolar Current Front (SACCF); and one south-east toward the SACCF (figure 4.2C).

4.4.1 Meso-scale trophic interactions

PEE information coincided with all meso-scale plankton patches for only three of the twenty-two trips included in the meso-scale analysis. For the remaining eighteen trips, patches coincided with PEE information only during the outward phase of the trip, until the seal reached the distal end of its foraging trip. Fitted light attenuation values from our cubic smoothing analysis revealed multiple meso-scale patches along seal tracks (figure 4.2C*;* for individual plots for each layer of plankton see appendix S4.7.5-S4.7.7). Meso-scale plankton densities in the upper euphotic zone increased with distance from the Iles Kerguelen (*i.e.* values peaked at the distal end of a seal's trip) (figure 4.3), although no trend was found between the distance from the colony and plankton densities in the lower euphotic zone, below the euphotic zone or PEE rate (table 4.2). However, PEE rates were

positively related to the P_{upper} and P_{lower} of meso-scale patches; though no clear trend existed as seals maximum dive depth exceeded 500 m (figure 4.4, table 4.3). Prey encounter event rates did not respond significantly to plankton density below the euphotic zone or $Biolum_{PEE}$ rates at the meso-scale (terms were not retained in the final model, table 4.3). Models that tested the relationship between PEE rate and meso-scale conditions did not retain either patch type (high- and low-density) or its interaction effect (see model rankings in appendix S4.7.8).

Finally, $Biolum_{PEE}$ rates were inversely related to P_{upper} and P_{below} irrespective of patch type, and to the P_{lower} of high-density plankton patches, though not the P_{lower} of low-density plankton patches (figure 4.5, table 4.4). This is because a relatively weak interaction term between P_{lower} and patch type was retained in the final model based on P_{lower} dive conditions (table 4.4). This same model also retained an interaction term between patch type and maximum dive depth that showed $Biolum_{PEE}$ rate in low-density plankton patches (*i.e.* surrounding waters) dropped significantly when seal maximum dive depth was above 500 m (figure 4.6).

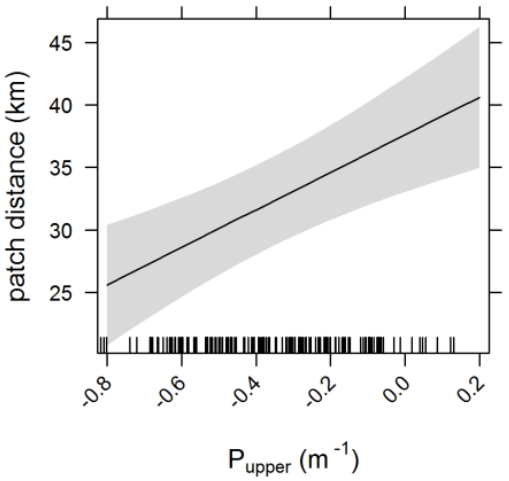

Figure 4.3. Distance from the colony (*i.e.* Isles Kerguelen) in response to the plankton density of meso-scale patches within the upper layer of the euphotic zone (P_{upper}). Shaded area indicates the confidence interval.

Table 4.2. Coefficient values of dive conditions and prey encounter event (PEE) rate from models at the meso-scale. Coefficients derived from the most parsimonious linear mixed-effects models relating distance from the colony to plankton density within different layers of the euphotic zone (P_{upper}, P_{lower}, P_{below}), and prey capture rate. Term coefficients are presented ± SE and *p*-values for each coefficient are also shown.

dive conditions	**intercept**					**explanatory**				
	coefficients	**SE**	***df***	***t*-value**	***p*-value**	**coefficients**	**SE**	***df***	***t*-value**	***p*-value**
P_{upper}	37.61	2.31	142	16.21	< 0.0001	15.01	3.88	142	3.86	0.0002
P_{lower}	27.66	7.38	138	3.74	0.0003	-4.93	8.15	138	-0.60	0.546
P_{below}	37.12	10.31	139	3.59	0.0004	3.15	7.93	139	0.397	0.6916
PEE rate	22.20	5.92	143	3.74	0.0003	1.65	1.00	143	1.63	0.1032

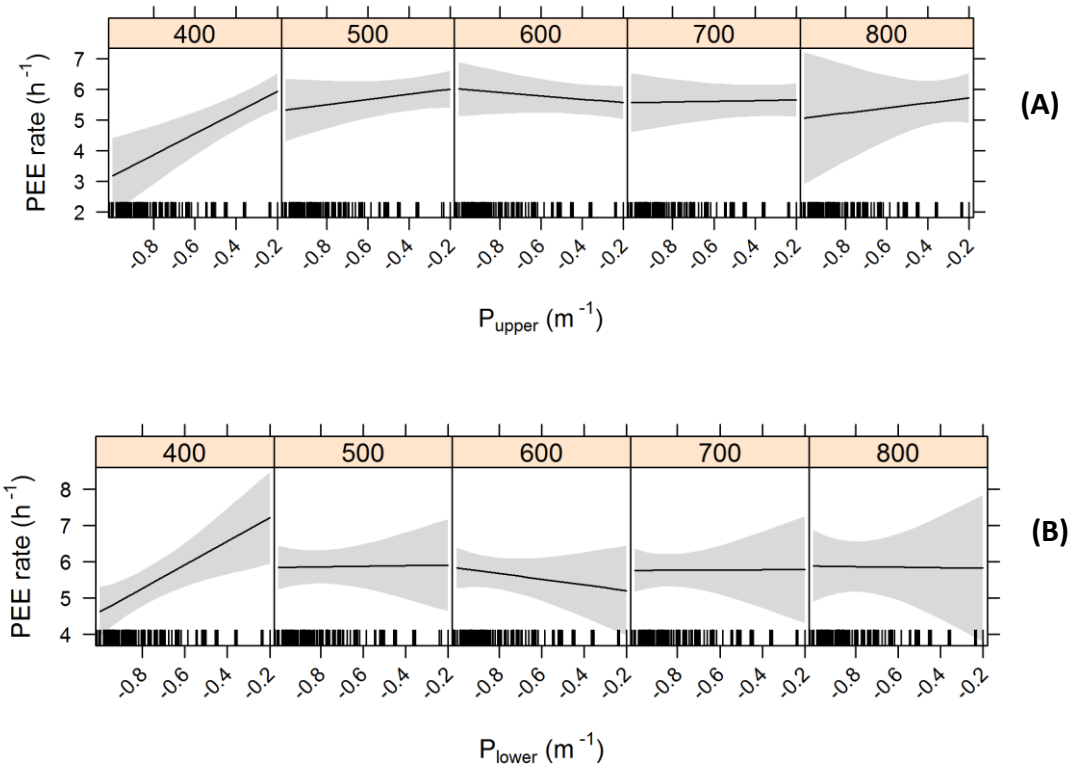

Figure 4.4. Prey encounter event (PEE) rate in response to the plankton density of meso-scale patches within the (A) upper and (B) lower layer of the euphotic zone (P_{upper} and P_{lower} respectively) according to the maximum dive depths performed within meso-scale plankton patches (grouped in 100 m depth bins from 400 to 800 m). Shaded area indicates the confidence interval.

Table 4.3. Coefficient values of dive conditions from models at the meso-scale. Coefficients are from our most parsimonious linear mixed-effects models relating prey capture rate to plankton density within different layers of the euphotic zone (P_{upper}, P_{lower}, P_{below}) and bioluminescent prey encounter (BPEE) rate, as well as seal maximum dive depth (depth) and interaction terms. Term coefficients are presented ± SE and *p*-values for each coefficient are also shown.

dive conditions		**coefficients**	**SE**	***df***	***t*-value**	***p*-value**
P_{upper}	(Intercept)	6.62	0.40	130	16.52	< 0.0001
	P_{upper}	3.45	0.85	130	4.04	< 0.0001
	depth (500)	-0.45	0.42	130	-1.07	0.2866
	depth (600)	-1.17	0.43	130	-2.74	0.0071
	depth (700)	-0.95	0.44	130	-2.18	0.0308
	depth (800)	-0.74	0.69	130	-1.07	0.2859
	P_{upper} : depth (500)	-2.60	0.98	130	-2.65	0.0089
	P_{upper} : depth (600)	-4.00	0.97	130	-4.11	< 0.0001
	P_{upper} : depth (700)	-3.34	1.02	130	-3.29	0.0013
	P_{upper} : depth (800)	-2.63	1.78	130	-1.48	0.1417
P_{lower}	(Intercept)	7.89	0.59	117	13.31	< 0.0001
	P_{upper}	3.27	0.73	117	4.45	< 0.0001
	depth (500)	-1.73	0.68	117	-2.55	0.0121
	depth (600)	-2.24	0.76	117	-2.94	0.0039
	depth (700)	-1.69	1.00	117	-1.69	0.0929
	depth (800)	-0.96	1.39	117	-0.69	0.4909
	P_{upper} : depth (500)	-2.90	0.87	117	-3.34	0.0011
	P_{upper} : depth (600)	-3.35	0.93	117	-3.60	0.0005
	P_{upper} : depth (700)	-2.71	1.19	117	-2.29	0.0239
	P_{upper} : depth (800)	-1.92	1.75	117	-1.10	0.2746
P_{below}	(Intercept)	5.72	0.25	122	22.86	< 0.0001
BPEE rate	(Intercept)	5.68	0.26	90	22.24	< 0.0001

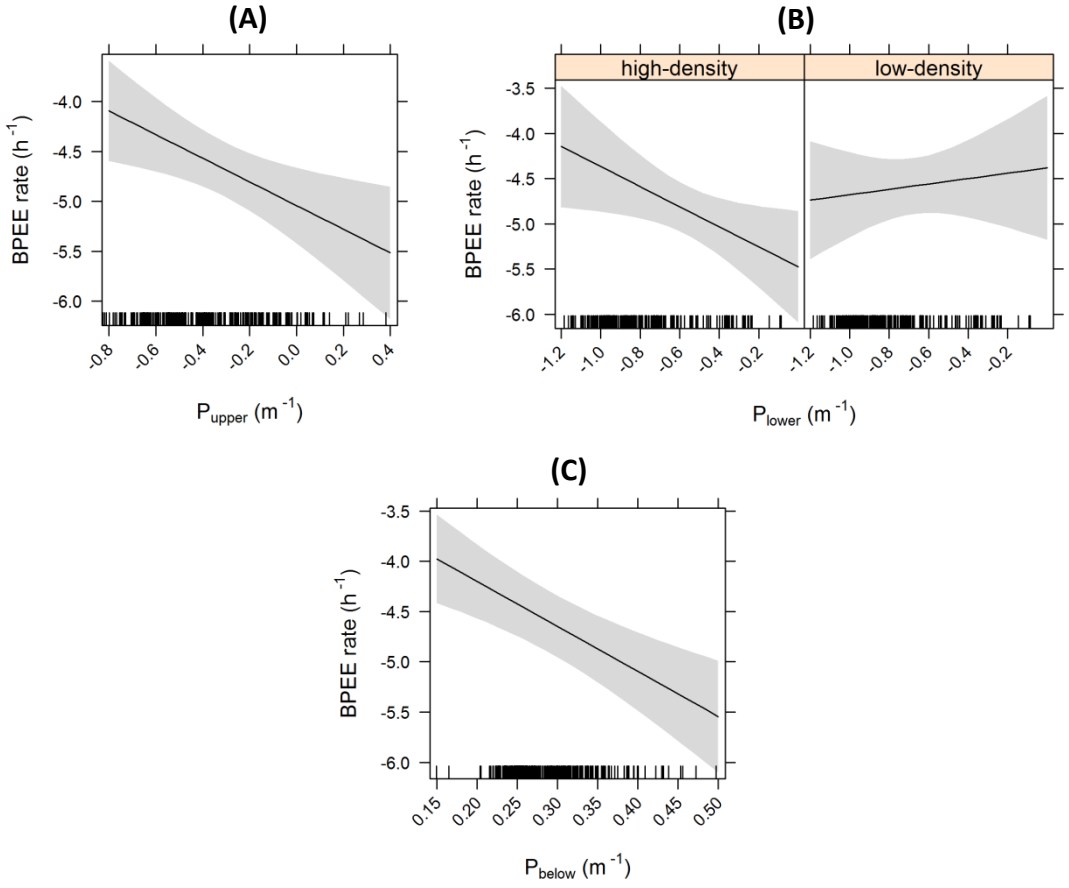

Figure 4.5. Bioluminescent prey encounter event (BPEE) rate in response to the plankton density of meso-scale plankton patches within different layers of the euphotic zone: (A) upper layer (0-75m); (B) lower layer (75-150m) according to high-density and low-density meso-scale plankton patches; and (C) below the euphotic zone (150-250m). Shaded area indicates the confidence interval.

Table 4.4. Coefficient values of dive conditions from models at the meso-scale. Coefficients are from our most parsimonious linear mixed-effects models relating bioluminescent encounter event (BPEE) rate to plankton density within different layers of the euphotic zone (P_{upper}, P_{lower}, P_{below}), seal maximum dive depth (depth), patch type (high-density or low-density) and interaction terms. Term coefficients are presented ± SE and *p*-values for each coefficient are also shown.

dive conditions		**coefficients**	**SE**	***df***	***t*-value**	***p*-value**
P_{upper}	(Intercept)	-5.77	0.27	235	-21.11	< 0.0001
	P_{upper}	-1.18	0.44	235	-2.69	0.0076
	depth (500)	0.72	0.26	235	2.80	0.0056
	depth (600)	0.66	0.24	235	2.71	0.0072
	depth (700)	0.76	0.24	235	3.14	0.0019
	depth (800)	1.26	0.29	235	4.40	< 0.0001
P_{lower}	(Intercept)	-5.44	0.39	218	-14.09	< 0.0001
	P_{lower}	-1.11	0.51	218	-2.19	0.0295
	patch type (low-density)	-0.19	0.56	218	-0.35	0.7301
	depth (500)	-0.43	0.37	218	-1.17	0.2449
	depth (600)	-0.05	0.35	218	-0.14	0.8893
	depth (700)	0.10	0.34	218	0.28	0.7765
	depth (800)	0.25	0.42	218	0.60	0.5468
	P_{lower} : patch type (low -density)	1.40	0.59	218	2.40	0.0173
	patch type (low-density) : depth (500)	1.90	0.50	218	3.82	0.0002
	patch type (low-density) : depth (600)	1.27	0.47	218	2.67	0.0081
	patch type (low-density) : depth (700)	1.23	0.47	218	2.65	0.0086
	patch type (low -density) : depth (800)	1.38	0.57	218	2.43	0.0160

Table 4.4. cont'

dive conditions		coefficients	SE	*df*	*t*-value	*p*-value
P_{below}	(Intercept)	-7.06	0.53	229	-13.37	< 0.0001
	P_{below}	-1.33	0.35	229	-3.84	0.0002
	depth (500)	0.69	0.29	229	2.42	0.0165
	depth (600)	0.79	0.28	229	2.79	0.0056
	depth (700)	0.87	0.28	229	3.09	0.0022
	depth (800)	1.13	0.34	229	3.35	0.0009

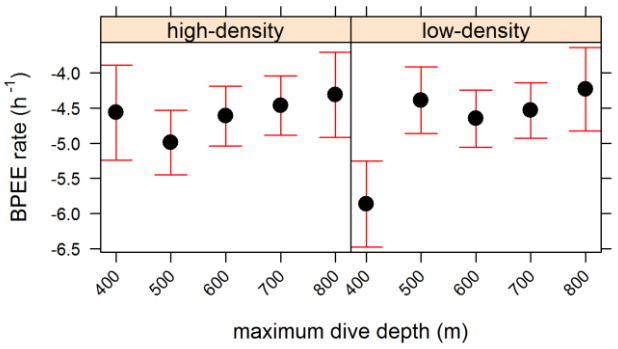

Figure 4.6. Bioluminescent prey encounter event (BPEE) rate in response to the maximum dive depth performed at the meso-scale according to high-density and low-density meso-scale plankton patches. Shaded area indicates the confidence interval.

4.4.2 Dive-scale trophic interactions

Patch type did not influence the trend between PEE rate and dive conditions (plankton or $Biolum_{PEE}$) at the dive-scale (see model rankings in appendix S4.7.9). Consequently, patch type was not considered in our dive-scale analysis and both complete and incomplete trip records were included (n=33) to maximise our sample size. Prey encounter event rates were most related ($p < 0.01$) with P_{lower} conditions encountered within the focal dive (d_0), as well as previous dives d_{-3} and d_{-1} (table 4.5). In each case PEE rates increased with P_{lower} dive conditions (figure 4.7). Similarly, PEE rates increased with P_{upper} dive conditions within the focal dives and surrounding dives (most notably post-dive conditions), though these trends were statistically weaker (table 4.5). PEE rates did not respond significantly with P_{below} conditions within focal dives or surrounding dives.

When only considering dives that coincided with $Biolum_{PEE}$ ($Biolum_{PEE}$ rate > 0), PEE rates increased significantly with P_{lower} conditions encountered within the focal dives and adjacent dives (*i.e.* d_{-1},d_{+1}), but not with P_{upper} conditions (table 4.6). We also showed PEE rate responded positively to $Biolum_{PEE}$ rate (figure 4.8). Finally, a positive trend between $Biolum_{PEE}$ rate and plankton density in the euphotic zone (*i.e.* P_{upper} and P_{lower}) at the dive-scale strengthened as seal maximum dive depth increased from 500 m to 700 m (figure 4.9A), but weakened when seals dived to depths between 600 m and 800 m (figure 4.9B, table 4.7).

Table 4.5. Coefficient values of dive conditions that coincide with prey capture activity from models at the dive-scale. Coefficients are from our most parsimonious linear mixed-effects models relating prey capture rate to plankton density within different layers of the euphotic zone (P_{upper}, P_{lower}, P_{below}). Term coefficients are presented ± SE and *p*-values for each coefficient are also shown.

dive conditions	biological conditions	intercept					explanatory				
		coefficients	**SE**	***df***	***t*-value**	***p*-value**	**coefficients**	**SE**	***df***	***t*-value**	***p*-value**
P_{upper}	d_{-5}	-0.71	0.10	16147	-7.03	< 0.0001	0.20	0.11	16147	1.77	0.0756
	d_{-4}	-0.65	0.09	16704	-6.56	< 0.0001	0.12	0.10	16704	1.23	0.217
	d_{-3}	-0.64	0.10	17230	-5.90	< 0.0001	0.12	0.12	17230	1.03	0.3018
	d_{-2}	-0.73	0.11	17640	-6.58	< 0.0001	0.23	0.12	17640	1.85	0.0635
	d_{-1}	-0.76	0.10	17787	-7.31	< 0.0001	0.24	0.11	17787	2.15	0.0314
	d_0	-0.80	0.11	18347	-7.31	< 0.0001	0.29	0.12	18347	2.38	0.0173
	d_{+1}	-0.78	0.10	17693	-7.20	< 0.0001	0.26	0.12	17693	2.13	0.0324
	d_{+2}	-0.73	0.10	17443	-7.30	< 0.0001	0.20	0.11	17443	1.84	0.0657
	d_{+3}	-0.78	0.09	16889	-8.21	< 0.0001	0.26	0.10	16889	2.52	0.0117
	d_{+4}	-0.77	0.11	16221	-6.82	< 0.0001	0.25	0.12	16221	1.98	0.0474
	d_{+5}	-0.77	0.11	15561	-7.03	< 0.0001	0.25	0.12	15561	1.96	0.0494
P_{lower}	d_{-5}	-0.69	0.10	16309	-6.71	< 0.0001	0.23	0.13	16309	1.68	0.0924
	d_{-4}	-0.68	0.11	16872	-5.70	< 0.0001	0.20	0.16	16872	1.25	0.211
	d_{-3}	-0.73	0.07	17408	-10.17	< 0.0001	0.28	0.07	17408	3.65	0.0003
	d_{-2}	-0.71	0.11	17828	-6.10	< 0.0001	0.25	0.15	17828	1.61	0.1053
	d_{-1}	-0.78	0.07	17974	-11.02	< 0.0001	0.34	0.07	17974	4.43	< 0.0001
	d_0	-0.45	0.05	18534	-8.96	< 0.0001	0.12	0.02	18534	4.73	< 0.0001
	d_{+1}	-0.77	0.12	17880	-6.35	< 0.0001	0.31	0.17	17880	1.82	0.0676
	d_{+2}	-0.79	0.11	17631	-7.17	< 0.0001	0.34	0.15	17631	2.26	0.0234
	d_{+3}	-0.66	0.11	17069	-5.92	< 0.0001	0.14	0.14	17069	0.99	0.321
	d_{+4}	-0.65	0.11	16385	-5.92	< 0.0001	0.12	0.15	16385	0.80	0.4215
	d_{+5}	-0.75	0.10	15722	-7.06	< 0.0001	0.27	0.14	15722	1.87	0.0602

Table 4.5 (cont')

dive conditions	biological conditions	intercept					explanatory				
		coefficients	**SE**	***df***	***t*-value**	***p*-value**	**coefficients**	**SE**	***df***	***t*-value**	***p*-value**
P_{below}	d_{-5}	-0.56	0.06	16309	-8.88	< 0.0001	0.05	0.07	16309	0.70	0.4808
	d_{-4}	-0.60	0.10	16872	-5.63	< 0.0001	0.11	0.14	16872	0.78	0.4304
	d_{-3}	-0.56	0.06	17408	-9.05	< 0.0001	0.03	0.07	17408	0.52	0.5998
	d_{-2}	-0.62	0.06	17828	-10.16	< 0.0001	0.15	0.07	17828	2.18	0.0287
	d_{-1}	-0.57	0.06	17974	-9.52	< 0.0001	0.05	0.07	17974	0.75	0.4486
	d_0	-0.57	0.05	18534	-9.65	< 0.0001	0.03	0.07	18534	0.43	0.6671
	d_{+1}	-0.60	0.08	17880	-6.71	< 0.0001	0.08	0.12	17880	0.65	0.5112
	d_{+2}	-0.59	0.09	17631	-6.62	< 0.0001	0.06	0.12	17631	0.48	0.626
	d_{+3}	-0.58	0.06	17069	-9.44	< 0.0001	0.04	0.07	17069	0.55	0.5803
	d_{+4}	-0.62	0.09	16385	-6.59	< 0.0001	0.10	0.14	16385	0.76	0.4426
	d_{+5}	-0.53	0.06	15722	-8.65	< 0.0001	-0.05	0.07	15722	-0.75	0.4528

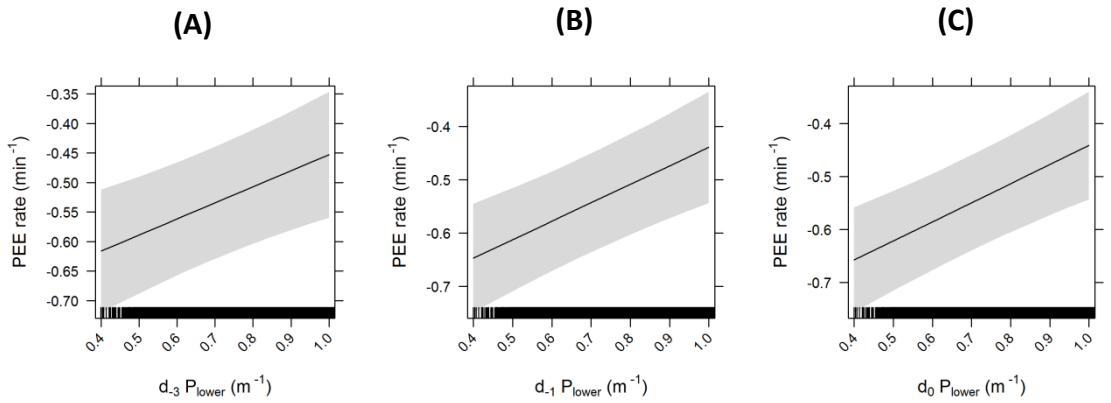

Figure 4.7. Prey encounter event (PEE) rate in response to the plankton density of surrounding dives within the lower layer of the euphotic zone (P_{lower}) at the dive-scale: (A) P_{lower} conditions 3 dives prior; (B) P_{lower} conditions 1 dive prior; and (C) P_{lower} conditions within the focal dive. Shaded area indicates the confidence interval.

Table 4.6. Coefficient values of dive conditions that coincide with prey capture activity from mixed models at the dive-scale. Coefficients are from our most parsimonious linear mixed-effects models relating prey capture rate to plankton density within different layers of the euphotic zone (P_{upper}, P_{lower}, P_{below}), and bioluminescence encounter rate (B_{rate}). Term coefficients are presented ± SE and *p*-values for each coefficient are also shown.

dive conditions	biological conditions	intercept					explanatory				
		coefficients	SE	*df*	*t*-value	*p*-value	coefficients	SE	*df*	*t*-value	*p*-value
P_{upper}	d_{-5}	-0.72	0.15	933	-4.69	< 0.0001	0.17	0.23	933	0.74	0.4610
	d_{-4}	-0.75	0.17	942	-4.27	< 0.0001	0.20	0.26	942	0.78	0.4382
	d_{-3}	-0.68	0.16	955	-4.33	< 0.0001	0.04	0.22	955	0.17	0.8685
	d_{-2}	-0.81	0.16	971	-5.20	< 0.0001	0.27	0.21	971	1.30	0.1935
	d_{-1}	-0.84	0.14	1006	-5.80	< 0.0001	0.32	0.20	1006	1.63	0.1043
	d_{0}	-1.03	0.33	1083	-3.11	0.0019	0.46	0.39	1083	1.16	0.2475
	d_{+1}	-0.73	0.16	1012	-4.51	< 0.0001	0.14	0.23	1012	0.60	0.5475
	d_{+2}	-0.91	0.19	965	-4.65	< 0.0001	0.35	0.26	965	1.35	0.1785
	d_{+3}	-0.83	0.13	918	-6.37	< 0.0001	0.24	0.18	918	1.33	0.1847
	d_{+4}	-0.88	0.15	911	-5.98	< 0.0001	0.30	0.22	911	1.38	0.1689
	d_{+5}	-0.92	0.16	884	-5.76	< 0.0001	0.37	0.24	884	1.54	0.1248
P_{lower}	d_{-5}	-0.49	0.13	1037	-3.71	0.0002	0.14	0.14	1037	1.00	0.3153
	d_{-4}	-0.51	0.16	1049	-3.24	0.0012	0.14	0.18	1049	0.82	0.4145
	d_{-3}	-0.51	0.12	1063	-4.31	< 0.0001	0.17	0.14	1063	1.25	0.2122
	d_{-2}	-0.50	0.15	1082	-3.37	0.0008	0.15	0.16	1082	0.94	0.3463
	d_{-1}	-0.36	0.13	1118	-2.84	0.0046	0.30	0.14	1118	2.05	0.0408
	d_{0}	-0.27	0.11	1196	-2.46	0.0142	0.44	0.13	1196	3.34	0.0009
	d_{+1}	-0.40	0.12	1126	-3.22	0.0013	0.27	0.12	1126	2.20	0.0283
	d_{+2}	-0.46	0.13	1078	-3.50	0.0005	0.25	0.14	1078	1.84	0.6587
	d_{+3}	-0.45	0.13	1028	-3.48	0.0005	0.26	0.15	1028	1.76	0.0787
	d_{+4}	-0.56	0.13	1015	-4.32	< 0.0001	0.13	0.13	1015	1.02	0.3099
	d_{+5}	-0.32	0.14	988	-2.34	0.0194	0.40	0.13	988	3.03	0.0025

Table 4.6 (cont')

dive conditions	biological conditions	intercept					explanatory				
		coefficients	**SE**	***df***	***t*-value**	***p*-value**	**coefficients**	**SE**	***df***	***t*-value**	***p*-value**
P_{below}	d_{-5}	-0.75	0.16	1037	-4.71	< 0.0001	0.51	0.61	1037	0.84	0.4002
	d_{-4}	-0.66	0.17	1049	-3.78	0.0002	0.08	0.66	1049	0.12	0.9033
	d_{-3}	-0.81	0.16	1063	-5.18	< 0.0001	0.58	0.47	1063	1.23	0.2207
	d_{-2}	-0.91	0.12	1082	-7.64	< 0.0001	1.04	0.40	1082	2.62	0.0090
	d_{-1}	-0.76	0.16	1118	-4.77	< 0.0001	0.49	0.46	1118	1.06	0.2885
	d_0	-0.76	0.14	1196	-5.24	< 0.0001	0.33	0.44	1196	0.75	0.4504
	d_{+1}	-0.66	0.15	1126	-4.50	< 0.0001	0.07	0.47	1126	0.15	0.8841
	d_{+2}	-0.83	0.16	1078	-5.25	< 0.0001	0.56	0.50	1078	1.11	0.2656
	d_{+3}	-0.85	0.15	1028	-5.77	< 0.0001	0.65	0.50	1028	1.32	0.1872
	d_{+4}	-0.91	0.12	1015	-7.28	< 0.0001	0.85	0.47	1015	1.80	0.0716
	d_{+5}	-0.85	0.15	988	-5.76	< 0.0001	0.66	0.44	988	1.51	0.1311
B_{rate}	d_{-5}	-0.64	0.10	1037	-6.25	< 0.0001	-0.01	0.04	1037	-0.33	0.7402
	d_{-4}	-0.47	0.14	1049	-3.43	0.0006	0.09	0.06	1049	1.49	0.1354
	d_{-3}	-0.67	0.07	1063	-9.30	< 0.0001	0.00	0.04	1063	0.10	0.9238
	d_{-2}	-0.52	0.11	1082	-4.84	< 0.0001	0.06	0.05	1082	1.22	0.2229
	d_{-1}	-0.62	0.09	1118	-6.84	< 0.0001	0.00	0.04	1118	0.08	0.9384
	d_0	-0.45	0.10	1196	-4.76	< 0.0001	0.12	0.04	1196	2.66	0.0079
	d_{+1}	-0.51	0.10	1126	-5.27	< 0.0001	0.07	0.05	1126	1.52	0.1286
	d_{+2}	-0.59	0.10	1078	-5.71	< 0.0001	0.05	0.05	1078	0.98	0.3283
	d_{+3}	-0.56	0.10	1028	-5.70	< 0.0001	0.06	0.04	1028	1.53	0.1268
	d_{+4}	-0.47	0.12	1015	-3.95	0.0001	0.11	0.05	1015	2.09	0.0366
	d_{+5}	-0.62	0.11	988	-5.43	< 0.0001	0.03	0.04	988	0.68	0.4996

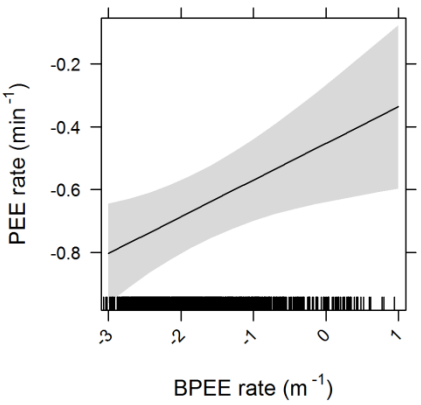

Figure 4.8. Prey encounter event (PEE) rate in response to the bioluminescent prey encounter event (BPEE) rate at the dive-scale. Shaded area indicates the confidence interval. Coefficient *p*-value <0.01 (*see* table 4.6).

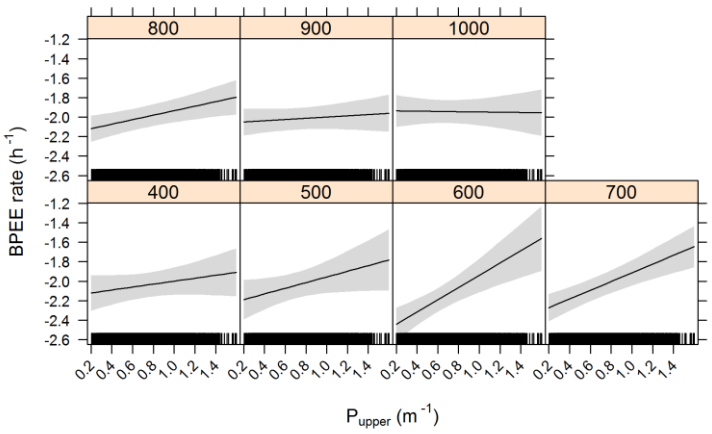

(A)

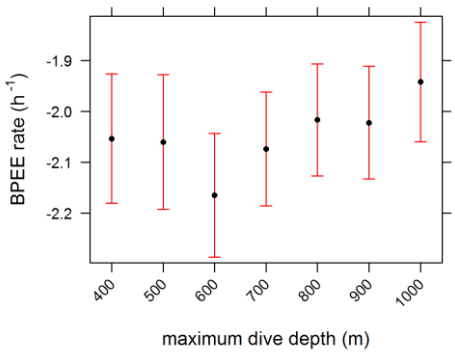

(B)

Figure 4.9. Bioluminescent prey encounter event (BPEE) rate in response to (A) the plankton density within the upper layer of the euphotic zone (P_{upper}) according to the maximum dive depths performed by the seals at the dive-scale (grouped in 100 m depth bins between 400 m and 1000 m); and (B) maximum dive depths performed by the seals at the dive-scale. Shaded area indicates the confidence interval.

Table 4.7. Coefficient values of dive conditions from models at the dive-scale. Coefficients derive from the most parsimonious linear mixed-effects models relating bioluminescent encounter rate to plankton density within different layers of the euphotic zone (P_{upper}, P_{lower}, P_{below}), as well as seal maximum dive depth (depth) and interaction terms. Term coefficients are presented ± SE and *p*-values for each coefficient are also shown.

dive conditions		**coefficients**	**SE**	***df***	***t*-value**	***p*-value**
P_{upper}	(Intercept)	-2.15	0.11	4794	-18.99	< 0.0001
	P_{upper}	0.15	0.12	4794	1.19	0.2332
	depth (500)	-0.09	0.13	4794	-0.72	0.4695
	depth (600)	-0.41	0.12	4794	-3.26	0.0011
	depth (700)	-0.21	0.10	4794	-1.97	0.0478
	depth (800)	-0.01	0.09	4794	-0.14	0.8810
	depth (900)	0.08	0.10	4794	0.84	0.3960
	depth (1000)	0.21	0.11	4794	1.83	0.0663
	P_{upper} : depth (500)	0.14	0.17	4794	0.79	0.4265
	P_{upper} : depth (600)	0.47	0.18	4794	2.55	0.0107
	P_{upper} : depth (700)	0.29	0.14	4794	2.07	0.0379
	P_{upper} : depth (800)	0.08	0.12	4794	0.63	0.5265
	P_{upper} : depth (900)	-0.08	0.13	4794	-0.65	0.5151
	P_{upper} : depth (1000)	-0.16	0.15	4794	-1.05	0.2901
P_{lower}	(Intercept)	-2.12	0.20	4801	-10.28	< 0.0001
	P_{lower}	0.09	0.30	4801	0.29	0.7668
	depth (500)	-0.14	0.31	4801	-0.46	0.6393
	depth (600)	-0.75	0.31	4801	-2.43	0.0149
	depth (700)	-0.39	0.24	4801	-1.58	0.1137
	depth (800)	-0.07	0.22	4801	-0.31	0.7515
	depth (900)	0.07	0.23	4801	0.31	0.7523
	depth (1000)	0.48	0.27	4801	1.77	0.0759
	P_{lower} : depth (500)	0.21	0.45	4801	0.46	0.6405
	P_{lower} : depth (600)	0.98	0.46	4801	2.10	0.0356
	P_{lower} : depth (700)	0.57	0.36	4801	1.57	0.1161
	P_{lower} : depth (800)	0.18	0.33	4801	0.55	0.5813
	P_{lower} : depth (900)	-0.04	0.34	4801	-0.14	0.8839
	P_{lower} : depth (1000)	-0.56	0.40	4801	-1.39	0.1619
P_{below}	(Intercept)	-2.06	0.06	4808	-32.88	< 0.0001
	depth (500)	0.01	0.04	4808	0.03	0.9704
	depth (600)	-0.12	0.04	4808	-2.84	0.0045
	depth (700)	-0.01	0.03	4808	-0.39	0.6934
	depth (800)	0.05	0.03	4808	1.48	0.1368
	depth (900)	0.05	0.03	4808	1.36	0.1734
	depth (1000)	0.13	0.04	4808	3.20	0.0014

Compared with the area closest to the colony (in the west), there was a clear contrast in the response of seal maximum dive depth to plankton density within the euphotic zone (P_{upper} and P_{lower}) in the area furthest from the colony (about 1000 km to 2000 km to the east). The maximum dive depth in response to plankton density below the euphotic zone (P_{below}) was not considered because preceding results showed no significant relationship between prey capture and plankton density. When seals encountered waters closest to the colony there was little or no significant positive relationship between maximum dive depth and P_{upper} or P_{lower} (*i.e.* seals dive deeper when plankton density increases) (table 4.8, figure 4.10A). Conversely, when seals encountered waters furthest from the colony there was a weak significant inverse relationship between maximum dive depth and P_{upper} or P_{lower} (*i.e.* seals dive shallower when plankton density increases) (table 4.8, figure 4.10B and figure 4.10C). Figure 4.10B and figure 4.10C suggested that seals in low-density plankton conditions dive approximately 50 m deeper compared with seals in high-density plankton conditions.

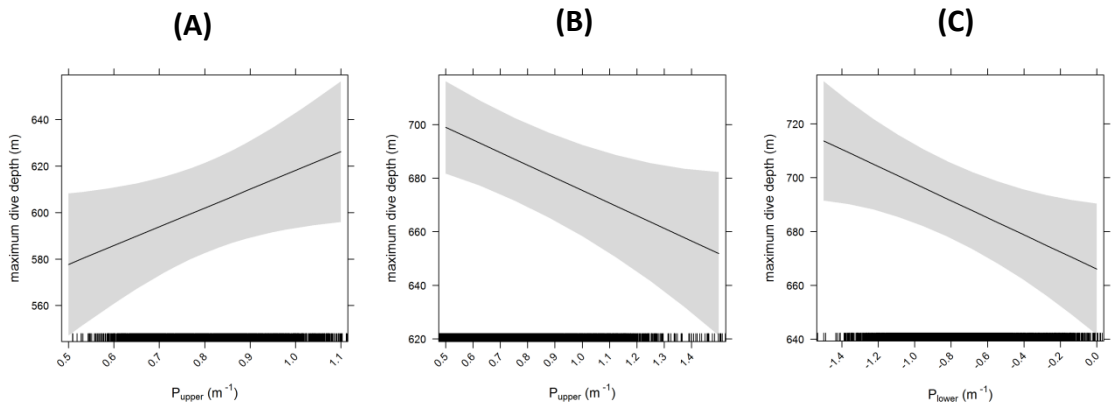

Figure 4.10. Maximum dive depth (MDD) in response to the plankton density at the dive-scale within meso-scale patches: (A) MDD verses plankton density within the upper layer of the euphotic zone (P_{upper}) within meso-scale patches nearest to the plume origin (*i.e.* closest to the colony); (B) MDD verses P_{upper} within meso-scale patches nearest to the plume front (*i.e.* furthest from the colony); and (C) MDD verses plankton density within the lower layer of the euphotic zone (P_{lower}) within meso-scale patches furthest from the colony. Shaded area indicates the confidence interval.

Table 4.8. Coefficient values of the maximum dive depth that coincide with plankton density within the upper (P_{upper}) and lower (P_{lower}) euphotic zone at the dive-scale within meso-scale patches: nearest to the origin of the plume in the west of the study site (plume origin); and nearest to the plume front in the east of the study site (plume front). Coefficients are from our most parsimonious linear mixed-effects model relating maximum dive depth to plankton density. Term coefficients are presented ± SE and *p*-values for each coefficient are also shown.

longitudinal position of meso-scale patch	**biotic conditions**	**intercept**					**explanatory**				
		coefficients	**SE**	***df***	***t*-value**	***p*-value**	**coefficients**	**SE**	***df***	***t*-value**	***p*-value**
west (plume origin)	P_{upper}	537.28	33.44	2810	16.07	< 0.0001	80.87	39.82	2810	2.03	0.0423
	P_{lower}	633.35	15.74	3302	40.24	< 0.0001	10.73	14.66	3302	0.73	0.464
east (plume front)	P_{upper}	722.50	15.69	4457	46.05	< 0.0001	-47.13	18.31	4457	-2.57	0.0101
	P_{lower}	666.06	12.43	4762	53.60	< 0.0001	-31.75	12.78	4762	-2.48	0.013

4.5 Discussion

Here, fine-scale data recorded by seal-borne sensors have provided unprecedented insights into the trophic coupling between a top marine predator and lower-trophic-levels in the open ocean environment, during the increase in biological production recurring in late spring – early summer. Some studies have found no clear relationship between the foraging behaviour of top marine predators and phytoplankton density estimates derived from satellite (Jaquet et al., 1996;Bradshaw et al., 2004); while others have found contrasting trends depending on scale (e.g. diving activity of fur seals, *Arctocephalus gazella*, negatively related to chlorophyll-a concentration at a small spatial scale but positively related at a larger scale; Guinet et al., 2001). These studies have likely been limited by three fundamental problems: 1) the spatio-temporal mismatch between the chlorophyll data (10s of kilometres and days) and animal foraging behaviour (10s of meters and minutes); 2) satellite data only provide information at the near-surface; and 3) these data lack information on prey fields, and are only likely to be proximally related to the actual prey of the predators.

Our assessment of seal prey encounter events (PEE) rates in response to two different *in situ* biological metrics (*i.e.* density of plankton estimated from the amount of light attenuated in the water column [plankton density] and seal bioluminescent prey encounters estimated from peak light levels below 550 m [$Biolum_{PEE}$]) give a picture of 3D resource distribution and their respective trophic interactions as seals migrate across an eastward-shifting phytoplankton plume in summer. Bioluminescent prey density declined as the seals moved eastward towards the Kerguelen plume front, while rates of prey encounter increased with plankton density. Moreover, while encountering waters around the Kerguelen plume front seals did not dive as deep when plankton density was high. However, it is important to remember that our light-based estimates of plankton density do not represent absolute plankton values, nor do our light-based estimates of $Biolum_{PEE}$ rates represent absolute counts of mid-trophic seal prey. Instead, these estimates provide two relative scales of lower-trophic-level patterns, namely plankton density (Teo et al., 2009;O'Toole et al., 2014b) and the mid-trophic prey of elephant seals (Vacquié-Garcia et al., 2012).

4.5.1 A deep-diving predator and its association with patches of plankton

The Kerguelen Plateau is a large bathymetric feature that diverts the flow of major fronts (*i.e.* sub-Antarctic Front and Polar Front) and creates meandering small scale eddies downstream (Park et al., 1991) that bring nutrient-rich Circumpolar Deep Water (CDW) to the surface (Park et al., 2014). The

growth rates of phytoplankton in areas of the Southern Ocean remote from land are predominately limited by iron availability (Boyd et al., 2000;de Baar et al., 2005) and rely on eastward advection by the Antarctic Circumpolar Current (ACC) to resupply open ocean regions with these nutrient-rich waters. Indeed, the Kerguelen Plateau sustains the most productive waters in the ACC (Moore and Abbott, 2000;Chever et al., 2010), which also enrich surface waters thousands of kilometres downstream via lateral advection (Blain et al., 2001;Sokolov and Rintoul, 2007;Mongin et al., 2009). These conditions are thought to facilitate recurrent phytoplankton blooms in the region (Boyd, 2002;Sokolov and Rintoul, 2007), driven by nutrient dispersal via upwelling and advection by meso-scale eddies (Palter et al., 2010), as well as the eastward flow of the ACC (Olbers et al., 2004). All post-breeding trips performed by female elephant seals in this study coincided with the phytoplankton bloom period in the late austral spring – early summer. The seals overlapped with the large Kerguelen phytoplankton plume that forms on the Kerguelen shelf and carried eastward by the ACC into the open ocean (Mongin et al., 2008). Our light-based estimates of plankton density showed that seals travelling throughout the plume encounter alternating areas of high and low-density plankton, which are likely driven by meso-scale eddy processes.

The trophic repercussions of a spring bloom can extend to deeper living species which are prey of deep-diving predators such as elephant seals (Donnelly et al., 2006). Plankton density increased as seals travelled further from the Iles Kerguelen, supporting the notion that post-breeding seals feed within the eastward-drifting Kerguelen plume. However, despite seals encountering multiple meso-scale patches of high-density plankton along their tracks, rates of prey encounter did not change between high- and low-density patches. The distribution of marine biota, including elephant seal prey, may be sufficiently concentrated at the scale of the Kerguelen plume (approximately 1500 km), to enable efficient resource acquisition by the seals (Cotté et al., 2014). However, the energy transfer via trophic links initiated by seasonal phytoplankton blooms often influences zooplankton and fish larvae (Henson et al., 2009), rather than adult fish species, and so there may be spatial and temporal disconnect between lower and upper trophic levels. Studies examining elephant seal foraging behaviour in such environments, have reported seal feeding activity in association with (sub-) meso-scale oceanographic features such as cold core eddies (Bailleul et al., 2010b;Dragon et al., 2012;Cotté et al., 2014 & Della Penna unpublished data) generated within these basin-scale plumes (Park et al., 2008b;Park et al., 2014). These features have important ecological implications because they may facilitate the transfer of energy via trophic linkages to top predators such as elephant seals (d'Ovidio et al., 2013). Specifically, strong meandering meso-scale eddies are thought to accumulate phytoplankton, and retain them for sufficient periods, to transfer energy via bottom-

up processes (d'Ovidio et al., 2013). However, these features may not necessarily be associated with elevated plankton densities due to heavy grazing pressure from zooplankton, which could explain the lack of difference between high- and low-density plankton patches in prey encounter rates.

Our interpretation of results at the meso-scale relies on our definition of patch type. The criterion we used identified the most significant peaks in plankton encountered by each seal, but we concede that the algorithm used does not always correspond with the plankton data when visually inspected. However, from recent work we know seal '2012-28' interacted with the edge of a cold-core eddy (Della Penna unpublished data), which often facilitate the accumulation of phytoplankton (d'Ovidio et al., 2013) (and most likely other trophic levels too; *see* (Godo et al., 2012)). Our meso-scale analysis reveals that seal '2012-28' encountered a major bloom event (high-density plankton patch) in the same point in space and time (*see* figure 4.2A and figure 4.2B) providing preliminary validation of our method.

The density of meso-scale plankton patches below the euphotic zone did not influence PEE or $Biolum_{PEE}$ rate, given that little or no plankton persists below the euphotic zone (Teo et al., 2009). Conversely, elevated plankton density within the euphotic zone (*i.e.* P_{upper} and P_{lower}) improved PEE rates. However, when seals fed at depths beyond the euphotic zone (*i.e.* > 600 m) both P_{upper} and P_{lower} had no effect. Elephant seal prey are often encountered between 400 m and 600 m, and encounter rates were significantly lower below 700 m (Guinet et al., 2014), which could be why we see the trend between plankton density and PEE weakening with depth. Moreover, PEE rate was more influenced by P_{lower}, rather than P_{upper} conditions, suggesting that the vertical distance between planktonic conditions (in lower euphotic zone, *i.e.* 75 m – 150 m) and seal feeding activity (below the euphotic zone, *i.e.* 400 m – 600 m) has an effect on their relationship with one another. How planktonic conditions may influence seal feeding activity is discussed in the following section.

4.5.2 Prey distribution and the downstream drift of the Kerguelen plume

Female southern elephant seals do not feed on phytoplankton, but instead feed on mid-trophic mesopelagic fish (Cherel et al., 2008). The trophic links between phytoplankton and mesopelagic fish can be highly dynamic and intermediate links such as zooplankton and fish often vary in space and time (i.e. match/mismatch hypothesis; Cushing, 1990) and do not necessarily coincide with primary producers. For instance, zooplankton proliferation follows phytoplankton blooms later in the season (Jouandet et al., 2011), which results in a temporal lag between these two lower-trophic levels.

Productive waters are also advected laterally over time so that the ecosystem closer to the initial bloom site has had more time for energy to transfer, via trophic links, to higher-trophic levels such as mesopelagic fish, and ultimately top predators (Smetacek et al., 2004). Conversely, the front of the advected productive waters would have had less time allocated for energy transfer to higher trophic levels. Consequently, we would expect a gradient in food web development along the west-east axis of open waters between the initial bloom site around the Kerguelen Plateau (where maximum time has been allocated for energy transfer along the food chain, *i.e.* 'biologically mature') and the front of the advected phytoplankton plume (where minimum time has been allocated for energy transfer along the food chain, *i.e.* 'biologically immature').

In this study, estimates of plankton density and PEE, coupled with $Biolum_{PEE}$ provide evidence that supports the notion of progressive food web development in open ocean ecosystems. Firstly, $Biolum_{PEE}$ rate was not related to PEE rate at the meso-scale. This may be because seals may also target non-bioluminescent prey (though majority of mesopelagic prey species are thought to be bioluminescent; (Widder, 2010)), as well as encounter bioluminescent organisms that are not prey. However, $Biolum_{PEE}$ rate was inversely related to the plankton density of meso-scale patches, while the plankton density of meso-scale patches increased with distance from the colony. This suggests that bioluminescent prey density was greater in waters closer to the origin of the Kerguelen plume (*i.e.* waters closely associated with the Kerguelen Plateau) where zooplankton grazing pressure is expected to have depleted phytoplankton biomass most. It is also where we would expect the ecosystem to be more 'biologically mature', *i.e.* where the time lag of seal prey relative to phytoplankton development was greater, thereby allowing more energy to be transferred to seal prey biomass. However, female elephant seals acquire resources at relatively constant rates over their post-breeding foraging trip (Thums et al., 2011;Naito et al., 2013). So why does PEE not change as seals travel towards the plume front, where the system is expected to be less mature? A west-east change from dense patches of small prey to patches of sparsely-distributed large prey could explain the drop in density. This has certainly been suggested by Guinet et al. (2014), though only along the latitudinal axis (*i.e.* north-south) and not along the longitudinal axis (*i.e.* west-east). Instead, it is likely that the seals are adjusting their foraging strategy to maximise prey acquisition as the density of the prey field decreases from west to east.

A broad range of marine taxonomic groups exhibit diel vertical migration and will dive deeper as ambient light levels increase in order to avoid predation by visual predators (see review, Hays, 2003). Indeed, the habitat of myctophid (*i.e.* lanternfish), an important mesopelagic prey of elephant seals

(Cherel et al., 2008), is highly dependent on water column light levels (myctophid often found higher in the water column when light levels decrease) (Duhamel et al., 2000;Widder, 2010). Dive-scale plankton densities affect light conditions (via shading) in the euphotic zone, and therefore below the euphotic layer as well (Morel, 1988). It is likely that increased shading from denser plankton aggregates means that the prey field will be higher in the water column, thereby mediating the vertical access of predators' to prey per dive. This will be particularly pronounced during daylight hours. Indeed, Guinet et al. (2014) found both seal dive depth and the depth of PEEs increased with integrated light attenuation within the euphotic zone (0 m – 150 m) during daylight hours. Seals may therefore increasingly utilise denser aggregates of plankton to gain vertical access to food (up to 600 m where most prey are found (Guinet et al., 2014) as the density of bioluminescent prey drops as seals approach the eastward-drifting plume front. Indeed, we showed that seals did not dive as deep where plankton density was high, but only in the east when in the vicinity of the plume front. This relationship was much less clear in the west where seals encountered waters closest to the origin of the plume. A behavioural adjustment such as this could buffer prey acquisition rate (*i.e.* PEE rate), via reduced vertical travel and search time, against lower prey densities that may be prevalent in the less mature biological system at the plume front. Certainly, in optimal foraging models prey acquisition rate is more important to energy maximisation than prey density (Arditi and Dacorogna, 1988). Behavioural adjustment in response to plankton density could be the primary reason that female elephant seals are still able to acquire resources at relatively constant rates over their post-breeding foraging trip despite variability in prey density.

However, the diving capabilities of elephant seals needs to be considered if we are to understand the benefit plankton shading effect provides to seals accessing their prey at depth. Elephant seals are able to maximise their oxygen stores while diving by adjusting their metabolic rate (reduce while diving; Hindell and Lea, 1998;Hindell et al., 2000) and behaviour (*e.g.* maintain slow swim speed while diving - Hindell and Lea, 1998;Hindell et al., 2000; and/or change dive angle – Sala et al., 2011), making them well-adapted for diving to a range of depths (up to 2000 m; McIntyre et al., 2012) for long periods of time (up to 2 h – Hindell et al., 1991a; on average 20 – 30 minutes – Boyd and Croxall, 1996). We showed that the effect difference of high- and low-density planktonic conditions on maximum dive depth is approximately 50 m. If we assume descent and ascent speed is constant at ~1 m s^{-1} (*see* Davis and Weihs, 2007) then it would take ~2 min for a seal to descend and ascend 50 m. For dives lasting 30 mins this represents ~7% of total dive duration dedicated to diving another 50 m in areas where plankton density is low. Whether this provides any real benefit to elephant seals, which are well-adapted for diving deep and for long periods of time, is still unclear. We suspect that

the shading effect of plankton may provide a relatively small benefit to elephant seal foraging efficiency.

Our light-based estimates of plankton density collected by elephant seals revealed the internal biological structure of a recurrent plume, driven by well-documented oceanographic processes within the ACC. Our findings also demonstrate how a marine predator responds to the spatio-temporal development of a mature ecosystem; specifically, how seals respond to the different developmental stages of lower-trophic distribution as a major plume drifts downstream from its point of origin in early spring until late summer. This improves our understanding of how a higher-trophic-level species, such as the elephant seal, utilises the spatial heterogeneity of plankton and the different stages of bottom-up processes within a major plume in the Southern Ocean to potentially maximise prey returns.

4.6 Acknowledgements

We thank all the people who contributed to the field work and data processing, with special thanks to Baptiste Picard for help with data access. The authors would also like to thank Jade Vacquié-Garcia for advice on bioluminescence detection.

4.7 Appendix

Appendix S4.7.1

At times a light level estimate at a given depth interval (75 m, 150 m or 250 m) is lower than the light level estimate at a deeper depth interval. If we use these light level estimates to calculate the plankton index value for the depth band between these two depth intervals we will be given a negative plankton index value. We show that most negative plankton index values are found within the deepest depth band (below the euphotic zone) during all daylight hours (sun angle > 0°) (figure S4.7.1.1).

Although it is possible that a luminescent spike may influence light conditions at depth (possibly a bioluminescent encounter, though we are unable to confirm these events at depths above 550 m), it is more likely that the on-board light sensors are unable to detect subtle differences in light level where light conditions are especially low (figure S4.7.1.2). In other instances we show that the light and depth sensors record erroneous values (figure S4.7.1.3).

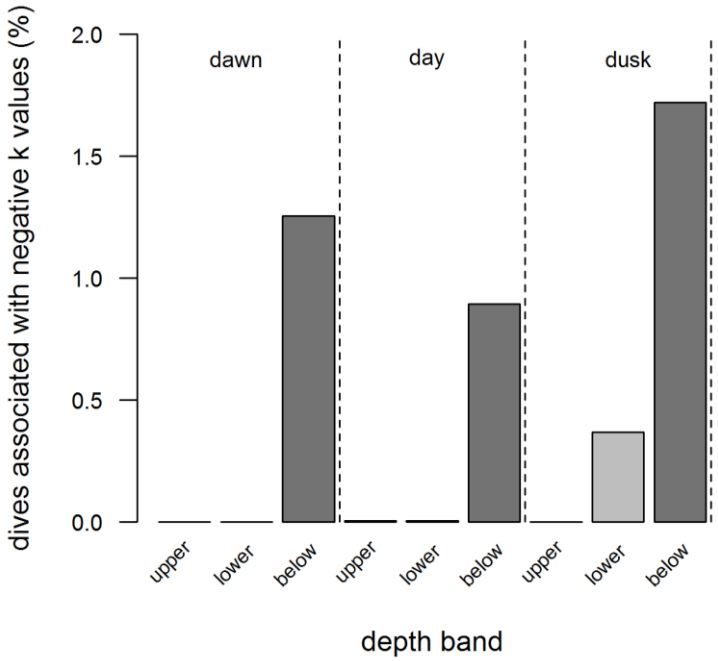

Figure S4.7.1.1. Percentage of dives associated with negative k values within each depth band according to the time of day (i.e. dawn, day and dusk). Vertical dashed lines indicate the interface between the times of day. Shaded bars represent each depth band: upper (light grey); lower (grey); and below (dark grey).

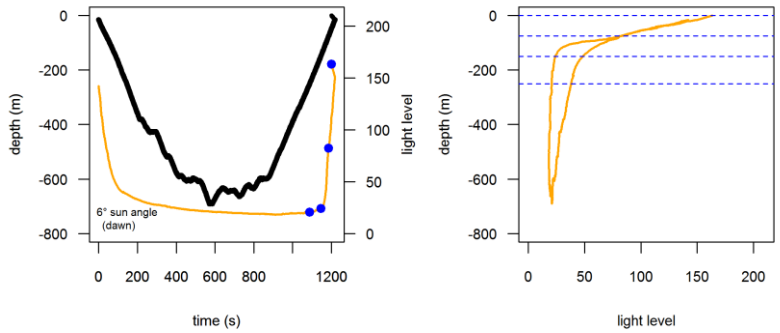

Figure S4.7.1.2. Examples of on-board sensors recording low light levels during a seal dive performed around mid-morning (sun angle = 7°). Time-depth profile (black) and time-light profile (orange) (*left*) and light-depth profile (*right*) from the seal 2011-28 dataset during dive 2051. Light level estimates at each depth interval (*i.e.* 75 m, 150 m and 250 m) are indicated by blue dots in the left plot and blue dashed lines in the right plot.

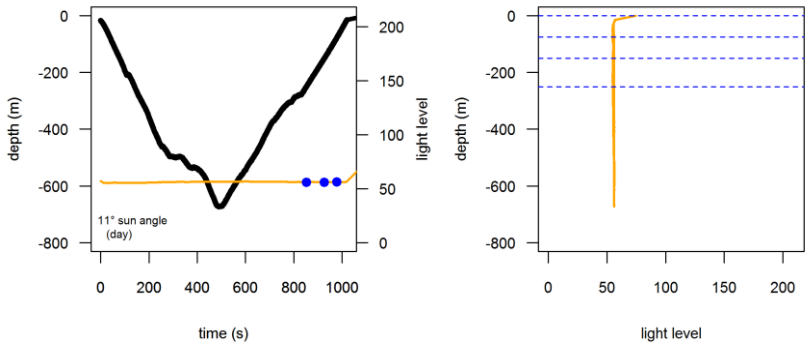

Figure S4.7.1.3. Examples of on-board sensors recording erroneous light levels during a seal dive performed around mid-morning (sun angle = 11°). Time-depth profile (black) and time-light profile (orange) (*left*) and light-depth profile (*right*) from the seal 2012-9 dataset during dive 2886. Light level estimates at each depth interval (*i.e.* 75 m, 150 m and 250 m) are indicated by blue dots in the left plot and blue dashed lines in the right plot.

Appendix S4.7.2

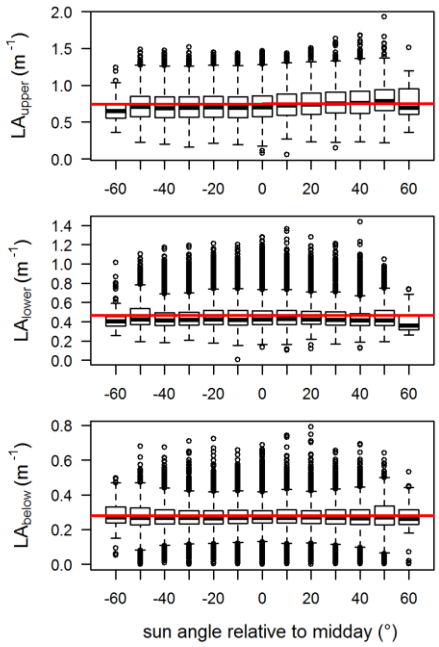

Figure S4.7.2. The relationship between sun angle and light attenuation within each depth band: LA_{upper} (top), LA_{lower} (middle) and LA_{below} (bottom) (also see Table S2.7.2 for ANOVA results). Light attenuation estimates were grouped into bins of sun angle at 10° intervals. The red line indicates the slope of the relationship according to analysis of variance.

Table S4.7.2. ANOVA output corresponding with data represented in figure S4.7.2

	df	**sum sq.**	**mean sq.**	**F-value**	**Pr(>F)**
LA_{upper} ~ angle					
Angle	1	12.3	12.291	273.8	<2e-16
Residuals	22496	1009.7	0.045		
LA_{lower} ~ angle					
Angle	1	0.1	0.06055	2.444	0.118
Residuals	22496	557.4	0.02478		
LA_{below} ~ angle					
Angle	1	0.02	0.020163	2.51	0.113
Residuals	22496	180.68	0.008032		

Appendix S4.7.3

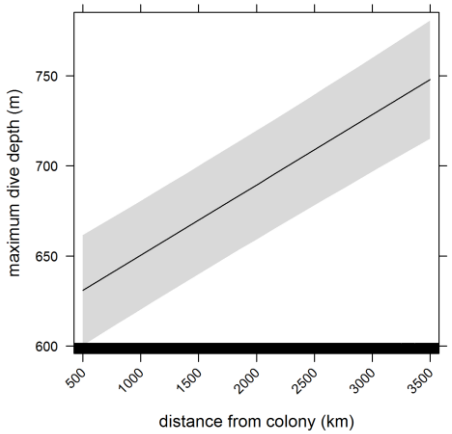

Figure S4.7.3. Maximum dive depth in response to distance from the colony (*i.e.* Isle Kerguelen) at the dive-scale. Shaded area indicates the confidence interval. Coefficient p-values <0.01 (see table S4.7.3).

Table S4.7.3. Coefficient values of the distance from the colony (*i.e.* Isle Kerguelen) that coincide with maximum dive depth from a mixed model at the dive-scale. Coefficients are from our most parsimonious linear mixed-effects model relating maximum dive depth to distance from the colony. Term coefficients are presented ± SE and *p*-values for each coefficient are also shown.

intercept					**explanatory**				
coefficients	**SE**	***df***	***t*-value**	***p*-value**	**coefficients**	**SE**	***df***	***t*-value**	***p*-value**
611.47	16.01	46126	38.18	< 0.0001	0.04	0.00	46126	11.85	< 0.0001

Appendix S4.7.4

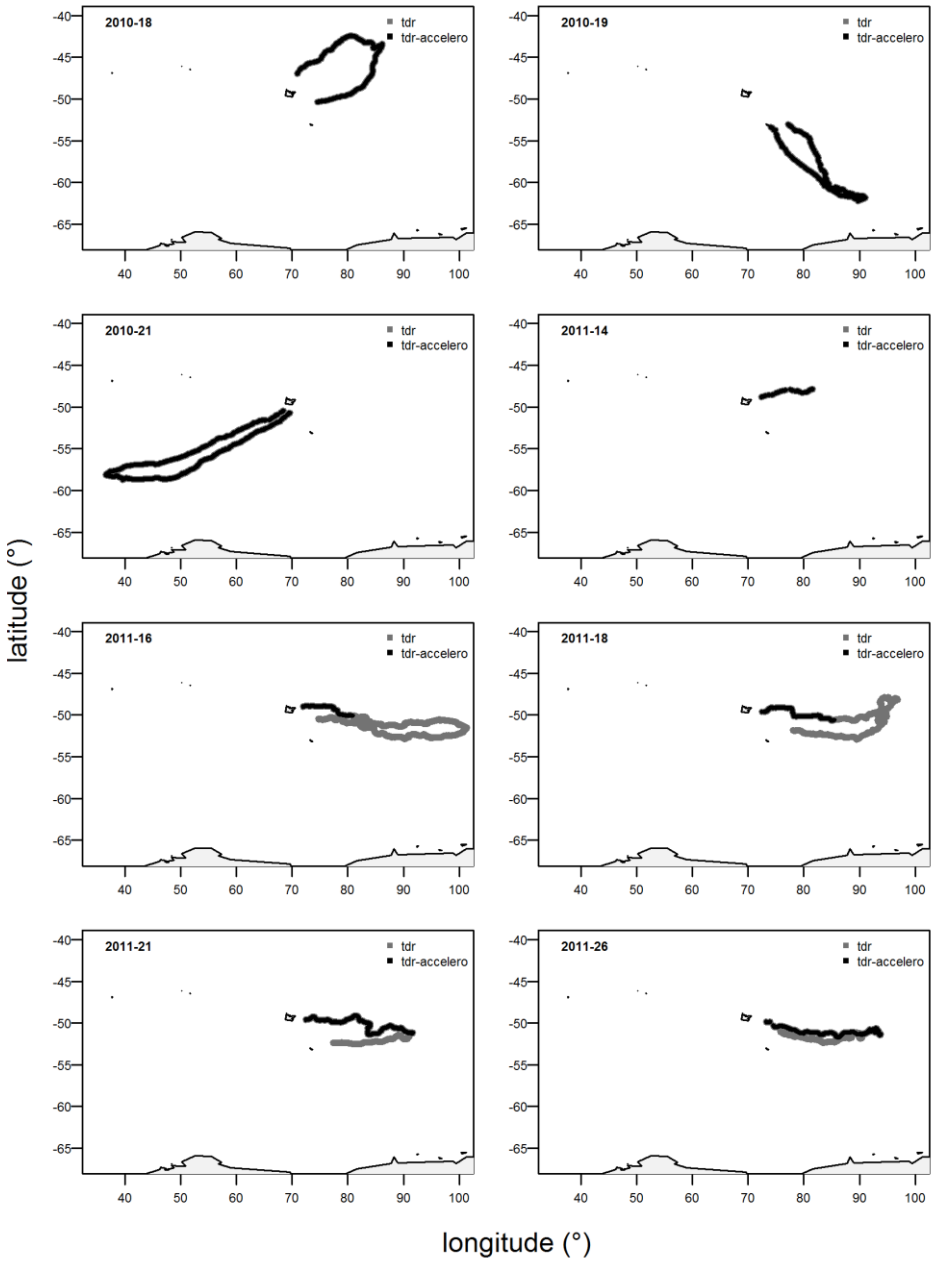

Figure S4.7.4. Tracks of each post-breeding female southern elephant seal in the pelagic zone of the southern Indian Ocean: each track corresponds with time-depth-light (light grey), plus complete or restricted accelerometry data (dark grey). Frontal structures are shown from north to south: subtropical front (dotted); subantarctic front (dashed); polar front (solid); Southern Antarctic Circumpolar Current Front (dotted-dashed); and Antarctic divergence (grey dashed). The Kerguelen and Antarctic shelf areas are considered from the coast to the 1000 m depth isobath (shaded grey).

Appendix S4.7.4 (cont')

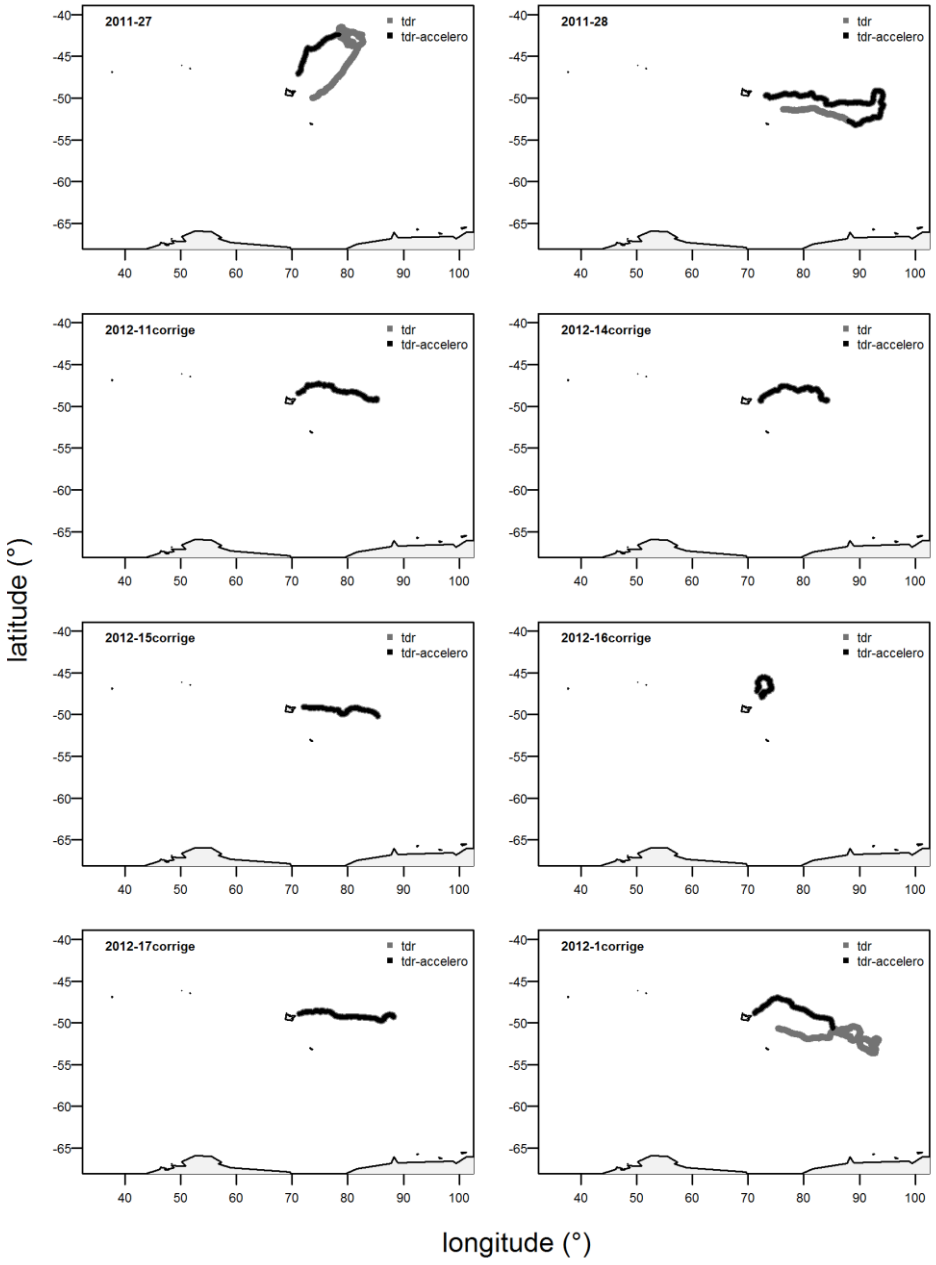

Figure S4.7.4 (cont') Tracks of each post-breeding female southern elephant seal in the pelagic zone of the southern Indian Ocean: each track corresponds with time-depth-light (light grey), plus complete or restricted accelerometry data (dark grey). Frontal structures are shown from north to south: subtropical front (dotted); subantarctic front (dashed); polar front (solid); Southern Antarctic Circumpolar Current Front (dotted-dashed); and Antarctic divergence (grey dashed). The Kerguelen and Antarctic shelf areas are considered from the coast to the 1000 m depth isobath (shaded grey).

Appendix S4.7.4 (cont')

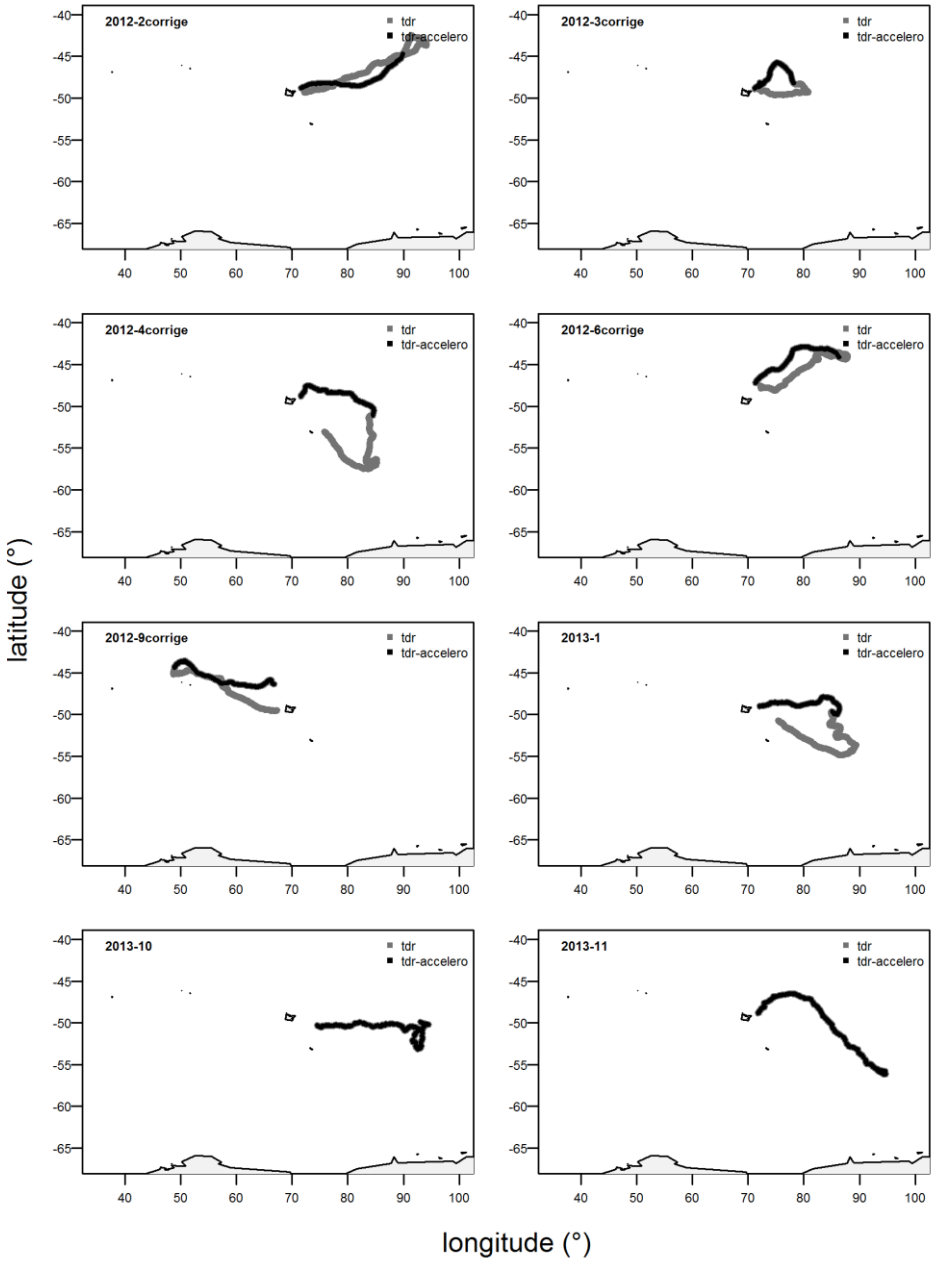

Figure S4.7.4 (cont') Tracks of each post-breeding female southern elephant seal in the pelagic zone of the southern Indian Ocean: each track corresponds with time-depth-light (light grey), plus complete or restricted accelerometry data (dark grey). Frontal structures are shown from north to south: subtropical front (dotted); subantarctic front (dashed); polar front (solid); Southern Antarctic Circumpolar Current Front (dotted-dashed); and Antarctic divergence (grey dashed). The Kerguelen and Antarctic shelf areas are considered from the coast to the 1000 m depth isobath (shaded grey).

Appendix S4.7.4 (cont')

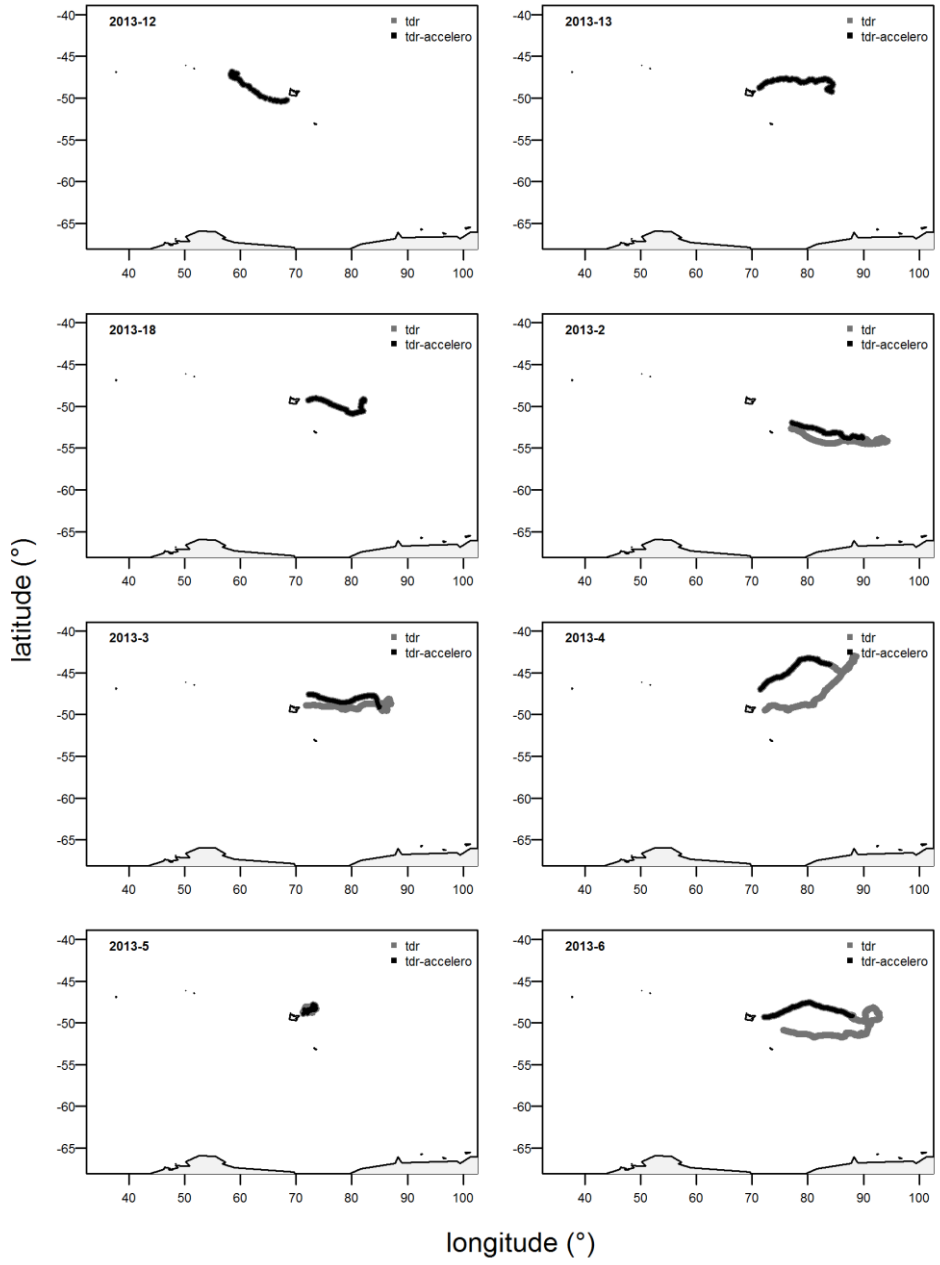

Figure S4.7.4 (cont') Tracks of each post-breeding female southern elephant seal in the pelagic zone of the southern Indian Ocean: each track corresponds with time-depth-light (light grey), plus complete or restricted accelerometry data (dark grey). Frontal structures are shown from north to south: subtropical front (dotted); subantarctic front (dashed); polar front (solid); Southern Antarctic Circumpolar Current Front (dotted-dashed); and Antarctic divergence (grey dashed). The Kerguelen and Antarctic shelf areas are considered from the coast to the 1000 m depth isobath (shaded grey).

Appendix S4.7.4 (cont')

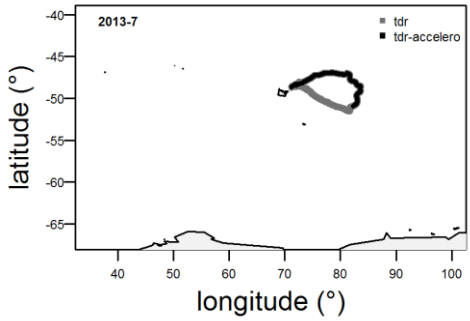

Figure S4.7.4 (cont') Tracks of each post-breeding female southern elephant seal in the pelagic zone of the southern Indian Ocean: each track corresponds with time-depth-light (light grey), plus complete or restricted accelerometry data (dark grey). Frontal structures are shown from north to south: subtropical front (dotted); subantarctic front (dashed); polar front (solid); Southern Antarctic Circumpolar Current Front (dotted-dashed); and Antarctic divergence (grey dashed). The Kerguelen and Antarctic shelf areas are considered from the coast to the 1000 m depth isobath (shaded grey).

Appendix S4.7.5

Meso-scale patches of plankton in the upper euphotic zone: bloom (red) and non-bloom (blue). A smoothing function applied to plankton values from each trip (n=22) reveals spatio-temporal bloom patterns encountered during each trip (*left*). Incomplete trip datasets were excluded from analysis (n=11, see table 1). For details of bloom definition see the methods section. Bloom and non-bloom patches encountered along the seal's track are enclosed in red and dashed blue boxes respectively. Spatial scale of each bloom patch is indicated at the top of each red box. Temporal records of prey capture rates are enclosed in the dashed grey box. Bloom (red) and non-bloom (blue) patches, and dives that coincided with prey capture records (grey) were mapped spatially, along the seal's track (*right*).

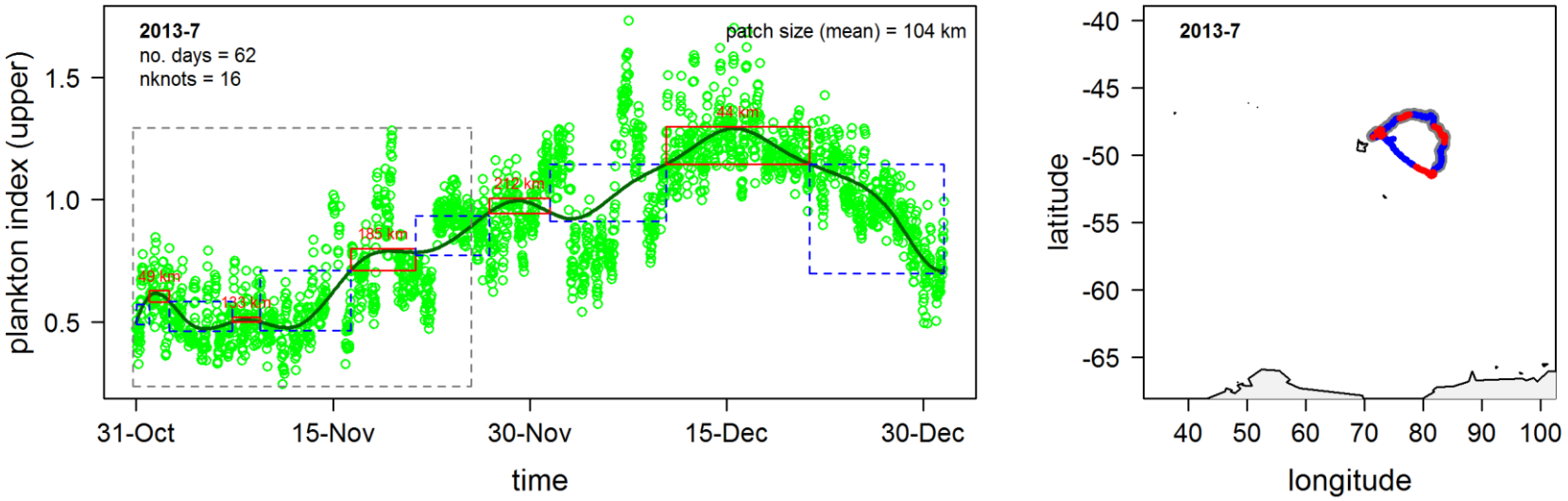

Appendix S4.7.5 (cont')

Meso-scale patches of plankton in the upper euphotic zone: bloom (red) and non-bloom (blue). A smoothing function applied to plankton values from each trip (n=22) reveals temporal bloom patterns encountered during each trip (*left*). Incomplete trip datasets were excluded from analysis (n=11, see table 1). For details of bloom definition see the methods section. Bloom and non-bloom patches encountered along the seal's track are enclosed in red and dashed blue boxes respectively. Spatial scale of each bloom patch is indicated at the top of each red box. Temporal records of prey capture rates are enclosed in the dashed grey box. Bloom (red) and non-bloom (blue) patches, and dives that coincided with prey capture records (grey) were mapped spatially, along the seal's track (*right*).

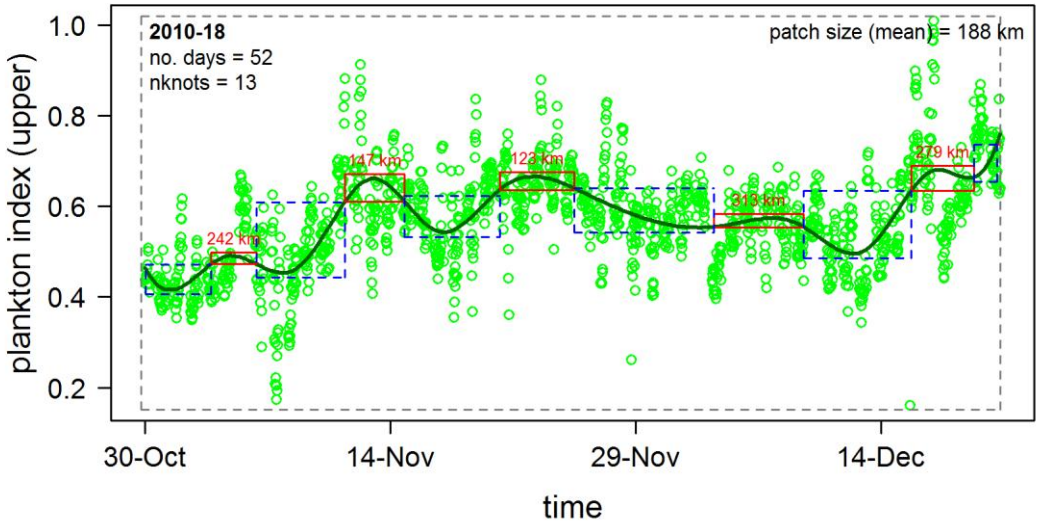

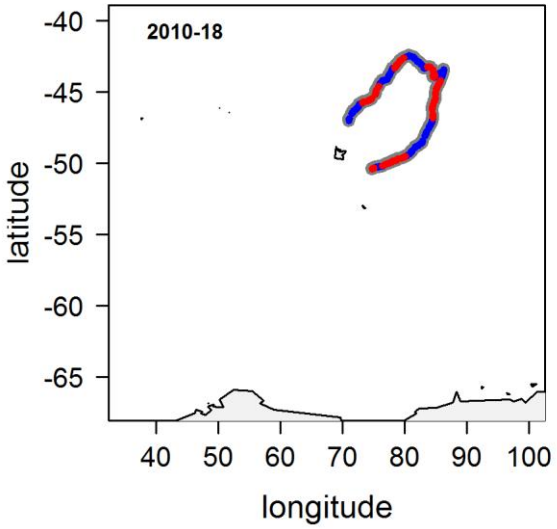

Appendix S4.7.5 (cont')

Meso-scale patches of plankton in the upper euphotic zone: bloom (red) and non-bloom (blue). A smoothing function applied to plankton values from each trip (n=22) reveals temporal bloom patterns encountered during each trip (*left*). Incomplete trip datasets were excluded from analysis (n=11, see table 1). For details of bloom definition see the methods section. Bloom and non-bloom patches encountered along the seal's track are enclosed in red and dashed blue boxes respectively. Spatial scale of each bloom patch is indicated at the top of each red box. Temporal records of prey capture rates are enclosed in the dashed grey box. Bloom (red) and non-bloom (blue) patches, and dives that coincided with prey capture records (grey) were mapped spatially, along the seal's track (*right*).

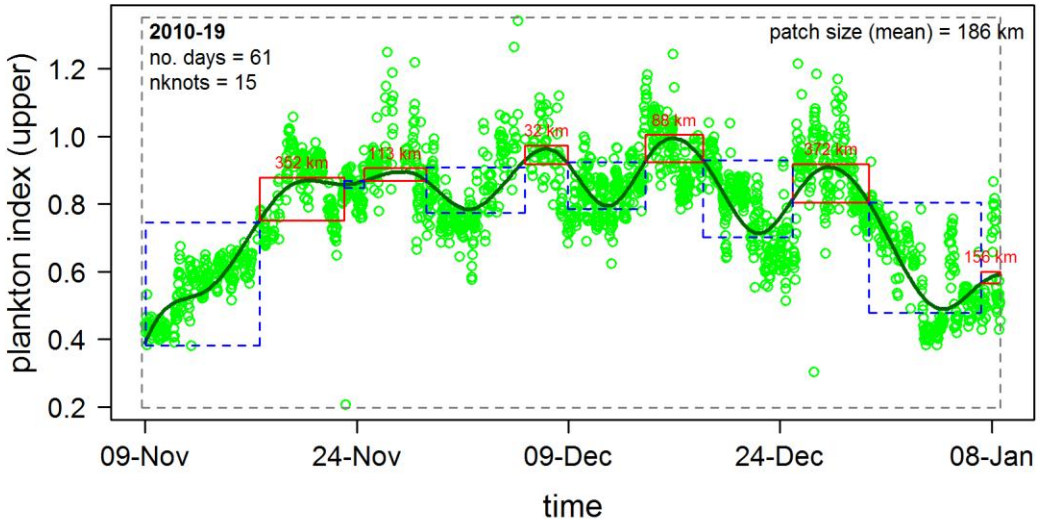

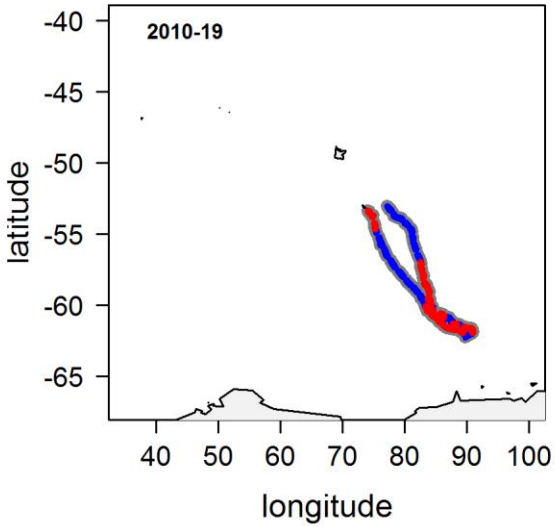

Appendix S4.7.5 (cont')

Meso-scale patches of plankton in the upper euphotic zone: bloom (red) and non-bloom (blue). A smoothing function applied to plankton values from each trip (n=22) reveals temporal bloom patterns encountered during each trip (*left*). Incomplete trip datasets were excluded from analysis (n=11, see table 1). For details of bloom definition see the methods section. Bloom and non-bloom patches encountered along the seal's track are enclosed in red and dashed blue boxes respectively. Spatial scale of each bloom patch is indicated at the top of each red box. Temporal records of prey capture rates are enclosed in the dashed grey box. Bloom (red) and non-bloom (blue) patches, and dives that coincided with prey capture records (grey) were mapped spatially, along the seal's track (*right*).

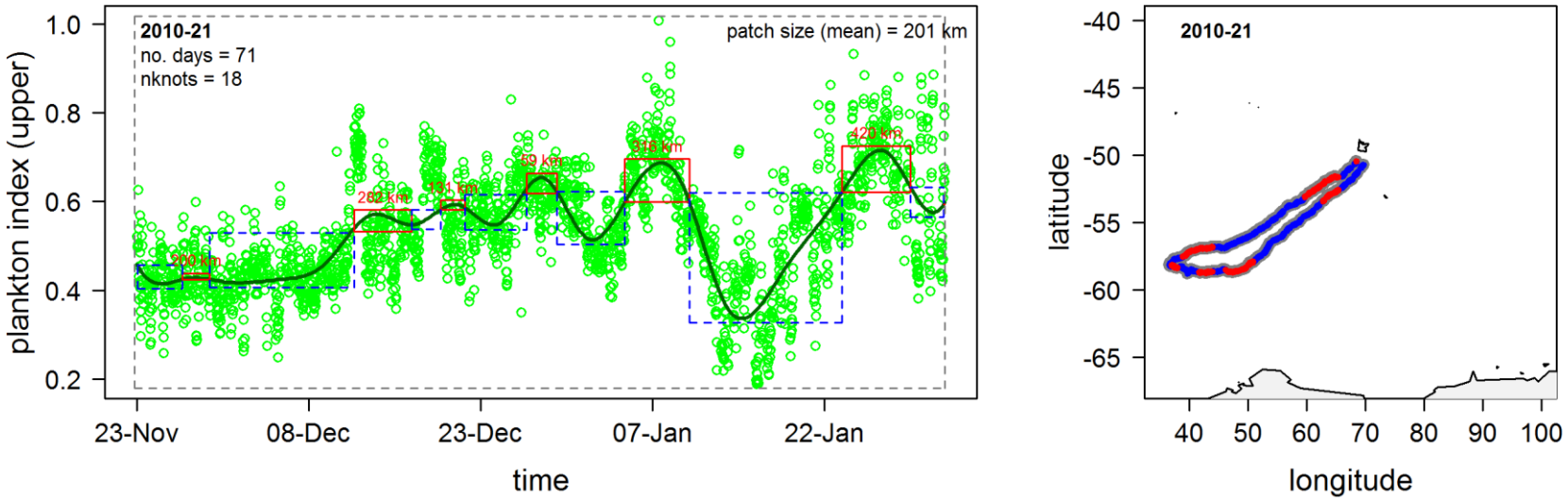

Appendix S4.7.5 (cont')

Meso-scale patches of plankton in the upper euphotic zone: bloom (red) and non-bloom (blue). A smoothing function applied to plankton values from each trip (n=22) reveals temporal bloom patterns encountered during each trip (*left*). Incomplete trip datasets were excluded from analysis (n=11, see table 1). For details of bloom definition see the methods section. Bloom and non-bloom patches encountered along the seal's track are enclosed in red and dashed blue boxes respectively. Spatial scale of each bloom patch is indicated at the top of each red box. Temporal records of prey capture rates are enclosed in the dashed grey box. Bloom (red) and non-bloom (blue) patches, and dives that coincided with prey capture records (grey) were mapped spatially, along the seal's track (*right*).

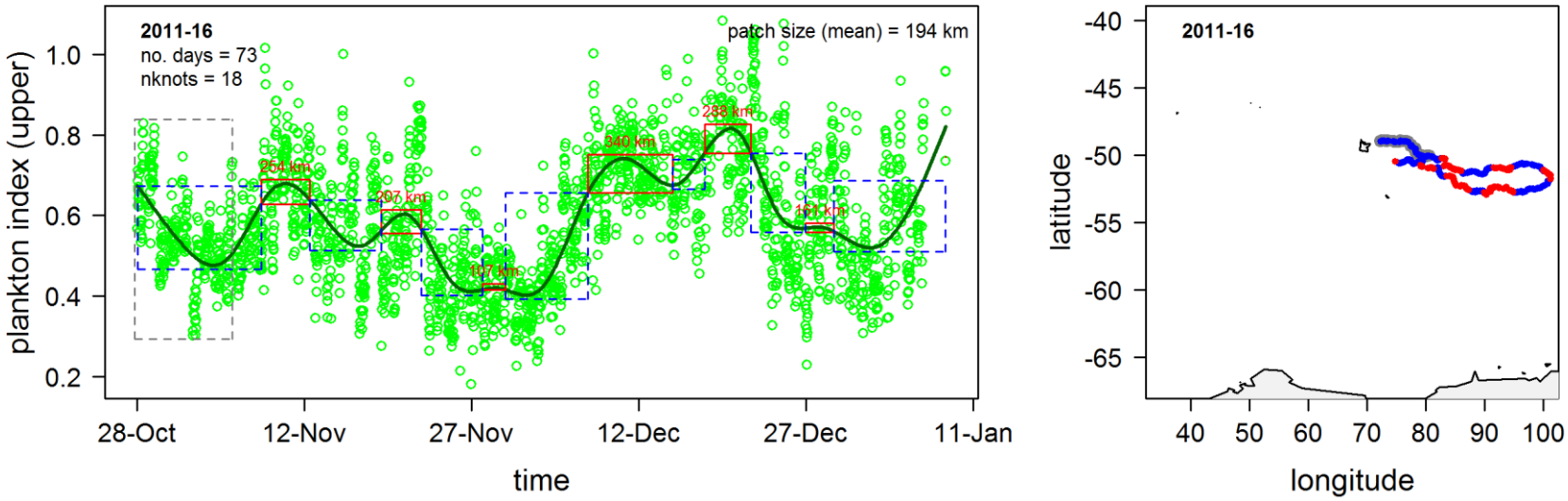

Appendix S4.7.5 (cont')

Meso-scale patches of plankton in the upper euphotic zone: bloom (red) and non-bloom (blue). A smoothing function applied to plankton values from each trip (n=22) reveals temporal bloom patterns encountered during each trip (*left*). Incomplete trip datasets were excluded from analysis (n=11, see table 1). For details of bloom definition see the methods section. Bloom and non-bloom patches encountered along the seal's track are enclosed in red and dashed blue boxes respectively. Spatial scale of each bloom patch is indicated at the top of each red box. Temporal records of prey capture rates are enclosed in the dashed grey box. Bloom (red) and non-bloom (blue) patches, and dives that coincided with prey capture records (grey) were mapped spatially, along the seal's track (*right*).

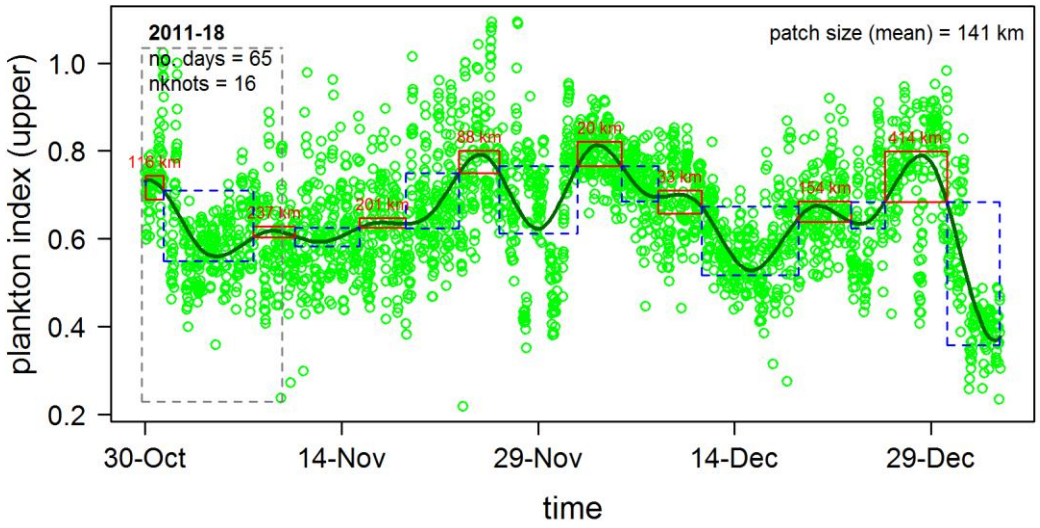

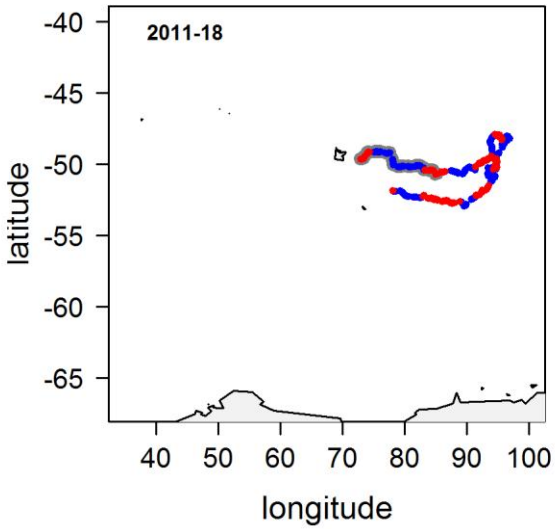

Appendix S4.7.5 (cont')

Meso-scale patches of plankton in the upper euphotic zone: bloom (red) and non-bloom (blue). A smoothing function applied to plankton values from each trip (n=22) reveals temporal bloom patterns encountered during each trip (*left*). Incomplete trip datasets were excluded from analysis (n=11, see table 1). For details of bloom definition see the methods section. Bloom and non-bloom patches encountered along the seal's track are enclosed in red and dashed blue boxes respectively. Spatial scale of each bloom patch is indicated at the top of each red box. Temporal records of prey capture rates are enclosed in the dashed grey box. Bloom (red) and non-bloom (blue) patches, and dives that coincided with prey capture records (grey) were mapped spatially, along the seal's track (*right*).

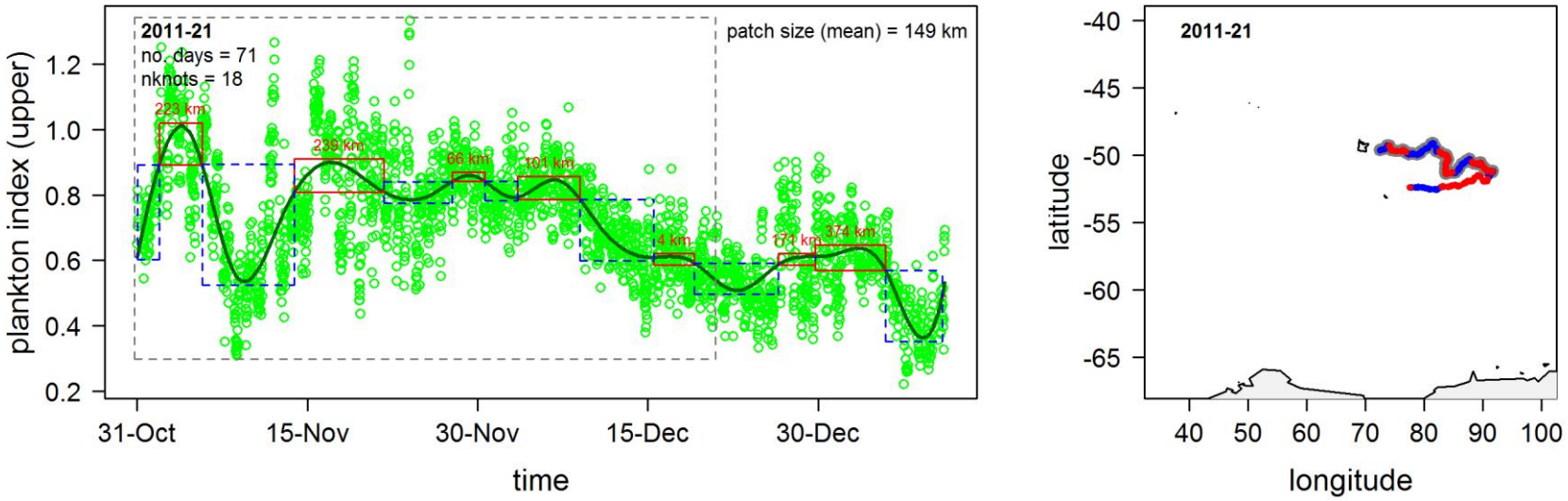

Appendix S4.7.5 (cont')

Meso-scale patches of plankton in the upper euphotic zone: bloom (red) and non-bloom (blue). A smoothing function applied to plankton values from each trip (n=22) reveals temporal bloom patterns encountered during each trip (*left*). Incomplete trip datasets were excluded from analysis (n=11, see table 1). For details of bloom definition see the methods section. Bloom and non-bloom patches encountered along the seal's track are enclosed in red and dashed blue boxes respectively. Spatial scale of each bloom patch is indicated at the top of each red box. Temporal records of prey capture rates are enclosed in the dashed grey box. Bloom (red) and non-bloom (blue) patches, and dives that coincided with prey capture records (grey) were mapped spatially, along the seal's track (*right*).

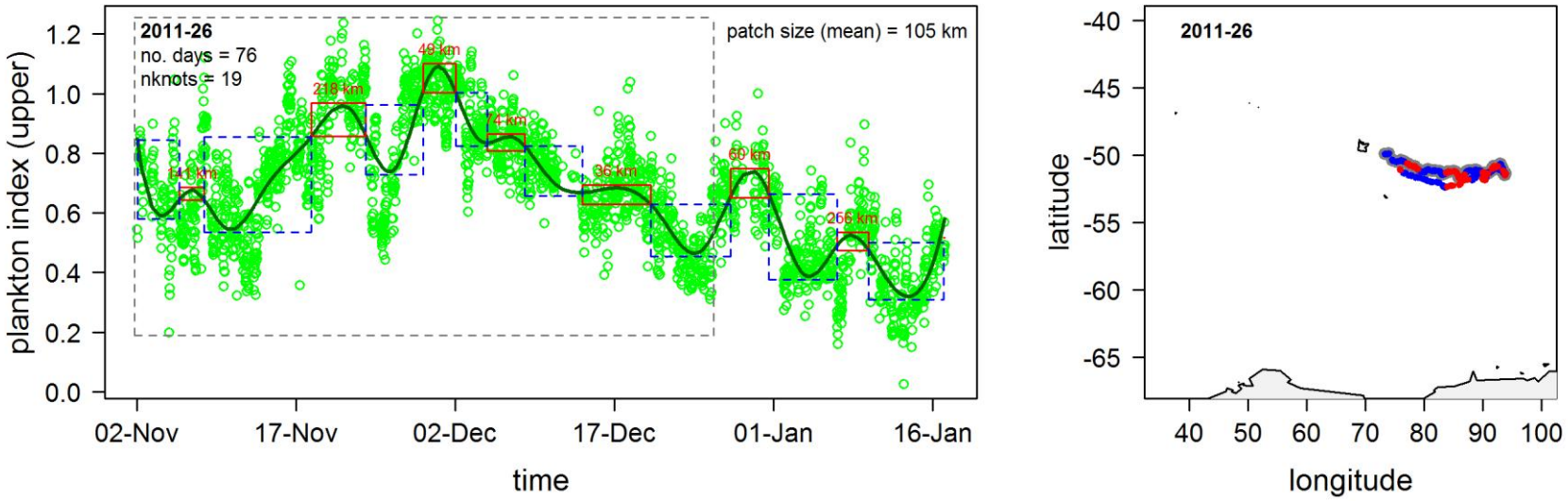

Appendix S4.7.5 (cont')

Meso-scale patches of plankton in the upper euphotic zone: bloom (red) and non-bloom (blue). A smoothing function applied to plankton values from each trip (n=22) reveals temporal bloom patterns encountered during each trip (*left*). Incomplete trip datasets were excluded from analysis (n=11, see table 1). For details of bloom definition see the methods section. Bloom and non-bloom patches encountered along the seal's track are enclosed in red and dashed blue boxes respectively. Spatial scale of each bloom patch is indicated at the top of each red box. Temporal records of prey capture rates are enclosed in the dashed grey box. Bloom (red) and non-bloom (blue) patches, and dives that coincided with prey capture records (grey) were mapped spatially, along the seal's track (*right*).

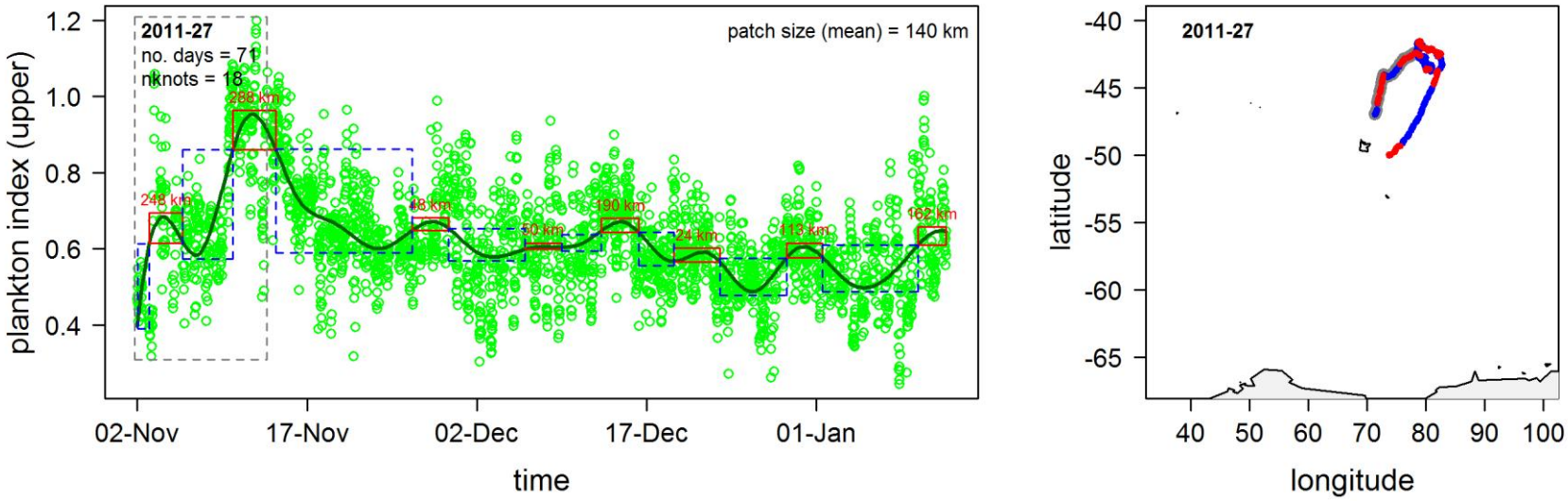

Appendix S4.7.5 (cont')

Meso-scale patches of plankton in the upper euphotic zone: bloom (red) and non-bloom (blue). A smoothing function applied to plankton values from each trip (n=22) reveals temporal bloom patterns encountered during each trip (*left*). Incomplete trip datasets were excluded from analysis (n=11, see table 1). For details of bloom definition see the methods section. Bloom and non-bloom patches encountered along the seal's track are enclosed in red and dashed blue boxes respectively. Spatial scale of each bloom patch is indicated at the top of each red box. Temporal records of prey capture rates are enclosed in the dashed grey box. Bloom (red) and non-bloom (blue) patches, and dives that coincided with prey capture records (grey) were mapped spatially, along the seal's track (*right*).

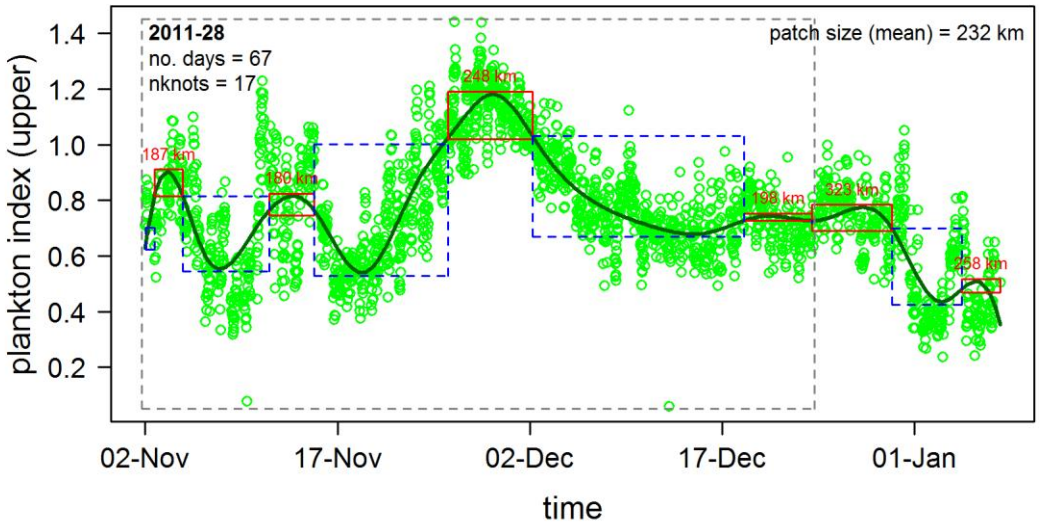

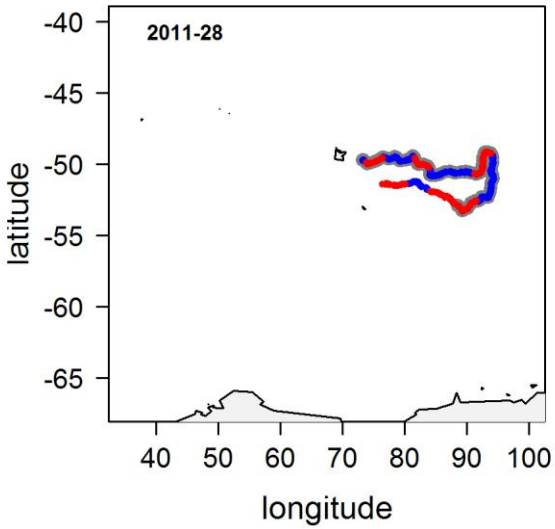

Appendix S4.7.5 (cont')

Meso-scale patches of plankton in the upper euphotic zone: bloom (red) and non-bloom (blue). A smoothing function applied to plankton values from each trip (n=22) reveals temporal bloom patterns encountered during each trip (*left*). Incomplete trip datasets were excluded from analysis (n=11, see table 1). For details of bloom definition see the methods section. Bloom and non-bloom patches encountered along the seal's track are enclosed in red and dashed blue boxes respectively. Spatial scale of each bloom patch is indicated at the top of each red box. Temporal records of prey capture rates are enclosed in the dashed grey box. Bloom (red) and non-bloom (blue) patches, and dives that coincided with prey capture records (grey) were mapped spatially, along the seal's track (*right*).

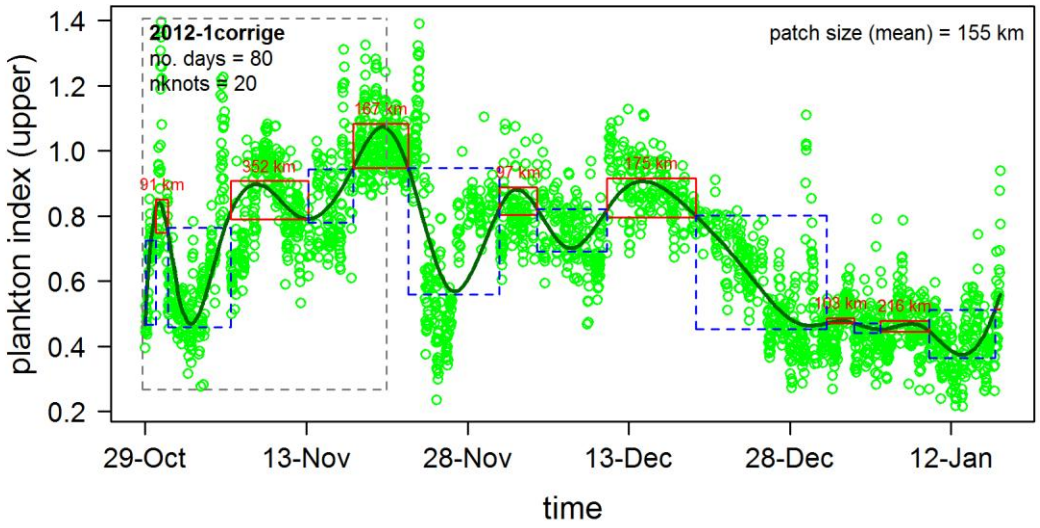

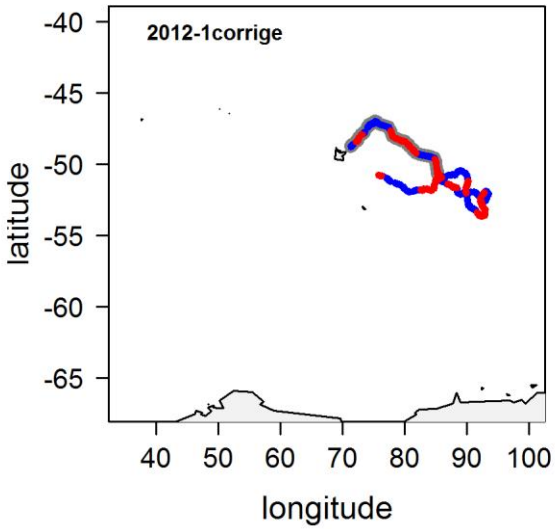

Appendix S4.7.5 (cont')

Meso-scale patches of plankton in the upper euphotic zone: bloom (red) and non-bloom (blue). A smoothing function applied to plankton values from each trip (n=22) reveals temporal bloom patterns encountered during each trip (*left*). Incomplete trip datasets were excluded from analysis (n=11, see table 1). For details of bloom definition see the methods section. Bloom and non-bloom patches encountered along the seal's track are enclosed in red and dashed blue boxes respectively. Spatial scale of each bloom patch is indicated at the top of each red box. Temporal records of prey capture rates are enclosed in the dashed grey box. Bloom (red) and non-bloom (blue) patches, and dives that coincided with prey capture records (grey) were mapped spatially, along the seal's track (*right*).

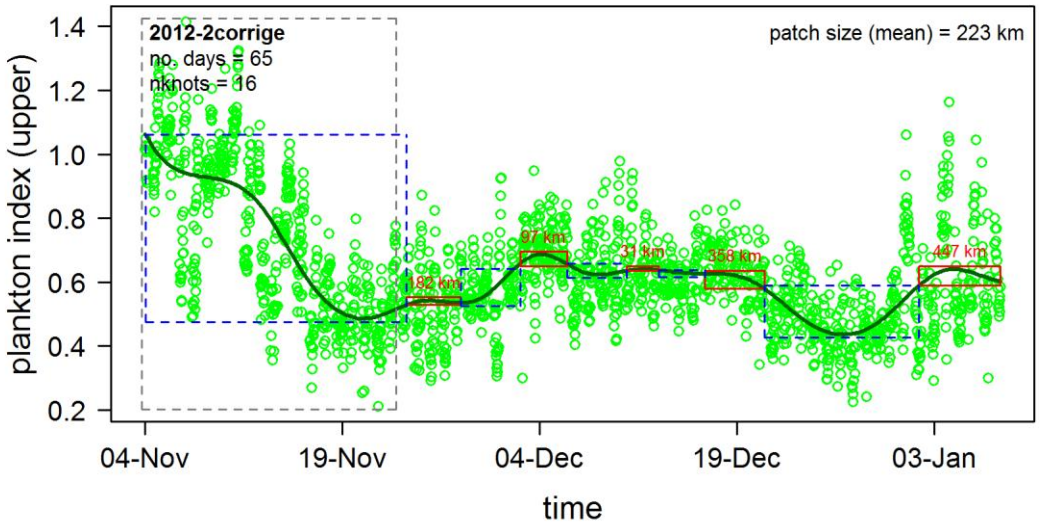

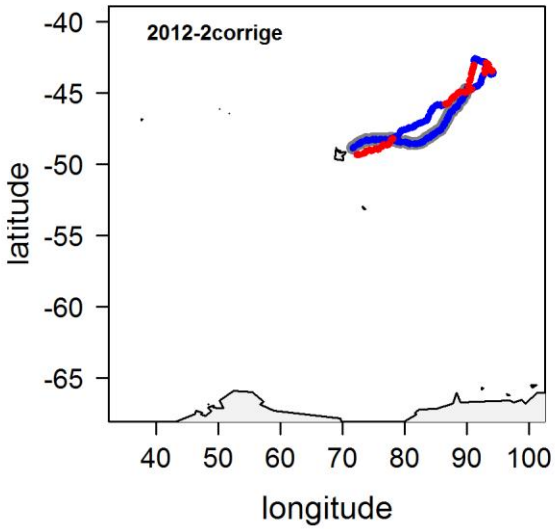

Appendix S4.7.5 (cont')

Meso-scale patches of plankton in the upper euphotic zone: bloom (red) and non-bloom (blue). A smoothing function applied to plankton values from each trip (n=22) reveals temporal bloom patterns encountered during each trip (*left*). Incomplete trip datasets were excluded from analysis (n=11, see table 1). For details of bloom definition see the methods section. Bloom and non-bloom patches encountered along the seal's track are enclosed in red and dashed blue boxes respectively. Spatial scale of each bloom patch is indicated at the top of each red box. Temporal records of prey capture rates are enclosed in the dashed grey box. Bloom (red) and non-bloom (blue) patches, and dives that coincided with prey capture records (grey) were mapped spatially, along the seal's track (*right*).

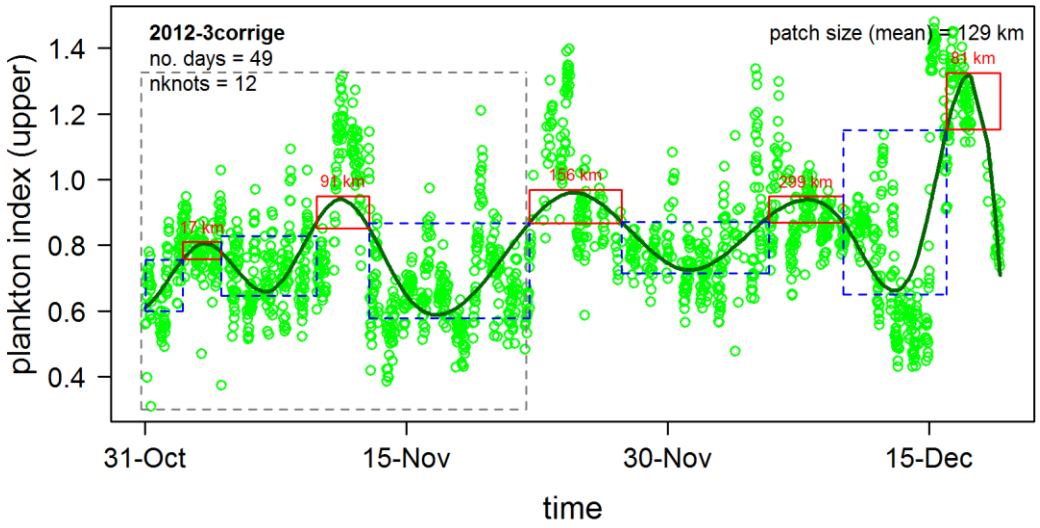

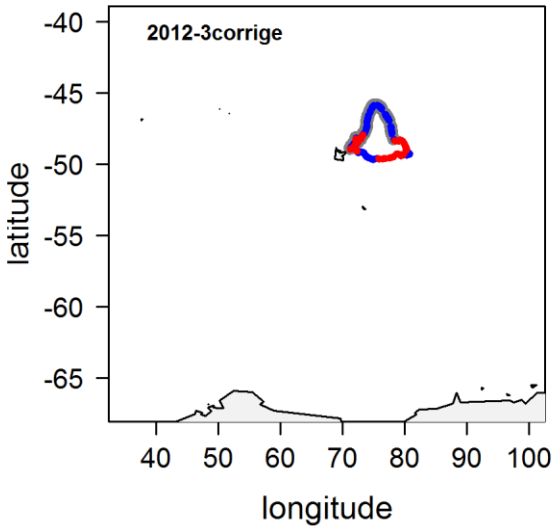

Appendix S4.7.5 (cont')

Meso-scale patches of plankton in the upper euphotic zone: bloom (red) and non-bloom (blue). A smoothing function applied to plankton values from each trip (n=22) reveals temporal bloom patterns encountered during each trip (*left*). Incomplete trip datasets were excluded from analysis (n=11, see table 1). For details of bloom definition see the methods section. Bloom and non-bloom patches encountered along the seal's track are enclosed in red and dashed blue boxes respectively. Spatial scale of each bloom patch is indicated at the top of each red box. Temporal records of prey capture rates are enclosed in the dashed grey box. Bloom (red) and non-bloom (blue) patches, and dives that coincided with prey capture records (grey) were mapped spatially, along the seal's track (*right*).

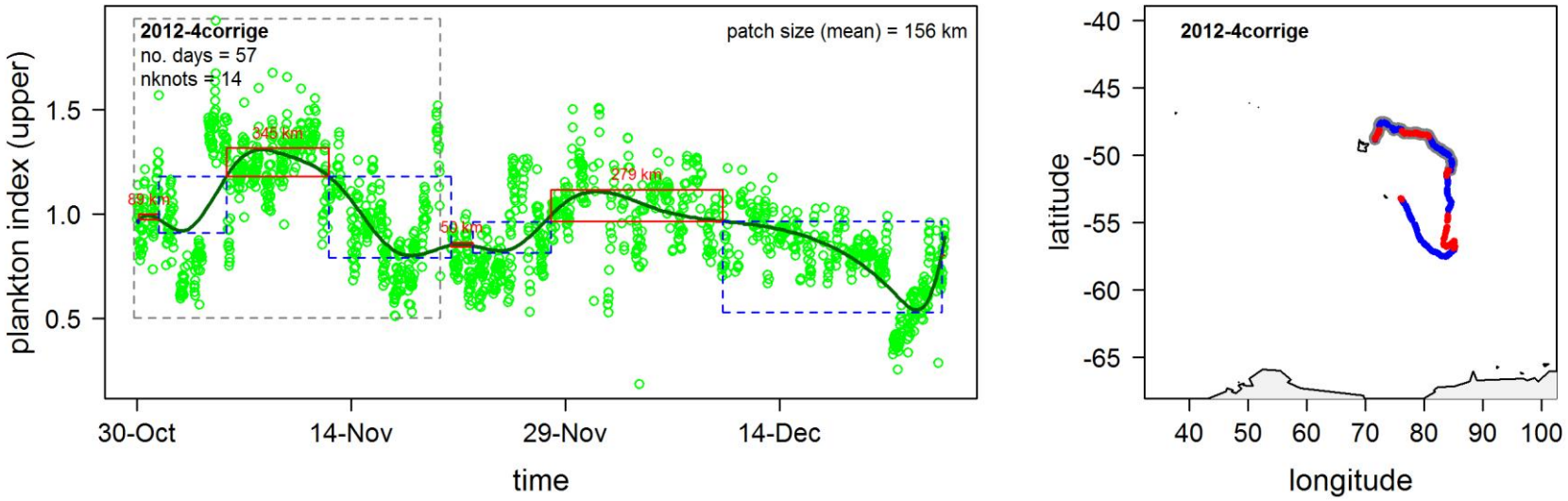

Appendix S4.7.5 (cont')

Meso-scale patches of plankton in the upper euphotic zone: bloom (red) and non-bloom (blue). A smoothing function applied to plankton values from each trip (n=22) reveals temporal bloom patterns encountered during each trip (*left*). Incomplete trip datasets were excluded from analysis (n=11, see table 1). For details of bloom definition see the methods section. Bloom and non-bloom patches encountered along the seal's track are enclosed in red and dashed blue boxes respectively. Spatial scale of each bloom patch is indicated at the top of each red box. Temporal records of prey capture rates are enclosed in the dashed grey box. Bloom (red) and non-bloom (blue) patches, and dives that coincided with prey capture records (grey) were mapped spatially, along the seal's track (*right*).

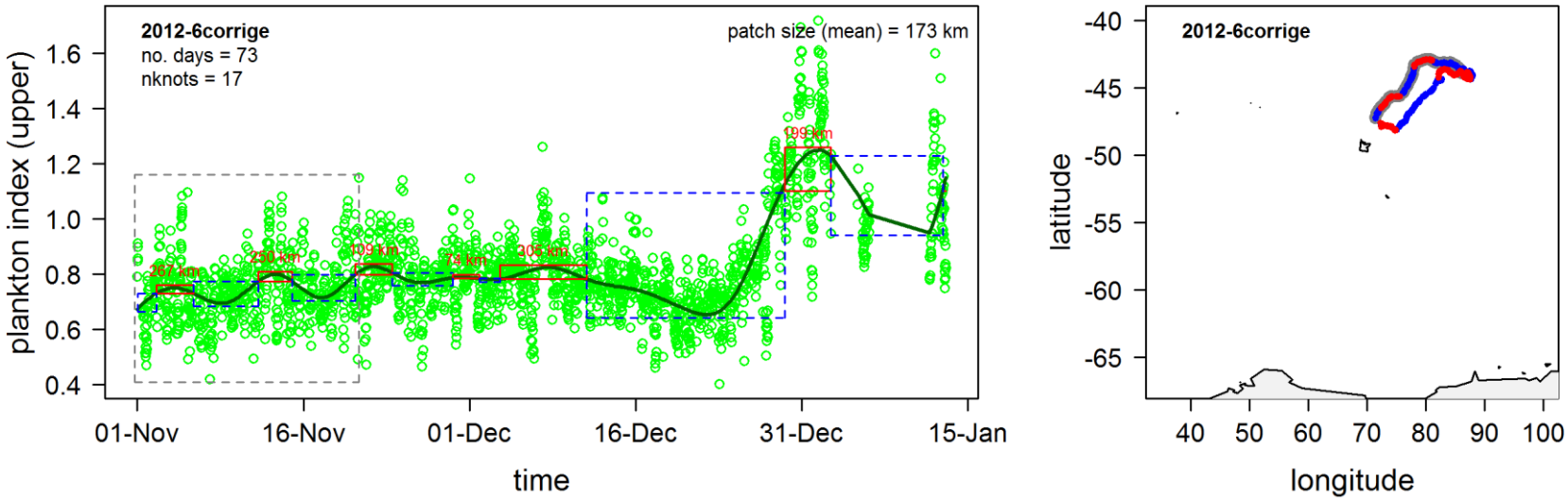

Appendix S4.7.5 (cont')

Meso-scale patches of plankton in the upper euphotic zone: bloom (red) and non-bloom (blue). A smoothing function applied to plankton values from each trip (n=22) reveals temporal bloom patterns encountered during each trip (*left*). Incomplete trip datasets were excluded from analysis (n=11, see table 1). For details of bloom definition see the methods section. Bloom and non-bloom patches encountered along the seal's track are enclosed in red and dashed blue boxes respectively. Spatial scale of each bloom patch is indicated at the top of each red box. Temporal records of prey capture rates are enclosed in the dashed grey box. Bloom (red) and non-bloom (blue) patches, and dives that coincided with prey capture records (grey) were mapped spatially, along the seal's track (*right*).

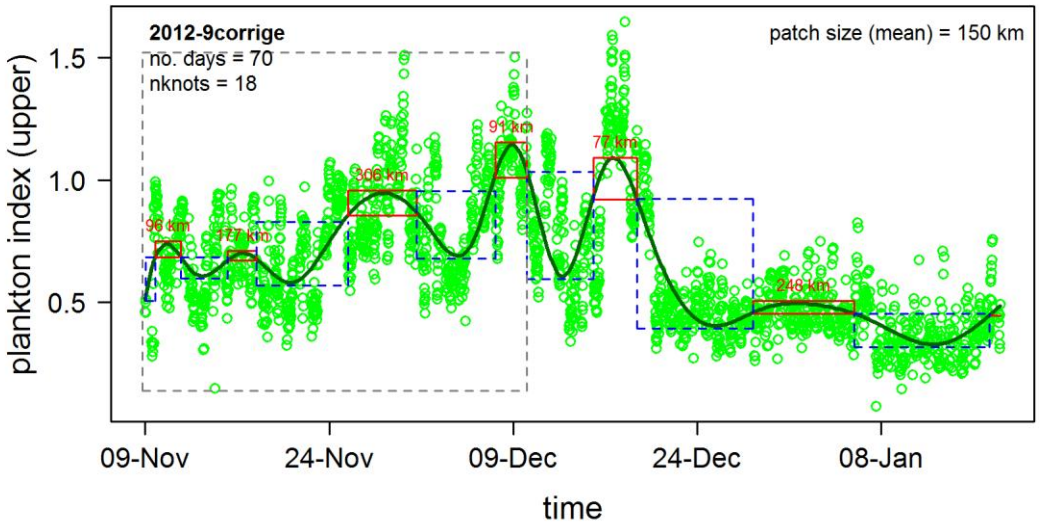

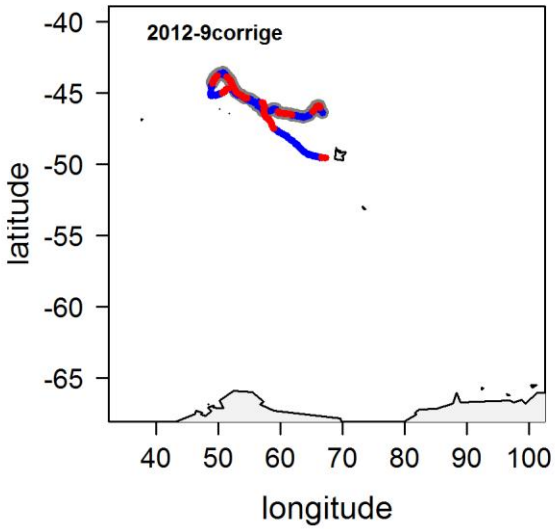

Appendix S4.7.5 (cont')

Meso-scale patches of plankton in the upper euphotic zone: bloom (red) and non-bloom (blue). A smoothing function applied to plankton values from each trip (n=22) reveals temporal bloom patterns encountered during each trip (*left*). Incomplete trip datasets were excluded from analysis (n=11, see table 1). For details of bloom definition see the methods section. Bloom and non-bloom patches encountered along the seal's track are enclosed in red and dashed blue boxes respectively. Spatial scale of each bloom patch is indicated at the top of each red box. Temporal records of prey capture rates are enclosed in the dashed grey box. Bloom (red) and non-bloom (blue) patches, and dives that coincided with prey capture records (grey) were mapped spatially, along the seal's track (*right*).

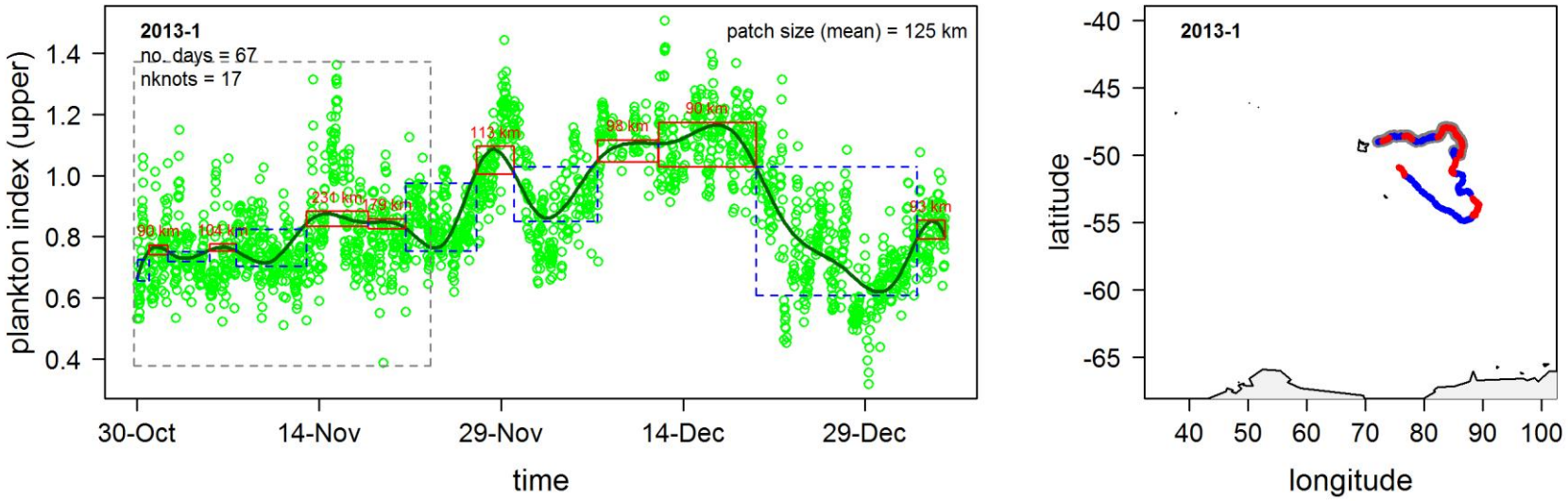

Appendix S4.7.5 (cont')

Meso-scale patches of plankton in the upper euphotic zone: bloom (red) and non-bloom (blue). A smoothing function applied to plankton values from each trip (n=22) reveals temporal bloom patterns encountered during each trip (*left*). Incomplete trip datasets were excluded from analysis (n=11, see table 1). For details of bloom definition see the methods section. Bloom and non-bloom patches encountered along the seal's track are enclosed in red and dashed blue boxes respectively. Spatial scale of each bloom patch is indicated at the top of each red box. Temporal records of prey capture rates are enclosed in the dashed grey box. Bloom (red) and non-bloom (blue) patches, and dives that coincided with prey capture records (grey) were mapped spatially, along the seal's track (*right*).

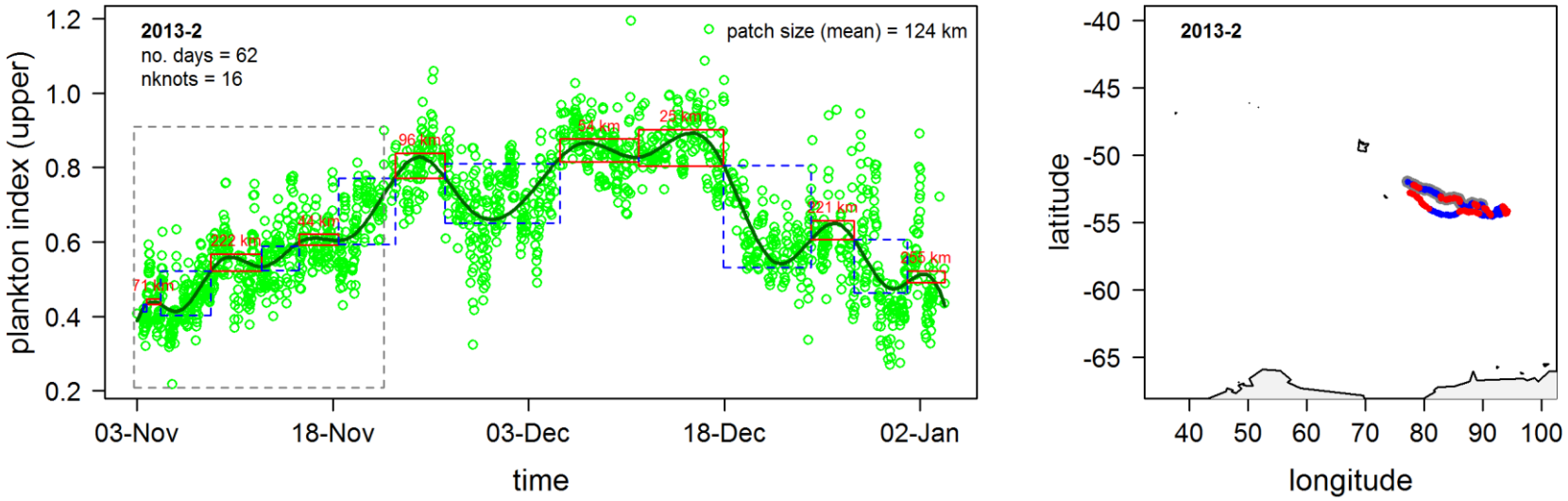

Appendix S4.7.5 (cont')

Meso-scale patches of plankton in the upper euphotic zone: bloom (red) and non-bloom (blue). A smoothing function applied to plankton values from each trip (n=22) reveals temporal bloom patterns encountered during each trip (*left*). Incomplete trip datasets were excluded from analysis (n=11, see table 1). For details of bloom definition see the methods section. Bloom and non-bloom patches encountered along the seal's track are enclosed in red and dashed blue boxes respectively. Spatial scale of each bloom patch is indicated at the top of each red box. Temporal records of prey capture rates are enclosed in the dashed grey box. Bloom (red) and non-bloom (blue) patches, and dives that coincided with prey capture records (grey) were mapped spatially, along the seal's track (*right*).

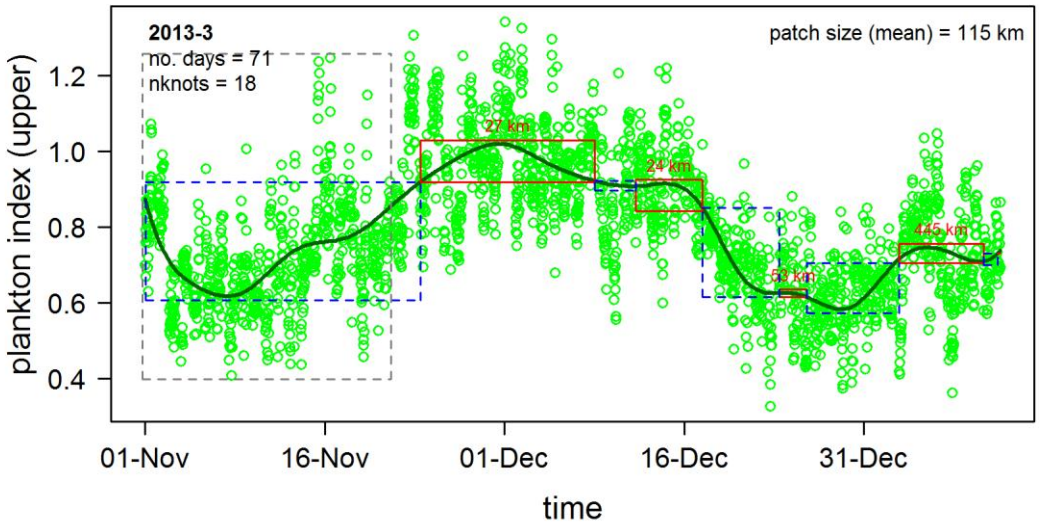

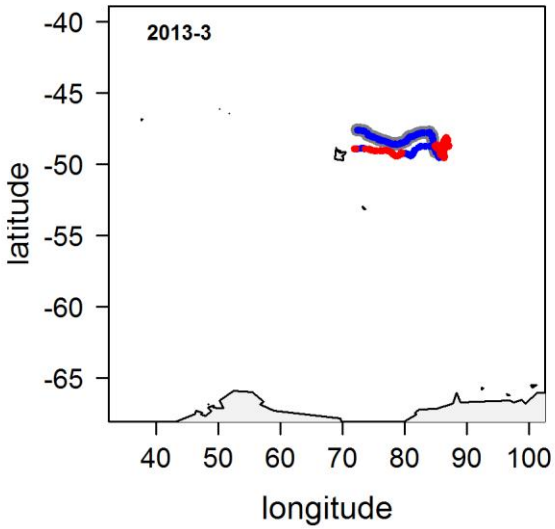

Appendix S4.7.5 (cont')

Meso-scale patches of plankton in the upper euphotic zone: bloom (red) and non-bloom (blue). A smoothing function applied to plankton values from each trip (n=22) reveals temporal bloom patterns encountered during each trip (*left*). Incomplete trip datasets were excluded from analysis (n=11, see table 1). For details of bloom definition see the methods section. Bloom and non-bloom patches encountered along the seal's track are enclosed in red and dashed blue boxes respectively. Spatial scale of each bloom patch is indicated at the top of each red box. Temporal records of prey capture rates are enclosed in the dashed grey box. Bloom (red) and non-bloom (blue) patches, and dives that coincided with prey capture records (grey) were mapped spatially, along the seal's track (*right*).

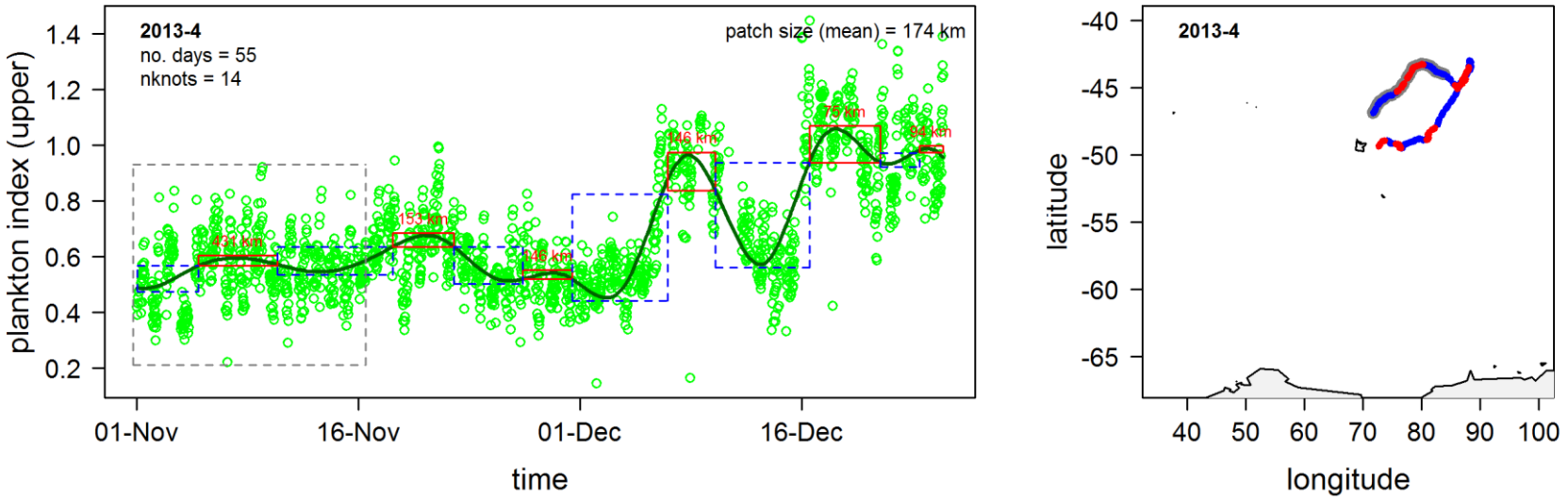

Appendix S4.7.5 (cont')

Meso-scale patches of plankton in the upper euphotic zone: bloom (red) and non-bloom (blue). A smoothing function applied to plankton values from each trip (n=22) reveals temporal bloom patterns encountered during each trip (*left*). Incomplete trip datasets were excluded from analysis (n=11, see table 1). For details of bloom definition see the methods section. Bloom and non-bloom patches encountered along the seal's track are enclosed in red and dashed blue boxes respectively. Spatial scale of each bloom patch is indicated at the top of each red box. Temporal records of prey capture rates are enclosed in the dashed grey box. Bloom (red) and non-bloom (blue) patches, and dives that coincided with prey capture records (grey) were mapped spatially, along the seal's track (*right*).

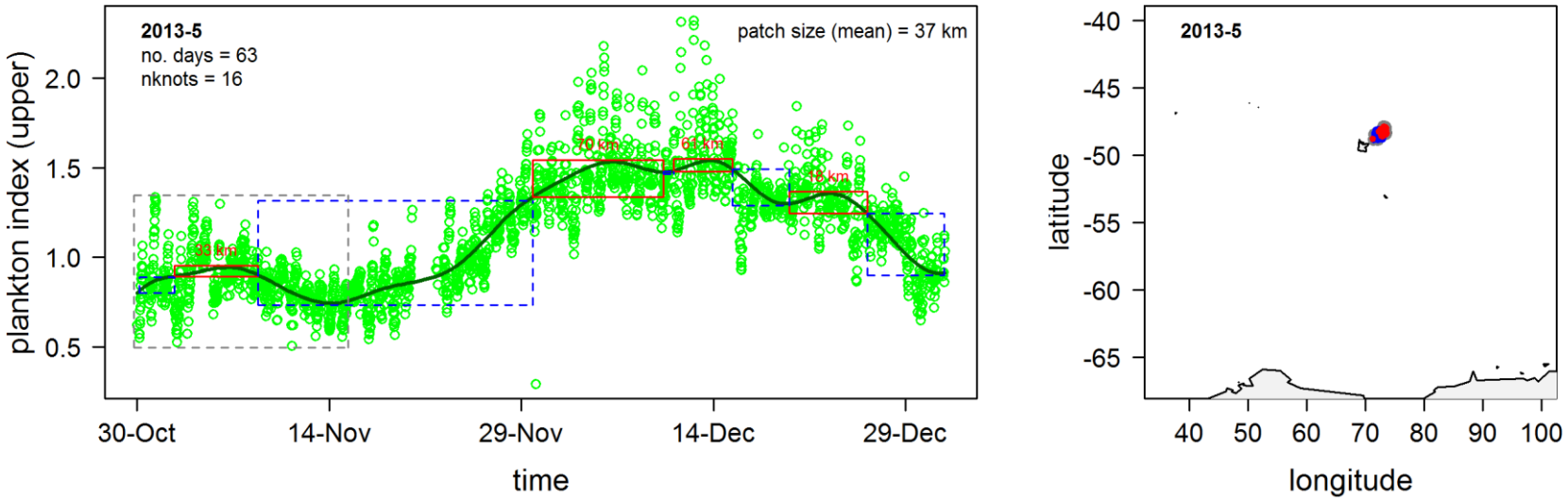

Appendix S4.7.5 (cont')

Meso-scale patches of plankton in the upper euphotic zone: bloom (red) and non-bloom (blue). A smoothing function applied to plankton values from each trip (n=22) reveals temporal bloom patterns encountered during each trip (*left*). Incomplete trip datasets were excluded from analysis (n=11, see table 1). For details of bloom definition see the methods section. Bloom and non-bloom patches encountered along the seal's track are enclosed in red and dashed blue boxes respectively. Spatial scale of each bloom patch is indicated at the top of each red box. Temporal records of prey capture rates are enclosed in the dashed grey box. Bloom (red) and non-bloom (blue) patches, and dives that coincided with prey capture records (grey) were mapped spatially, along the seal's track (*right*).

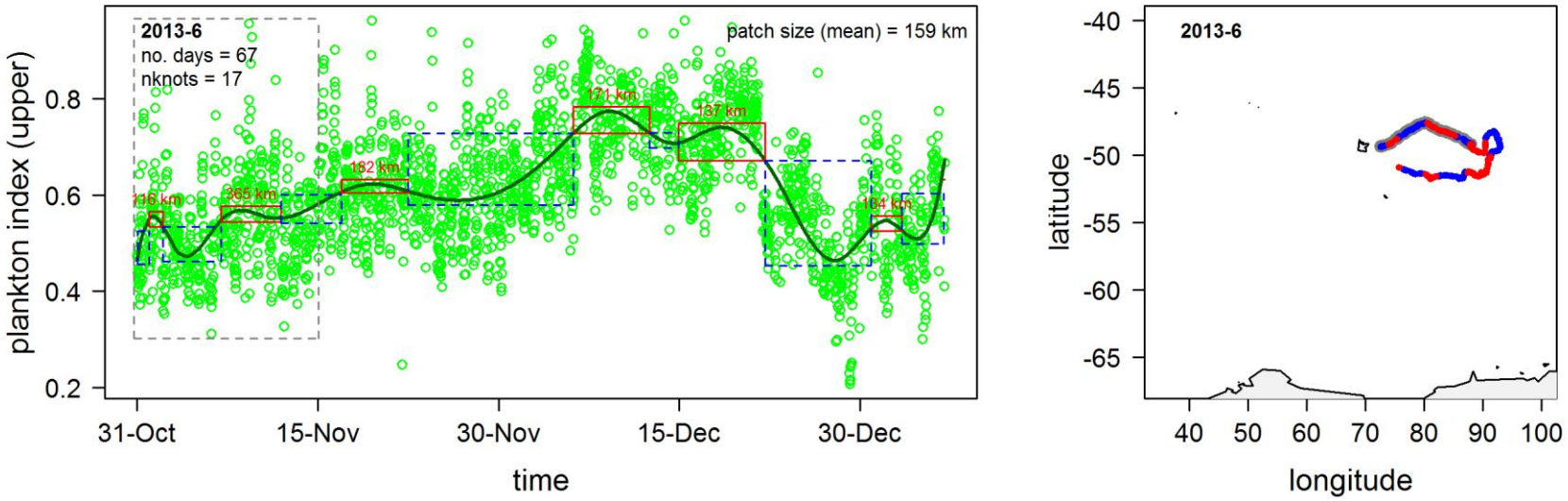

Appendix S4.7.6

Meso-scale patches of plankton in the lower euphotic zone: bloom (red) and non-bloom (blue). A smoothing function applied to plankton values from each trip (n=22) reveals temporal bloom patterns encountered during each trip (*left*). Incomplete trip datasets were excluded from analysis (n=11, see table 1). For details of bloom definition see the methods section. Bloom and non-bloom patches encountered along the seal's track are enclosed in red and dashed blue boxes respectively. Spatial scale of each bloom patch is indicated at the top of each red box. Temporal records of prey capture rates are enclosed in the dashed grey box. Bloom (red) and non-bloom (blue) patches, and dives that coincided with prey capture records (grey) were mapped spatially, along the seal's track (*right*).

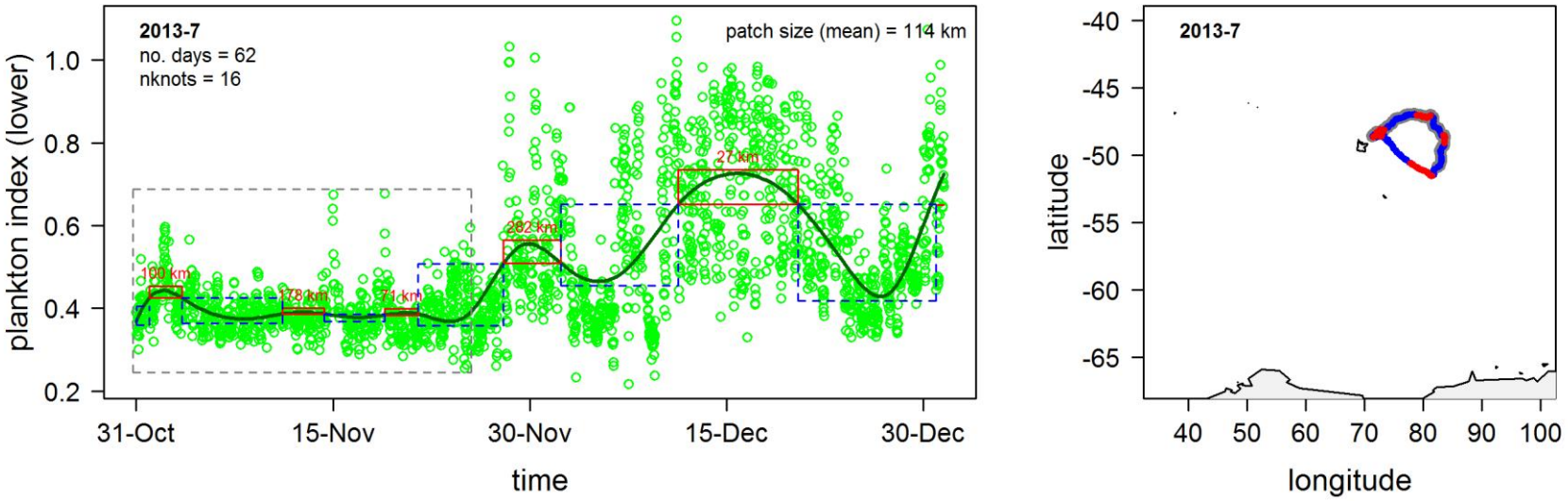

Appendix S4.7.6 (cont')

Meso-scale patches of plankton in the lower euphotic zone: bloom (red) and non-bloom (blue). A smoothing function applied to plankton values from each trip (n=22) reveals temporal bloom patterns encountered during each trip (*left*). Incomplete trip datasets were excluded from analysis (n=11, see table 1). For details of bloom definition see the methods section. Bloom and non-bloom patches encountered along the seal's track are enclosed in red and dashed blue boxes respectively. Spatial scale of each bloom patch is indicated at the top of each red box. Temporal records of prey capture rates are enclosed in the dashed grey box. Bloom (red) and non-bloom (blue) patches, and dives that coincided with prey capture records (grey) were mapped spatially, along the seal's track (*right*).

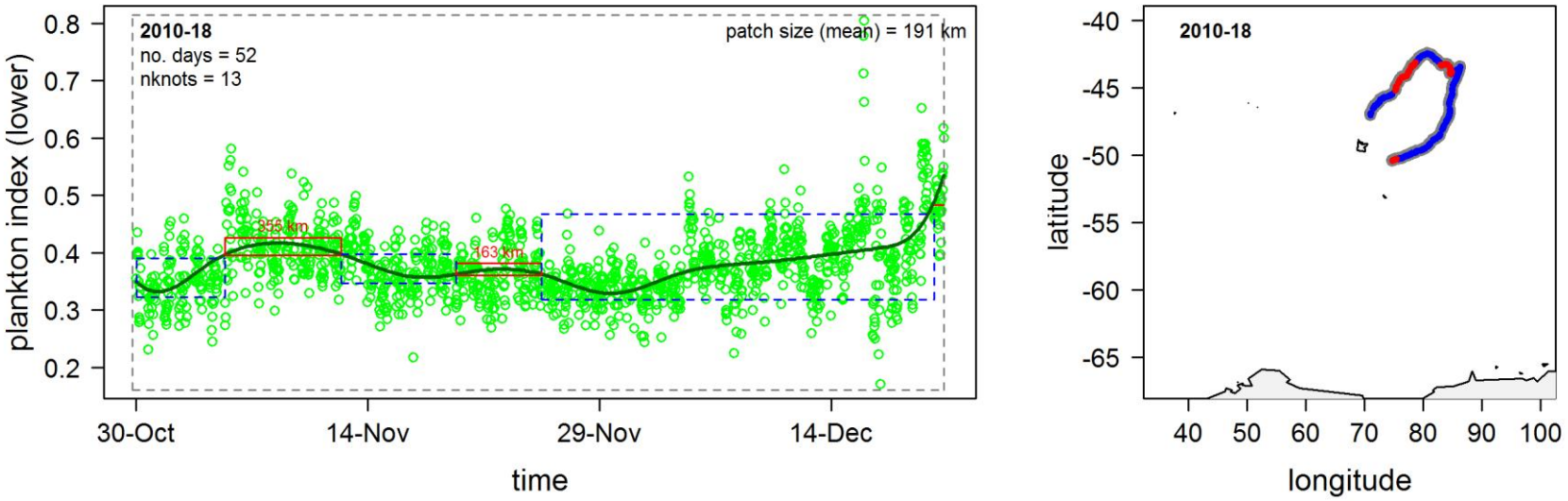

Appendix S4.7.6 (cont')

Meso-scale patches of plankton in the lower euphotic zone: bloom (red) and non-bloom (blue). A smoothing function applied to plankton values from each trip (n=22) reveals temporal bloom patterns encountered during each trip (*left*). Incomplete trip datasets were excluded from analysis (n=11, see table 1). For details of bloom definition see the methods section. Bloom and non-bloom patches encountered along the seal's track are enclosed in red and dashed blue boxes respectively. Spatial scale of each bloom patch is indicated at the top of each red box. Temporal records of prey capture rates are enclosed in the dashed grey box. Bloom (red) and non-bloom (blue) patches, and dives that coincided with prey capture records (grey) were mapped spatially, along the seal's track (*right*).

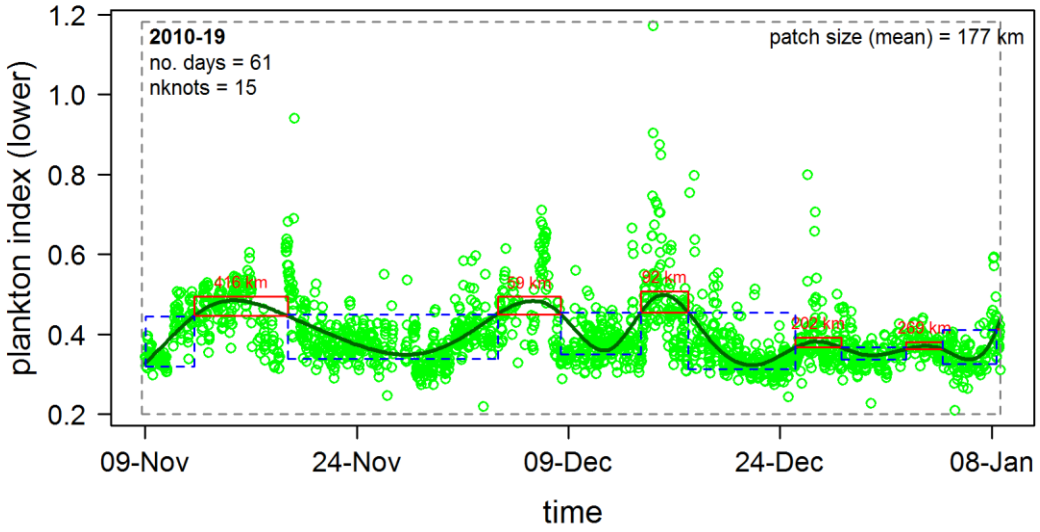

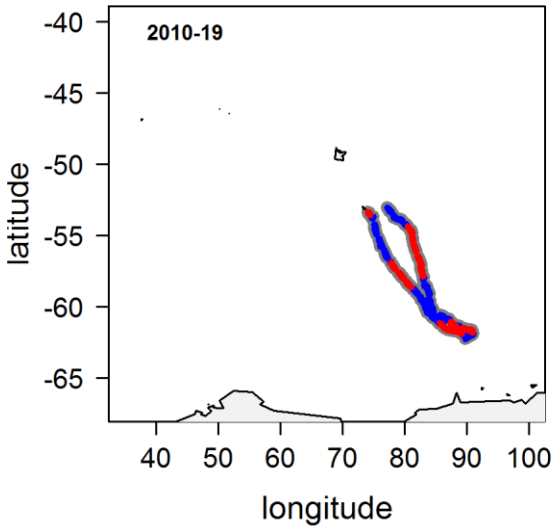

Appendix S4.7.6 (cont')

Meso-scale patches of plankton in the lower euphotic zone: bloom (red) and non-bloom (blue). A smoothing function applied to plankton values from each trip (n=22) reveals temporal bloom patterns encountered during each trip (*left*). Incomplete trip datasets were excluded from analysis (n=11, see table 1). For details of bloom definition see the methods section. Bloom and non-bloom patches encountered along the seal's track are enclosed in red and dashed blue boxes respectively. Spatial scale of each bloom patch is indicated at the top of each red box. Temporal records of prey capture rates are enclosed in the dashed grey box. Bloom (red) and non-bloom (blue) patches, and dives that coincided with prey capture records (grey) were mapped spatially, along the seal's track (*right*).

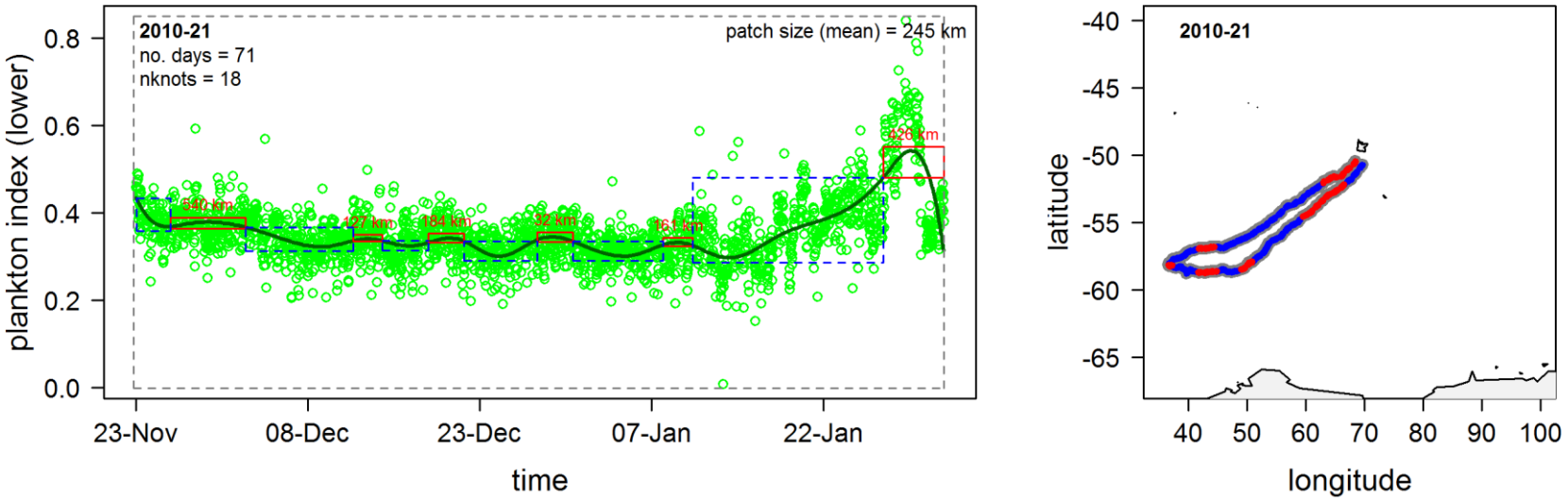

Appendix S4.7.6 (cont')

Meso-scale patches of plankton in the lower euphotic zone: bloom (red) and non-bloom (blue). A smoothing function applied to plankton values from each trip (n=22) reveals temporal bloom patterns encountered during each trip (*left*). Incomplete trip datasets were excluded from analysis (n=11, see table 1). For details of bloom definition see the methods section. Bloom and non-bloom patches encountered along the seal's track are enclosed in red and dashed blue boxes respectively. Spatial scale of each bloom patch is indicated at the top of each red box. Temporal records of prey capture rates are enclosed in the dashed grey box. Bloom (red) and non-bloom (blue) patches, and dives that coincided with prey capture records (grey) were mapped spatially, along the seal's track (*right*).

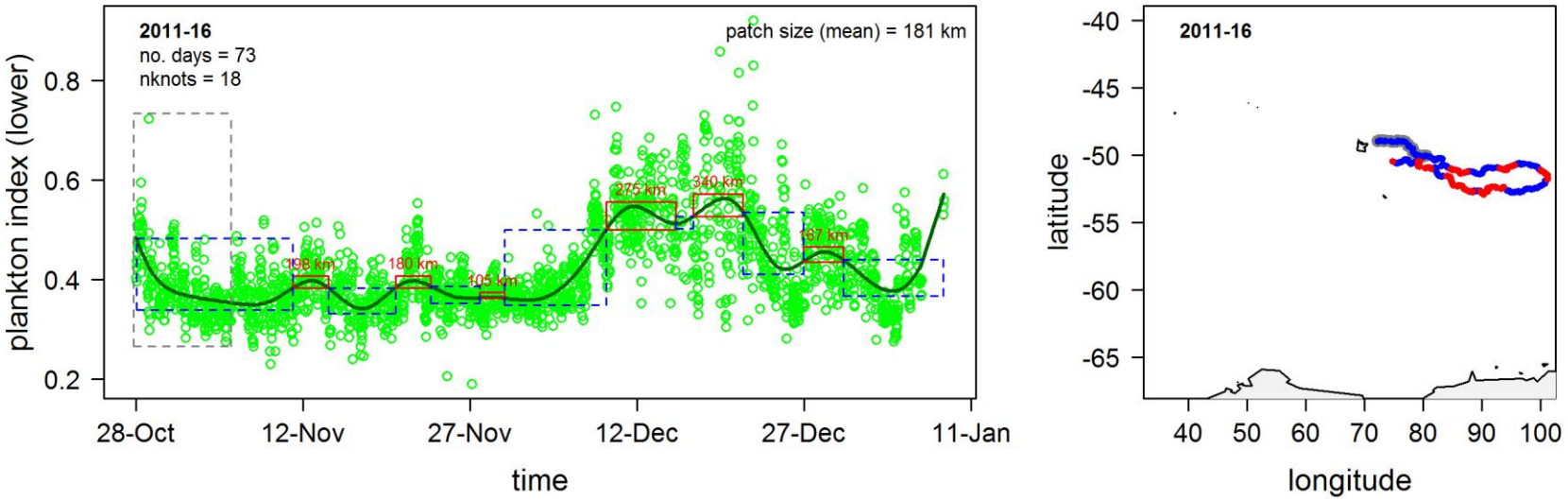

Appendix S4.7.6 (cont')

Meso-scale patches of plankton in the lower euphotic zone: bloom (red) and non-bloom (blue). A smoothing function applied to plankton values from each trip (n=22) reveals temporal bloom patterns encountered during each trip (*left*). Incomplete trip datasets were excluded from analysis (n=11, see table 1). For details of bloom definition see the methods section. Bloom and non-bloom patches encountered along the seal's track are enclosed in red and dashed blue boxes respectively. Spatial scale of each bloom patch is indicated at the top of each red box. Temporal records of prey capture rates are enclosed in the dashed grey box. Bloom (red) and non-bloom (blue) patches, and dives that coincided with prey capture records (grey) were mapped spatially, along the seal's track (*right*).

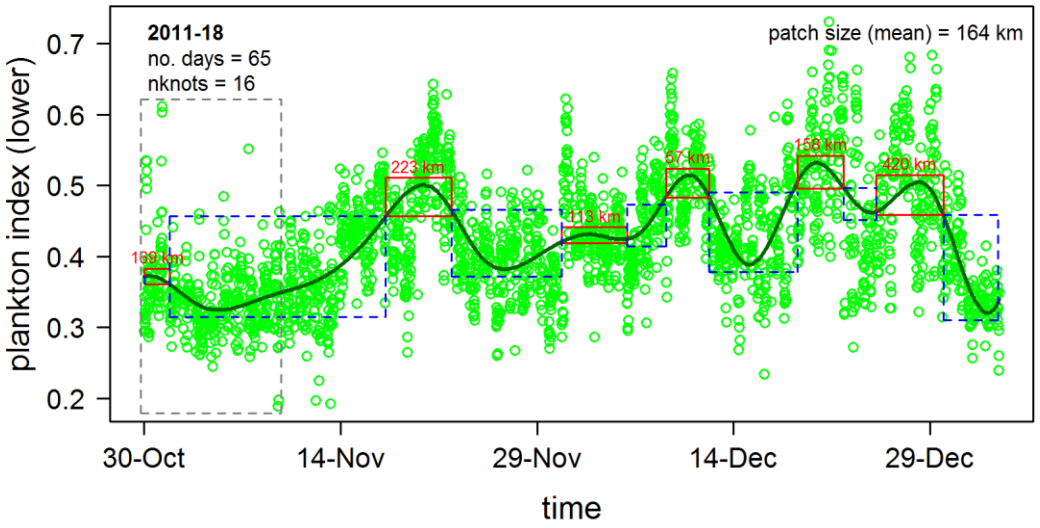

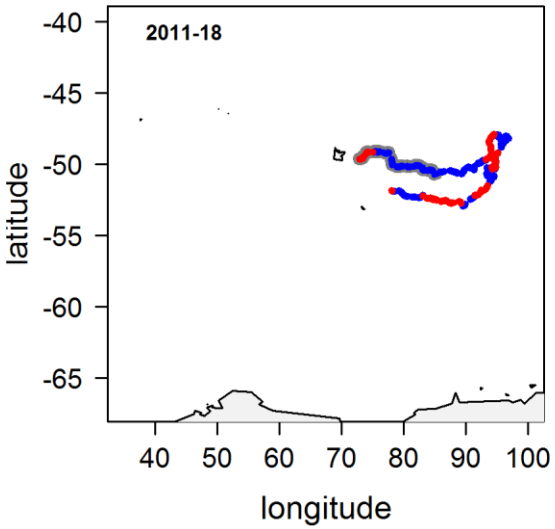

Appendix S4.7.6 (cont')

Meso-scale patches of plankton in the lower euphotic zone: bloom (red) and non-bloom (blue). A smoothing function applied to plankton values from each trip (n=22) reveals temporal bloom patterns encountered during each trip (*left*). Incomplete trip datasets were excluded from analysis (n=11, see table 1). For details of bloom definition see the methods section. Bloom and non-bloom patches encountered along the seal's track are enclosed in red and dashed blue boxes respectively. Spatial scale of each bloom patch is indicated at the top of each red box. Temporal records of prey capture rates are enclosed in the dashed grey box. Bloom (red) and non-bloom (blue) patches, and dives that coincided with prey capture records (grey) were mapped spatially, along the seal's track (*right*).

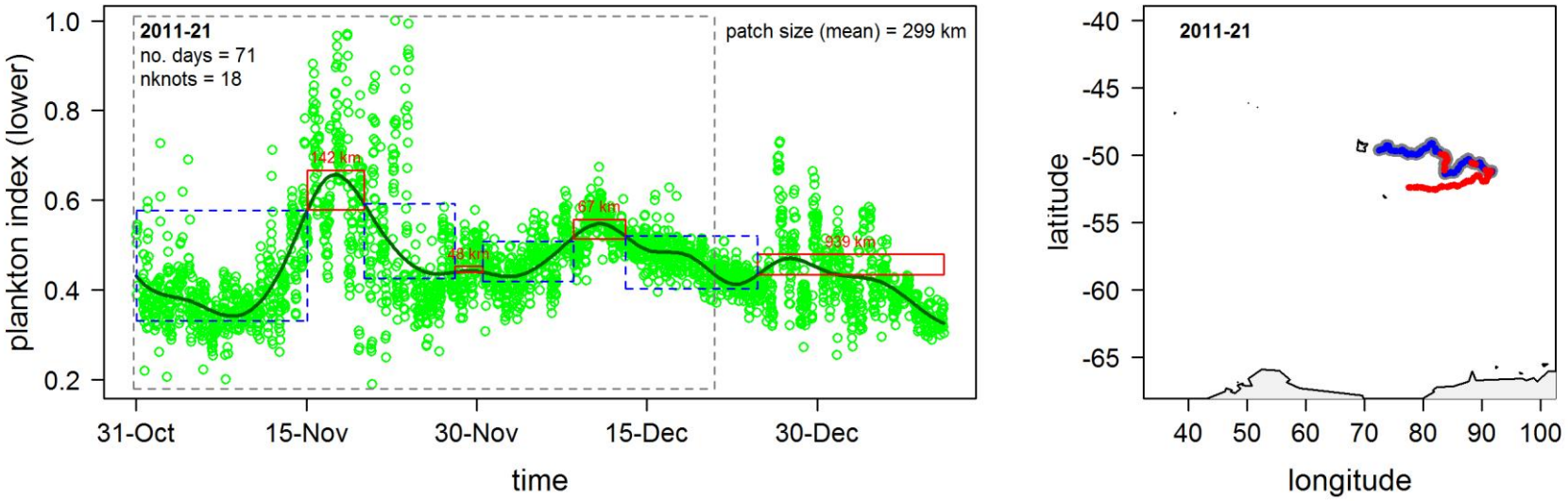

Appendix S4.7.6 (cont')

Meso-scale patches of plankton in the lower euphotic zone: bloom (red) and non-bloom (blue). A smoothing function applied to plankton values from each trip (n=22) reveals temporal bloom patterns encountered during each trip (*left*). Incomplete trip datasets were excluded from analysis (n=11, see table 1). For details of bloom definition see the methods section. Bloom and non-bloom patches encountered along the seal's track are enclosed in red and dashed blue boxes respectively. Spatial scale of each bloom patch is indicated at the top of each red box. Temporal records of prey capture rates are enclosed in the dashed grey box. Bloom (red) and non-bloom (blue) patches, and dives that coincided with prey capture records (grey) were mapped spatially, along the seal's track (*right*).

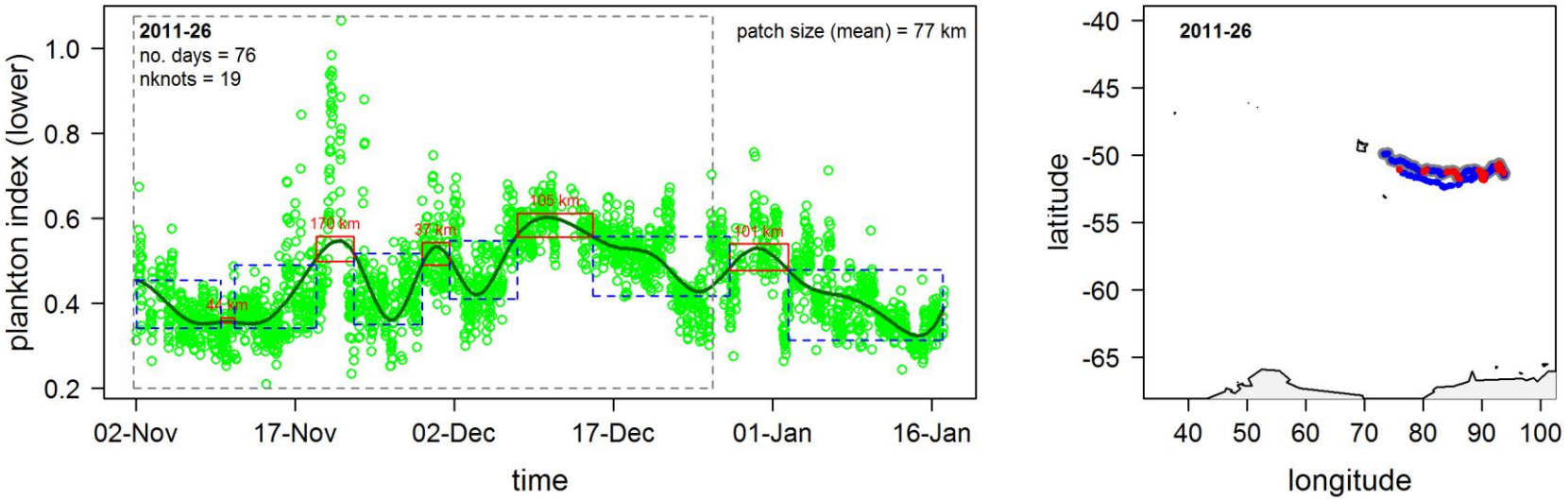

Appendix S4.7.6 (cont')

Meso-scale patches of plankton in the lower euphotic zone: bloom (red) and non-bloom (blue). A smoothing function applied to plankton values from each trip (n=22) reveals temporal bloom patterns encountered during each trip (*left*). Incomplete trip datasets were excluded from analysis (n=11, see table 1). For details of bloom definition see the methods section. Bloom and non-bloom patches encountered along the seal's track are enclosed in red and dashed blue boxes respectively. Spatial scale of each bloom patch is indicated at the top of each red box. Temporal records of prey capture rates are enclosed in the dashed grey box. Bloom (red) and non-bloom (blue) patches, and dives that coincided with prey capture records (grey) were mapped spatially, along the seal's track (*right*).

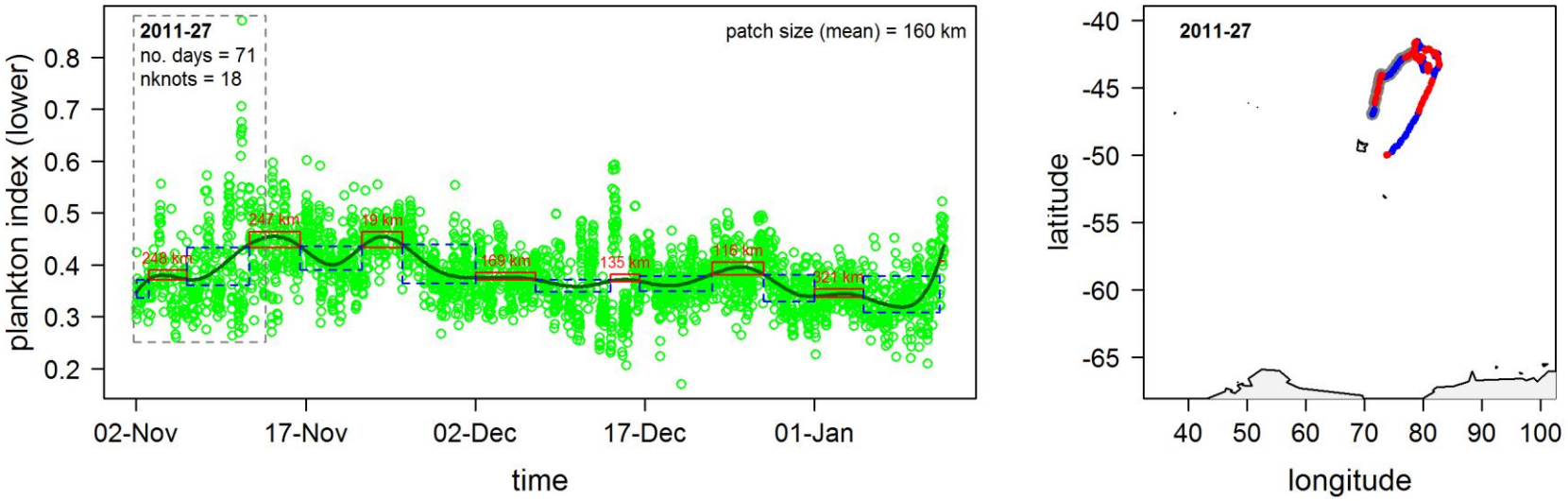

Appendix S4.7.6 (cont')

Meso-scale patches of plankton in the lower euphotic zone: bloom (red) and non-bloom (blue). A smoothing function applied to plankton values from each trip (n=22) reveals temporal bloom patterns encountered during each trip (*left*). Incomplete trip datasets were excluded from analysis (n=11, see table 1). For details of bloom definition see the methods section. Bloom and non-bloom patches encountered along the seal's track are enclosed in red and dashed blue boxes respectively. Spatial scale of each bloom patch is indicated at the top of each red box. Temporal records of prey capture rates are enclosed in the dashed grey box. Bloom (red) and non-bloom (blue) patches, and dives that coincided with prey capture records (grey) were mapped spatially, along the seal's track (*right*).

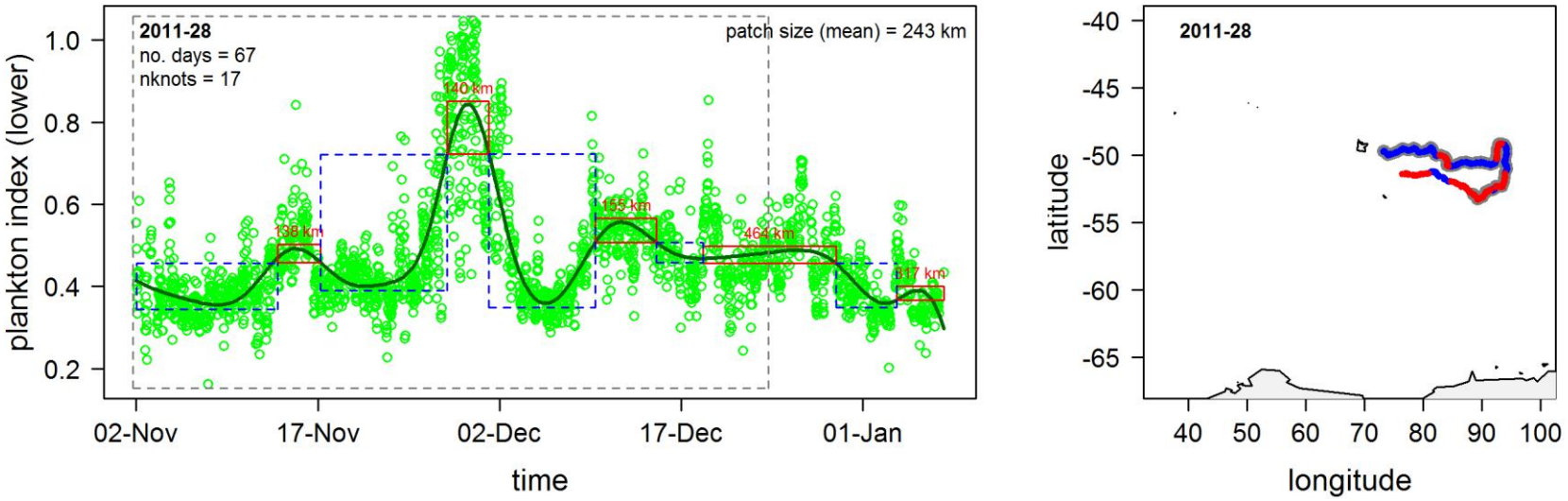

Appendix S4.7.6 (cont')

Meso-scale patches of plankton in the lower euphotic zone: bloom (red) and non-bloom (blue). A smoothing function applied to plankton values from each trip (n=22) reveals temporal bloom patterns encountered during each trip (*left*). Incomplete trip datasets were excluded from analysis (n=11, see table 1). For details of bloom definition see the methods section. Bloom and non-bloom patches encountered along the seal's track are enclosed in red and dashed blue boxes respectively. Spatial scale of each bloom patch is indicated at the top of each red box. Temporal records of prey capture rates are enclosed in the dashed grey box. Bloom (red) and non-bloom (blue) patches, and dives that coincided with prey capture records (grey) were mapped spatially, along the seal's track (*right*).

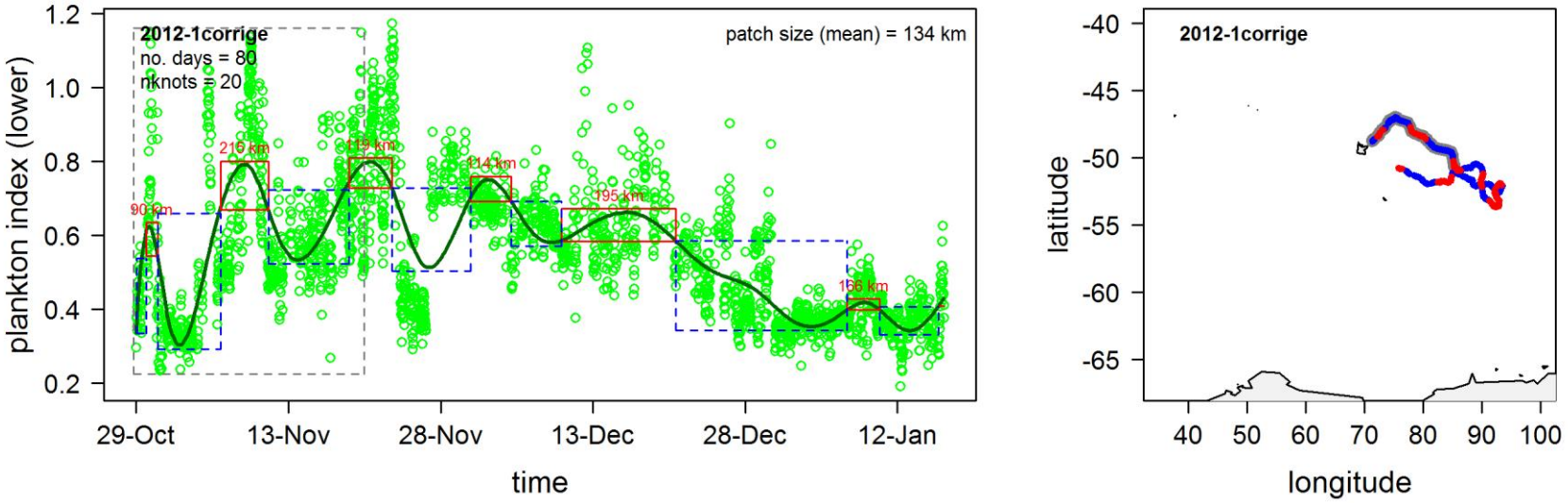

Appendix S4.7.6 (cont')

Meso-scale patches of plankton in the lower euphotic zone: bloom (red) and non-bloom (blue). A smoothing function applied to plankton values from each trip (n=22) reveals temporal bloom patterns encountered during each trip (*left*). Incomplete trip datasets were excluded from analysis (n=11, see table 1). For details of bloom definition see the methods section. Bloom and non-bloom patches encountered along the seal's track are enclosed in red and dashed blue boxes respectively. Spatial scale of each bloom patch is indicated at the top of each red box. Temporal records of prey capture rates are enclosed in the dashed grey box. Bloom (red) and non-bloom (blue) patches, and dives that coincided with prey capture records (grey) were mapped spatially, along the seal's track (*right*).

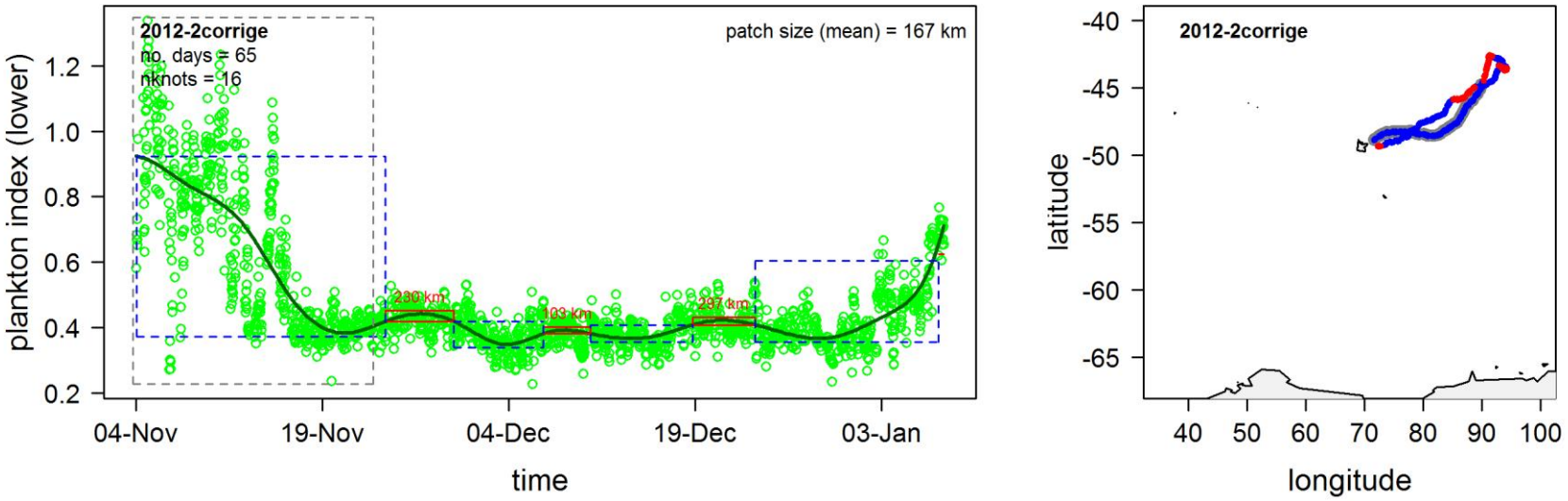

Appendix S4.7.6 (cont')

Meso-scale patches of plankton in the lower euphotic zone: bloom (red) and non-bloom (blue). A smoothing function applied to plankton values from each trip (n=22) reveals temporal bloom patterns encountered during each trip (*left*). Incomplete trip datasets were excluded from analysis (n=11, see table 1). For details of bloom definition see the methods section. Bloom and non-bloom patches encountered along the seal's track are enclosed in red and dashed blue boxes respectively. Spatial scale of each bloom patch is indicated at the top of each red box. Temporal records of prey capture rates are enclosed in the dashed grey box. Bloom (red) and non-bloom (blue) patches, and dives that coincided with prey capture records (grey) were mapped spatially, along the seal's track (*right*).

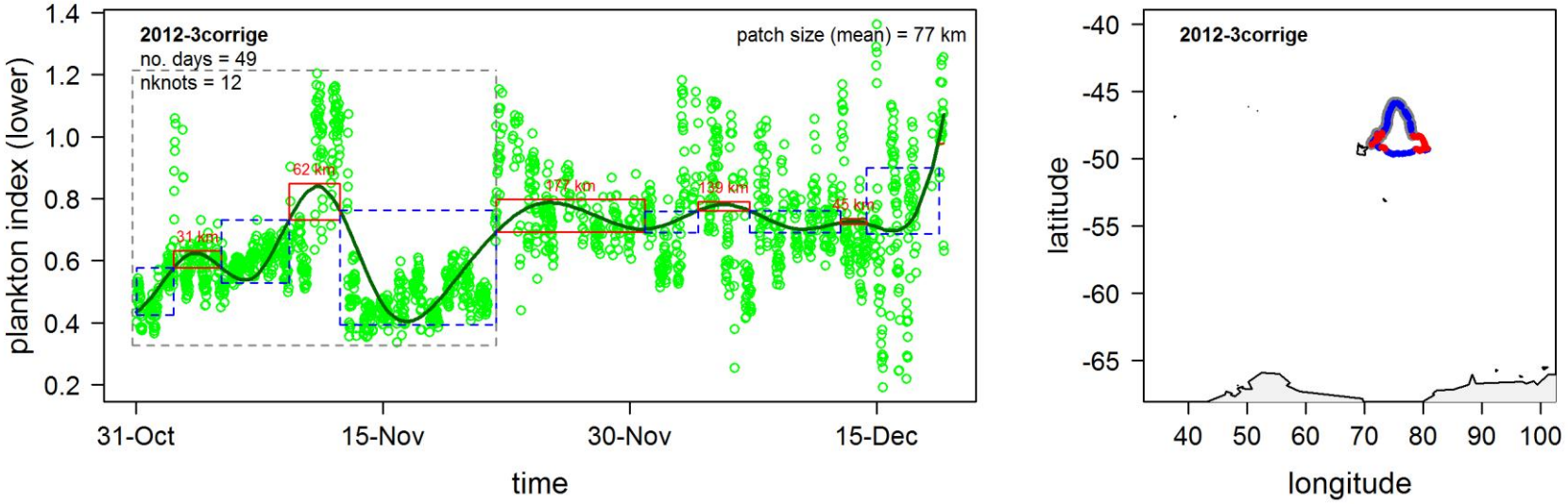

Appendix S4.7.6 (cont')

Meso-scale patches of plankton in the lower euphotic zone: bloom (red) and non-bloom (blue). A smoothing function applied to plankton values from each trip (n=22) reveals temporal bloom patterns encountered during each trip (*left*). Incomplete trip datasets were excluded from analysis (n=11, see table 1). For details of bloom definition see the methods section. Bloom and non-bloom patches encountered along the seal's track are enclosed in red and dashed blue boxes respectively. Spatial scale of each bloom patch is indicated at the top of each red box. Temporal records of prey capture rates are enclosed in the dashed grey box. Bloom (red) and non-bloom (blue) patches, and dives that coincided with prey capture records (grey) were mapped spatially, along the seal's track (*right*).

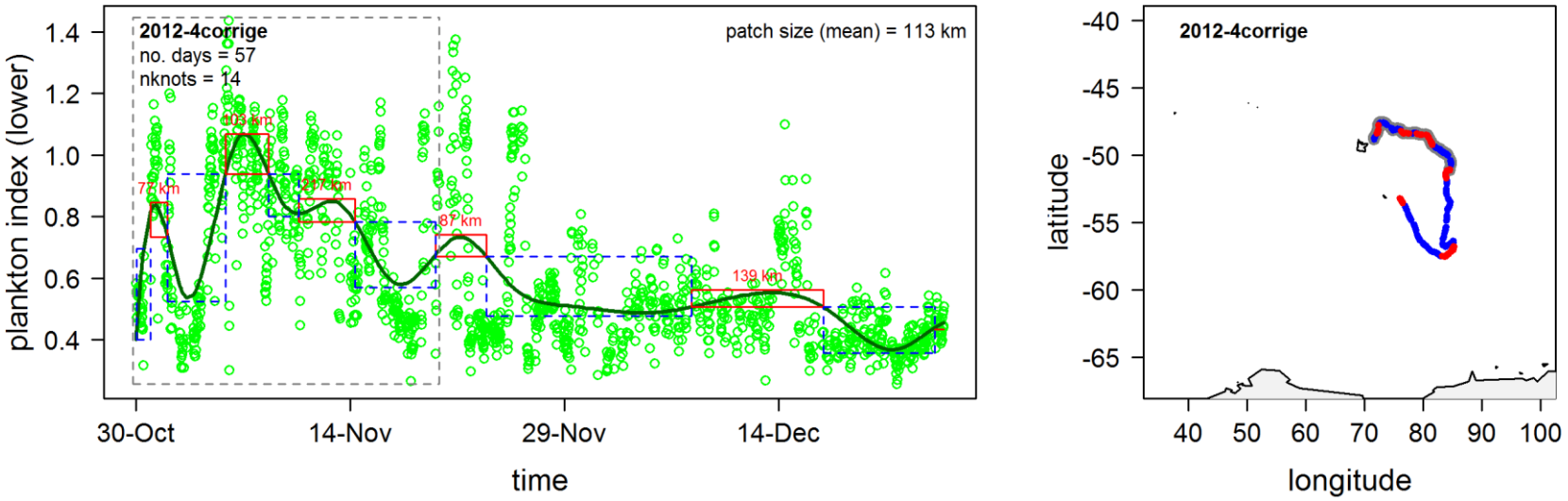

Appendix S4.7.6 (cont')

Meso-scale patches of plankton in the lower euphotic zone: bloom (red) and non-bloom (blue). A smoothing function applied to plankton values from each trip (n=22) reveals temporal bloom patterns encountered during each trip (*left*). Incomplete trip datasets were excluded from analysis (n=11, see table 1). For details of bloom definition see the methods section. Bloom and non-bloom patches encountered along the seal's track are enclosed in red and dashed blue boxes respectively. Spatial scale of each bloom patch is indicated at the top of each red box. Temporal records of prey capture rates are enclosed in the dashed grey box. Bloom (red) and non-bloom (blue) patches, and dives that coincided with prey capture records (grey) were mapped spatially, along the seal's track (*right*).

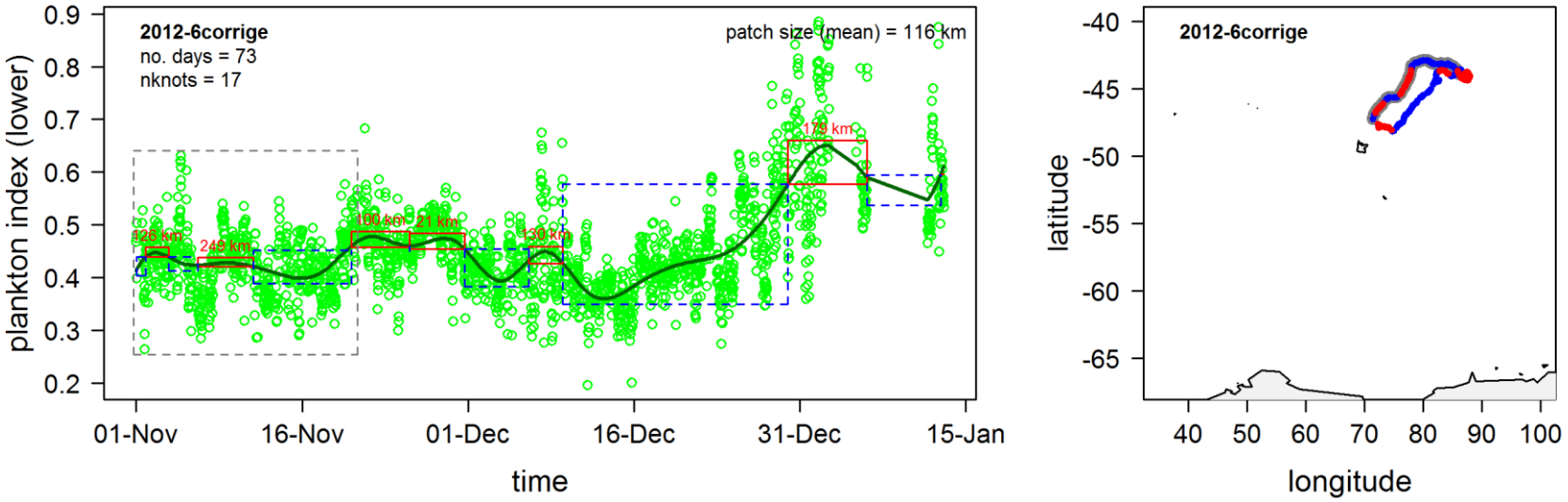

Appendix S4.7.6 (cont')

Meso-scale patches of plankton in the lower euphotic zone: bloom (red) and non-bloom (blue). A smoothing function applied to plankton values from each trip (n=22) reveals temporal bloom patterns encountered during each trip (*left*). Incomplete trip datasets were excluded from analysis (n=11, see table 1). For details of bloom definition see the methods section. Bloom and non-bloom patches encountered along the seal's track are enclosed in red and dashed blue boxes respectively. Spatial scale of each bloom patch is indicated at the top of each red box. Temporal records of prey capture rates are enclosed in the dashed grey box. Bloom (red) and non-bloom (blue) patches, and dives that coincided with prey capture records (grey) were mapped spatially, along the seal's track (*right*).

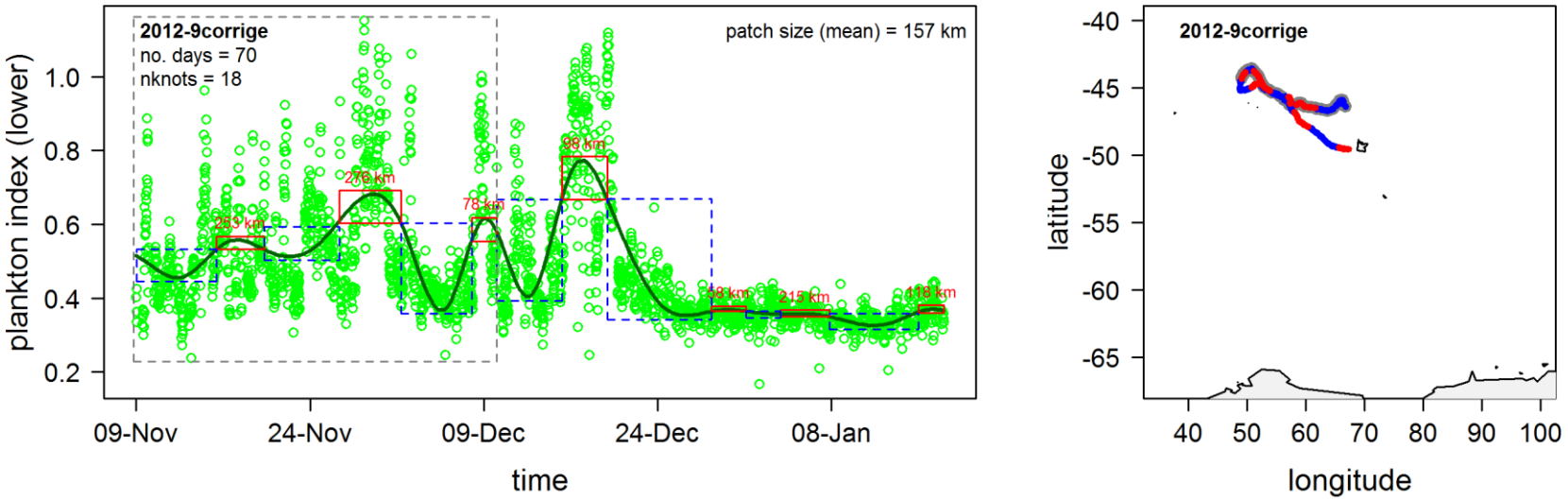

Appendix S4.7.6 (cont')

Meso-scale patches of plankton in the lower euphotic zone: bloom (red) and non-bloom (blue). A smoothing function applied to plankton values from each trip (n=22) reveals temporal bloom patterns encountered during each trip (*left*). Incomplete trip datasets were excluded from analysis (n=11, see table 1). For details of bloom definition see the methods section. Bloom and non-bloom patches encountered along the seal's track are enclosed in red and dashed blue boxes respectively. Spatial scale of each bloom patch is indicated at the top of each red box. Temporal records of prey capture rates are enclosed in the dashed grey box. Bloom (red) and non-bloom (blue) patches, and dives that coincided with prey capture records (grey) were mapped spatially, along the seal's track (*right*).

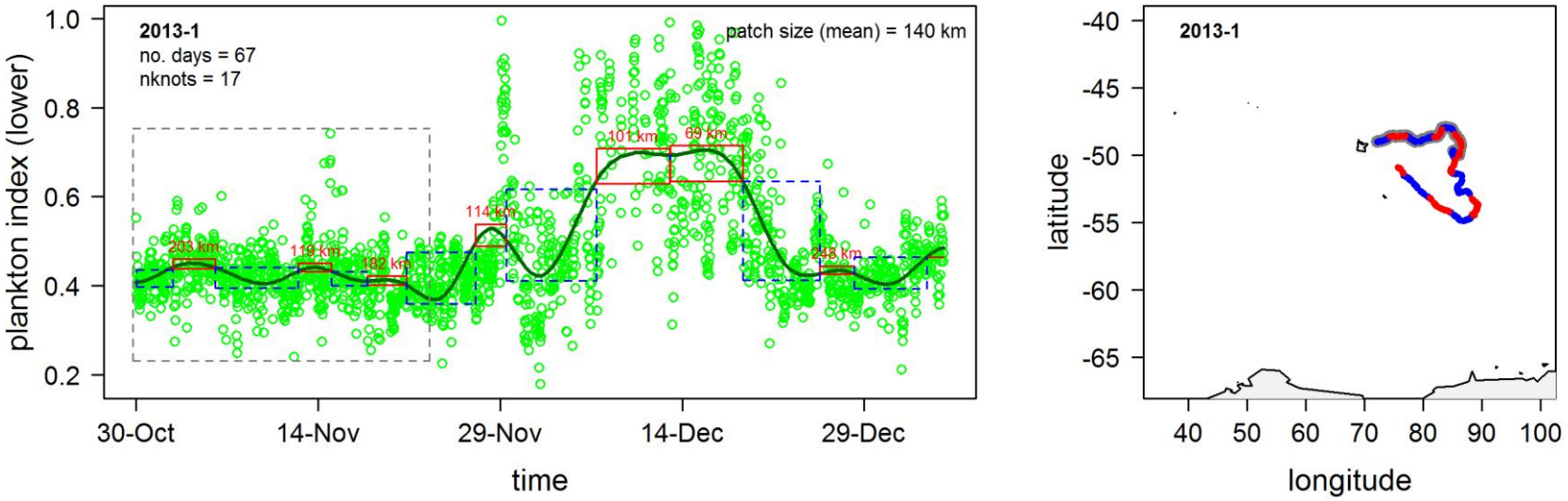

Appendix S4.7.6 (cont')

Meso-scale patches of plankton in the lower euphotic zone: bloom (red) and non-bloom (blue). A smoothing function applied to plankton values from each trip (n=22) reveals temporal bloom patterns encountered during each trip (*left*). Incomplete trip datasets were excluded from analysis (n=11, see table 1). For details of bloom definition see the methods section. Bloom and non-bloom patches encountered along the seal's track are enclosed in red and dashed blue boxes respectively. Spatial scale of each bloom patch is indicated at the top of each red box. Temporal records of prey capture rates are enclosed in the dashed grey box. Bloom (red) and non-bloom (blue) patches, and dives that coincided with prey capture records (grey) were mapped spatially, along the seal's track (*right*).

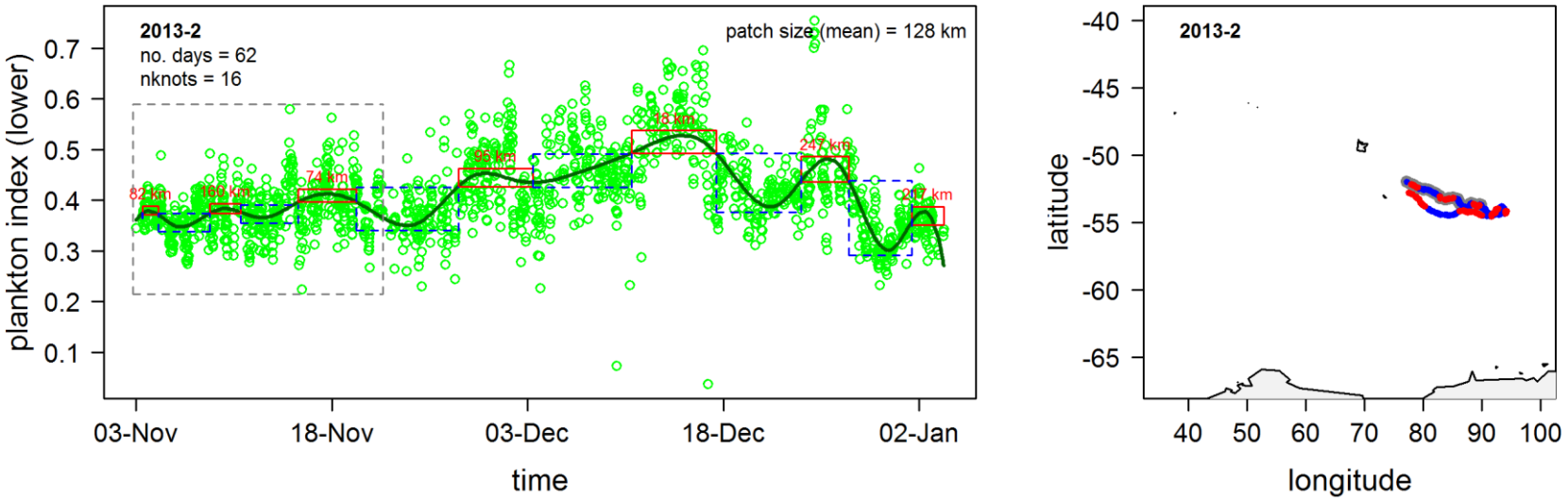

Appendix S4.7.6 (cont')

Meso-scale patches of plankton in the lower euphotic zone: bloom (red) and non-bloom (blue). A smoothing function applied to plankton values from each trip (n=22) reveals temporal bloom patterns encountered during each trip (*left*). Incomplete trip datasets were excluded from analysis (n=11, see table 1). For details of bloom definition see the methods section. Bloom and non-bloom patches encountered along the seal's track are enclosed in red and dashed blue boxes respectively. Spatial scale of each bloom patch is indicated at the top of each red box. Temporal records of prey capture rates are enclosed in the dashed grey box. Bloom (red) and non-bloom (blue) patches, and dives that coincided with prey capture records (grey) were mapped spatially, along the seal's track (*right*).

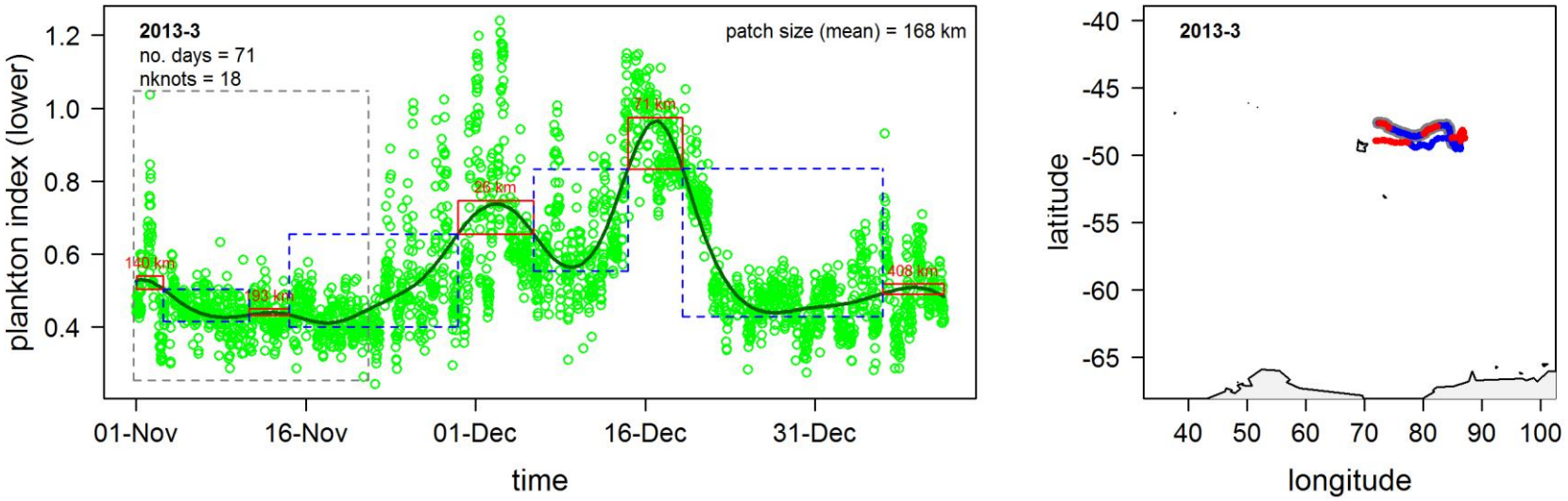

Appendix S4.7.6 (cont')

Meso-scale patches of plankton in the lower euphotic zone: bloom (red) and non-bloom (blue). A smoothing function applied to plankton values from each trip (n=22) reveals temporal bloom patterns encountered during each trip (*left*). Incomplete trip datasets were excluded from analysis (n=11, see table 1). For details of bloom definition see the methods section. Bloom and non-bloom patches encountered along the seal's track are enclosed in red and dashed blue boxes respectively. Spatial scale of each bloom patch is indicated at the top of each red box. Temporal records of prey capture rates are enclosed in the dashed grey box. Bloom (red) and non-bloom (blue) patches, and dives that coincided with prey capture records (grey) were mapped spatially, along the seal's track (*right*).

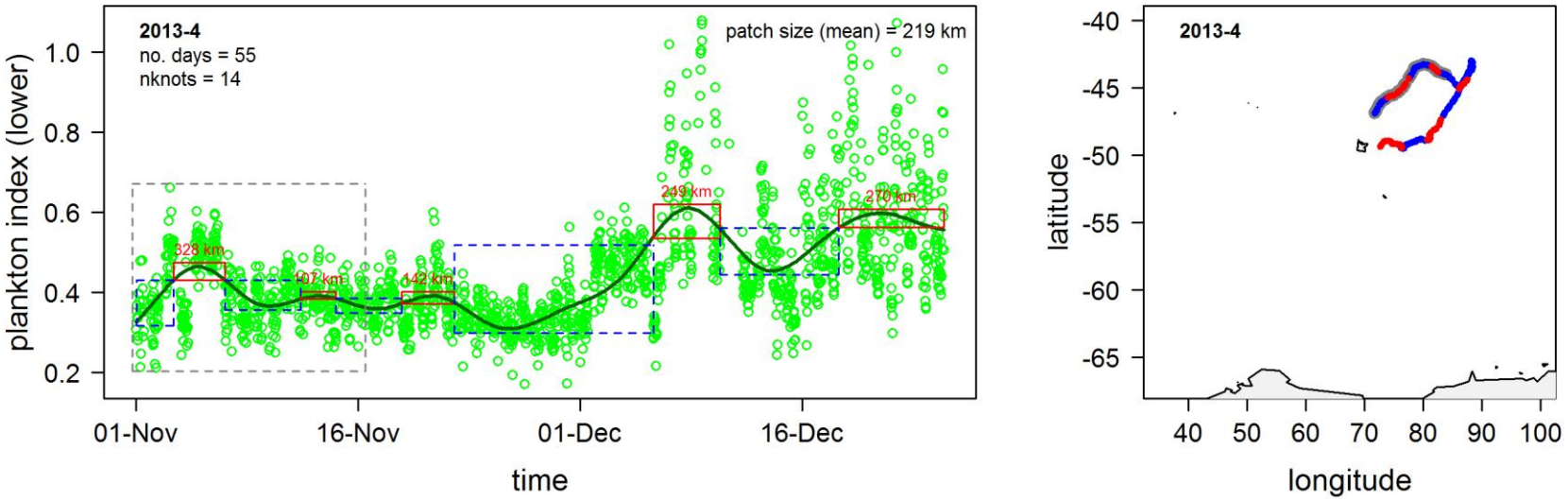

Appendix S4.7.6 (cont')

Meso-scale patches of plankton in the lower euphotic zone: bloom (red) and non-bloom (blue). A smoothing function applied to plankton values from each trip (n=22) reveals temporal bloom patterns encountered during each trip (*left*). Incomplete trip datasets were excluded from analysis (n=11, see table 1). For details of bloom definition see the methods section. Bloom and non-bloom patches encountered along the seal's track are enclosed in red and dashed blue boxes respectively. Spatial scale of each bloom patch is indicated at the top of each red box. Temporal records of prey capture rates are enclosed in the dashed grey box. Bloom (red) and non-bloom (blue) patches, and dives that coincided with prey capture records (grey) were mapped spatially, along the seal's track (*right*).

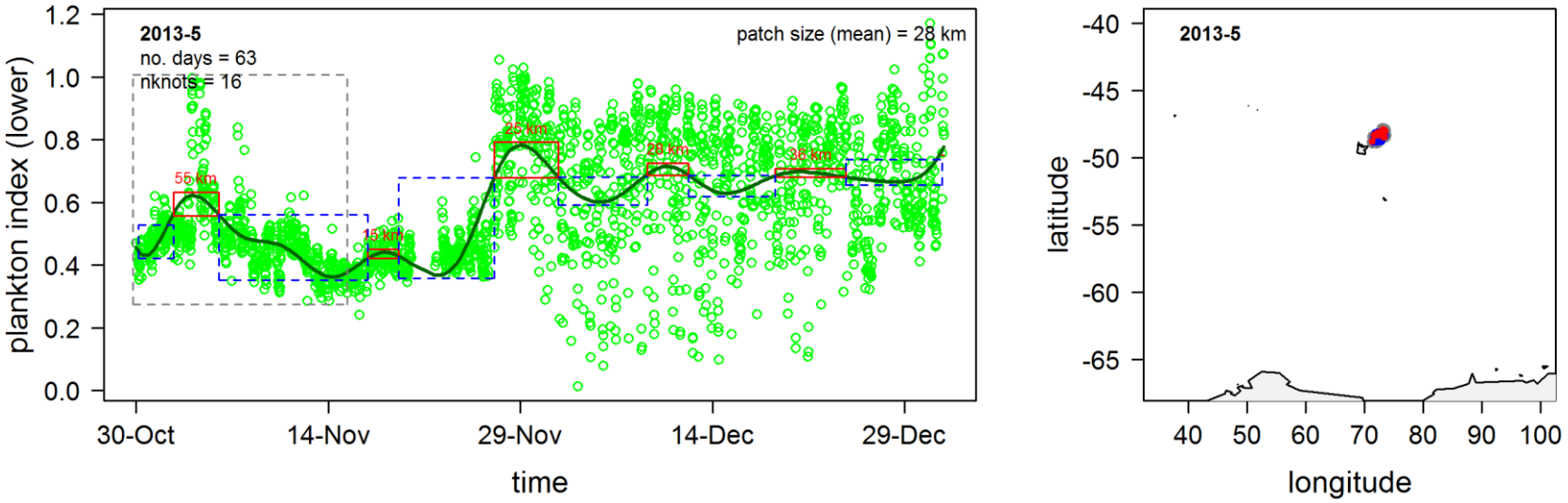

Appendix S4.7.6 (cont')

Meso-scale patches of plankton in the lower euphotic zone: bloom (red) and non-bloom (blue). A smoothing function applied to plankton values from each trip (n=22) reveals temporal bloom patterns encountered during each trip (*left*). Incomplete trip datasets were excluded from analysis (n=11, see table 1). For details of bloom definition see the methods section. Bloom and non-bloom patches encountered along the seal's track are enclosed in red and dashed blue boxes respectively. Spatial scale of each bloom patch is indicated at the top of each red box. Temporal records of prey capture rates are enclosed in the dashed grey box. Bloom (red) and non-bloom (blue) patches, and dives that coincided with prey capture records (grey) were mapped spatially, along the seal's track (*right*).

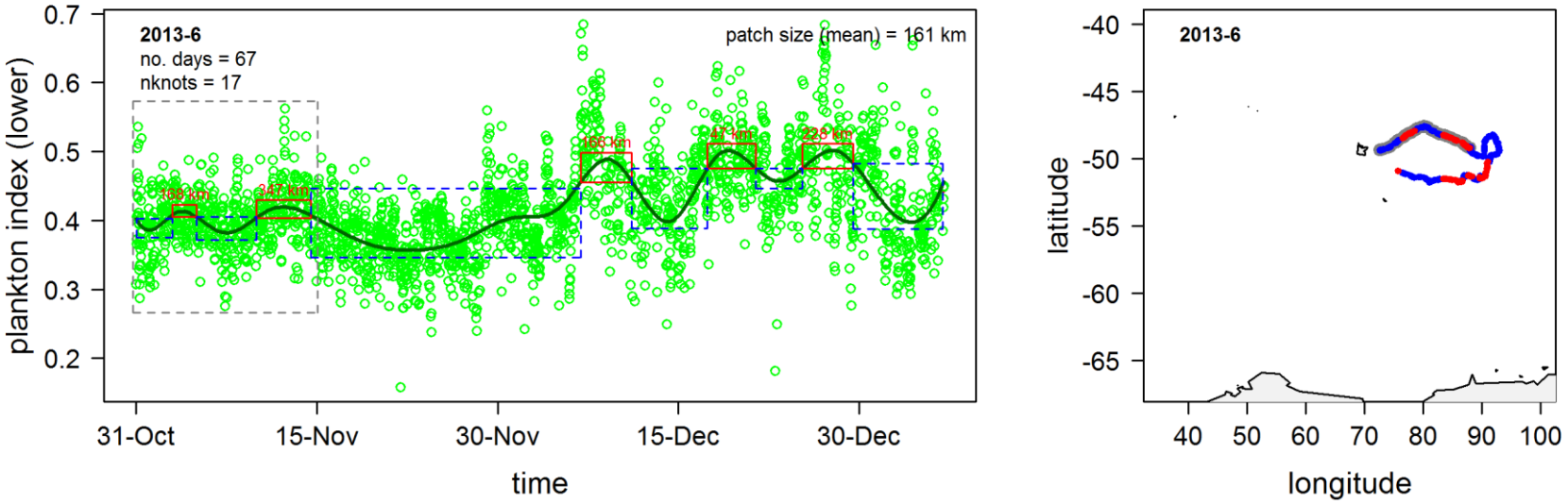

Appendix S4.7.7

Meso-scale patches of plankton below the euphotic zone: bloom (red) and non-bloom (blue). A smoothing function applied to plankton values from each trip (n=22) reveals temporal bloom patterns encountered during each trip (*left*). Incomplete trip datasets were excluded from analysis (n=11, see table 1). For details of bloom definition see the methods section. Bloom and non-bloom patches encountered along the seal's track are enclosed in red and dashed blue boxes respectively. Spatial scale of each bloom patch is indicated at the top of each red box. Temporal records of prey capture rates are enclosed in the dashed grey box. Bloom (red) and non-bloom (blue) patches, and dives that coincided with prey capture records (grey) were mapped spatially, along the seal's track (*right*).

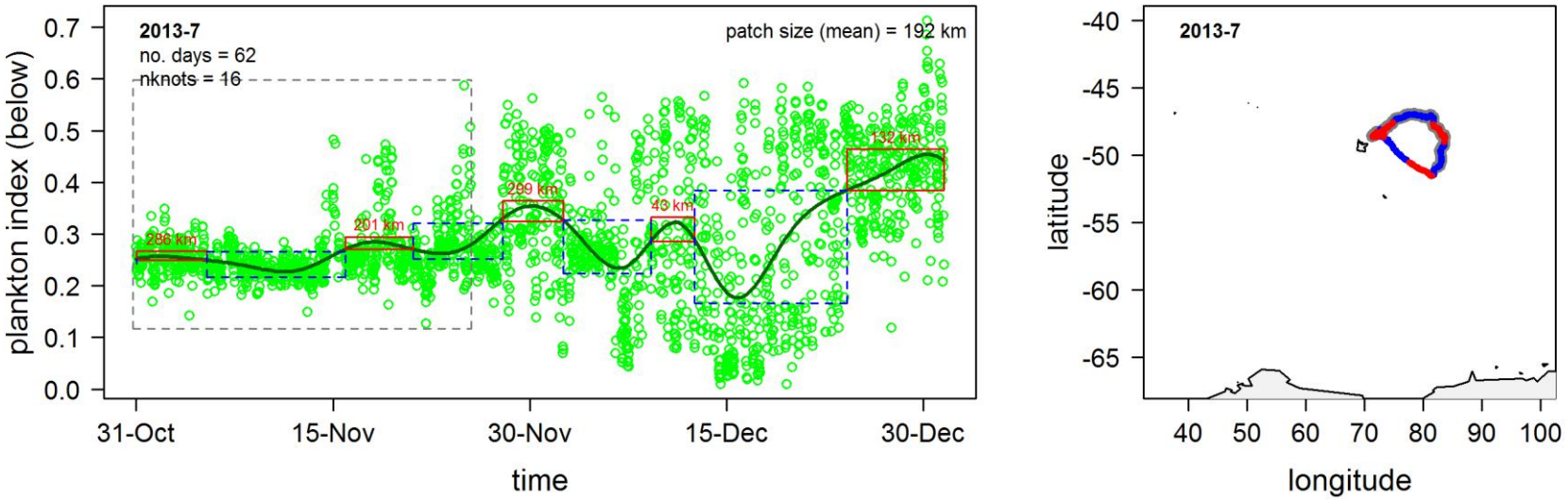

Appendix S4.7.7 (cont')

Meso-scale patches of plankton below the euphotic zone: bloom (red) and non-bloom (blue). A smoothing function applied to plankton values from each trip (n=22) reveals temporal bloom patterns encountered during each trip (*left*). Incomplete trip datasets were excluded from analysis (n=11, see table 1). For details of bloom definition see the methods section. Bloom and non-bloom patches encountered along the seal's track are enclosed in red and dashed blue boxes respectively. Spatial scale of each bloom patch is indicated at the top of each red box. Temporal records of prey capture rates are enclosed in the dashed grey box. Bloom (red) and non-bloom (blue) patches, and dives that coincided with prey capture records (grey) were mapped spatially, along the seal's track (*right*).

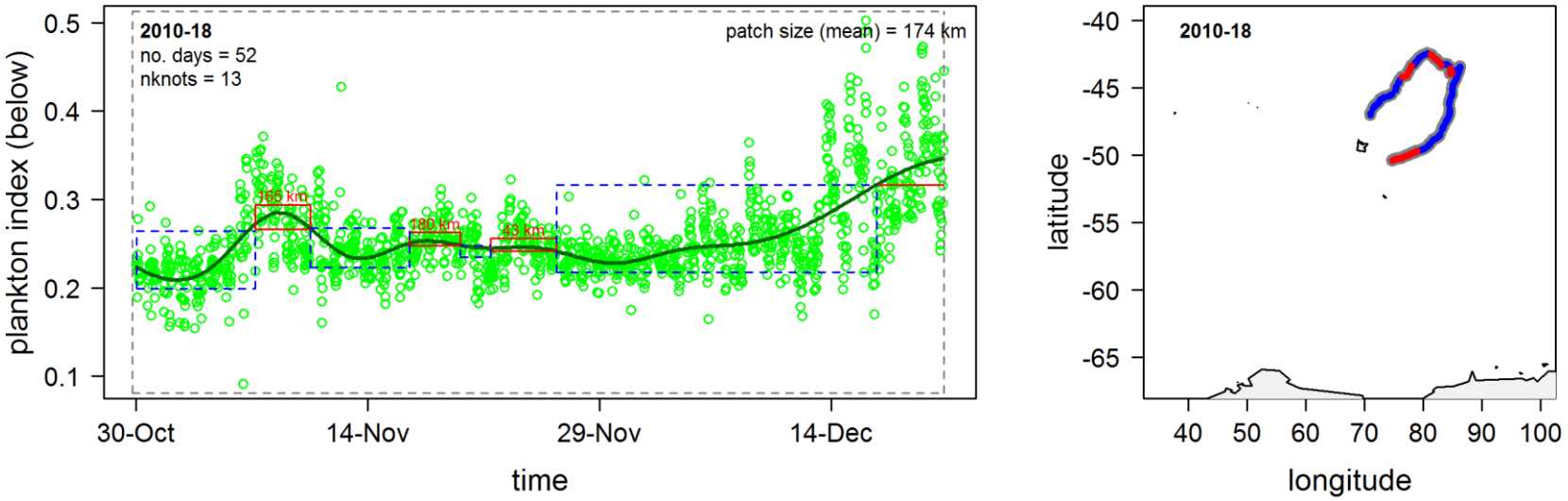

Appendix S4.7.7 (cont')

Meso-scale patches of plankton below the euphotic zone: bloom (red) and non-bloom (blue). A smoothing function applied to plankton values from each trip (n=22) reveals temporal bloom patterns encountered during each trip (*left*). Incomplete trip datasets were excluded from analysis (n=11, see table 1). For details of bloom definition see the methods section. Bloom and non-bloom patches encountered along the seal's track are enclosed in red and dashed blue boxes respectively. Spatial scale of each bloom patch is indicated at the top of each red box. Temporal records of prey capture rates are enclosed in the dashed grey box. Bloom (red) and non-bloom (blue) patches, and dives that coincided with prey capture records (grey) were mapped spatially, along the seal's track (*right*).

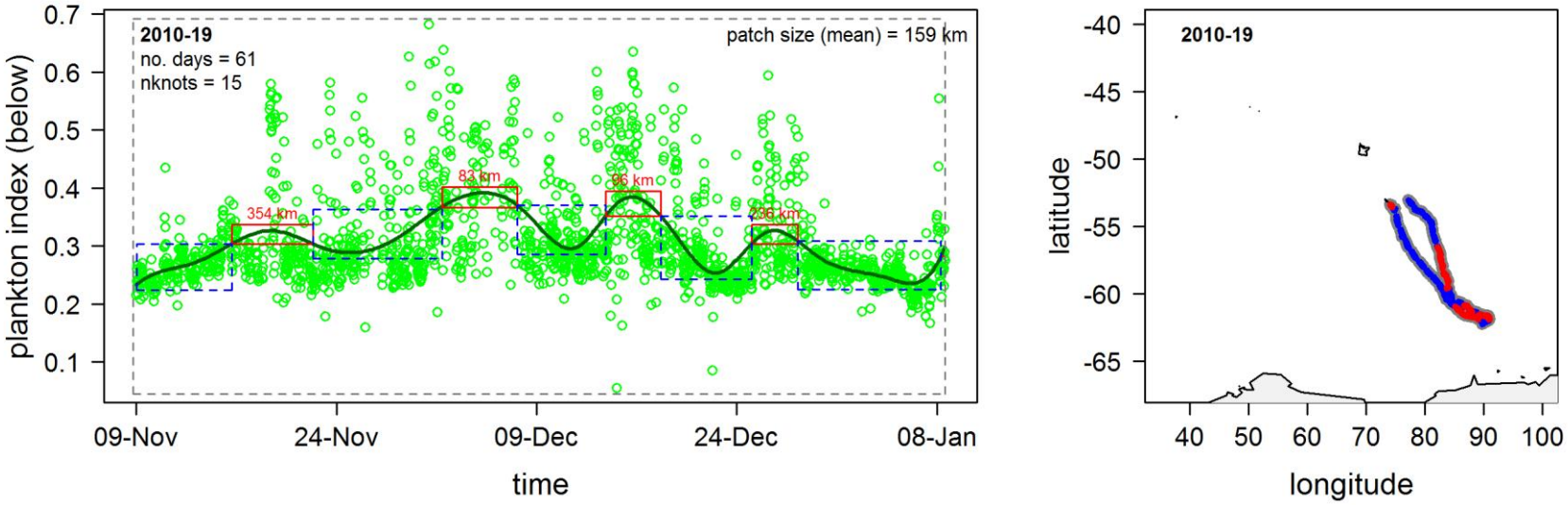

Appendix S4.7.7 (cont')

Meso-scale patches of plankton below the euphotic zone: bloom (red) and non-bloom (blue). A smoothing function applied to plankton values from each trip (n=22) reveals temporal bloom patterns encountered during each trip (*left*). Incomplete trip datasets were excluded from analysis (n=11, see table 1). For details of bloom definition see the methods section. Bloom and non-bloom patches encountered along the seal's track are enclosed in red and dashed blue boxes respectively. Spatial scale of each bloom patch is indicated at the top of each red box. Temporal records of prey capture rates are enclosed in the dashed grey box. Bloom (red) and non-bloom (blue) patches, and dives that coincided with prey capture records (grey) were mapped spatially, along the seal's track (*right*).

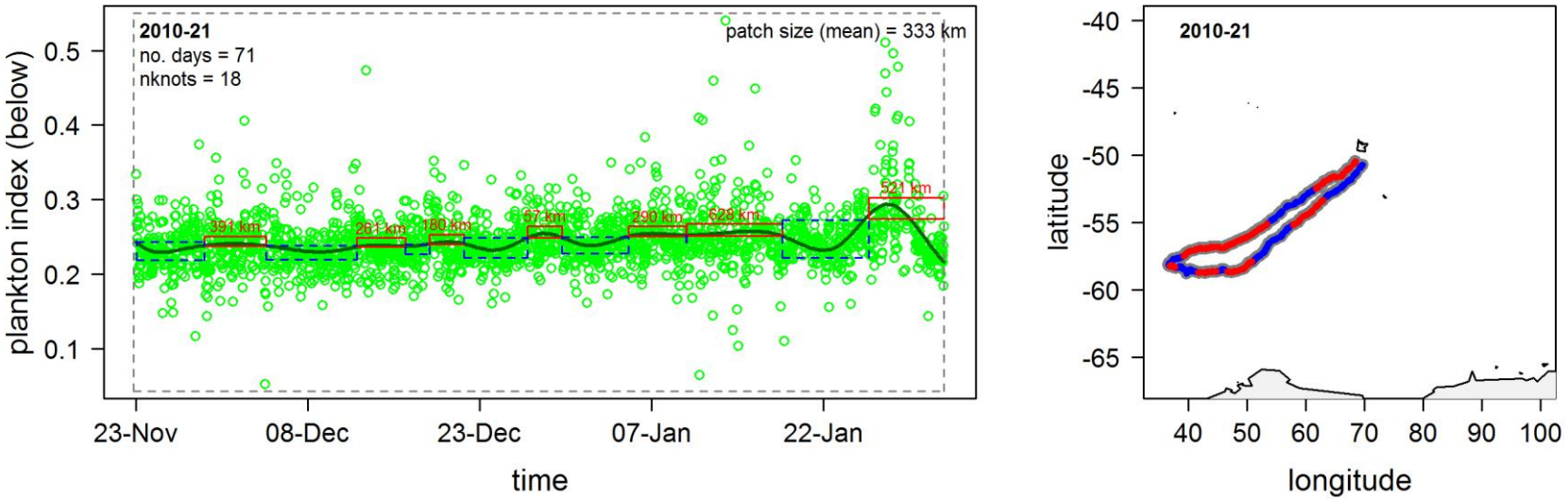

Appendix S4.7.7 (cont')

Meso-scale patches of plankton below the euphotic zone: bloom (red) and non-bloom (blue). A smoothing function applied to plankton values from each trip (n=22) reveals temporal bloom patterns encountered during each trip (*left*). Incomplete trip datasets were excluded from analysis (n=11, see table 1). For details of bloom definition see the methods section. Bloom and non-bloom patches encountered along the seal's track are enclosed in red and dashed blue boxes respectively. Spatial scale of each bloom patch is indicated at the top of each red box. Temporal records of prey capture rates are enclosed in the dashed grey box. Bloom (red) and non-bloom (blue) patches, and dives that coincided with prey capture records (grey) were mapped spatially, along the seal's track (*right*).

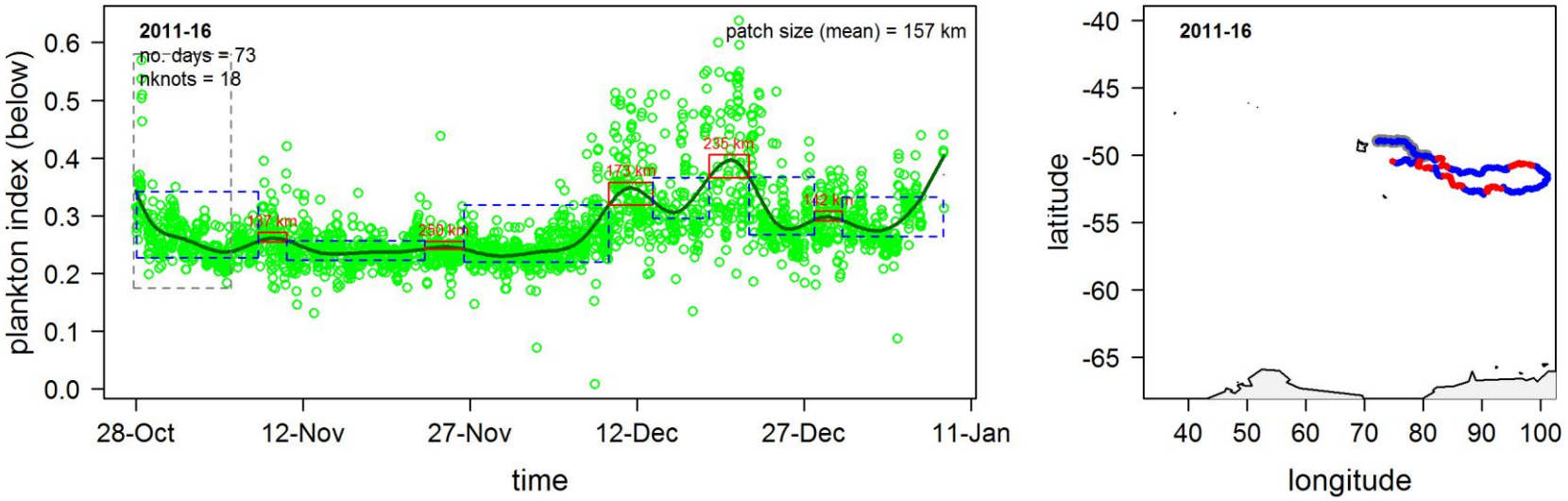

Appendix S4.7.7 (cont')

Meso-scale patches of plankton below the euphotic zone: bloom (red) and non-bloom (blue). A smoothing function applied to plankton values from each trip (n=22) reveals temporal bloom patterns encountered during each trip (*left*). Incomplete trip datasets were excluded from analysis (n=11, see table 1). For details of bloom definition see the methods section. Bloom and non-bloom patches encountered along the seal's track are enclosed in red and dashed blue boxes respectively. Spatial scale of each bloom patch is indicated at the top of each red box. Temporal records of prey capture rates are enclosed in the dashed grey box. Bloom (red) and non-bloom (blue) patches, and dives that coincided with prey capture records (grey) were mapped spatially, along the seal's track (*right*).

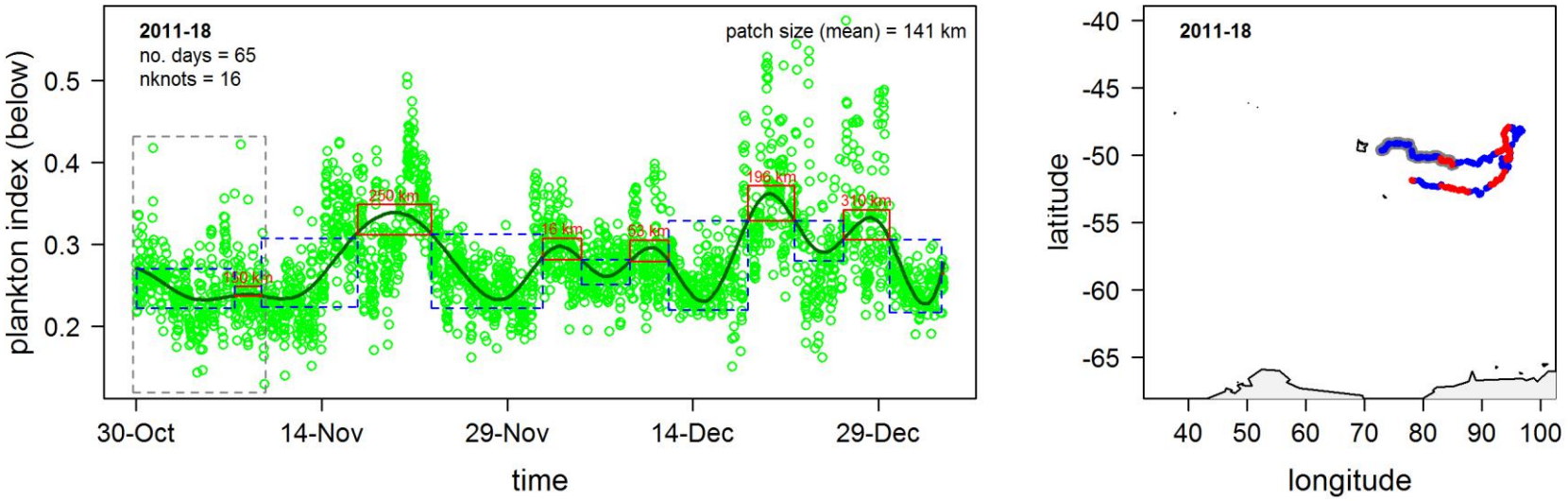

Appendix S4.7.7 (cont')

Meso-scale patches of plankton below the euphotic zone: bloom (red) and non-bloom (blue). A smoothing function applied to plankton values from each trip (n=22) reveals temporal bloom patterns encountered during each trip (*left*). Incomplete trip datasets were excluded from analysis (n=11, see table 1). For details of bloom definition see the methods section. Bloom and non-bloom patches encountered along the seal's track are enclosed in red and dashed blue boxes respectively. Spatial scale of each bloom patch is indicated at the top of each red box. Temporal records of prey capture rates are enclosed in the dashed grey box. Bloom (red) and non-bloom (blue) patches, and dives that coincided with prey capture records (grey) were mapped spatially, along the seal's track (*right*).

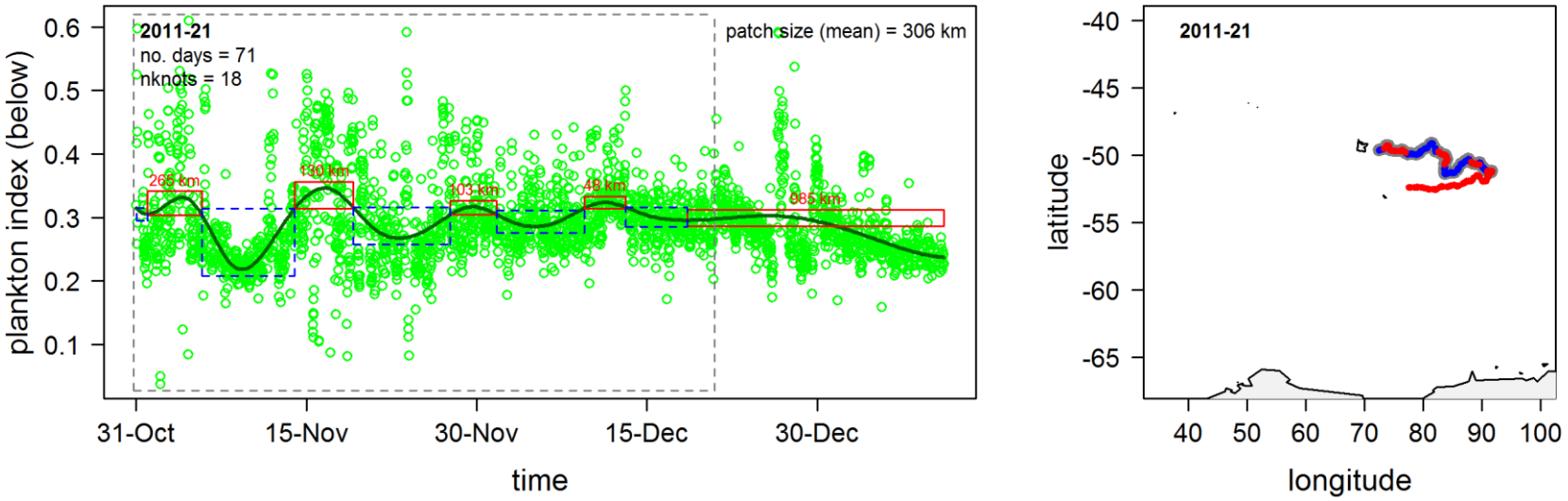

Appendix S4.7.7 (cont')

Meso-scale patches of plankton below the euphotic zone: bloom (red) and non-bloom (blue). A smoothing function applied to plankton values from each trip (n=22) reveals temporal bloom patterns encountered during each trip (*left*). Incomplete trip datasets were excluded from analysis (n=11, see table 1). For details of bloom definition see the methods section. Bloom and non-bloom patches encountered along the seal's track are enclosed in red and dashed blue boxes respectively. Spatial scale of each bloom patch is indicated at the top of each red box. Temporal records of prey capture rates are enclosed in the dashed grey box. Bloom (red) and non-bloom (blue) patches, and dives that coincided with prey capture records (grey) were mapped spatially, along the seal's track (*right*).

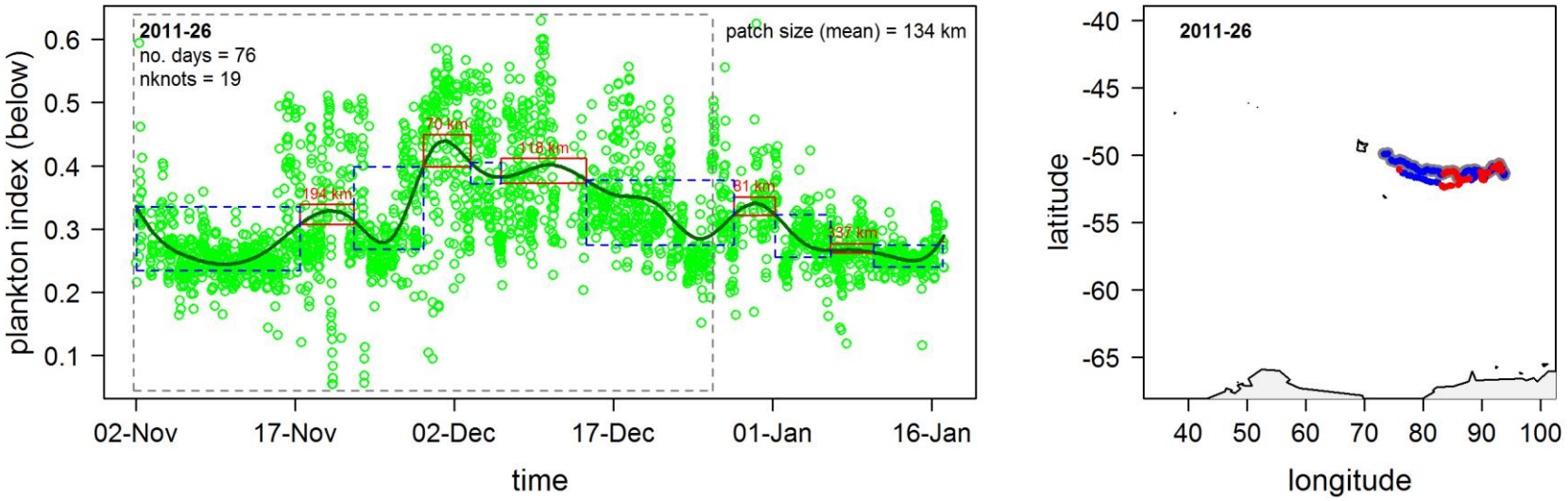

Appendix S4.7.7 (cont')

Meso-scale patches of plankton below the euphotic zone: bloom (red) and non-bloom (blue). A smoothing function applied to plankton values from each trip (n=22) reveals temporal bloom patterns encountered during each trip (*left*). Incomplete trip datasets were excluded from analysis (n=11, see table 1). For details of bloom definition see the methods section. Bloom and non-bloom patches encountered along the seal's track are enclosed in red and dashed blue boxes respectively. Spatial scale of each bloom patch is indicated at the top of each red box. Temporal records of prey capture rates are enclosed in the dashed grey box. Bloom (red) and non-bloom (blue) patches, and dives that coincided with prey capture records (grey) were mapped spatially, along the seal's track (*right*).

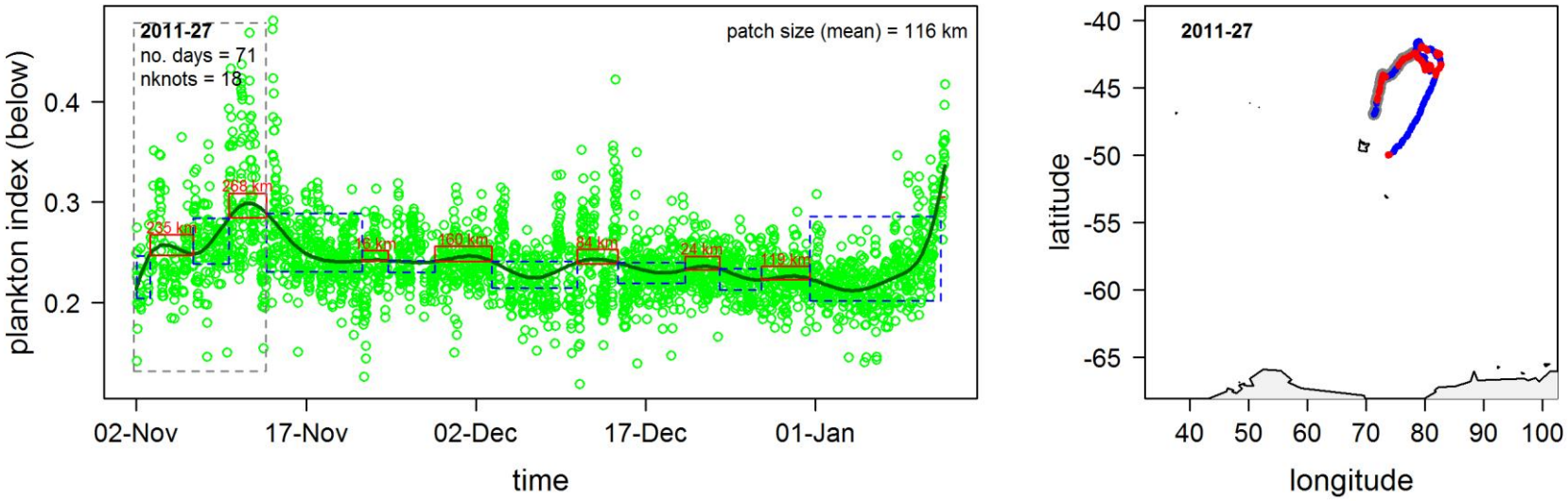

Appendix S4.7.7 (cont')

Meso-scale patches of plankton below the euphotic zone: bloom (red) and non-bloom (blue). A smoothing function applied to plankton values from each trip (n=22) reveals temporal bloom patterns encountered during each trip (*left*). Incomplete trip datasets were excluded from analysis (n=11, see table 1). For details of bloom definition see the methods section. Bloom and non-bloom patches encountered along the seal's track are enclosed in red and dashed blue boxes respectively. Spatial scale of each bloom patch is indicated at the top of each red box. Temporal records of prey capture rates are enclosed in the dashed grey box. Bloom (red) and non-bloom (blue) patches, and dives that coincided with prey capture records (grey) were mapped spatially, along the seal's track (*right*).

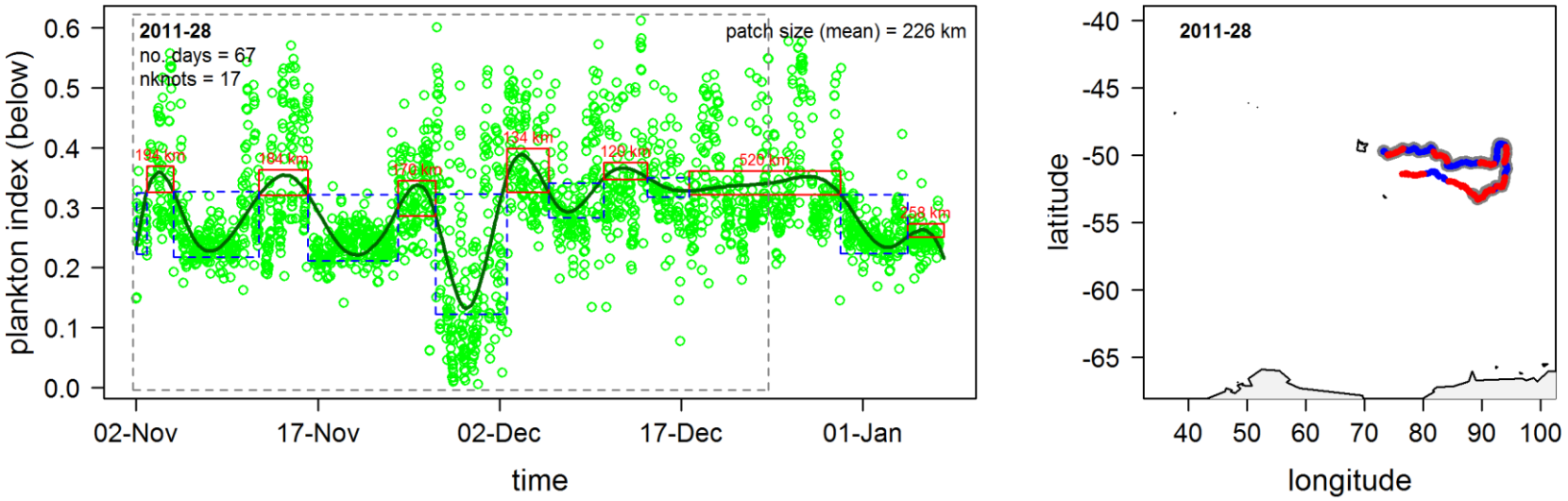

Appendix S4.7.7 (cont')

Meso-scale patches of plankton below the euphotic zone: bloom (red) and non-bloom (blue). A smoothing function applied to plankton values from each trip (n=22) reveals temporal bloom patterns encountered during each trip (*left*). Incomplete trip datasets were excluded from analysis (n=11, see table 1). For details of bloom definition see the methods section. Bloom and non-bloom patches encountered along the seal's track are enclosed in red and dashed blue boxes respectively. Spatial scale of each bloom patch is indicated at the top of each red box. Temporal records of prey capture rates are enclosed in the dashed grey box. Bloom (red) and non-bloom (blue) patches, and dives that coincided with prey capture records (grey) were mapped spatially, along the seal's track (*right*).

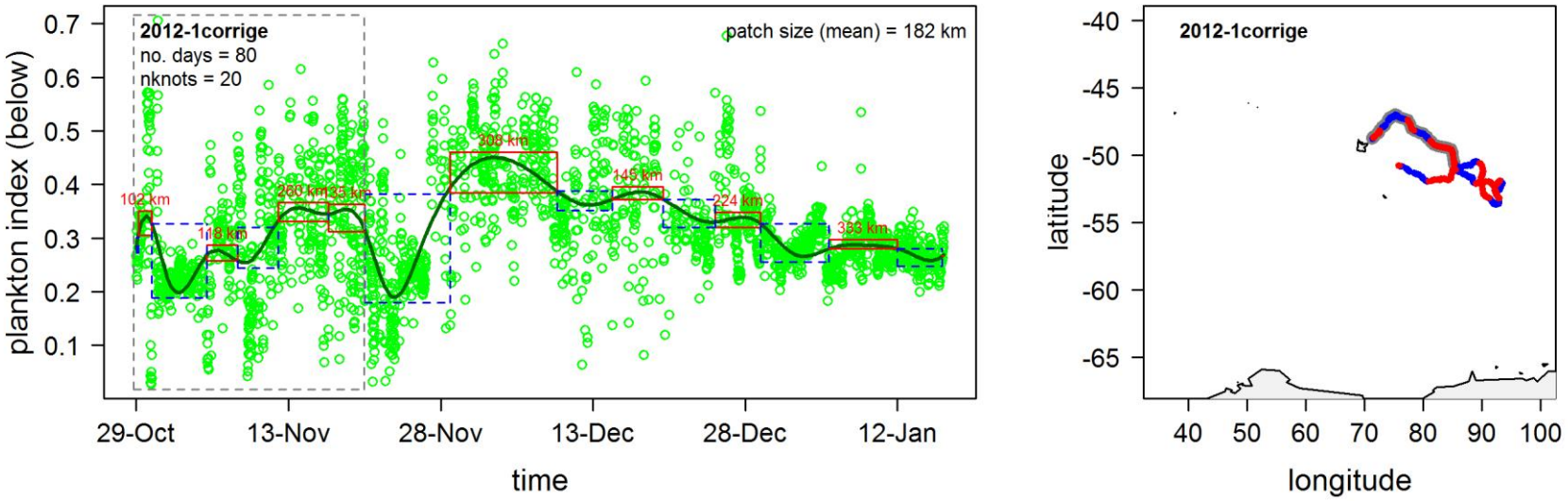

Appendix S4.7.7 (cont')

Meso-scale patches of plankton below the euphotic zone: bloom (red) and non-bloom (blue). A smoothing function applied to plankton values from each trip (n=22) reveals temporal bloom patterns encountered during each trip (*left*). Incomplete trip datasets were excluded from analysis (n=11, see table 1). For details of bloom definition see the methods section. Bloom and non-bloom patches encountered along the seal's track are enclosed in red and dashed blue boxes respectively. Spatial scale of each bloom patch is indicated at the top of each red box. Temporal records of prey capture rates are enclosed in the dashed grey box. Bloom (red) and non-bloom (blue) patches, and dives that coincided with prey capture records (grey) were mapped spatially, along the seal's track (*right*).

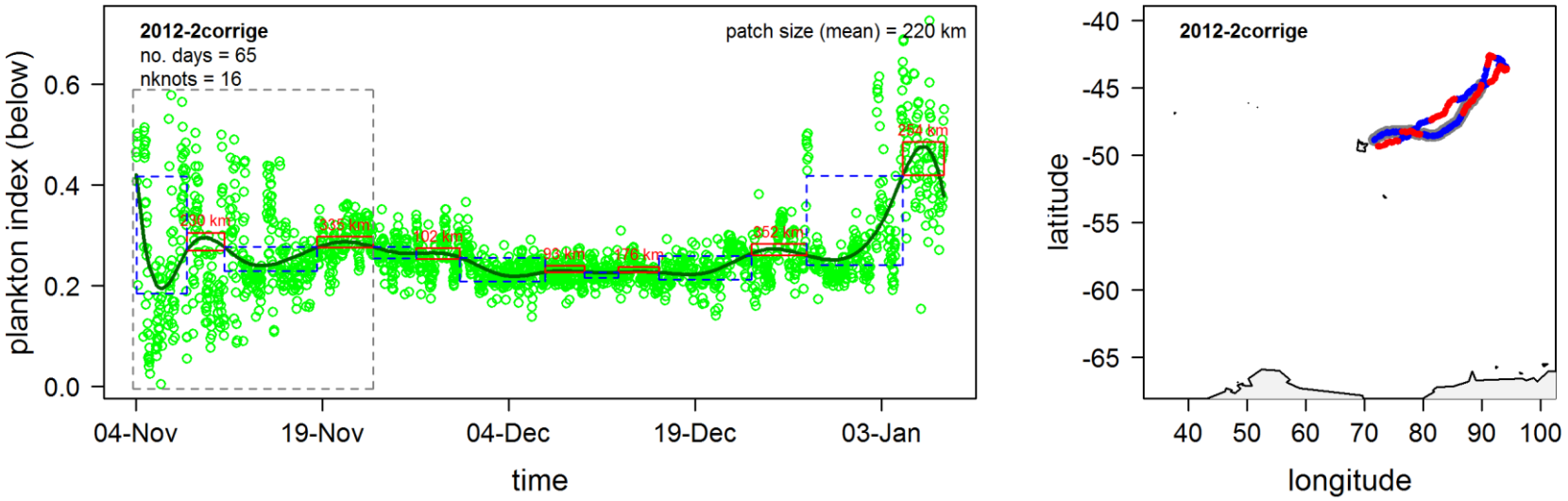

Appendix S4.7.7 (cont')

Meso-scale patches of plankton below the euphotic zone: bloom (red) and non-bloom (blue). A smoothing function applied to plankton values from each trip (n=22) reveals temporal bloom patterns encountered during each trip (*left*). Incomplete trip datasets were excluded from analysis (n=11, see table 1). For details of bloom definition see the methods section. Bloom and non-bloom patches encountered along the seal's track are enclosed in red and dashed blue boxes respectively. Spatial scale of each bloom patch is indicated at the top of each red box. Temporal records of prey capture rates are enclosed in the dashed grey box. Bloom (red) and non-bloom (blue) patches, and dives that coincided with prey capture records (grey) were mapped spatially, along the seal's track (*right*).

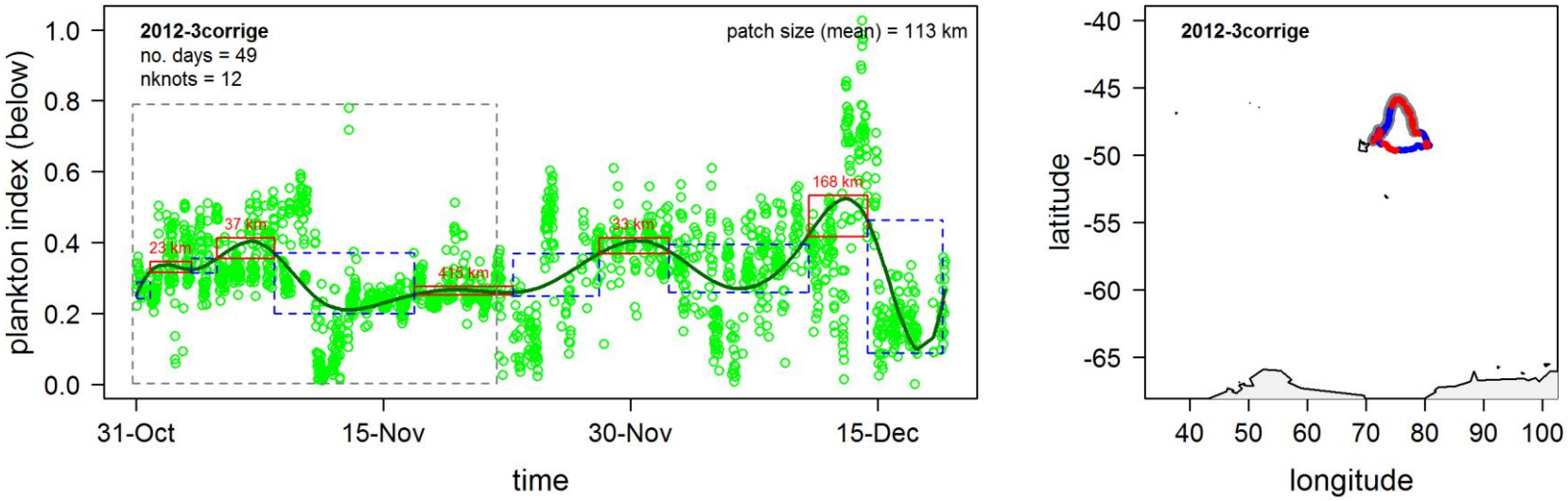

Appendix S4.7.7 (cont')

Meso-scale patches of plankton below the euphotic zone: bloom (red) and non-bloom (blue). A smoothing function applied to plankton values from each trip (n=22) reveals temporal bloom patterns encountered during each trip (*left*). Incomplete trip datasets were excluded from analysis (n=11, see table 1). For details of bloom definition see the methods section. Bloom and non-bloom patches encountered along the seal's track are enclosed in red and dashed blue boxes respectively. Spatial scale of each bloom patch is indicated at the top of each red box. Temporal records of prey capture rates are enclosed in the dashed grey box. Bloom (red) and non-bloom (blue) patches, and dives that coincided with prey capture records (grey) were mapped spatially, along the seal's track (*right*).

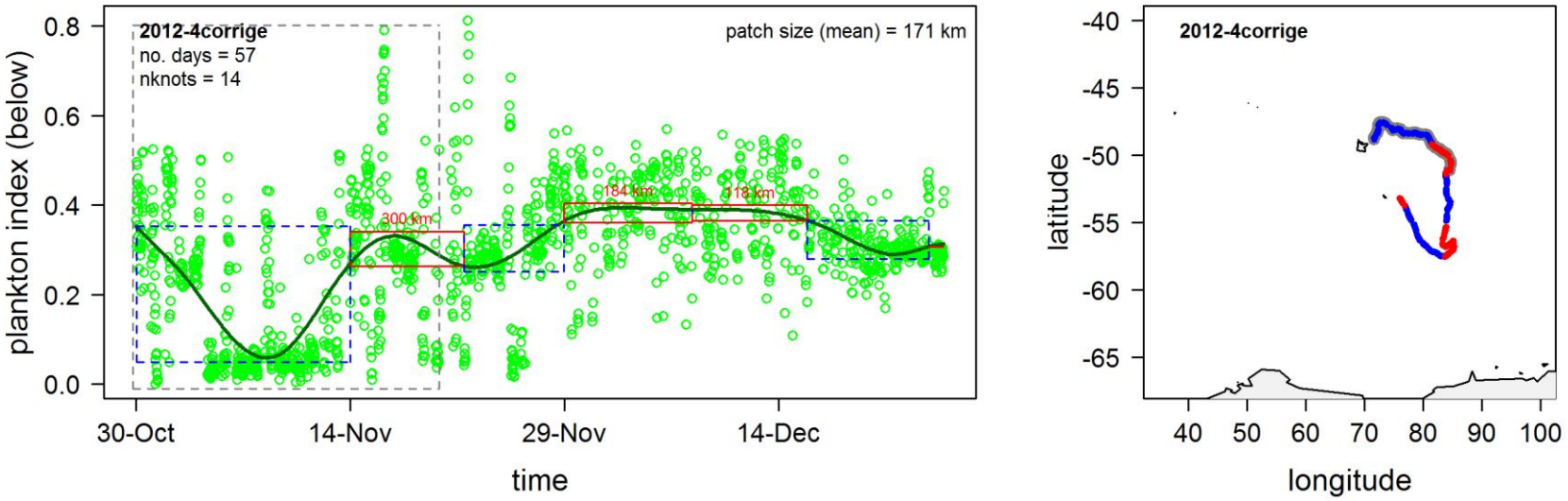

Appendix S4.7.7 (cont')

Meso-scale patches of plankton below the euphotic zone: bloom (red) and non-bloom (blue). A smoothing function applied to plankton values from each trip (n=22) reveals temporal bloom patterns encountered during each trip (*left*). Incomplete trip datasets were excluded from analysis (n=11, see table 1). For details of bloom definition see the methods section. Bloom and non-bloom patches encountered along the seal's track are enclosed in red and dashed blue boxes respectively. Spatial scale of each bloom patch is indicated at the top of each red box. Temporal records of prey capture rates are enclosed in the dashed grey box. Bloom (red) and non-bloom (blue) patches, and dives that coincided with prey capture records (grey) were mapped spatially, along the seal's track (*right*).

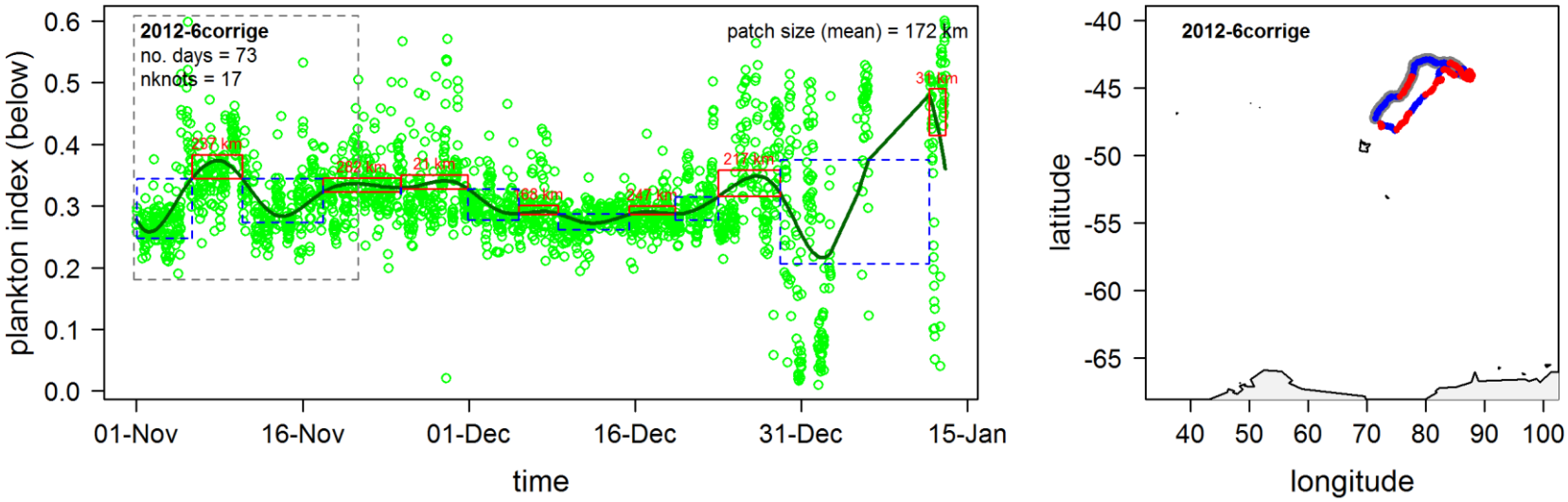

Appendix S4.7.7 (cont')

Meso-scale patches of plankton below the euphotic zone: bloom (red) and non-bloom (blue). A smoothing function applied to plankton values from each trip (n=22) reveals temporal bloom patterns encountered during each trip (*left*). Incomplete trip datasets were excluded from analysis (n=11, see table 1). For details of bloom definition see the methods section. Bloom and non-bloom patches encountered along the seal's track are enclosed in red and dashed blue boxes respectively. Spatial scale of each bloom patch is indicated at the top of each red box. Temporal records of prey capture rates are enclosed in the dashed grey box. Bloom (red) and non-bloom (blue) patches, and dives that coincided with prey capture records (grey) were mapped spatially, along the seal's track (*right*).

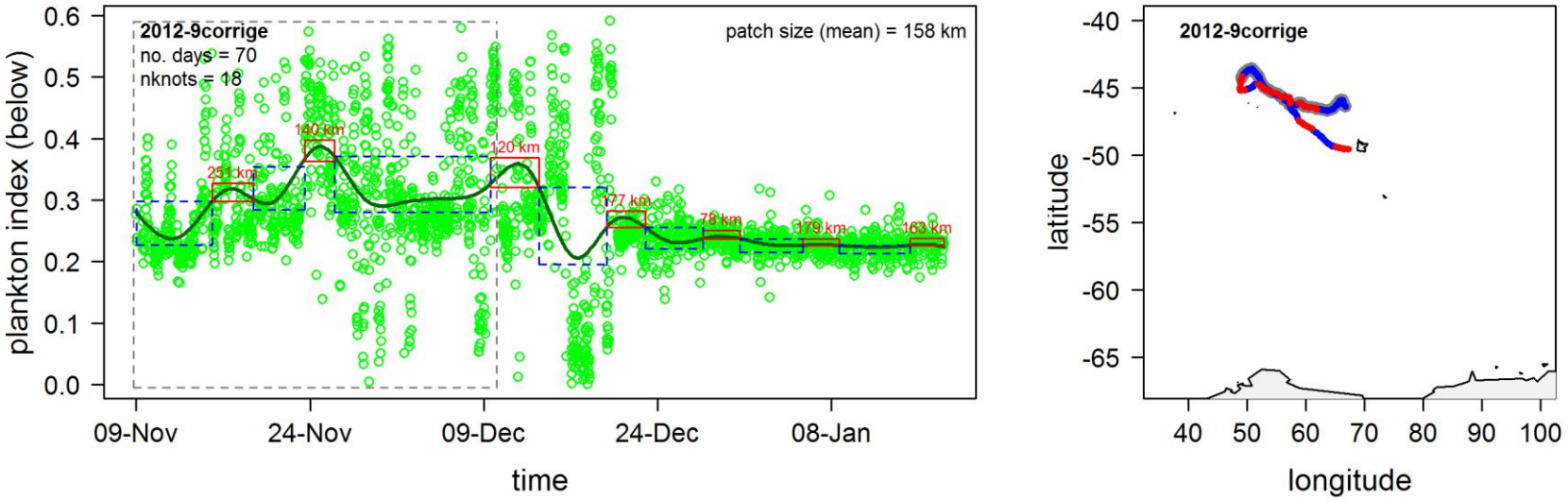

Appendix S4.7.7 (cont')

Meso-scale patches of plankton below the euphotic zone: bloom (red) and non-bloom (blue). A smoothing function applied to plankton values from each trip (n=22) reveals temporal bloom patterns encountered during each trip (*left*). Incomplete trip datasets were excluded from analysis (n=11, see table 1). For details of bloom definition see the methods section. Bloom and non-bloom patches encountered along the seal's track are enclosed in red and dashed blue boxes respectively. Spatial scale of each bloom patch is indicated at the top of each red box. Temporal records of prey capture rates are enclosed in the dashed grey box. Bloom (red) and non-bloom (blue) patches, and dives that coincided with prey capture records (grey) were mapped spatially, along the seal's track (*right*).

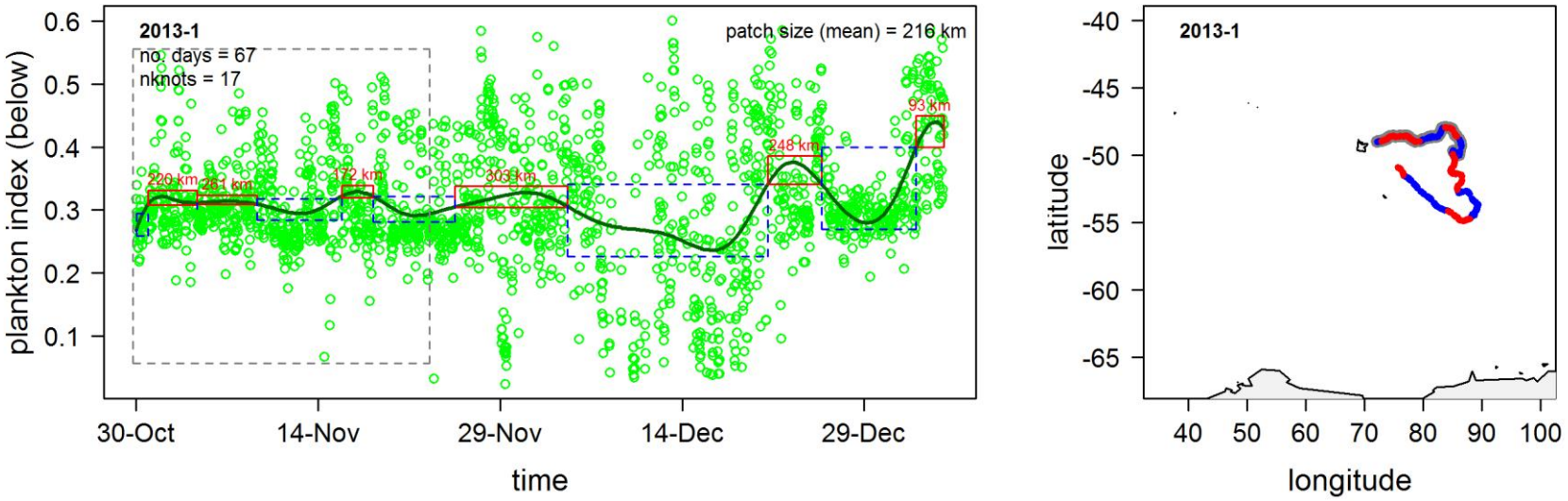

Appendix S4.7.7 (cont')

Meso-scale patches of plankton below the euphotic zone: bloom (red) and non-bloom (blue). A smoothing function applied to plankton values from each trip (n=22) reveals temporal bloom patterns encountered during each trip (*left*). Incomplete trip datasets were excluded from analysis (n=11, see table 1). For details of bloom definition see the methods section. Bloom and non-bloom patches encountered along the seal's track are enclosed in red and dashed blue boxes respectively. Spatial scale of each bloom patch is indicated at the top of each red box. Temporal records of prey capture rates are enclosed in the dashed grey box. Bloom (red) and non-bloom (blue) patches, and dives that coincided with prey capture records (grey) were mapped spatially, along the seal's track (*right*).

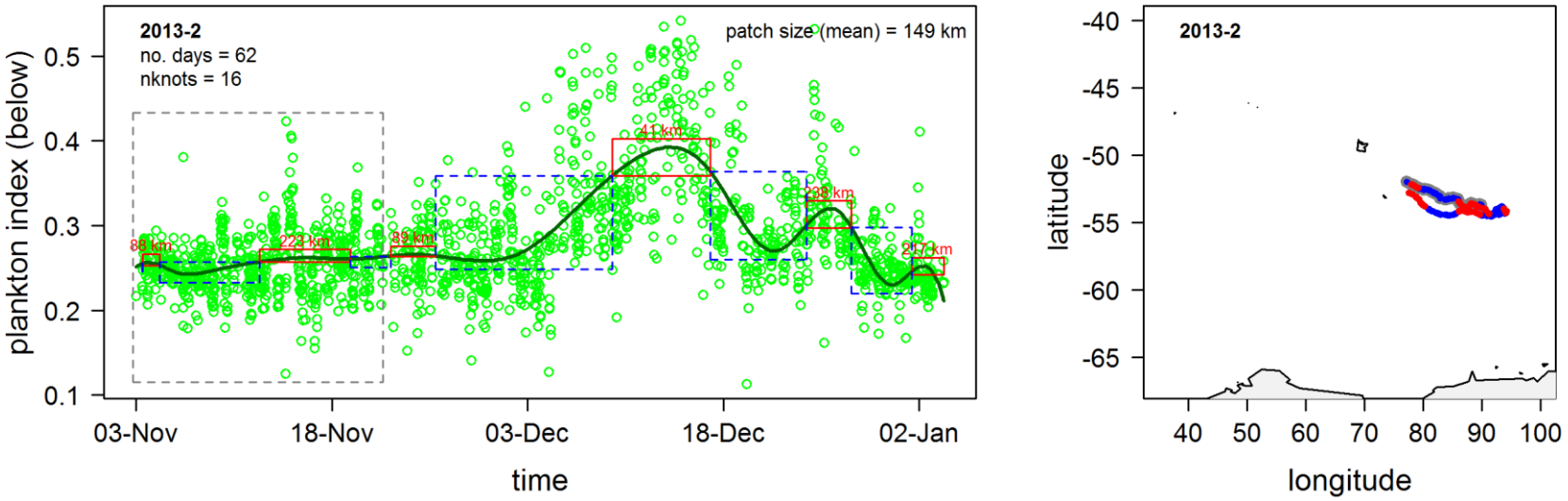

Appendix S4.7.7 (cont')

Meso-scale patches of plankton below the euphotic zone: bloom (red) and non-bloom (blue). A smoothing function applied to plankton values from each trip (n=22) reveals temporal bloom patterns encountered during each trip (*left*). Incomplete trip datasets were excluded from analysis (n=11, see table 1). For details of bloom definition see the methods section. Bloom and non-bloom patches encountered along the seal's track are enclosed in red and dashed blue boxes respectively. Spatial scale of each bloom patch is indicated at the top of each red box. Temporal records of prey capture rates are enclosed in the dashed grey box. Bloom (red) and non-bloom (blue) patches, and dives that coincided with prey capture records (grey) were mapped spatially, along the seal's track (*right*).

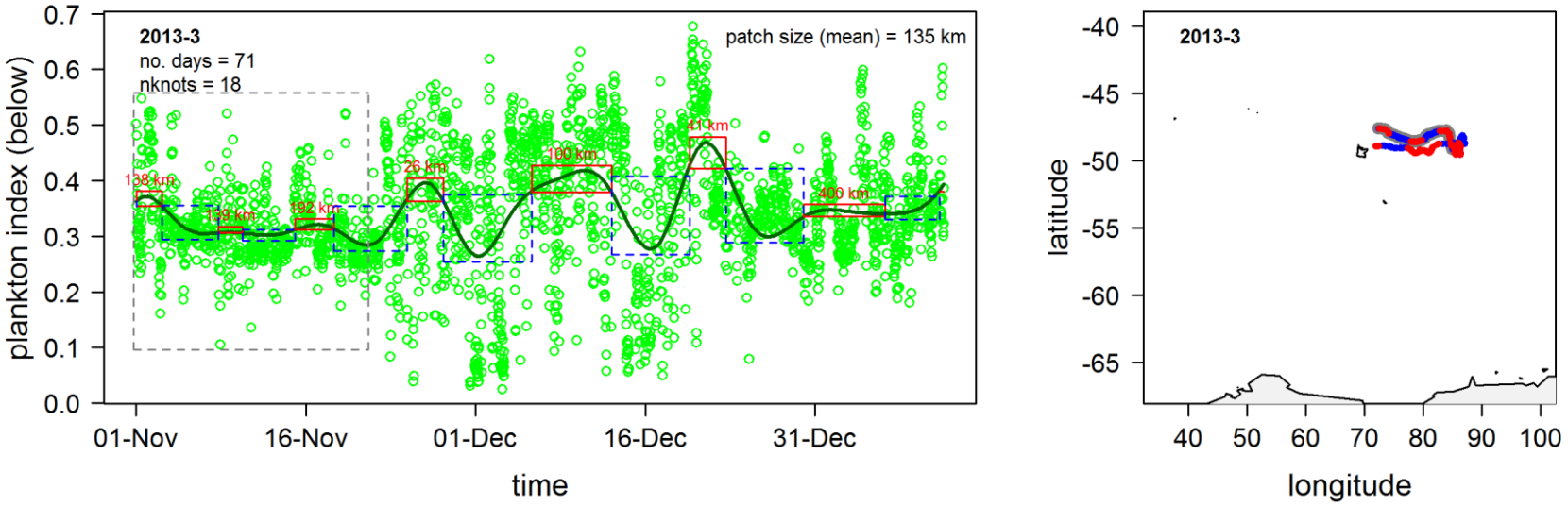

Appendix S4.7.7 (cont')

Meso-scale patches of plankton below the euphotic zone: bloom (red) and non-bloom (blue). A smoothing function applied to plankton values from each trip (n=22) reveals temporal bloom patterns encountered during each trip (*left*). Incomplete trip datasets were excluded from analysis (n=11, see table 1). For details of bloom definition see the methods section. Bloom and non-bloom patches encountered along the seal's track are enclosed in red and dashed blue boxes respectively. Spatial scale of each bloom patch is indicated at the top of each red box. Temporal records of prey capture rates are enclosed in the dashed grey box. Bloom (red) and non-bloom (blue) patches, and dives that coincided with prey capture records (grey) were mapped spatially, along the seal's track (*right*).

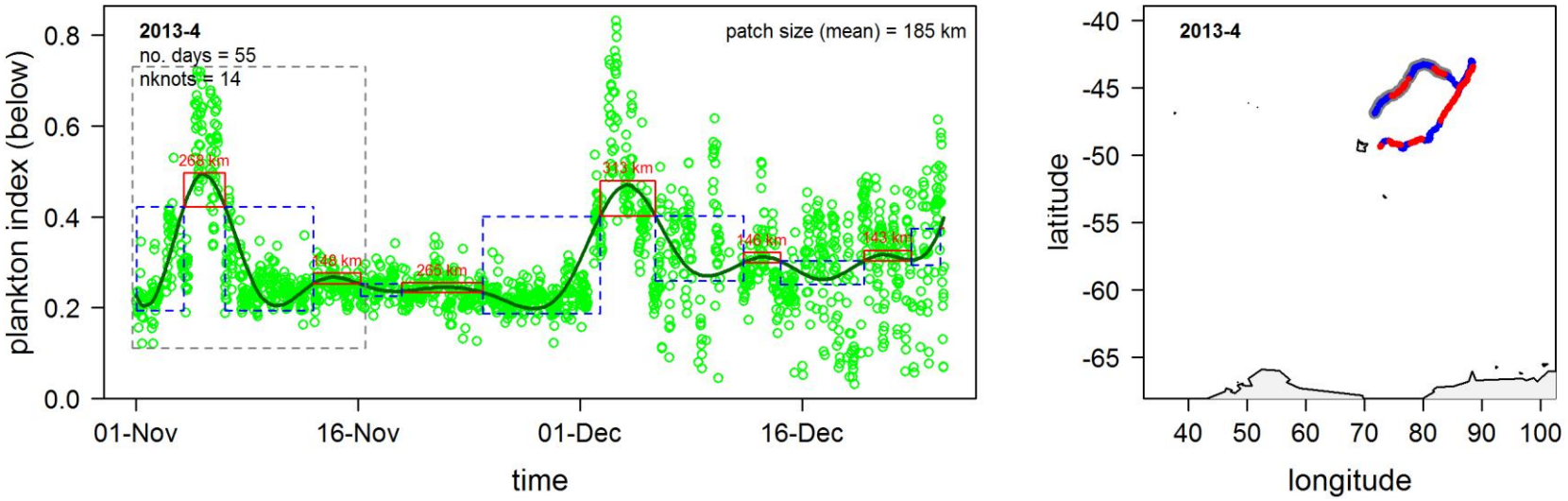

Appendix S4.7.7 (cont')

Meso-scale patches of plankton below the euphotic zone: bloom (red) and non-bloom (blue). A smoothing function applied to plankton values from each trip (n=22) reveals temporal bloom patterns encountered during each trip (*left*). Incomplete trip datasets were excluded from analysis (n=11, see table 1). For details of bloom definition see the methods section. Bloom and non-bloom patches encountered along the seal's track are enclosed in red and dashed blue boxes respectively. Spatial scale of each bloom patch is indicated at the top of each red box. Temporal records of prey capture rates are enclosed in the dashed grey box. Bloom (red) and non-bloom (blue) patches, and dives that coincided with prey capture records (grey) were mapped spatially, along the seal's track (*right*).

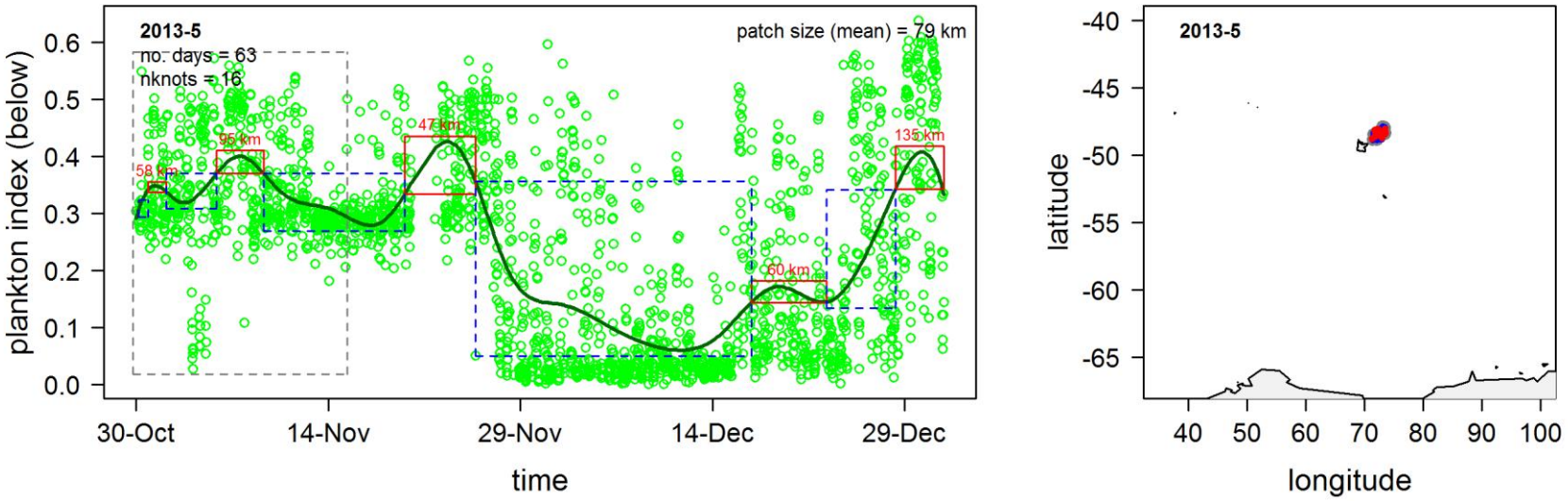

Appendix S4.7.7 (cont')

Meso-scale patches of plankton below the euphotic zone: bloom (red) and non-bloom (blue). A smoothing function applied to plankton values from each trip (n=22) reveals temporal bloom patterns encountered during each trip (*left*). Incomplete trip datasets were excluded from analysis (n=11, see table 1). For details of bloom definition see the methods section. Bloom and non-bloom patches encountered along the seal's track are enclosed in red and dashed blue boxes respectively. Spatial scale of each bloom patch is indicated at the top of each red box. Temporal records of prey capture rates are enclosed in the dashed grey box. Bloom (red) and non-bloom (blue) patches, and dives that coincided with prey capture records (grey) were mapped spatially, along the seal's track (*right*).

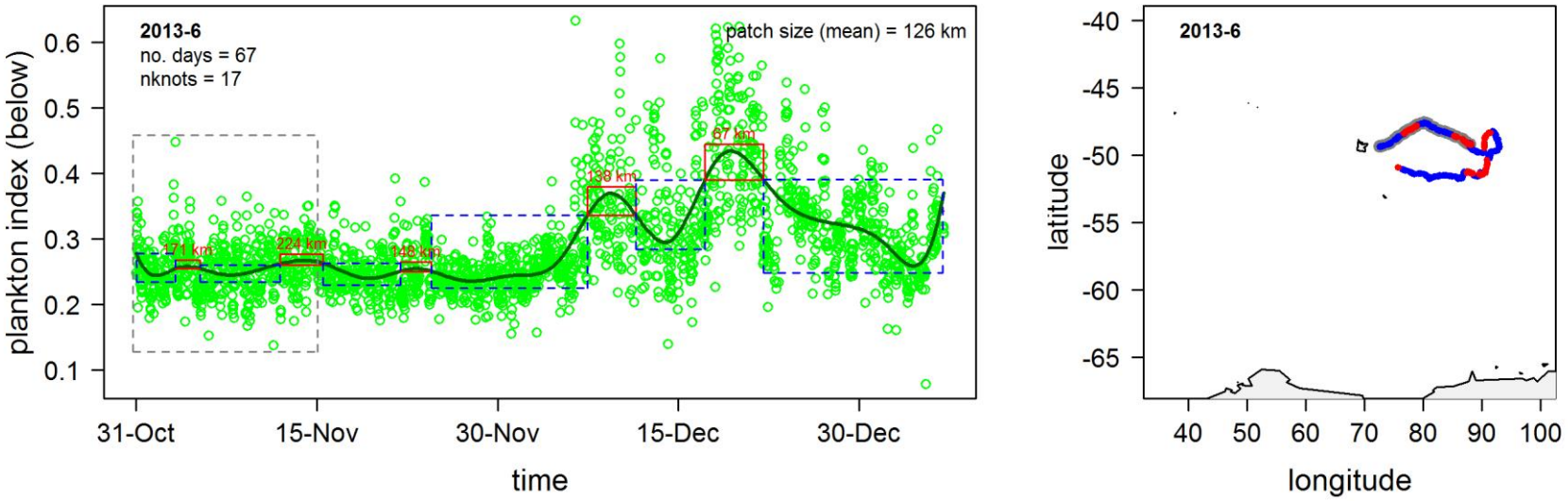

Appendix S4.7.8

Table S4.7.8. Model ranking: prey encounter event (PEE) rate is tested against plankton density (P_{upper}, P_{lower} or P_{below}), maximum dive depth (D), patch type (PT) and their interaction effects at the meso-scale. Explanatory variables are retained sequentially according to their significance. Model parsimony is checked by ranking via Akaike Information Criterion (Burnham and Anderson, 2002). Tables present degrees of freedom (*df*), Akaike Information Criterion (AIC), divergence of a candidate model from the most parsimonious model according to AIC (△AIC), and maximum log-likelihood (LL).

Model	***df***	**AIC**	**△AIC**	**LL**
PEE ~ P_{upper} + D	12	470.6	0	-223.3
PEE ~ P_{upper} + PT + D + P_{upper}:D	13	472.5	2	-223.3
PEE ~ P_{upper} + PT + D + P_{upper}:PT + P_{upper}:D (full model)	14	474.2	3.7	-223.1
PEE ~ P_{upper} + PT + D	9	482.1	11.6	-232.1
PEE ~ P_{upper} + PT + D + P_{upper}:PT	10	483.2	12.6	-231.6
PEE ~ 1 (null model)	2	569.6	99.1	-282.8

Model	***df***	**AIC**	**△AIC**	**LL**
PEE ~ P_{lower} + D	15	399.6	0	-184.8
PEE ~ P_{lower} + PT + D + P_{lower}:D	16	401.6	2	-184.8
PEE ~ P_{lower} + PT + D + P_{lower}:PT + P_{lower}:D (full model)	17	403.6	4	-184.8
PEE ~ P_{lower} + PT + D	12	412.1	12.5	-194
PEE ~ P_{lower} + PT + D + P_{lower}:PT	13	413.9	14.3	-194
PEE ~ 1 (null model)	2	514.5	114.9	-255.2

Model	***df***	**AIC**	**△AIC**	**LL**
PEE ~ 1 (null model)	6	414	0	-201
PEE ~ PT + D	11	414.6	0.6	-196.3
PEE ~ D	10	415.1	1.1	-197.5
PEE ~ P_{below} + PT + D	12	416.4	2.4	-196.2
PEE ~ P_{below} + PT + D + P_{below}:PT	13	418.3	4.3	-196.2
PEE ~ P_{below} + PT + D + P_{below}:D	16	423.9	9.9	-195.9
PEE ~ P_{below} + PT + D + P_{below}:PT + P_{below}:D (full model)	17	425.9	11.9	-195.9

Appendix S4.7.9

Table S4.7.9. Model ranking: prey encounter event (PEE) rate is tested against plankton density (P_{upper}, P_{lower} or P_{below}) within focal dives and surrounding dives ($d_{-5}…d_0…d_{+5}$); patch type (PT) and their interaction effects at the dive-scale. Explanatory variables are retained sequentially according to their significance. Model parsimony is checked by ranking via Akaike Information Criterion (Burnham and Anderson, 2002). Tables present degrees of freedom (*df*), Akaike Information Criterion (AIC), divergence of a candidate model from the most parsimonious model according to AIC (∆AIC), and maximum log-likelihood (LL).

Dive conditions	Plankton layer	Model	*df*	AIC	∆AIC	logLik
d_{-5}	P_{upper}	PEE ~ P	10	27685.8	0	-13832.9
		PEE ~ 1 (null model)	9	27685.8	0	-13833.9
		PEE ~ P + PT	11	27686.6	0.9	-13832.3
		PEE ~ P + PT + P:PT (full model)	12	27688.6	2.9	-13832.3
	P_{lower}	PEE ~ 1 (null model)	6	27694.5	0	-13841.3
		PEE ~ P	7	27695.3	0.8	-13840.6
		PEE ~ P + PT	8	27697.1	2.6	-13840.5
		PEE ~ P + PT + P:PT (full model)	9	27698.2	3.7	-13840.1
	P_{below}	PEE ~ 1 (null model)	6	27686.8	0	-13837.4
		PEE ~ P	7	27687.9	1.1	-13837
		PEE ~ P + PT	8	27689.9	3.1	-13836.9
		PEE ~ P + PT + P:PT (full model)	9	27691.7	4.9	-13836.8
d_{-4}	P_{upper}	PEE ~ 1 (null model)	6	28033.4	0	-14010.7
		PEE ~ P	7	28034.2	0.8	-14010.1
		PEE ~ P + PT	8	28036.1	2.7	-14010
		PEE ~ P + PT + P:PT (full model)	9	28038	4.7	-14010
	P_{lower}	PEE ~ 1 (null model)	6	28033.4	0	-14010.7
		PEE ~ P	7	28034.2	0.8	-14010.1
		PEE ~ P + PT	8	28036.1	2.7	-14010
		PEE ~ P + PT + P:PT (full model)	9	28038	4.7	-14010
	P_{below}	PEE ~ 1 (null model)	6	28025.7	0	-14006.9
		PEE ~ P	7	28027.6	1.9	-14006.8
		PEE ~ P + PT	8	28029.6	3.9	-14006.8
		PEE ~ P + PT + P:PT (full model)	9	28030.8	5.1	-14006.4
d_{-3}	P_{upper}	PEE ~ P	10	28307	0	-14143.5
		PEE ~ P + PT	11	28307.4	0.4	-14142.7

		PEE ~ P + PT + P:PT (full model)	12	28309.2	2.2	-14142.6
		PEE ~ 1 (null model)	9	28310.3	3.3	-14146.1
	P_{lower}	PEE ~ 1 (null model)	6	28216.7	0	-14102.3
		PEE ~ P	7	28218.3	1.6	-14102.1
		PEE ~ P + PT	8	28220.3	3.6	-14102.1
		PEE ~ P + PT + P:PT (full model)	9	28222.2	5.5	-14102.1
	P_{below}	PEE ~ 1 (null model)	6	28216.7	0	-14102.3
		PEE ~ P	7	28218.3	1.6	-14102.1
		PEE ~ P + PT	8	28220.3	3.6	-14102.1
		PEE ~ P + PT + P:PT (full model)	9	28222.2	5.5	-14102.1
	P_{upper}	PEE ~ P	10	28307	0	-14143.5
		PEE ~ P + PT	11	28307.4	0.4	-14142.7
		PEE ~ P + PT + P:PT (full model)	12	28309.2	2.2	-14142.6
		PEE ~ 1 (null model)	9	28310.3	3.3	-14146.1
d_{-2}	P_{lower}	PEE ~ P	7	28242.1	0	-14114
		PEE ~ 1 (null model)	6	28244	2	-14116
		PEE ~ P + PT	8	28244.1	2	-14114
		PEE ~ P + PT + P:PT (full model)	9	28245.1	3	-14113.5
	P_{below}	PEE ~ 1 (null model)	6	28262.2	0	-14125.1
		PEE ~ P	7	28263.1	0.9	-14124.6
		PEE ~ P + PT	8	28265.1	2.9	-14124.5
		PEE ~ P + PT + P:PT (full model)	9	28265.7	3.5	-14123.9
	P_{upper}	PEE ~ P	10	28416.1	0	-14198.1
		PEE ~ 1 (null model)	9	28417.4	1.3	-14199.7
		PEE ~ P + PT	11	28417.9	1.8	-14198
		PEE ~ P + PT + P:PT (full model)	12	28419.5	3.3	-14197.7
d_{-1}	P_{lower}	PEE ~ P	7	28358.4	0	-14172.2
		PEE ~ 1 (null model)	6	28358.9	0.5	-14173.4
		PEE ~ P + PT	8	28360.4	2	-14172.2
		PEE ~ P + PT + P:PT (full model)	9	28362.4	3.9	-14172.2
	P_{below}	PEE ~ 1 (null model)	6	28371.4	0	-14179.7
		PEE ~ P	7	28372.4	1	-14179.2
		PEE ~ P + PT	8	28373.2	1.9	-14178.6
		PEE ~ P + PT + P:PT (full model)	9	28375.2	3.8	-14178.6
d_0	P_{upper}	PEE ~ P	10	29200.4	0	-14590.2

		PEE ~ P + PT	11	29200.8	0.4	-14589.4
		PEE ~ P + PT + P:PT (full model)	12	29202.1	1.6	-14589
		PEE ~ 1 (null model)	9	29202.7	2.2	-14592.3
	P_{lower}	PEE ~ P	7	29132.1	0	-14559
		PEE ~ 1 (null model)	6	29134	1.9	-14561
		PEE ~ P + PT	8	29134.1	2	-14559
		PEE ~ P + PT + P:PT (full model)	9	29135.6	3.5	-14558.8
	P_{below}	PEE ~ 1 (null model)	6	29128.4	0	-14558.2
		PEE ~ P	7	29129.7	1.3	-14557.8
		PEE ~ P + PT	8	29131.3	2.9	-14557.7
		PEE ~ P + PT + P:PT (full model)	9	29133.1	4.6	-14557.5
	P_{upper}	PEE ~ P	10	28598	0	-14289
		PEE ~ P + PT	11	28598.4	0.5	-14288.2
		PEE ~ 1 (null model)	9	28598.6	0.6	-14290.3
		PEE ~ P + PT + P:PT (full model)	12	28600.3	2.3	-14288.2
d_{+1}	P_{lower}	PEE ~ P	7	28475.7	0	-14230.8
		PEE ~ 1 (null model)	6	28476.4	0.8	-14232.2
		PEE ~ P + PT	8	28477.6	1.9	-14230.8
		PEE ~ P + PT + P:PT (full model)	9	28478.6	2.9	-14230.3
	P_{below}	PEE ~ 1 (null model)	6	28502.2	0	-14245.1
		PEE ~ P	7	28504	1.8	-14245
		PEE ~ P + PT	8	28505.7	3.5	-14244.8
		PEE ~ P + PT + P:PT (full model)	9	28507.6	5.4	-14244.8
	P_{upper}	PEE ~ P	10	28242.8	0	-14111.4
		PEE ~ 1 (null model)	9	28243.5	0.7	-14112.7
		PEE ~ P + PT	11	28244.4	1.6	-14111.2
		PEE ~ P + PT + P:PT (full model)	12	28246.2	3.4	-14111.1
d_{+2}	P_{lower}	PEE ~ P	7	28089.8	0	-14037.9
		PEE ~ P + PT	8	28091.8	2	-14037.9
		PEE ~ 1 (null model)	6	28091.8	2	-14039.9
		PEE ~ P + PT + P:PT (full model)	9	28093.7	3.9	-14037.8
	P_{below}	PEE ~ 1 (null model)	6	28111.2	0	-14049.6
		PEE ~ P	7	28113.1	1.8	-14049.5
		PEE ~ P + PT	8	28115	3.8	-14049.5
		PEE ~ P + PT + P:PT (full model)	9	28115.1	3.9	-14048.6

	P_{upper}	PEE ~ P	10	28232.1	0	-14106
		PEE ~ 1 (null model)	9	28232.5	0.4	-14107.3
		PEE ~ P + PT	11	28233.8	1.7	-14105.9
		PEE ~ P + PT + P:PT (full model)	12	28235.5	3.4	-14105.7
d_{+3}	P_{lower}	PEE ~ 1 (null model)	6	28108.6	0	-14048.3
		PEE ~ P	7	28109	0.4	-14047.5
		PEE ~ P + PT	8	28110.9	2.4	-14047.5
		PEE ~ P + PT + P:PT (full model)	9	28112.5	3.9	-14047.2
	P_{below}	PEE ~ 1 (null model)	6	28120	0	-14054
		PEE ~ P	7	28121.5	1.5	-14053.7
		PEE ~ P + PT	8	28122.9	3	-14053.5
		PEE ~ P + PT + P:PT (full model)	9	28123.5	3.6	-14052.8
	P_{upper}	PEE ~ P	10	27987.5	0	-13983.7
		PEE ~ 1 (null model)	9	27987.7	0.2	-13984.9
		PEE ~ P + PT	11	27988.8	1.3	-13983.4
		PEE ~ P + PT + P:PT (full model)	12	27990.6	3.1	-13983.3
d_{+4}	P_{lower}	PEE ~ 1 (null model)	6	27889.9	0	-13939
		PEE ~ P	7	27890.1	0.1	-13938
		PEE ~ P + PT	8	27891.7	1.8	-13937.9
		PEE ~ P + PT + P:PT (full model)	9	27893.7	3.8	-13937.8
	P_{below}	PEE ~ 1 (null model)	6	27897	0	-13942.5
		PEE ~ P	7	27898.7	1.7	-13942.4
		PEE ~ P + PT	8	27900.6	3.6	-13942.3
		PEE ~ P + PT + P:PT (full model)	9	27901.5	4.5	-13941.8
	P_{upper}	PEE ~ 1 (null model)	9	27470.5	0	-13726.2
		PEE ~ P	10	27471.4	0.9	-13725.7
		PEE ~ P + PT	11	27472.8	2.3	-13725.4
		PEE ~ P + PT + P:PT (full model)	12	27474.8	4.3	-13725.4
d_{+5}	P_{lower}	PEE ~ 1 (null model)	6	27396.2	0	-13692.1
		PEE ~ P	7	27396.7	0.4	-13691.3
		PEE ~ P + PT	8	27398.4	2.2	-13691.2
		PEE ~ P + PT + P:PT (full model)	9	27400.3	4.1	-13691.2
	P_{below}	PEE ~ 1 (null model)	6	27425.8	0	-13706.9
		PEE ~ P	7	27427.7	1.9	-13706.9
		PEE ~ P + PT + P:PT (full model)	9	27429.5	3.7	-13705.7
		PEE ~ P + PT	8	27429.6	3.8	-13706.8

Chapter 5: General discussion

5.1 Preface

The advent of bio-logging technology has enabled the examination of the three-dimensional physical structure of the marine environment and the identification of hydrological features important to marine predators in the Southern Ocean (Bost et al., 2009b;Evans et al., 2013). However, the data collected by marine predators rarely includes *in situ* biological information (although chlorophyll estimates have been derived from recently deployed fluorometers; Blain et al., 2013), but rather have detailed information on physical parameters such as temperature, salinity (Bailleul et al., 2007;Biuw et al., 2007) and light (Bradshaw et al., 2002;Guinet et al., 2014). These data have provided vital insight into habitat use by marine predators and the consequences of oceanographic fluctuations in relation to climate change (Bost et al., 2009b). Nonetheless, productivity is a major factor influencing food web and ecosystem dynamics in natural systems (Odum, 1969), but biophysical processes in the Southern Ocean means that resources for higher-trophic level species are often patchily distributed. Small-scale marine structures (*e.g.* meandering eddies, cold water filaments) are thought to change plankton distributions more rapidly than large-scale marine structures (*e.g.* frontal zones) (Haury et al., 1978). The continuously changing spatio-temporal pattern of prey is therefore expected to respond to complex heterogeneity at different scales (Russell et al., 1992). Foraging behaviour of predators is by necessity linked to the distribution and abundance of prey and therefore has the potential to reveal changes in prey distribution and abundance (Hindell et al 2003). Because of difficulties inherent in locating food in such a complex environment, both models (e.g. Fauchald, 1999) and empirical evidence (e.g. Grémillet et al., 2001;Weimerskirch et al., 2005) reiterate the strong selection for efficient foraging, and that predators adopt specific foraging behaviours to manage these dynamic conditions. Feeding and activity patterns are therefore central themes to life-history evolution (Stearns, 1993).

The main objective of this thesis was to examine biological patterns in open ocean systems, as well as improve our understanding of how an apex predator, southern elephant seals, optimises their foraging strategies in relation to seasonally variable primary productivity. This was dependent on the ability to estimate plankton density in the water column and to relate this to concurrent seal foraging behaviour at appropriate spatial and temporal scales.

5.2 Light-based estimates of plankton distribution

Studies have used satellite-derived chlorophyll estimates to predict predator habitat on the basis of productivity, but these have a number of limitations due to the paucity of data concurrent with animal movement on the horizontal (Bradshaw et al., 2004; satellite sensors limited by heavy cloud cover and/or low data resolution) and vertical axes (Grémillet et al., 2008; satellite sensors cannot detect chlorophyll below the surface or zooplankton). This spatio-temporal mismatch between satellite-derived chlorophyll-a data and animal foraging behaviour often limits studies to broad scale analyses (e.g. weeks or months; Bradshaw et al., 2004) (see chapter 2). The approach outlined in chapter 2 (*i.e.* uses animal-borne light sensors to estimate plankton density distribution) and allowed predator foraging behaviour to be examined in response to plankton distribution at multiple scales, including at the daily scale (chapter 3), as well as the meso- and dive-scale (chapter 4). This meant that light data collected by elephant seals allowed seasonal plankton distribution patterns to be analysed at scales relevant to elephant seal foraging behaviour.

The shading effect of plankton in the water column (*i.e.* plankton density index – PDI) was detectable from the on-board light sensors deployed on elephant seals and correlated well with concurrent seasonal chlorophyll-a estimates derived from satellite ocean colour. Recent studies have also found similar results by comparing light estimates, collected from animal-borne sensors, with florescence (Jaud et al., 2012), as well as water samples of phytoplankton collected at stations in the vicinity of the tagged animal (Teo et al., 2009). Moreover, Teo et al. (2009) demonstrated the application of this approach along the vertical axis by estimating *in situ* subsurface chlorophyll profiles concurrent with Pacific bluefin tuna (*Thunnus orientalis*) dive behaviour. In chapter 4, elephant seals responded to plankton densities in the lower euphotic zone (75 m – 150 m), suggesting that deep chlorophyll maxima (*i.e.* secondary peaks in phytoplankton biomass) were influencing deep-diving predators. Light-based estimates of plankton density collected by elephant seals also demonstrated typical trans-seasonal plankton patterns north of the Ross Sea (chapter 2 and chapter 3), as well as the full extent of a major recurrent plume in the southern Indian Ocean, spanning more than two-thousand kilometres east of the Kerguelen Plateau (chapter 4). However, despite the utility of using light to estimate plankton density in the water column, it should be stressed that the effectiveness of this method largely relies on measurements being taken in Case I waters, whereby most particulates in the euphotic zone are assumed to be phytoplankton (Morel and Prieur, 1977;Morel and Maritorena, 2001; for details see chapter 2).

5.3 Predator foraging behaviour and marine productivity

Marine ecosystems are vast and complex biological networks, dynamic in structure at a range of spatial and temporal scales (Nicol et al 2000), and are driven by physical processes (Olson and Hood, 1994), as well as biotic top-down processes (Baum and Worm, 2009) that determine oceanic habitat. Seasonal variability has important repercussions for the geographic patterns and abundance of primary productivity (*i.e.* phytoplankton), which in turn contributes to the distribution and abundance of zooplankton, fish and ultimately, top predators. Consequently, top predators are thought to exploit zones of intense primary productivity that are expected to be extremely profitable foraging grounds characterised by high prey availability (typical bottom-up processes, Ware and Thomson, 2005). However, temporal delays in the food web introduced by microbial recycling pathways and grazing zooplankton (Smetacek et al., 2004) will lead to spatial disconnect between areas of primary production and consumption by higher trophic levels as resources are advected in the ocean (Grossmann, 1994;Grossmann and Dieckmann, 1994). Resources are therefore often patchily distributed, and individuals must respond to local prey distribution and abundance by adjusting their behaviour accordingly to maximise energy intake (Cantrell et al., 2010).

In many of the world's oceans it is well known that some apex predators are often associated with frontal structures where it is thought they find profitable prey patches (table 5.1). It is thought that these productive waters are due to the enhancement of local primary production, as well as aggregation of prey due to convergence processes (e.g. Hunt Jr, 1997;Spear et al., 2001;Van Franeker et al., 2002;d'Ovidio et al., 2013;Cotté et al., 2014). In the Southern Ocean there is much literature reporting how seabirds and mammals use fronts and how this may influence their diving activity and feeding success (for review see Bost et al., 2009b). However, the relatively poor performance of habitat models that are based on physical parameters (e.g. Bradshaw et al., 2004;O'Toole et al., 2014a) may suggest that predators are instead directly driven by resource distribution, rather than the processes that generate them. Rather than focus on physical attributes of the marine environment (*e.g.* temperature, salinity), studies in chapter 3 and chapter 4 examined how the foraging behaviour of elephant seals in response to plankton distribution (inferred using a light-based plankton density index introduced in chapter 2) in the pelagic realm. Overall, it was revealed that elephant seal foraging behaviour was influenced by areas of elevated plankton, which are expected to coincide with their mesopelagic fish prey. This is commonly observed in upwelling systems where nutrient input and local productivity overlap with top marine predators and their prey (e.g. Croll et al., 2005;Biuw et al., 2010).

Table 5.1. Examples of marine predators and their use of fronts in different sectors of the global ocean.

region	predator *spp.*	frontal structure	predator association	publication
Bering Sea	Murres (*Uria lomvia* and *U. aalge*)	shelf fronts around the Pribilof Islands	concentration of birds near the fronts	Kinder et al 1983
Mozambique Channel	Great frigatebirds (*Fregata minor*)	mesoscale anticyclonic gyres	remained at the edge of cold-core eddies	Weimerskirch et al 2004
Northeat Pacific	Sooty and Pink-footed shearwaters (*Puffinus griseus* and *P. creatopus*)	California Boundary Current System	attracted to the edge of the most recently upwelled water	Ainley et al 2005
waters off Southern California	Blue whales (*Balaenoptera musculus*)	California Current	foraging activity downstream from an upwelling	Croll et al 1998
Southern Indian Ocean	King penguins (*Aptenodytes patagonicus*)	Polar Front	prefered waters below the surface mixed layer	Charrassin & Bost 2001

In a highly dynamic environment where resources are patchily distributed, animals need to evolve efficient ways to locate food. Interestingly, the positive relationship between seal foraging behaviour and plankton density at the daily scale occurred year-round (chapter 3) despite distinct differences in productivity between summer and winter (Behrenfeld and Falkowski, 1997;Garibotti et al., 2005;Thomalla et al., 2011). This suggests that seals continued to locate sufficient food during both the bloom period during summer (*i.e.* post-breeding migration) and the relatively oligotrophic period during winter (*i.e.* post-moulting migration). With this in mind, elephant seals seem to be capable of changing foraging strategies according to resource distribution in order to maintain prey acquisition year-round. Based on this relative broad-scale study it appears that seals foraging during their post-breeding migration likely respond to large-scale biological cues (*i.e.* plankton density) in summer when resources are relatively homogeneous; seals during their post-moulting migration likely respond to (sub) meso-scale biological cues in winter when resources are more patchily distributed (see discussion in chapter 3). Simmons et al. (2010) alludes to similar foraging strategies adopted by northern elephant seals (*Mirounga angustirostris*) to exploit environments with different degrees of heterogeneity: seals exhibiting higher encounter rates of lower quality patches for short post-breeding migrations and lower encounter rates of higher quality patches for longer post-moulting migrations. Flying seabirds, such as Masked boobies (*Sula dactylatra*), also exhibit similar strategies when faced with a trade-off between local and distant trips: locally these birds only have access to low quality patches, but encounter these patches often; by travelling further they are able to access higher quality patches, but these patches are encountered much less often (Sommerfeld et al., 2015).

Certainly, nowhere else but in the polar regions are such stark seasonal environmental changes encountered by marine predators. The plasticity of top predators foraging in the open ocean highlights the value of different foraging strategies adopted by individuals exploiting resources that are patchy in space and time. Authier et al (2012) suggest that female southern elephant seals from Isle Kerguelen may use the inter-frontal zone because food is much more predictable here than in Antarctic waters; though less profitable. The findings discussed in the following section (based on chapter 4 analyses) will propose the dynamic structure and trophic interactions within the inter-frontal zone in a seemingly homogeneous phytoplankton plume that appears to influence the foraging behaviour of post-breeding elephant seals.

5.4 Tropho-dynamics within the Antarctic Circumpolar Current

Elephant seals do not feed on lower-trophic primary producers, but rather on mid-trophic mesopelagic fish and squid (Cherel et al., 2008;Newland et al., 2009;Newland et al., 2011;Banks et al., 2014) that are often found well below the euphotic zone (Catul et al., 2011). These trophic links can be highly dynamic and intermediate components (such as zooplankton and fish) often vary in space and time and do not necessarily coincide with lower-trophic levels such as phytoplankton. The match/mismatch hypothesis, first proposed by Cushing (1969), seeks to explain this recruitment variation in populations by focusing on seasonal timing of different trophic levels and how they compare with each other in space and time (also see Cushing, 1990). For example, a mismatch between primary productivity and upper-trophic levels can be due to life history strategies. Llopiz and Hobday (2014) have revealed spawning adults and larvae of zooplankton in lower latitude waters occur when chlorophyll concentrations near a seasonal minimum (*i.e.* low food availability) to take advantage of warmer water temperatures necessary for rapid growth.

A change in the food web structure of an ecosystem due to anthropogenic impacts (*e.g.* overfishing) can also result in trophic mismatch. Grémillet et al. (2008) suggested the life history strategies of a coastal breeding seabird (Cape gannets, *Morus capensis*) have adapted to targeting areas of intense primary productivity where their prey once aggregated off the Atlantic coast of South Africa. Cape gannet populations continue to target these areas despite depleted prey stocks from commercial fishing, leading to a superficial link between phytoplankton distribution and a top predator. Trophic mismatch may also simply arise due to the temporal lag between typical marine recruitment processes: the lag between nutrient input and phytoplankton growth can range between days to

weeks (Dugdale and Wilkerson, 1989;Dugdale et al., 2006) or between phytoplankton and changes in zooplankton biomass that can range between weeks and months (Hayward and Venrick, 1998). The examples of different match/mismatch types presented above are summarised in table 5.2.

Table 5.2. A summary of three different match/mismatch types in the marine environment and examples for each type.

match/mismatch type	**example scenario**	**publication**
life history strategy	spawning adults and larvae of zooplankton coincide with low chlorophyll concentrations to take advantage of warm water for rapid growth	Llopiz & Hobday 2014
antrhopegenic impact alters food web dynamics	seabirds target areas of intense primary production despite low prey abundance due to overfishing	Gremillet et al 2008
temporal lag between recruitment	nutrient input is followed days to weeks later by phytoplankton growth; zooplankton then takes weeks to months to respond to phytoplankton	Hayward and Venrick 1998

In chapter 4, data collected by elephant seals migrating eastward from Isles Kerguelen was effectively a longitudinal transect through a major recurrent phytoplankton plume (figure 5.1A) that originates from productive waters generated over the Kerguelen Plateau at the beginning of the spring/summer bloom period. During the bloom period phytoplankton biomass in this region is highly dynamic in space and time (figure 5.1B-D). The growth rates of phytoplankton in areas of the Southern Ocean remote from land are predominately limited by iron availability (Boyd et al., 2000;de Baar et al., 2005) and rely on eastward advection by the ACC to resupply open ocean regions (for details see chapter 1.3). The efficient recycling and retention of nutrients in the mixed layer by Southern Ocean microbes, protozoa and metazoa (Smetacek et al., 2004) also suggests that much of the productive waters generated around the Kerguelen Plateau would be slowly advected eastward by the ACC over large distances before being depleted. In accordance with temporal lags between the recruitment each trophic-level group (see table 5.2), zooplankton biomass will proliferate in response to primary production over summer as these nutrient-rich waters are advected across open ocean before energy is transferred to higher-trophic levels such as mesopelagic fish (figure 5.2), and ultimately top predators (Smetacek et al., 2004).

A trophic lag would mean that the ecosystem closer to the initial plume site (*i.e.* the Kerguelen Plateau) has had more time for energy transfer from lower- to higher-trophic species and nutrient recycling, compared with the ecosystem closer to the plume front (*i.e.* furthest eastward-advected waters from the initial plume site) (figure 5.3). As seals travel further from the initial plume site, but

closer to the eastward-drifting plume front, less time has been allocated to food web development, meaning less energy has been transferred to their mid-trophic prey via bottom-up processes (higher-trophic levels driven by phytoplankton distribution and abundance). Seals may therefore encounter lower mesopelagic fish densities as they travel further from the initial plume site. This notion was supported by the use of light as a proxy for bioluminescent prey that suggests prey density decreases as seals approached the plume front (chapter 4).

Although a temporal lag is expected between the initial phytoplankton bloom and zooplankton proliferation (e.g. Croll et al., 2005;Grémillet et al., 2008), high densities of myctophid are known to co-occur with their zooplankton prey within the Polar Frontal Zone at the meso-scale (Pakhomov et al., 1996). Therefore, it could be that bottom-up processes during the summer bloom period are delayed primarily by the temporal mismatch between phytoplankton and zooplankton as productive waters drift eastward.

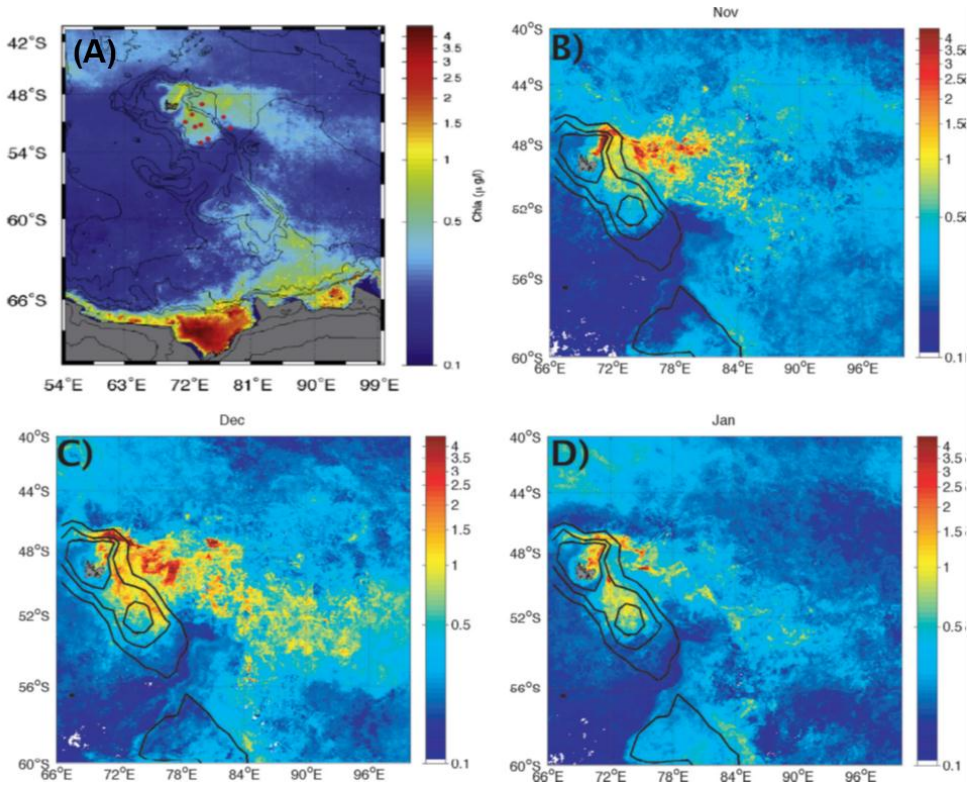

Figure 5.1. Map of the Kerguelen Plateau area, showing major topography (black lines) and sea-surface chlorophyll-*a* climatology (1997 – 2007) from the MODIS AQUA sensor: (A) annual average of recurrent Kerguelen plume in the north and productive Antarctic waters in the south (modified from Mongin et al., 2008); and averages for (B) November; (C) December; and (D) January (modified from Mongin et al., 2009).

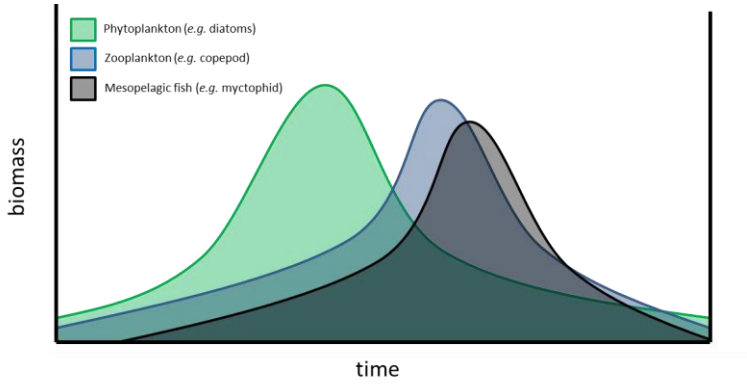

Figure 5.2. A graphical representation of three trophic-level groups (phytoplankton, zooplankton and mesopelagic fish) according to their biomass over time, and the temporal lag between the recruitment (*i.e.* peak biomass) of each trophic-level group (see table 5.2).

Superficial overlap between phytoplankton and top predators, such as those caused by overfishing in temperate waters off the west coast of South Africa (see Grémillet et al., 2008), can blur the functional link between primary production and top predator feeding success. Without an understanding of intermediate trophic levels it can be difficult to quantify trophic linkages, particularly in the open ocean pelagic system where food web processes are highly dynamic in time, as well as in space (see chapter 1.3). Scale-dependent analysis of seal feeding in the plume structure and bioluminescent prey distribution in chapter 4 suggests the possible role of plankton in a seal's attempt to access prey. It was proposed that the shading effect of plankton may assist female elephant seals to access vertically-migrating prey to compensate for lower prey densities encountered closer to the plume front. The stimulus for vertical migration of many pelagic species is changes in light intensity (Frank and Widder, 1997): a trade-off between feeding near the surface and minimising the risk of predation by diving to deeper refuges (Hays, 2003). As central place foragers, deep-diving predators are expected to increase their energy gain to compensate for travel costs as vertical distances to food increases (Mori, 1998). Female elephant seals may increasingly utilise the shading effect of plankton as a way to improve vertical accessibility (reduce vertical distance to food) as prey densities drop (decreased energy gain). This response could be even more important for other predator species with poorer diving capabilities (*e.g.* fur seals, penguins) that also respond to the light-regulated vertical migration of their prey (Horning and Trillmich, 1999;Georges et al., 2000;Blanchet et al., 2013;Sterling et al., 2014).

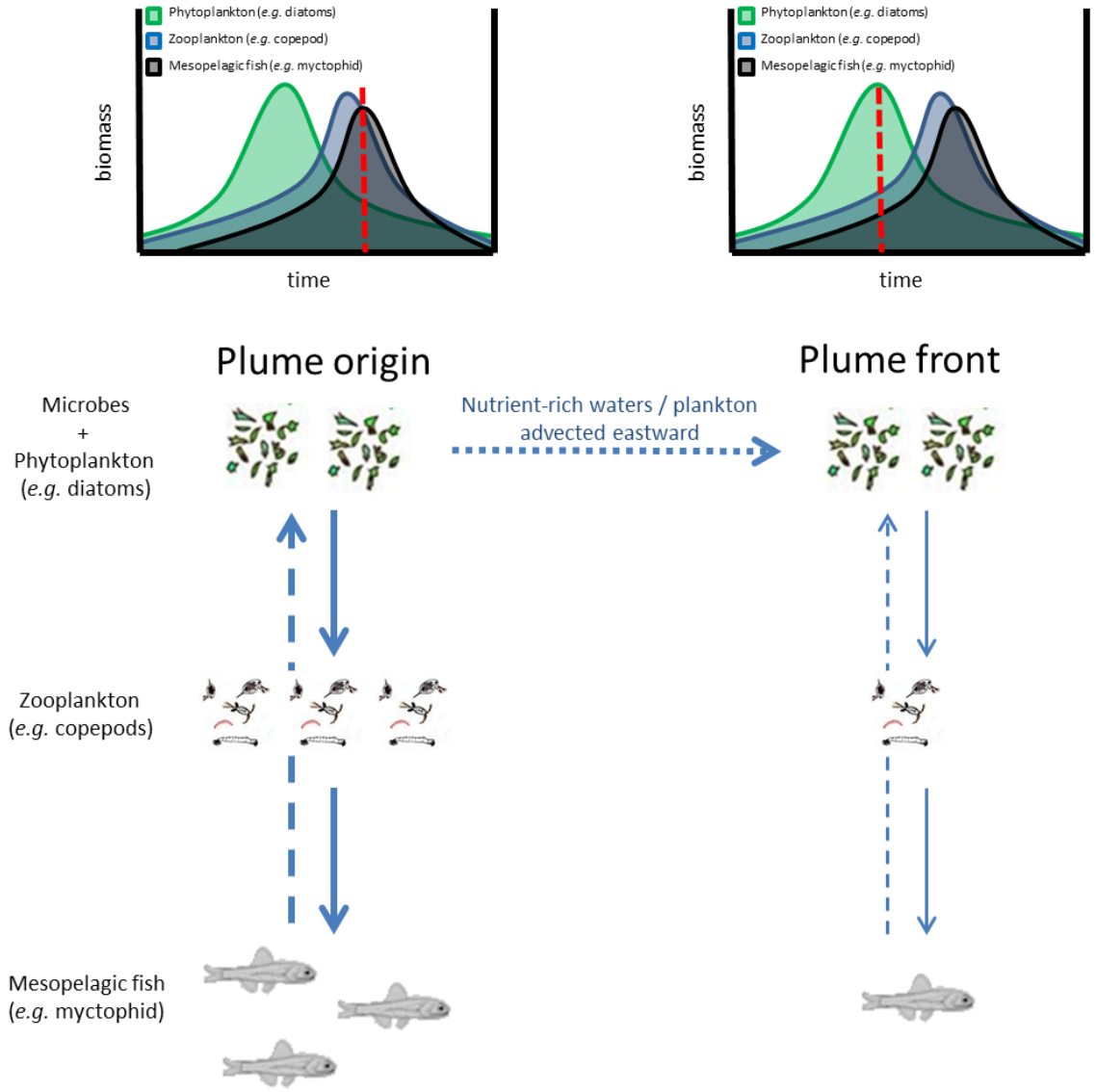

Figure 5.3. A simplistic food chain at the origin (plume origin) and front (plume front) of the eastward-advected Kerguelen plume at different recruitment stages. Recruitment stage is indicated by the vertical red dashed line shown in the top plots adapted from figure 5.2: plume origin is where the most time has passed since phytoplankton recruitment; site of the plume front is where the least amount of time has passed since phytoplankton recruitment. The bottom diagram represents the food chain and biomass of each trophic level according to the recruitment stage at the plume origin (*i.e.* where more time has allowed greater energy transfer to higher-trophic level groups) and front (*i.e.* where less time has allowed the least amount of energy transfer to higher-trophic level groups). Vertical blue arrows represent energy transfer to higher-trophic level groups (solid) and recycled nutrients (dashed); arrow thickness represents relative amount of energy transferred and recycled. Horizontal blue dotted arrow represents the eastward-advected productive waters (*i.e.* nutrients/microbes/plankton).

There are other examples of other marine predators that use their environment to aid their capture of prey. Ropert-Coudert et al. (2006) suggested that little penguins (*Eudyptula minor*) in the Bass Strait off Tasmania may use the thermocline, either to reduce the escape field or to concentrate prey. Individuals from the same population of little penguins are also thought to use the seafloor to trap their prey (Ropert-Coudert et al., 2006). Burns et al. (2008) has suggested that this same foraging strategy is used by crabeater seals (*Lobodon carcinophagus*) to feed on krill aggregates around waters of the Western Antarctic Peninsula. Bernard and Steinberg (2013) has also shown that Adélie penguins (*Pygoscelis adeliae*) that forage nearshore of the Western Antarctic Peninsula coastline improve their vertical access to Antarctic krill (*Euphausia superba*) by favouring diurnal tides associated with shallower prey aggregations. Ultimately, these strategies – including the one proposed in chapter 4 to deal with a gradient of food web developmental stages – all follow the same premise, which is to minimise the cost of travel to food and maximise energy intake (Schoener, 1971). A summary of these proposed prey capture strategies are outlined in table 5.3.

Table 5.3. Examples of proposed prey capture strategies adopted by marine predators in different oceanic regions.

proposed prey capture strategy	**predator *spp.***	**region**	**publication**
(1) use the thermocline to reduce escape field or concentrate prey; and (2) use seafloor to trap prey	little penguins (*Eudyptula minor*)	Bass straight, Australia	Ropert-Coudert et al 2006
use seafloor to trap prey	crabeater seals (*Lobodon carcinophagus*)	Western Antarctic Peninsula	Burns et al 2008
use diurnal tides to aggregate prey	Adélie penguins (*Pygoscelis adeliae*)	Western Antarctic Peninsula	Bernard et al (2013)
use shading effect of plankton to improve vertical access to mesopelagic prey	southern elephant seals	southern Indian Ocean	Guinet et al (2014); chapter 4 of this thesis

In contrast, seals foraging in relatively oligotrophic winter waters may be more strongly associated with physical structures such as meso-scale eddies or cold water filaments that drive the accumulation/retention of plankton and subsequent energy transfer up the food chain (d'Ovidio et al., 2013; for more details see the discussion in chapter 3). Consequently, the shading effect of plankton is likely to be less important to seals in winter; rather, plankton is more likely to coincide

with distinct profitable prey patches because of the accumulative/retentive effect of meso-scale eddies and cold water filaments on marine resources in winter. Comparisons of analysis in chapter 4 with similar high-resolution data collected in winter – when primary productivity is comparatively low – could allow a holistic understanding of the seasonal function of plankton in relation to elephant seal foraging strategies (*i.e.* does the shading effect of plankton influence seal foraging success in both summer and winter?). Chapter 4 underlines the importance of understanding spatial dynamics across all relevant trophic levels, as well as the utility of scale-dependent studies.

5.5 Perspective

Despite the relatively poor fit of habitat models that are based on physical parameters, very few studies have considered biological conditions at scales relevant to the animal. While this thesis does not dispute the importance of oceanographic features, ecological interpretation may well be distorted without the relevant biological parameters that influence predator movement patterns and habitat use. It is vital that the ecological links between the measured parameters of top predators and the associated environmental parameters are understood so that observed responses can be interpreted correctly (Hindell et al., 2003a). The dynamics between predators and their prey needs to be well understood before long term trends can provide any meaningful ecological insight (Hindell et al., 2003a). Observational studies in ecology attempt to examine patterns and disentangle responses of organisms from other processes. The aim of this thesis was to make more reliable inferences about the underlying causes of observed ecosystem changes. Light collected by animal-borne sensors allowed inferences to be made about local and broad biological conditions at different trophic levels (*i.e.* lower- and mid-trophic groups), and alluded to the significant impact of ecological interactions on seal foraging strategies that may have evolved in response to these environmental features. Such seasonal and local variation at the population level may be an important factor in the species plasticity with significant consequences on how predation may respond to environmental variability.

A better understanding of the functioning of biological processes and structures in the open ocean is crucial to improve our knowledge of top predator behaviour. For this purpose, the use of animal-borne light sensors to estimate biological indices in real time concurrent with recorded animal foraging behaviour at sea has proved successful, demonstrating the utility of bio-logging devices to collect light data. Light data allowed scale-dependent analysis of predator response to biotic

conditions in the water column, including smaller scale where the relationship between physical parameters and predator/prey distribution become less clear (Bost et al 2009). Moreover, like physical data now collected by animal-borne sensors (e.g. Boehme et al 2008; Charrassin et al 2002; Charrassin et al 2008; Charrassin et al 2010), this information also has potential applications by broader research communities. For example, resource patterns revealed by tag data in this thesis may benefit biological oceanographers and their interpretation of large- and small-scale biophysical processes in the ocean realm. Coupled with other animal-borne sensors (*e.g.* oxygen, temperature, salinity, fluorometer), light-based biotic indices could help considerably our understanding of marine ecosystem dynamics and predator response to physical verses biotic parameters while foraging at sea.

References

Alvain, S., Moulin, C., Dandonneau, Y., and Breon, F.M. (2005). Remote sensing of phytoplankton groups in case 1 waters from global SeaWiFS imagery. *Deep-Sea Research Part I-Oceanographic Research Papers* 52**,** 1989-2004. doi: 10.1016/j.dsr.2005.06.015.

Araújo, M.B., and Guisan, A. (2006). Five (or so) challenges for species distribution modelling. *Journal of Biogeography* 33**,** 1677-1688.

Arditi, R., and Dacorogna, B. (1988). Optimal foraging on arbitrary food distributions and the definition of habitat patches. *American Naturalist* 131**,** 837-846.

Arrigo, K.R., Van Dijken, G.L., and Bushinsky, S. (2008). Primary production in the Southern Ocean, 1997-2006. *Journal of Geophysical Research C: Oceans* 113.

Bailleul, F., Authier, M., Ducatez, S., Roquet, F., Charrassin, J.-B., Cherel, Y., and Guinet, C. (2010a). Looking at the unseen: combining animal bio-logging and stable isotopes to reveal a shift in the ecological niche of a deep diving predator. *Ecography* 33**,** 709-719. doi: 10.1111/j.1600-0587.2009.06034.x.

Bailleul, F., Charrassin, J.B., Monestiez, P., Roquet, F., Biuw, M., and Guinet, C. (2007). Successful foraging zones of southern elephant seals from the Kerguelen Islands in relation to oceanographic conditions. *Philosophical Transactions of the Royal Society B-Biological Sciences* 362**,** 2169-2181. doi: 10.1098/rstb.2007.2109.

Bailleul, F., Cotte, C., and Guinet, C. (2010b). Mesoscale eddies as foraging area of a deep-diving predator, the southern elephant seal. *Marine Ecology-Progress Series* 408**,** 251-264. doi: 10.3354/meps08560.

Bailleul, F., Pinaud, D., Hindell, M., Charrassin, J.B., and Guinet, C. (2008). Assessment of scale-dependent foraging behaviour in southern elephant seals incorporating the vertical dimension: a development of the First Passage Time method. *Journal of Animal Ecology* 77**,** 948-957. doi: 10.1111/j.1365-2656.2008.01407.x.

Banks, J., Lea, M.A., Wall, S., Mcmahon, G.R., and Hindell, M.A. (2014). Combining bio-logging and fatty acid signature analysis indicates spatio-temporal variation in the diet of the southern elephant seal, Mirounga leonina. *Journal of Experimental Marine Biology and Ecology* 450**,** 79-90. doi: 10.1016/j.jembe.2013.10.024.

Baum, J.K., and Worm, B. (2009). Cascading top-down effects of changing oceanic predator abundances. *Journal of Animal Ecology* 78**,** 699-714. doi: 10.1111/j.1365-2656.2009.01531.x.

Begon, M., Townsend, C.R., and Harper, J.L. (2006). *Ecology: from individuals to ecosystems.* Oxford: Blackwell Publishing.

Behrenfeld, M.J., and Falkowski, P.G. (1997). Photosynthetic rates derived from satellite-based chlorophyll concentration. *Limnology and Oceanography* 42**,** 1-20.

Benitez-Nelson, C.R., and Mcgillicuddy Jr, D.J. (2008). Mesoscale physical-biological-biogeochemical linkages in the open ocean: An introduction to the results of the E-Flux and EDDIES programs. *Deep-Sea Research Part II: Topical Studies in Oceanography* 55**,** 1133-1138.

Bernard, K.S., and Steinberg, D.K. (2013). Krill biomass and aggregation structure in relation to tidal cycle in a penguin foraging region off the Western Antarctic Peninsula. *Ices Journal of Marine Science* 70**,** 834-849.

Bestley, S., Patterson, T.A., Hindell, M.A., and Gunn, J.S. (2010). Predicting feeding success in a migratory predator: integrating telemetry, environment, and modeling techniques. *Ecology* 91**,** 2373-2384. doi: 10.1890/08-2019.1.

Biggs, D.C. (1992). Nutrients, plankton, and productivity in a warm-core ring in the western Gulf of Mexico. *Journal of Geophysical Research* 97**,** 2143-2154.

Biuw, M., Boehme, L., Guinet, C., Hindell, M., Costa, D., Charrassin, J.-B., Roquet, F., Bailleul, F., Meredith, M., Thorpe, S., Tremblay, Y., Mcdonald, B., Park, Y.-H., Rintoul, S.R., Bindoff, N.,

Goebel, M., Crocker, D., Lovell, P., Nicholson, J., Monks, F., and Fedak, M.A. (2007). Variations in behavior and condition of a Southern Ocean top predator in relation to in situ oceanographic conditions. *Proceedings of the National Academy of Sciences* 104**,** 13705-13710. doi: 10.1073/pnas.0701121104.

Biuw, M., Mcconnell, B., Bradshaw, C.J.A., Burton, H., and Fedak, M. (2003). Blubber and buoyancy: monitoring the body condition of free-ranging seals using simple dive characteristics. *Journal of Experimental Biology* 206**,** 3405-3423. doi: 10.1242/jeb.00583.

Biuw, M., Nøst, O.A., Stien, A., Zhou, Q., Lydersen, C., and Kovacs, K.M. (2010). Effects of hydrographic variability on the spatial, seasonal and diel diving patterns of southern elephant seals in the eastern Weddell Sea. *Plos One* 5**,** e13816.

Blain, S., Quéguiner, B., Armand, L., Belviso, S., Bombled, B., Bopp, L., Bowie, A., Brunet, C., Brussaard, C., Carlotti, F., Christaki, U., Corbière, A., Durand, I., Ebersbach, F., Fuda, J.L., Garcia, N., Gerringa, L., Griffiths, B., Guigue, C., Guillerm, C., Jacquet, S., Jeandel, C., Laan, P., Lefèvre, D., Lo Monaco, C., Malits, A., Mosseri, J., Obernosterer, I., Park, Y.H., Picheral, M., Pondaven, P., Remenyi, T., Sandroni, V., Sarthou, G., Savoye, N., Scouarnec, L., Souhaut, M., Thuiller, D., Timmermans, K., Trull, T., Uitz, J., Van Beek, P., Veldhuis, M., Vincent, D., Viollier, E., Vong, L., and Wagener, T. (2007). Effect of natural iron fertilization on carbon sequestration in the Southern Ocean. *Nature* 446**,** 1070-1074.

Blain, S., Renaut, S., Xing, X., Claustre, H., and Guinet, C. (2013). Instrumented elephant seals reveal the seasonality in chlorophyll and light-mixing regime in the iron-fertilized Southern Ocean. *Geophysical Research Letters* 40**,** 6368-6372.

Blain, S., Tréguer, P., Belviso, S., Bucciarelli, E., Denis, M., Desabre, S., Fiala, M., Martin Jézéquel, V., Le Fèvre, J., Mayzaud, P., Marty, J.C., and Razouls, S. (2001). A biogeochemical study of the island mass effect in the context of the iron hypothesis: Kerguelen Islands, Southern Ocean. *Deep-Sea Research Part I: Oceanographic Research Papers* 48**,** 163-187.

Blanchet, M.A., Biuw, M., Hofmeyr, G.J.G., De Bruyn, P.J.N., Lydersen, C., and Kovacs, K.M. (2013). At-sea behaviour of three krill predators breeding at Bouvetøya- Antarctic fur seals, macaroni penguins and chinstrap penguins. *Marine Ecology Progress Series* 477**,** 285-302.

Block, B.A., Jonsen, I.D., Jorgensen, S.J., Winship, A.J., Shaffer, S.A., Bograd, S.J., Hazen, E.L., Foley, D.G., Breed, G.A., Harrison, A.L., Ganong, J.E., Swithenbank, A., Castleton, M., Dewar, H., Mate, B.R., Shillinger, G.L., Schaefer, K.M., Benson, S.R., Weise, M.J., Henry, R.W., and Costa, D.P. (2011). Tracking apex marine predator movements in a dynamic ocean. *Nature* 475**,** 86-90.

Bolker, B.M. (2010). "Evolution of dispersal scale and shape in heterogeneous environments: a correlation equation " in *Spatial Ecology,* eds. R.S. Cantrell, C. Cosner & S. Ruan. CRC Press), 231-249.

Bost, C., Thiebot, J., Pinaud, D., Cherel, Y., and Trathan, P.N. (2009a). Where do penguins go during the inter-breeding period? Using geolocation to track the winter dispersion of the macaroni penguin. *Biology Letters* 5**,** 473-476.

Bost, C.A., Cotté, C., Bailleul, F., Cherel, Y., Charrassin, J.B., Guinet, C., Ainley, D.G., and Weimerskirch, H. (2009b). The importance of oceanographic fronts to marine birds and mammals of the southern oceans. *Journal of Marine Systems* 78**,** 363-376.

Bown, J., Boye, M., Laan, P., Bowie, A.R., Park, Y.H., Jeandel, C., and Nelson, D.M. (2012). Imprint of a dissolved cobalt basaltic source on the Kerguelen Plateau. *Biogeosciences* 9**,** 5279-5290.

Boyd, I.L., and Croxall, J.P. (1996). Dive durations in pinnipeds and seabirds. *Canadian Journal of Zoology* 74**,** 1696-1705.

Boyd, I.L., Kato, A., and Ropert-Coudert, Y. (2004). Bio-logging science: sensing beyond the boundaries. *Memoirs of the National Institute of Polar Research* 58**,** 1-14.

Boyd, I.L., Walker, T.R., Taylor, R.I., and Mccafferty, D.J. (1999). Can marine mammals be used to monitor oceanographic conditions? *Marine biology* 134**,** 387-395.

Boyd, P.W. (2002). Environmental factors controlling phytoplankton processes in the Southern Ocean. *Journal of Phycology* 38**,** 844-861.

Boyd, P.W., Crossley, A.C., Ditullio, G.R., Griffiths, F.B., Hutchins, D.A., Queguiner, B., Sedwick, P.N., and Trull, T.W. (2001). Control of phytoplankton growth by iron supply and irradiance in the subantarctic Southern Ocean: Experimental results from the SAZ Project. *Journal of Geophysical Research: Oceans* 106**,** 31573-31583.

Boyd, P.W., Jickells, T., Law, C.S., Blain, S., Boyle, E.A., Buesseler, K.O., Coale, K.H., Cullen, J.J., De Baar, H.J.W., Follows, M., Harvey, M., Lancelot, C., Levasseur, M., Owens, N.P.J., Pollard, R., Rivkin, R.B., Sarmiento, J., Schoemann, V., Smetacek, V., Takeda, S., Tsuda, A., Turner, S., and Watson, A.J. (2007). Mesoscale iron enrichment experiments 1993-2005: Synthesis and future directions. *Science* 315**,** 612-617.

Boyd, P.W., Watson, A.J., Law, C.S., Abraham, E.R., Trull, T., Murdoch, R., Bakker, D.C.E., Bowie, A.R., Buesseler, K.O., Chang, H., Charette, M., Croot, P., Downing, K., Frew, R., Gall, M., Hadfield, M., Hall, J., Harvey, M., Jameson, G., Laroche, J., Liddicoat, M., Ling, R., Maldonado, M.T., Mckay, R.M., Nodder, S., Pickmere, S., Pridmore, R., Rintoul, S., Safi, K., Sutton, P., Strzepek, R., Tanneberger, K., Turner, S., Waite, A., and Zeldis, J. (2000). A mesoscale phytoplankton bloom in the polar Southern Ocean stimulated by iron fertilization. *Nature* 407**,** 695-702.

Bradshaw, C.J.A., Higgins, J., Michael, K.J., Wotherspoon, S.J., and Hindell, M.A. (2004). At-sea distribution of female southern elephant seals relative to variation in ocean surface properties. *Ices Journal of Marine Science* 61**,** 1014-1027. doi: 10.1016/j.icesjms.2004.07.012.

Bradshaw, C.J.A., Hindell, M.A., Michael, K.J., and Sumner, M.D. (2002). The optimal spatial scale for the analysis of elephant seal foraging as determined by geo-location in relation to sea surface temperatures. *ICES Journal of Marine Science* 59**,** 770-781.

Bricaud, A., Morel, A., Babin, M., Allali, K., and Claustre, H. (1998). Variations of light absorption by suspended particles with chlorophyll a concentration in oceanic (case 1) waters: Analysis and implications for bio-optical models. *Journal of Geophysical Research: Oceans* 103**,** 31033-31044. doi: 10.1029/98jc02712.

Bricaud, A., Morel, A., and Prieur, L. (1981). Absorption by dissolved organic matter of the sea (yellow substance) in the UV and visible domains. *Limnol. Oceanogr* 26**,** 43-53.

Burghart, S.E., Hopkins, T.L., Vargo, G.A., and Torres, J.J. (1999). Effects of a rapidly receding ice edge on the abundance, age structure and feeding of three dominant calanoid copepods in the Weddell Sea, Antarctica. *Polar Biology* 22**,** 279-288. doi: 10.1007/s003000050421.

Burnham, K.P., and Anderson, D.R. (2002). *Model Selection and Multi-Model Inference: A Practical Information-Theoretic Approach.* Springer.

Burns, J.M., Hindell, M.A., Bradshaw, C.J.A., and Costa, D.P. (2008). Fine-scale habitat selection of crabeater seals as determined by diving behavior. *Deep-Sea Research Part II: Topical Studies in Oceanography* 55**,** 500-514.

Campagna, C., Dignani, J., Blackwell, S.B., and Marin, M.R. (2001). Detecting bioluminsecence with an irradiance time-depth recorder deployed on southern elephant seals. *Marine Mammal Science* 17**,** 402-414. doi: 10.1111/j.1748-7692.2001.tb01283.x.

Campagna, C., Fedak, M.A., and Mcconnell, B.J. (1999). Post-breeding distribution and diving behavior of adult male southern elephant seals from Patagonia. *Journal of Mammalogy* 80**,** 1341-1352.

Cantrell, R.S., Cosner, C., and Lou, Y. (2010). "Evolution of dispersal in heterogeneous landscapes," in *Spatial Ecology,* eds. R.S. Cantrell, C. Cosner & S. Ruan. CRC Press), 213-229.

Catul, V., Gauns, M., and Karuppasamy, P.K. (2011). A review on mesopelagic fishes belonging to family Myctophidae. *Reviews in Fish Biology and Fisheries* 21**,** 339-354.

Cavalieri, D.J., Parkinson, C.L., Gloersen, P., and Zwally, H. (2012, updated yearly). "Sea Ice Concentrations from Nimbus-7 SMMR and DMSP SSM/I-SSMIS Passive Microwave Data". (Boulder, Colorado USA: NASA DAAC at the National Snow and Ice Data Center).

Charnov, E.L. (1976). Optimal foraging, the marginal value theorem. *Theoretical Population Biology* 9**,** 129-136.

Charrassin, J.-B., Hindell, M., Rintoul, S.R., Roquet, F., Sokolov, S., Biuw, M., Costa, D., Boehme, L., Lovell, P., Coleman, R., Timmermann, R., Meijers, A., Meredith, M., Park, Y.-H., Bailleul, F., Goebel, M., Tremblay, Y., Bost, C.-A., Mcmahon, C.R., Field, I.C., Fedak, M.A., and Guinet, C. (2008). Southern Ocean frontal structure and sea-ice formation rates revealed by elephant seals. *Proceedings of the National Academy of Sciences* 105**,** 11634-11639. doi: 10.1073/pnas.0800790105.

Charrassin, J.B., Park, Y.H., Maho, Y.L., and Bost, C.A. (2002). Penguins as oceanographers unravel hidden mechanisms of marine productivity. *Ecology Letters* 5**,** 317-319.

Charrassin, J.B., Roquet, F., Park, Y.H., Bailleul, F., Guinet, C., Meredith, M., Nicholls, K., Thorpe, S., Tremblay, Y., Costa, D., Göbel, M., Muelbert, M., Bester, M.N., Plötz, J., Bornemann, H., Timmermann, R., Hindell, M., Meijers, A., Coleman, R.C., Field, I.C., Mcmahon, C., Rintoul, S., Sokolov, S., Fedak, M., Lovell, P., Biuw, M., Kovacs, K., and Lydersen, C. (2010). New insights into Southern Ocean physical and biological processes revealed by instrumented elephant seals. *Proceedings of OceanObs 09: Sustained Ocean Observations and Information for Society* 2.

Chavez, F.P., Messié, M., and Pennington, J.T. (2011). Marine primary production in relation to climate variability and change. *Annual Review of Marine Science* 3**,** 227-260.

Chelton, D.B., Schlax, M.G., Samelson, R.M., and De Szoeke, R.A. (2007). Global observations of large oceanic eddies. *Geophysical Research Letters* 34.

Cherel, Y., Ducatez, S., Fontaine, C., Richard, P., and Guinet, C. (2008). Stable isotopes reveal the trophic position and mesopelagic fish diet of female southern elephant seals breeding on the Kerguelen Islands. *Marine Ecology Progress Series* 370**,** 239-247.

Chever, F., Sarthou, G., Bucciarelli, E., Blain, S., and Bowie, A.R. (2010). An iron budget during the natural iron fertilisation experiment KEOPS (Kerguelen Islands, Southern Ocean). *Biogeosciences* 7**,** 455-468.

Cleeland, J.B., Lea, M.A., and Hindell, M.A. (2013). Use of the Southern Ocean by breeding Short-tailed shearwaters (Puffinus tenuirostris). *Journal of Experimental Marine Biology and Ecology* 450**,** 109-117.

Constable, A.J., De Lamare, W.K., Agnew, D.J., Everson, I., and Miller, D. (2000). Managing fisheries to conserve the Antarctic marine ecosystem: Practical implementation of the Convention on the Conservation of Antarctic Marine Living Resources (CCAMLR). *Ices Journal of Marine Science* 57**,** 778-791.

Constable, A.J., Melbourne-Thomas, J., Corney, S.P., Arrigo, K.R., Barbraud, C., Barnes, D.K.A., Bindoff, N.L., Boyd, P.W., Brandt, A., Costa, D.P., Davidson, A.T., Ducklow, H.W., Emmerson, L., Fukuchi, M., Gutt, J., Hindell, M.A., Hofmann, E.E., Hosie, G.W., Iida, T., Jacob, S., Johnston, N.M., Kawaguchi, S., Kokubun, N., Koubbi, P., Lea, M.A., Makhado, A., Massom, R.A., Meiners, K., Meredith, M.P., Murphy, E.J., Nicol, S., Reid, K., Richerson, K., Riddle, M.J., Rintoul, S.R., Smith, W.O., Southwell, C., Stark, J.S., Sumner, M., Swadling, K.M., Takahashi, K.T., Trathan, P.N., Welsford, D.C., Weimerskirch, H., Westwood, K.J., Wienecke, B.C., Wolf-Gladrow, D., Wright, S.W., Xavier, J.C., and Ziegler, P. (2014). Climate change and Southern Ocean ecosystems I: How changes in physical habitats directly affect marine biota. *Global Change Biology*.

Convey, P., Bindschadler, R., Di Prisco, G., Fahrbach, E., Gutt, J., Hodgson, D.A., Mayewski, P.A., Summerhayes, C.P., and Turner, J. (2009). Antarctic climate change and the environment. *Antarctic Science* 21**,** 541-563.

Costa, D.P., Breed, G.A., and Robinson, P.W. (2012). New Insights into Pelagic Migrations: Implications for Ecology and Conservation. *Annual Review of Ecology, Evolution, and Systematics* 43**,** null. doi: doi:10.1146/annurev-ecolsys-102710-145045.

Costa, D.P., Crocker, D.E., and Boehlert, G. (2002). Foraging behavior of northern elephant seals relative to frontal features in the North Pacific Ocean. *Integrative and Comparative Biology* 42**,** 1212-1212.

Costa, D.P., Huckstadt, L.A., Crocker, D.E., Mcdonald, B.I., Goebel, M.E., and Fedak, M.A. (2010a). Approaches to Studying Climatic Change and its Role on the Habitat Selection of Antarctic Pinnipeds. *Integrative and Comparative Biology* 50**,** 1018-1030. doi: 10.1093/icb/icq054.

Costa, D.P., Robinson, P.W., Arnould, J.P.Y., Harrison, A.-L., Simmons, S.E., Hassrick, J.L., Hoskins, A.J., Kirkman, S.P., Oosthuizen, H., Villegas-Amtmann, S., and Crocker, D.E. (2010b). Accuracy of ARGOS Locations of Pinnipeds at-Sea Estimated Using Fastloc GPS. *Plos One* 5**,** e8677. doi: 10.1371/journal.pone.0008677.

Cotté, C., D'ovidio, F., Dragon, A.-C., Guinet, C., and Lévy, M. (2014). Flexible preference of southern elephant seals for distinct mesoscale features within the Antarctic Circumpolar Current. *Progress in Oceanography*. doi: http://dx.doi.org/10.1016/j.pocean.2014.11.011.

Croll, D.A., Marinovic, B., Benson, S., Chavez, F.P., Black, N., Ternullo, R., and Tershy, B.R. (2005). From wind to whales: Trophic links in a coastal upwelling system. *Marine Ecology Progress Series* 289**,** 117-130.

Cury, P., Bakun, A., Crawford, R.J.M., Jarre, A., Quiñones, R.A., Shannon, L.J., and Verheye, H.M. (2000). Small pelagics in upwelling systems: Patterns of interaction and structural changes in 'wasp-waist' ecosystems. *Ices Journal of Marine Science* 57**,** 603-618.

Cushing, D.H. (1969). The Regularity of the Spawning Season of Some Fishes. *Journal du Conseil* 33**,** 81-92. doi: 10.1093/icesjms/33.1.81.

Cushing, D.H. (1990). "Plankton Production and Year-class Strength in Fish Populations: an Update of the Match/Mismatch Hypothesis", in: *Advances in Marine Biology.*).

D'ovidio, F., De Monte, S., Alvain, S., Dandonneau, Y., and Lévy, M. (2010). Fluid dynamical niches of phytoplankton types. *Proceedings of the National Academy of Sciences of the United States of America* 107**,** 18366-18370. doi: 10.1073/pnas.1004620107.

D'ovidio, F., Monte, S.D., Penna, A.D., Cotté, C., and Guinet, C. (2013). Ecological implications of eddy retention in the open ocean: a Lagrangian approach. *Journal of Physics A: Mathematical and Theoretical* 46**,** 254023.

Davis, R.W., and Weihs, D. (2007). Locomotion in diving elephant seals: Physical and physiological constraints. *Philosophical Transactions of the Royal Society B: Biological Sciences* 362**,** 2141-2150.

Day, J. (2008). The need and practice of monitoring, evaluating and adapting marine planning and management-lessons from the Great Barrier Reef. *Marine Policy* 32**,** 823-831.

De Baar, H.J.W., Boyd, P.W., Coale, K.H., Landry, M.R., Tsuda, A., Assmy, P., Bakker, D.C.E., Bozec, Y., Barber, R.T., Brzezinski, M.A., Buesseler, K.O., Boyé, M., Croot, P.L., Gervais, F., Gorbunov, M.Y., Harrison, P.J., Hiscock, W.T., Laan, P., Lancelot, C., Law, C.S., Levasseur, M., Marchetti, A., Millero, F.J., Nishioka, J., Nojiri, Y., Van Oijen, T., Riebesell, U., Rijkenberg, M.J.A., Saito, H., Takeda, S., Timmermans, K.R., Veldhuis, M.J.W., Waite, A.M., and Wong, C.S. (2005). Synthesis of iron fertilization experiments: From the iron age in the age of enlightenment. *Journal of Geophysical Research C: Oceans* 110**,** 1-24.

Delong, R.L. (1992). Documenting migrations of northern elephant seals using day length. *Marine Mammal Science* 8**,** 155-159. doi: 10.1111/j.1748-7692.1992.tb00375.x.

Donnelly, J., Sutton, T.T., and Torres, J.J. (2006). Distribution and abundance of micronekton and macrozooplankton in the NW Weddell Sea: Relation to a spring ice-edge bloom. *Polar Biology* 29**,** 280-293. doi: 10.1007/s00300-005-0051-z.

Dragon, A.C., Bar-Hen, A., Monestiez, P., and Guinet, C. (2012). Horizontal and vertical movements as predictors of foraging success in a marine predator. *Marine Ecology Progress Series* 447**,** 243-257. doi: 10.3354/meps09498.

Dragon, A.C., Monestiez, P., Bar-Hen, A., and Guinet, C. (2010). Linking foraging behaviour to physical oceanographic structures: Southern elephant seals and mesoscale eddies east of Kerguelen Islands. *Progress in Oceanography* 87**,** 61-71. doi: 10.1016/j.pocean.2010.09.025.

Dugdale, R.C., and Wilkerson, F.P. (1989). New production in the upwelling center at Point Conception, California: temporal and spatial patterns. *Deep Sea Research Part A, Oceanographic Research Papers* 36**,** 985-1007.

Dugdale, R.C., Wilkerson, F.P., Hogue, V.E., and Marchi, A. (2006). Nutrient controls on new production in the Bodega Bay, California, coastal upwelling plume. *Deep-Sea Research Part II: Topical Studies in Oceanography* 53**,** 3049-3062.

Duhamel, G., Koubbi, P., and Ravier, C. (2000). Day and night mesopelagic fish assemblages off the Kerguelen Islands (Southern Ocean). *Polar Biology* 23**,** 106-112.

Ekstrom, P.A. (2004). An advance in geolocation by light. *Memoirs of the National Insitute of Polar Research, Special Issue* 58**,** 210-226.

El-Sayed, S.Z., Biggs, D.C., and Holm-Hansen, O. (1983). Phytoplankton standing crop, primary productivity, and near-surface nitrogenous nutrient fields in the Ross Sea, Antarctica. *Deep Sea Research Part A. Oceanographic Research Papers* 30**,** 871-886. doi: http://dx.doi.org/10.1016/0198-0149(83)90005-5.

Erikstad, K.E., Fauchald, P., Tveraa, T., and Steen, H. (1998). On the cost of reproduction in long-lived birds: The influence of environmental variability. *Ecology* 79**,** 1781-1788.

Estes, J.A., and Palmisano, J.F. (1974). Sea otters: Their role in structuring nearshore communities. *Science* 185**,** 1058-1060.

Evans, K., Lea, M.A., and Patterson, T.A. (2013). Recent advances in bio-logging science: Technologies and methods for understanding animal behaviour and physiology and their environments. *Deep-Sea Research Part II: Topical Studies in Oceanography* 88-89**,** 1-6.

Fahrig, L. (2003). "Effects of Habitat Fragmentation on Biodiversity", in: *Annual Review of Ecology, Evolution, and Systematics*.).

Fauchald, P. (1999). Foraging in a hierarchical patch system. *American Naturalist* 153**,** 603-613.

Fedak, M. (2013). The impact of animal platforms on polar ocean observation. *Deep Sea Research Part II: Topical Studies in Oceanography* 88-89**,** 7-13.

Fenton, N., Priddle, J., and Tett, P. (1994). Regional variations in bio-optical properties of the surface waters in the Southern Ocean. *Antarctic Science* 6**,** 443-448.

Field, I., Hindell, M., Slip, D., and Michael, K. (2001). Foraging strategies of southern elephant seals (*Mirounga leonina*) in relation to frontal zones and water masses. *Antarctic Science* 13**,** 371-379.

Field, I.C., Bradshaw, C.J.A., Burton, H.R., and Hindell, M.A. (2007). Differential resource allocation strategies in juvenile elephant seals in the highly seasonal Southern Ocean. *Marine Ecology Progress Series* 331**,** 281-290.

Field, I.C., Bradshaw, C.J.A., Mcmahon, C.R., Harrington, J., and Burton, H.R. (2002). Effects of age, size and condition of elephant seals (*Mirounga leonina*) on their intravenous anaesthesia with tiletamine and zolazepam. *Veterinary Record* 151**,** 235-240.

Forcada, J., Trathan, P.N., Reid, K., and Murphy, E.J. (2005). The effects of global climate variability in pup production of antarctic fur seals. *Ecology* 86**,** 2408-2417.

Frank, T.M., and Widder, E.A. (1997). The correlation of downwelling irradiance and staggered vertical migration patterns of zooplankton in Wilkinson Basin, Gulf of Maine. *Journal of Plankton Research* 19**,** 1975-1991.

Gallon, S., Bailleul, F., Charrassin, J.B., Guinet, C., Bost, C.A., Handrich, Y., and Hindell, M. (2013). Identifying foraging events in deep diving southern elephant seals, Mirounga leonina, using acceleration data loggers. *Deep-Sea Research Part II: Topical Studies in Oceanography* 88-89**,** 14-22.

Garcia-Munoz, C., Lubian, L.M., Garcia, C.M., Marrero-Diaz, A., Sangra, P., and Vernet, M. (2013). A mesoscale study of phytoplankton assemblages around the South Shetland Islands (Antarctica). *Polar Biology* 36**,** 1107-1123. doi: 10.1007/s00300-013-1333-5.

Garibotti, I.A., Vernet, M., Smith, R.C., and Ferrario, M.E. (2005). Interannual variability in the distribution of the phytoplankton standing stock across the seasonal sea-ice zone west of the Antarctic Peninsula. *Journal of Plankton Research* 27**,** 825-843. doi: 10.1093/plankt/fbi056.

Georges, J.Y., Tremblay, Y., and Guinet, C. (2000). Seasonal diving behaviour in lactating subantarctic fur seals on Amsterdam Island. *Polar Biology* 23**,** 59-69.

Godo, O.R., Samuelsen, A., Macaulay, G.J., Patel, R., Hjollo, S.S., Horne, J., Kaartvedt, S., and Johannessen, J.A. (2012). Mesoscale Eddies Are Oases for Higher Trophic Marine Life. *Plos One* 7. doi: 10.1371/journal.pone.0030161.

Grémillet, D., Lewis, S., Drapeau, L., Van Der Lingen, C.D., Huggett, J.A., Coetzee, J.C., Verheye, H.M., Daunt, F., Wanless, S., and Ryan, P.G. (2008). Spatial match–mismatch in the Benguela upwelling zone: should we expect chlorophyll and sea-surface temperature to predict marine predator distributions? *Journal of Applied Ecology* 45**,** 610-621. doi: 10.1111/j.1365-2664.2007.01447.x.

Grémillet, D., Wanless, S., Carss, D.N., Linton, D., Harris, M.P., Speakman, J.R., and Maho, Y.L. (2001). Foraging energetics of arctic cormorants and the evolution of diving birds. *Ecology Letters* 4**,** 180-184.

Grossmann, S. (1994). Bacterial activity in sea ice and open water of the Weddell Sea, Antarctica: A microautoradiographic study. *Microbial Ecology* 28**,** 1-18.

Grossmann, S., and Dieckmann, G.S. (1994). Bacterial standing stock, activity, and carbon production during formation and growth of sea ice in the Weddell Sea, Antarctica. *Applied and Environmental Microbiology* 60**,** 2746-2753.

Guinet, C., Dubroca, L., Lea, M.A., Goldsworthy, S., Cherel, Y., Duhamel, G., Bonadonna, F., and Donnay, J.-P. (2001). Spatial distribution of foraging in female Antarctic fur seals Arctocephalus gazella in relation to oceanographic variables: a scale-dependent approach using geographic information systems. *Marine Ecology Progress Series* 219**,** 251-264.

Guinet, C., Vacquié-Garcia, J., Picard, B., Bessigneul, G., Lebras, Y., Dragon, A.C., Viviant, M., Arnould, J.P.Y., and Bailleul, F. (2014). Southern elephant seal foraging success in relation to temperature and light conditions: insight into prey distribution. *Marine Ecology Progress Series* 499**,** 285-301. doi: 10.3354/meps10660.

Guinet, C., Xing, X., Walker, E., Monestiez, P., Marchand, S., Picard, B., Jaud, T., Authier, M., Cotte, C., and Dragon, A.-C. (2013). Calibration procedures and first dataset of Southern Ocean chlorophyll a profiles collected by elephant seals equipped with a newly developed CTD-fluorescence tags. *Earth System Science Data* 5**,** 15-29.

Guisan, A., and Thuiller, W. (2005). Predicting species distribution: Offering more than simple habitat models. *Ecology Letters* 8**,** 993-1009.

Haury, L.R., Mcgowan, J.A., and Wiebe, P.H. (1978). "Patterns and Processes in the Time-Space Scales of Plankton Distributions," in *Spatial Pattern in Plankton Communities,* ed. J. Steele. Springer US), 277-327.

Hays, G.C. (2003). A review of the adaptive significance and ecosystem consequences of zooplankton diel vertical migrations. *Hydrobiologia* 503**,** 163-170.

Hays, G.C., Hobson, V.J., Metcalfe, J.D., Righton, D., and Sims, D.W. (2006). Flexible foraging movements of leatherback turtles across the North Atlantic ocean. *Ecology* 87**,** 2647-2656.

Hayward, T.L., and Venrick, E.L. (1998). Nearsurface pattern in the California Current: Coupling between physical and biological structure. *Deep-Sea Research Part II: Topical Studies in Oceanography* 45**,** 1617-1638.

Heerah, K., Andrews-Goff, V., Williams, G., Sultan, E., Hindell, M., Patterson, T., and Charrassin, J.-B. (2013). Ecology of Weddell seals during winter: Influence of environmental parameters on their foraging behaviour. *Deep Sea Research Part II: Topical Studies in Oceanography* 88–89**,** 23-33. doi: http://dx.doi.org/10.1016/j.dsr2.2012.08.025.

Heerah, K., Hindell, M., Guinet, C., and Charrassin, J.-B. (2014). A New Method to Quantify within Dive Foraging Behaviour in Marine Predators. *Plos One* 9**,** e99329. doi: 10.1371/journal.pone.0099329.

Henson, S.A., Dunne, J.P., and Sarmiento, J.L. (2009). Decadal variability in North Atlantic phytoplankton blooms. *Journal of Geophysical Research C: Oceans* 114.

Hernández-León, S., Montero, I., Almeida, C., Portillo-Hahnefeld, A., and Bruce-Lauli, E. (2008). Mesozooplankton biomass and indices of grazing and metabolic activity in Antarctic waters. *Polar Biology* 31**,** 1373-1382. doi: 10.1007/s00300-008-0477-1.

Hill, R.D. (1994). Theory of geolocation by light levels. *Elephant seals: population ecology, behavior, and physiology. University of California Press, Berkeley***,** 227-236.

Hill, R.D., and Braun, M.J. (2001). "Geolocation by light level," in *Electronic tagging and tracking in marine fisheries*. Springer), 315-330.

Hindell, M., Crocker, D., Mori, Y., and Tyack, P. (2010). "Foraging Behaviour," in *Marine Mammal Ecology and Conservation: A Handbook of Techniques,* eds. I.L. Boyd, W.D. Bowen & S.J. Iverson. (Oxford: Oxford University Press), 241-262.

Hindell, M., Lea, M., Bost, C., Charrassin, J., Gales, N., Goldsworthy, S., Page, B., Robertson, G., Wienecke, B., O'toole, M., and Guinet, C. (2011). "Foraging habitats of top predators, and Areas of Ecological Significance, on the Kerguelen Plateau," in *The Kerguelen Plateau: marine ecosystem and fisheries,* eds. G. Duhamel & D. Welsford. (Abbeville, France: Société Française d'Ichtyologie), 203-215.

Hindell, M., Slip, D., and Burton, H. (1991a). The Diving Behavior of Adult Male and Female Southern Elephant Seals, Mirounga-Leonina (Pinnipedia, Phocidae). *Australian Journal of Zoology* 39**,** 595-619.

Hindell, M.A., Bradshaw, C.J.A., Harcourt, R., and Guinet, C. (2003a). "Ecosystem monitoring: are seals a potential tool for monitoring change in marine systems?," in *Marine Mammals, Fisheries, Tourism and Management Issues,* eds. N.J. Gales, M.A. Hindell & R. Kirkwood. (Melbourne: CSIRO Publishing), 330-343.

Hindell, M.A., Bradshaw, C.J.A., Sumner, M.D., Michael, K.J., and Burton, H.R. (2003b). Dispersal of female southern elephant seals and their prey consumption during the austral summer: Relevance to management and oceanographic zones. *Journal of Applied Ecology* 40**,** 703-715.

Hindell, M.A., Burton, H.R., and Slip, D.J. (1991b). Foraging areas of southern elephant seals, Mirounga leonina, as inferred from water temperature data. *Australian Journal of Marine & Freshwater Research* 42**,** 115-128.

Hindell, M.A., and Lea, M.A. (1998). Heart rate, swimming speed, and estimated oxygen consumption of a free-ranging southern elephant seal. *Physiological Zoology* 71**,** 74-84.

Hindell, M.A., Lea, M.A., Morrice, M.G., and Macmahon, C.R. (2000). Metabolic limits on dive duration and swimming speed in the southern elephant seal Mirounga leonina. *Physiological and Biochemical Zoology* 73**,** 790-798.

Hindell, M.A., and Mcmahon, C.R. (2000). Long distance movement of a southern elephant seal (Mirounga leonina) from Macquarie Island to Peter 1 Øy. *Marine Mammal Science* 16**,** 504-507.

Hindell, M.A., and Slip, D.J. (1997). "The importance of being fat: maternal expenditure in the southern elephant seal *Mirounga leonina*," in *Marine mammal research in the Southern Hemisphere: Status, ecology and medicine,* eds. M.A. Hindell & C.M. Kemper. Surrey Beatty & Sons), 72-77.

Hirawake, T., Satoh, H., Ishimaru, T., Yamaguchi, Y., and Kishino, M. (2000). Bio-optical relationship of case I waters: the difference between the low- and mid-latitude waters and the Southern Ocean. *Journal of Oceanography* 56**,** 245-260.

Hoelzel, A.R. (2009). *Marine mammal biology: an evolutionary approach.* John Wiley & Sons.

Hoelzel, A.R., Campagna, C., and Arnbom, T. (2001). Genetic and morphometric differentiation between island and mainland southern elephant seal populations. *Proceedings of the Royal Society B: Biological Sciences* 268**,** 325-332.

Holm-Hansen, O., Kahru, M., and Hewes, C.D. (2005). Deep chlorophyll a maxima (DCMs) in pelagic Antarctic waters. II. Relation to bathymetric features and dissolved iron concentrations. *Marine Ecology Progress Series* 297**,** 71-81.

Horning, M., and Trillmich, F. (1999). Lunar cycles in diel prey migrations exert a stronger effect on the diving of juveniles than adult Galapagos fur seals. *Proceedings of the Royal Society B: Biological Sciences* 266**,** 1127-1132.

Houston, A.I., and Mcnamara, J.M. (1985). A general theory of central place foraging for single-prey loaders. *Theoretical Population Biology* 28**,** 233-262.

Hunt Jr, G.L. (1997). Physics, zooplankton, and the distribution of least auklets in the Bering Sea - A review. *Ices Journal of Marine Science* 54**,** 600-607.

Jaquet, N., Whitehead, H., and Lewis, M. (1996). Coherence between 19th century sperm whale distributions and satellite- derived pigments in the tropical pacific. *Marine Ecology Progress Series* 145**,** 1-10.

Jaud, T., Dragon, A.-C., Garcia, J.V., and Guinet, C. (2012). Relationship between Chlorophyll a Concentration, Light Attenuation and Diving Depth of the Southern Elephant Seal *Mirounga leonina*. *PLoS One* 7**,** e47444. doi: 10.1371/journal.pone.0047444.

Johnson, R., Strutton, P.G., Wright, S.W., Mcminn, A., and Meiners, K.M. (2013). Three improved satellite chlorophyll algorithms for the Southern Ocean. *Journal of Geophysical Research: Oceans* 118**,** 3694-3703. doi: 10.1002/jgrc.20270.

Jonker, F.C., and Bester, M.N. (1998). Seasonal movements and foraging areas of adult southern female elephant seals, Mirounga leonina, from Marion Island. *Antarctic Science* 10**,** 21-30.

Jonsen, I.D., Flemming, J.M., and Myers, R.A. (2005). Robust state-space modeling of animal movement data. *Ecology* 86**,** 2874-2880.

Jouandet, M.P., Trull, T.W., Guidi, L., Picheral, M., Ebersbach, F., Stemmann, L., and Blain, S. (2011). Optical imaging of mesopelagic particles indicates deep carbon flux beneath a natural iron-fertilized bloom in the Southern Ocean. *Limnology and Oceanography* 56**,** 1130-1140.

Kara, A.B., Rochford, P.A., and Hurlburt, H.E. (2003). Mixed layer depth variability over the global ocean. *Journal of Geophysical Research C: Oceans* 108**,** 24-21.

Kiørboe, T. (1993). "Turbulence, Phytoplankton Cell Size, and the Structure of Pelagic Food Webs," in *Advances in Marine Biology,* eds. J.H.S. Blaxter & A.J. Southward. Academic Press), 1-72.

Kirk, J.T.O. (1994). *Light and Photosynthesis in Aquatic Ecosystems.* Cambridge University Press.

Knox, G.A. (2007). *Biology of the Southern Ocean.* Boca Raton: CRC Press/Taylor & Francis.

Kooyman, G.L. (2004). Genesis and evolution of bio-logging devices: 1963-2002. *Memoirs of the National Insitute of Polar Research, Special Issue***,** 15-22.

Kostianoy, A.G., Ginzburg, A.I., Lebedev, S.A., Frankignoulle, M., and Delille, B. (2003). Fronts and mesoscale variability in the Southern Indian Ocean as inferred from the TOPEX/POSEIDON and ERS-2 altimetry data. *Oceanology* 43**,** 632-642.

Koubbi, P., De Broyer, C., Griffiths, H.J., Raymond, B., D'udekem D'acoz, C., Van De Putte, A.P., Danis, B., David, B., Grant, S., Gutt, J., Held, C., Hosie, G., Huettmann, F., Post, A., Ropert-Coudert, Y., Stoddart, M., Swadling, K.M., and Wadley, V. (2014). "Conclusions: Present and future of Southern Ocean biogeography," in *Biogeographic Atlas of the Southern Ocean,* eds. C. De Broyer, P. Koubbi, H.J. Griffiths, B. Raymond, C. Udekem D'acoz, A.P. Van De Putte, B. Danis,

B. David, S. Grant, J. Gutt, C. Held, G. Hosie, F. Huettmann, A. Post & Y. Ropert-Coudert. (Cambridge: Scientific Committee on Antarctic Research), 470-475.

Labat, J.P., Gasparini, S., Mousseau, L., Prieur, L., Boutoute, M., and Mayzaud, P. (2009). Mesoscale distribution of zooplankton biomass in the northeast Atlantic Ocean determined with an Optical Plankton Counter: Relationships with environmental structures. *Deep-Sea Research Part I-Oceanographic Research Papers* 56**,** 1742-1756. doi: 10.1016/j.dsr.2009.05.013.

Laidre, K.L., Heide-Jørgensen, M.P., Logsdon, M.L., Delwiche, L., and Nielsen, T.G. (2010). A whale of an opportunity: Examining the vertical structure of chlorophyll-a in high Arctic waters using instrumented marine predators. *Marine Biology Research* 6**,** 519-529.

Langlais, C., Rintoul, S., and Schiller, A. (2011). Variability and mesoscale activity of the Southern Ocean fronts: Identification of a circumpolar coordinate system. *Ocean Modelling* 39**,** 79-96.

Laws, R.M. (1994). "History and present status of southern elephant seal populations," in *Elephant Seals: Population Ecology, Behavior, and Physiology,* eds. B.J.L. Boeuf & R.M. Laws. University of California Press), 49-65.

Le Boeuf, B.J., and Crocker, D.E. (2005). Ocean climate and seal condition. *BMC Biology* 3.

Lea, M.-A., Guinet, C., Cherel, Y., Duhamel, G., Dubroca, L., Pruvost, P., and Hindell, M. (2006). Impacts of climatic anomalies on provisioning strategies of a Southern Ocean predator. *Marine Ecology Progress Series* 310**,** 77-94. doi: 10.3354/meps310077.

Lizorre, M.P. (2001). The contributions of sea ice algae to antarctic marine primary production. *American Zoologist* 41**,** 57-73.

Llopiz, J.K., and Hobday, A.J. (2014). A global comparative analysis of the feeding dynamics and environmental conditions of larval tunas, mackerels, and billfishes. *Deep-Sea Research Part II: Topical Studies in Oceanography*.

Locher, R., Ruckstuhl, A., and Al., E. (2012). "IDPmisc: Utilities of Institute of Data Analyses and Process Design (**Error! Hyperlink reference not valid.**. R package version 1.1.17 ed.).

Loisel, H., Nicolas, J.M., Deschamps, P.Y., and Frouin, R. (2002). Seasonal and inter-annual variability of particulate organic matter in the global ocean. *Geophysical Research Letters* 29. doi: 10.1029/2002gl015948.

Lopez, R., Malardé, J.P., Royer, F., and Gaspar, P. (2014). Improving argos doppler location using multiple-model kalman filtering. *IEEE Transactions on Geoscience and Remote Sensing* 52**,** 4744-4755.

Martin, J.H., and Fitzwater, S.E. (1988). Iron deficiency limits phytoplankton growth in the north-east pacific subarctic. *Nature* 331**,** 341-343.

Martin, J.H., Fitzwater, S.E., and Gordon, R.M. (1990). Iron deficiency limits phytoplankton growth in Antarctic waters. *Global Biogeochemical Cycles* 4**,** 5-12.

Martinez, N.D., and Lawton, J.H. (1995). Scale and food-web structure - From local to global. *Oikos* 73**,** 148-154.

Mccafferty, D.J., Walker, T.R., and Boyd, I.L. (2004). Using time-depth-light recorders to measure light levels experienced by a diving marine mammal. *Marine Biology* 146**,** 191-199. doi: 10.1007/s00227-004-1428-1.

Mcclain, C.R., Cleave, M.L., Feldman, G.C., Gregg, W.W., and Et Al. (1998). Science quality sea WiFS data for global biosphere research. *Sea Technology* 39**,** 10.

Mcconnell, B.J., Chambers, C., and Fedak, M.A. (1992). Foraging ecology of southern elephant seals in relation to the bathymetry and productivity of the Southern Ocean. *Antarctic Science* 4**,** 393-398.

Mcintyre, T., Bornemann, H., Plötz, J., Tosh, C.A., and Bester, M.N. (2012). Deep divers in even deeper seas: Habitat use of male southern elephant seals from Marion Island. *Antarctic Science* 24**,** 561-570.

Mcintyre, T., De Bruyn, P.J.N., Ansorge, I.J., Bester, M.N., Bornemann, H., Plötz, J., and Tosh, C.A. (2010). A lifetime at depth: Vertical distribution of southern elephant seals in the water column. *Polar Biology* 33**,** 1037-1048.

Mcmahon, C.R., Burton, H., Mclean, S., Slip, D., and Bester, M. (2000). Field immobilisation of southern elephant seals with intravenous tiletamine and zolazepam. *Veterinary Record* 146**,** 251-254.

Mcmahon, C.R., and Burton, H.R. (2005). Climate change and seal survival: Evidence for environmentally mediated changes in elephant seal, Mirounga leonina, pup survival. *Proceedings of the Royal Society B: Biological Sciences* 272**,** 923-928.

Mcmahon, C.R., Field, I.C., Bradshaw, C.J.A., White, G.C., and Hindell, M.A. (2008). Tracking and data–logging devices attached to elephant seals do not affect individual mass gain or survival. *Journal of Experimental Marine Biology and Ecology* 360**,** 71-77. doi: http://dx.doi.org/10.1016/j.jembe.2008.03.012.

Mcpeek, M.A., and Holt, R.D. (1992). The evolution of dispersal in spatially and temporally varying environments. *American Naturalist* 140**,** 1010-1027.

Mellard, J.P., Yoshiyama, K., Litchman, E., and Klausmeier, C.A. (2011). The vertical distribution of phytoplankton in stratified water columns. *Journal of Theoretical Biology* 269**,** 16-30.

Meredith, M.P., and King, J.C. (2005). Rapid climate change in the ocean west of the Antarctic Peninsula during the second half of the 20th century. *Geophysical Research Letters* 32**,** L19604. doi: 10.1029/2005gl024042.

Mitchell, B.G., Brody, E.A., Holm-Hansen, O., Mcclain, C., and Bishop, J. (1991). Light limitation of phytoplankton biomass and macronutrient utilization in the Southern Ocean. *Limnology & Oceanography* 36**,** 1662-1677.

Mongin, M., Molina, E., and Trull, T.W. (2008). Seasonality and scale of the Kerguelen plateau phytoplankton bloom: A remote sensing and modeling analysis of the influence of natural iron fertilization in the Southern Ocean. *Deep-Sea Research Part II: Topical Studies in Oceanography* 55**,** 880-892.

Mongin, M.M., Abraham, E.R., and Trull, T.W. (2009). Winter advection of iron can explain the Summer phytoplankton bloom that extends 1000 km downstream of the Kerguelen plateau in the Southern Ocean. *Journal of Marine Research* 67**,** 225-237.

Moore, J.K., and Abbott, M.R. (2000). Phytoplankton chlorophyll distributions and primary production in the Southern Ocean. *Journal of Geophysical Research: Oceans* 105**,** 28709-28722. doi: 10.1029/1999jc000043.

Moore, J.K., and Abbott, M.R. (2002). Surface chlorophyll concentrations in relation to the Antarctic Polar Front: Seasonal and spatial patterns from satellite observations. *Journal of Marine Systems* 37**,** 69-86.

Moore, J.K., Abbott, M.R., and Richman, J.G. (1999). Location and dynamics of the Antarctic Polar Front from satellite sea surface temperature data. *Journal of Geophysical Research: Oceans* 104**,** 3059-3073.

Morales, J.M., Haydon, D.T., Frair, J., Holsiner, K.E., and Fryxell, J.M. (2004). Extracting more out of relocation data: Building movement models as mixtures of random walks. *Ecology* 85**,** 2436-2445. doi: 10.1890/03-0269.

Morel, A. (1988). Optical modeling of the upper ocean in relation to its biogenous matter content (case I waters). *Journal of Geophysical Research: Oceans* 93**,** 10749-10768. doi: 10.1029/JC093iC09p10749.

Morel, A., and Maritorena, S. (2001). Bio-optical properties of oceanic waters: A reappraisal. *Journal of Geophysical Research* 106**,** 7163-7180. doi: 10.1029/2000jc000319.

Morel, A., and Prieur, L. (1977). Analysis of variations in ocean color. *Limnology and Oceanography* 22**,** 709-722.

Mori, Y. (1998). Optimal choice of foraging depth in divers. *Journal of Zoology* 245**,** 279-283.

Naito, Y. (2007). How can we observe the underwater feeding behavior of endotherms? *Polar Science* 1**,** 101-111.

Naito, Y., Bornemann, H., Takahashi, A., Mcintyre, T., and Plötz, J. (2010). Fine-scale feeding behavior of Weddell seals revealed by a mandible accelerometer. *Polar Science* 4**,** 309-316.

Naito, Y., Costa, D.P., Adachi, T., Robinson, P.W., Fowler, M., and Takahashi, A. (2013). Unravelling the mysteries of a mesopelagic diet: A large apex predator specializes on small prey. *Functional Ecology* 27**,** 710-717.

Newland, C., Field, I.C., Cherel, Y., Guinet, C., Bradshaw, C.J.A., Mcmahon, C.R., and Hindell, M.A. (2011). Diet of juvenile southern elephant seals reappraised by stable isotopes in whiskers. *Marine Ecology Progress Series* 424**,** 247-258.

Newland, C., Field, I.C., Nichols, P.D., Bradshaw, C.J.A., and Hindell, M.A. (2009). Blubber fatty acid profiles indicate dietary resource partitioning between adult and juvenile southern elephant seals. *Marine Ecology Progress Series* 384**,** 303-312.

Nishimoto, M.M., and Washburn, L. (2002). Patterns of coastal eddy circulation and abundance of pelagic juvenile fish in the Santa Barbara Channel, California, USA. *Marine Ecology Progress Series* 241**,** 183-199.

O'toole, M., Hindell, M.A., Charrassin, J.B., and Guinet, C. (2014a). Foraging behaviour of southern elephant seals over the Kerguelen Plateau. *Marine Ecology Progress Series* 502**,** 281-294.

O'toole, M.D., Lea, M.-A., Guinet, C., and Hindell, M.A. (2014b). Estimating Trans-Seasonal Variability in Water Column Biomass for a Highly Migratory, Deep Diving Predator. *Plos One* 9**,** e113171. doi: 10.1371/journal.pone.0113171.

Odum, E.P. (1969). The strategy of ecosystem development. *Science* 164**,** 262-270.

Olbers, D., Borowski, D., Völker, C., and Wölff, J.O. (2004). The dynamical balance, transport and circulation of the Antarctic Circumpolar Current. *Antarctic Science* 16**,** 439-470.

Olson, D.B., and Hood, R.R. (1994). Modelling pelagic biogeography. *Progress in Oceanography* 34**,** 161-205.

Orians, G.H., and Pearson, N.E. (1979). *On the theory of central place foraging.*

Orsi, A.H., Whitworth Iii, T., and Nowlin Jr, W.D. (1995). On the meridional extent and fronts of the Antarctic Circumpolar Current. *Deep Sea Research Part I: Oceanographic Research Papers* 42**,** 641-673. doi: http://dx.doi.org/10.1016/0967-0637(95)00021-W.

Pakhomov, E., Perissinotto, R., and Mcquaid, C. (1996). Prey composition and daily rations of myctophid fishes in the Southern Ocean. *Marine ecology progress series. Oldendorf* 134**,** 1-14.

Palter, J.B., Sarmiento, J.L., Gnanadesikan, A., Simeon, J., and Slater, R.D. (2010). Fueling export production: Nutrient return pathways from the deep ocean and their dependence on the Meridional Overturning Circulation. *Biogeosciences* 7**,** 3549-3568.

Park, Y.-H., Durand, I., Kestenare, E., Rougier, G., Zhou, M., D'ovidio, F., Cotté, C., and Lee, J.-H. (2014). Polar Front around the Kerguelen Islands: An up-to-date determination and associated circulation of surface/subsurface waters. *Journal of Geophysical Research: Oceans* 119**,** 6575-6592. doi: 10.1002/2014jc010061.

Park, Y.-H., Gambéroni, L., and Charriaud, E. (1991). Frontal structure and transport of the Antarctic Circumpolar Current in the south Indian Ocean sector, 40–80 E. *Marine Chemistry* 35**,** 45-62.

Park, Y.H., Charriaud, E., Pino, D.R., and Jeandel, C. (1998). Seasonal and interannual variability of the mixed layer properties and steric height at station KERFIX, southwest of Kerguelen. *Journal of Marine Systems* 17**,** 571-586.

Park, Y.H., Fuda, J.L., Durand, I., and Naveira Garabato, A.C. (2008a). Internal tides and vertical mixing over the Kerguelen Plateau. *Deep-Sea Research Part II: Topical Studies in Oceanography* 55**,** 582-593.

Park, Y.H., Roquet, F., Durand, I., and Fuda, J.L. (2008b). Large-scale circulation over and around the Northern Kerguelen Plateau. *Deep-Sea Research Part II: Topical Studies in Oceanography* 55**,** 566-581.

Parmesan, C. (2006). Ecological and Evolutionary Responses to Recent Climate Change. *Annual Review of Ecology, Evolution, and Systematics* 37**,** 637-669. doi: 10.2307/30033846.

Pellet, J., Fleishman, E., Dobkin, D.S., Gander, A., and Murphy, D.D. (2007). An empirical evaluation of the area and isolation paradigm of metapopulation dynamics. *Biological Conservation* 136**,** 483-495.

Pendoley, K.L., Schofield, G., Whittock, P.A., Ierodiaconou, D., and Hays, G.C. (2014). Protected species use of a coastal marine migratory corridor connecting marine protected areas. *Marine biology* 161**,** 1455-1466.

Perruche, C., Rivière, P., Lapeyre, G., Carton, X., and Pondaven, P. (2011). Effects of surface quasi-geostrophic turbulence on phytoplankton competition and coexistence. *Journal of Marine Research* 69**,** 105-135.

Pinheiro, J., Bates, D., Debroy, S., Sarkar, D., and R Development Core Team (2012a). "nlme: Linear and Nonlinear Mixed Effects Models".).

Pinheiro, J., Bates, D., Debroy, S., Sarkar, D., and Team, T.R.D.C. (2012b). nlme: Linear and Nonlinear Mixed Effects Models.

Polovina, J.J., Mitchum, G.T., and Evans, G.T. (1995). Decadal and basin-scale variation in mixed layer depth and the impact on biological production in the Central and North Pacific, 1960-88. *Deep-Sea Research Part I* 42**,** 1701-1716.

Post, A.L., Meijers, A.J.S., Fraser, A.D., Meiners, K.M., Ayers, J., Bindoff, N.L., Griffiths, H.J., Van De Putte, A.P., O'brien, P.E., Swadling, K.M., and Raymond, B. (2014). "Environmental setting," in *Biogeographic Atlas of the Southern Ocean,* eds. C. De Broyer, P. Koubbi, H.J. Griffiths, B. Raymond, C. Udekem D'acoz, A.P. Van De Putte, B. Danis, B. David, S. Grant, J. Gutt, C. Held, G. Hosie, F. Huettmann, A. Post & Y. Ropert-Coudert. (Cambridge: Scientific Committee on Antarctic Research), 46-64.

Purves, D., Scharlemann, J.P.W., Harfoot, M., Newbold, T., Tittensor, D.P., Hutton, J., and Emmott, S. (2013). Ecosystems: Time to model all life on Earth. *Nature* 493**,** 295-297.

R Development Core Team (2014). "R: A Language and Environment for Statistical Computing". (Vienna, Austria: R Foundation for Statistical Computing).

Riandey, V., Champalbert, G., Carlotti, F., Taupier-Letage, I., and Thibault-Botha, D. (2005). Zooplankton distribution related to the hydrodynamic features in the Algerian Basin (western Mediterranean Sea) in summer 1997. *Deep-Sea Research Part I: Oceanographic Research Papers* 52**,** 2029-2048.

Robins, D.B., Harris, R.P., Bedo, A.W., Fernandez, E., Fileman, T.W., Harbour, D.S., and Head, R.N. (1995). The relationship between suspended particulate material, phytoplankton and zooplankton during the retreat of the marginal ice zone in the Bellingshausen Sea. *Deep Sea Research Part II: Topical Studies in Oceanography* 42**,** 1137-1158. doi: http://dx.doi.org/10.1016/0967-0645(95)00058-X.

Ropert-Coudert, Y., Kato, A., Wilson, R.P., and Cannell, B. (2006). Foraging strategies and prey encounter rate of free-ranging Little Penguins. *Marine biology* 149**,** 139-148. doi: 10.1007/s00227-005-0188-x.

Rosen, D.a.S., and Trites, A.W. (2000). Digestive efficiency and dry-matter digestibility in Steller sea lions fed herring, pollock, squid, and salmon. *Canadian Journal of Zoology-Revue Canadienne De Zoologie* 78**,** 234-239. doi: 10.1139/cjz-78-2-234.

Russell, R.W., Hunt Jr, G.L., Coyle, K.O., and Cooney, R.T. (1992). Foraging in a fractal environment: Spatial patterns in a marine predator-prey system. *Landscape Ecology* 7**,** 195-209.

Sahrhage, D. (1988). "Some Indications for Environmental and Krill Resources Variability in the Southern Ocean," in *Antarctic Ocean and Resources Variability,* ed. D. Sahrhage. Springer Berlin Heidelberg), 33-40.

Sala, J., Quintana, F., Wilson, R., Dignani, J., Lewis, M., and Campagna, C. (2011). Pitching a new angle on elephant seal dive patterns. *Polar Biology* 34**,** 1197-1209. doi: 10.1007/s00300-011-0981-6.

Schick, R.S., New, L.F., Thomas, L., Costa, D.P., Hindell, M.A., Mcmahon, C.R., Robinson, P.W., Simmons, S.E., Thums, M., and Harwood, J. (2013). Estimating resource acquisition and at‐sea body condition of a marine predator. *Journal of Animal Ecology*.

Schoener, T.W. (1971). Theory of Feeding Strategies. *Annual Review of Ecology and Systematics* 2**,** 369-404. doi: doi:10.1146/annurev.es.02.110171.002101.

Schofield, O., Glenn, S., and Moline, M. (2013). The robot ocean network. *American Scientist* 101**,** 434-441.

Schreer, J.F., Kovacs, K.M., and Hines, R.J.O. (2001). Comparative diving patterns of pinnipeds and seabirds. *Ecological Monographs* 71**,** 137-162. doi: 10.1890/0012-9615(2001)071[0137:cdpopa]2.0.co;2.

Simmons, S.E., Crocker, D.E., Hassrick, J.L., Kuhn, C.E., Robinson, P.W., Tremblay, Y., and Costa, D.P. (2010). Climate-scale hydrographic features related to foraging success in a capital breeder, the northern elephant seal Mirounga angustirostris. *Endangered Species Research* 10**,** 233-243.

Sims, D.W., Witt, M.J., Richardson, A.J., Southall, E.J., and Metcalfe, J.D. (2006). Encounter success of free-ranging marine predator movements across a dynamic prey landscape. *Proceedings. Biological sciences / The Royal Society* 273**,** 1195-1201.

Slade, R.W., Moritz, C., Hoelzel, A.R., and Burton, H.R. (1998). Molecular population genetics of the southern elephant seal Mirounga leonina. *Genetics* 149**,** 1945-1957.

Smetacek, V., Assmy, P., and Henjes, J. (2004). The role of grazing in structuring Southern Ocean pelagic ecosystems and biogeochemical cycles. *Antarctic Science* 16**,** 541-558. doi: 10.1017/s0954102004002317.

Smith, R.C., and Baker, K.S. (1978). The bio-optical state of ocean waters and remote sensing. *Limnology and Oceanography* 23**,** 247-259.

Sokolov, S. (2008). Chlorophyll blooms in the Antarctic Zone south of Australia and New Zealand in reference to the Antarctic Circumpolar Current fronts and sea ice forcing. *J. Geophys. Res.* 113**,** C03022. doi: 10.1029/2007jc004329.

Sokolov, S., and Rintoul, S.R. (2007). On the relationship between fronts of the Antarctic Circumpolar Current and surface chlorophyll concentrations in the Southern Ocean. *Journal of Geophysical Research* 112**,** C07030. doi: 10.1029/2006jc004072.

Sokolov, S., and Rintoul, S.R. (2009). Circumpolar structure and distribution of the antarctic circumpolar current fronts: 1. Mean98 circumpolar paths. *Journal of Geophysical Research: Oceans* 114.

Sommerfeld, J., Kato, A., Ropert-Coudert, Y., Garthe, S., Wilcox, C., and Hindell, M.A. (2015). Flexible foraging behaviour in a marine predator, the Masked booby (Sula dactylatra), according to foraging locations and environmental conditions. *Journal of Experimental Marine Biology and Ecology* 463**,** 79-86.

Spear, L.B., Ballance, L.T., and Ainley, D.G. (2001). Response of seabirds to thermal boundaries in the tropical Pacific: the thermocline versus the Equatorial Front. *Marine Ecology Progress Series* 219**,** 275-289.

Stearns, S.C. (1993). "The Evolution of Life Histories," in *Journal of Evolutionary Biology,* eds. M.R. Rose & L.D. Mueller. (Oxford University Press, London: Blackwell Science Ltd), 304-306.

Sterling, J.T., Springer, A.M., Iverson, S.J., Johnson, S.P., Pelland, N.A., Johnson, D.S., Lea, M.A., and Bond, N.A. (2014). The sun, moon, wind, and biological imperative-shaping contrasting

wintertime migration and foraging strategies of adult male and female northern fur seals (Callorhinus ursinus). *Plos One* 9.

Stewart, B.S., and Delong, R.L. (1995). Double migrations of the northern elephant seal, Mirounga angustirostris. *Journal of Mammalogy* 76**,** 196-205.

Stramski, D., Bricaud, A., and Morel, A. (2001). Modeling the inherent optical properties of the ocean based on the detailed composition of the planktonic community. *Applied Optics* 40**,** 2929-2945. doi: 10.1364/ao.40.002929.

Sumner, M., and Wotherspoon, S. (2014). "Metropolis sampler and supporting functions for estimating animal movement from archival tags and satellite fixes". R package version 0.0-41 ed.).

Sumner, M.D., Michael, K.J., Bradshaw, C.J.A., and Hindell, M.A. (2003). Remote sensing of Southern Ocean sea surface temperature: implications for marine biophysical models. *Remote Sensing of Environment* 84**,** 161-173. doi: http://dx.doi.org/10.1016/S0034-4257(02)00103-7.

Sumner, M.D., Wotherspoon, S.J., and Hindell, M.A. (2009). Bayesian estimation of animal movement from archival and satellite tags. *PLoS One* 4**,** e7324.

Suryan, R.M., Santora, J.A., and Sydeman, W.J. (2012). New approach for using remotely sensed chlorophyll a to identify seabird hotspots. *Marine Ecology Progress Series* 451**,** 213-225.

Sutton, T.T. (2013). Vertical ecology of the pelagic ocean: Classical patterns and new perspectives. *Journal of Fish Biology* 83**,** 1508-1527.

Teo, S.L.H., Boustany, A., Blackwell, S., Walli, A., Weng, K.C., and Block, B.A. (2004). Validation of geolocation estimates based on light level and sea surface temperature from electronic tags. *Marine Ecology Progress Series* 283**,** 81-98.

Teo, S.L.H., Kudela, R.M., Rais, A., Perle, C., Costa, D.P., and Block, B.A. (2009). Estimating chlorophyll profiles from electronic tags deployed on pelagic animals. *Aquatic Biology* 5**,** 195-207. doi: 10.3354/ab00152.

Thomalla, S.J., Fauchereau, N., Swart, S., and Monteiro, P.M.S. (2011). Regional scale characteristics of the seasonal cycle of chlorophyll in the Southern Ocean. *Biogeosciences* 8**,** 2849-2866. doi: 10.5194/bg-8-2849-2011.

Thums, M., Bradshaw, C.J.A., and Hindell, M.A. (2008a). A validated approach for supervised dive classification in diving vertebrates. *Journal of Experimental Marine Biology and Ecology* 363**,** 75-83. doi: http://dx.doi.org/10.1016/j.jembe.2008.06.024.

Thums, M., Bradshaw, C.J.A., and Hindell, M.A. (2011). In situ measures of foraging success and prey encounter reveal marine habitat-dependent search strategies. *Ecology* 92**,** 1258-1270. doi: 10.1890/09-1299.1.

Thums, M., Cja, B., and Ma, H. (2008b). Tracking changes in relative body composition of southern elephant seals using swim speed data. *Marine Ecology Progress Series* 370**,** 249-261. doi: 10.3354/meps07613.

Trathan, P.N., Forcada, J., and Murphy, E.J. (2007). *Environmental forcing and Southern Ocean marine predator populations: effects of climate change and variability.*

Turner, W., Spector, S., Gardiner, N., Fladeland, M., Sterling, E., and Steininger, M. (2003). Remote sensing for biodiversity science and conservation. *Trends in Ecology and Evolution* 18**,** 306-314.

Vacquié-Garcia, J. (In Preparation). Verifying foraging success using accelerometers to detect prey encounter rates.

Vacquié-Garcia, J., Royer, F., Dragon, A.-C., Viviant, M., Bailleul, F., and Guinet, C. (2012). Foraging in the Darkness of the Southern Ocean: Influence of Bioluminescence on a Deep Diving Predator. *PLoS One* 7**,** e43565. doi: 10.1371/journal.pone.0043565.

Van Franeker, J.A., Van Den Brink, N.W., Bathmann, U.V., Pollard, R.T., De Baar, H.J.W., and Wolff, W.J. (2002). Responses of seabirds, in particular prions (Pachyptila sp.), to small-scale

processes in the Antarctic Polar Front. *Deep-Sea Research Part II: Topical Studies in Oceanography* 49**,** 3931-3950.

Vilchis, L.I., Ballance, L.T., and Fiedler, P.C. (2006). Pelagic habitat of seabirds in the eastern tropical Pacific: Effects of foraging ecology on habitat selection. *Marine Ecology Progress Series* 315**,** 279-292.

Viviant, M., Trites, A.W., Rosen, D.a.S., Monestiez, P., and Guinet, C. (2010). Prey capture attempts can be detected in Steller sea lions and other marine predators using accelerometers. *Polar Biology* 33**,** 713-719. doi: 10.1007/s00300-009-0750-y.

Walther, G.-R., Post, E., Convey, P., Menzel, A., Parmesan, C., Beebee, T.J.C., Fromentin, J.-M., Hoegh-Guldberg, O., and Bairlein, F. (2002). Ecological responses to recent climate change. *Nature* 416**,** 389-395.

Ware, D.M., and Thomson, R.E. (2005). Ecology: Bottom-up ecosystem trophic dynamics determine fish production in the northeast pacific. *Science* 308**,** 1280-1284.

Watanabe, Y.Y., and Takahashi, A. (2013). Linking animal-borne video to accelerometers reveals prey capture variability. *Proceedings of the National Academy of Sciences of the United States of America* 110**,** 2199-2204. doi: 10.1073/pnas.1216244110.

Webb, P.M., Crocker, D.E., Blackwell, S.B., Costa, D.P., and Le Boeuf, B.J. (1998). Effects of buoyancy on the diving behavior of northern elephant seals. *Journal of Experimental Biology* 201**,** 2349-2358.

Weimerskirch, H., Gault, A., and Cherel, Y. (2005). Prey distribution and patchiness: Factors in foraging success and efficiency of Wandering Albatrosses. *Ecology* 86**,** 2611-2622.

Widder, E.A. (2010). Bioluminescence in the ocean: Origins of biological, chemical, and ecological diversity. *Science* 328**,** 704-708.

Zainuddin, M., Kiyofuji, H., Saitoh, K., and Saitoh, S.I. (2006). Using multi-sensor satellite remote sensing and catch data to detect ocean hot spots for albacore (Thunnus alalunga) in the northwestern North Pacific. *Deep-Sea Research Part II: Topical Studies in Oceanography* 53**,** 419-431.

Zhao, L., Zhao, Y., Zhang, W.C., Zhou, F., Zhang, C.X., Ren, J.L., Ni, X.B., Denis, M., and Xiao, T. (2013). Picoplankton distribution in different water masses of the East China Sea in autumn and winter. *Chinese Journal of Oceanology and Limnology* 31**,** 247-266. doi: 10.1007/s00343-013-2085-3.

Zuur, A.F., Ieno, E.N., and Elphick, C.S. (2010). A protocol for data exploration to avoid common statistical problems. *Methods in Ecology and Evolution* 1**,** 3-14. doi: 10.1111/j.2041-210X.2009.00001.x.

Zuur, A.F., Leno, E.N., Walker, N.J., Saveliev, A.A., and Smith, G.M. (2009). *Mixed effects models and extensions in ecology with R.* Springer.